Post-Punching Behavior of Reinforced Concrete Slabs

THÈSE N^{O} 4613 (2010)

PRÉSENTÉE LE 12 MAI 2010

À LA FACULTÉ ENVIRONNEMENT NATUREL, ARCHITECTURAL ET CONSTRUIT

LABORATOIRE DE CONSTRUCTION EN BÉTON

PROGRAMME DOCTORAL EN STRUCTURES

ÉCOLE POLYTECHNIQUE FÉDÉRALE DE LAUSANNE

POUR L'OBTENTION DU GRADE DE DOCTEUR ÈS SCIENCES

PAR

Yaser MIRZAEI

acceptée sur proposition du jury:

Prof. J.-P. Lebet, président du jury
Prof. A. Muttoni, directeur de thèse
Prof. E. Brühwiler, rapporteur
Prof. P. Gambarova, rapporteur
Prof. T. Vogel, rapporteur

ÉCOLE POLYTECHNIQUE
FÉDÉRALE DE LAUSANNE

Suisse
2010

To my mom and dad

Acknowledgement

There are many people to thank for their support and encouragement, without whom this thesis would not have been possible. First of all, I would like to express my gratitude to my supervisor Prof. Dr. Aurelio Muttoni who welcomed me in his research group, giving me the possibility to work in excellent conditions and the opportunity to learn a new language and to get familiar with the Swiss culture.

The research project was supported and financed by the Swiss association of the cement industry (CEMSUISSE), which is gratefully acknowledged.

I would like to thank Prof. Eugen Brühwiler, the head of the Laboratory of Maintenance and Safety of Structures (MCS) at the EPFL, Prof. Pietro Gambarova, the head of the Structural Engineering Department of Politecnico di Milano, and Prof. Thomas Vogel, the chair of the Structural Engineering - Structural Design and Conservation at the ETH Zurich, for having accepted to be part of my jury and for their valuable comments allowing the improvement of the thesis. Special thanks to Prof. Jean-Paul Lebet, the president of the jury.

I would like to thank Dr. Miguel Fernández Ruiz and Dr. Olivier Burdet for the numerous discussions and technical comments on this dissertation. The support and help of our secretary Mrs. Yvonne Bühl is very much appreciated. A big thank you goes to my officemate Stefan Lips and my compatriot Talayeh Noshiravani for reading the manuscript and proposing valuable suggestions.

Special thanks go to the technical staff of the Civil Engineering Institute, namely Sylvain Demierre, Gilles Guignet, Patrice Gallay, Roland Gysler, Hans-Jakob Reist, and François Perrin, who taught me all I know about experimental techniques and helped me with my lab tests.

I would like to thank all my friends inside and outside school for the pleasant moments spent together over recent years. I would like to thank the present and the former members of the Concrete Structural Laboratory IBETON, with whom I have passed many pleasurable moments. Many thanks to Hadi Kamyab and the other members of the MCS for their friendship during the past several years.

Finally and above all, I would like to thank my family, my parents and siblings, for their never ending support and love during all those years of my studies - without you I would probably never have gotten this far.

Summary

Reinforced concrete flat slabs are extensively used in buildings and parking garages. Their design is governed by deflection at the serviceability limit state and punching shear at the ultimate limit state. When no punching shear reinforcement is provided, failure develops in a brittle manner. Punching shear failure occurs with almost no warning signs, because deflections are small and cracks at the top side of the slab are usually not visible.

Over the past decades, several structural collapses occurred due to punching shear failure resulting in human casualties and large damages. These collapses revealed some shortcomings in codes of practice and the necessity of reconsidering punching provisions. The investigations of these collapses showed that the collapse initiated from a local punching failure and propagated throughout the structure, in a progressive collapse. The term progressive collapse refers to the spreading of an initial local failure triggered by the loss of one or more load carrying members and leading to partial or total collapse of the structure in a manner analogous to the chain reaction. As a local punching failure can trigger progressive collapse, the study of the post-punching behavior can help adopting constructive solutions to avoid progressive collapse.

The post-punching behavior of flat slabs supported by columns has not yet been thoroughly investigated. Therefore, an extensive experimental campaign was performed in the framework of this dissertation to investigate the post-punching behavior of 24 slabs with various reinforcement layouts. The effects of bending reinforcement, integrity reinforcement, bent-up bars, steel type, and anchorage conditions on the post-punching behavior of slab-column connections were investigated. The performance and robustness of the various solutions was investigated to obtain physical explanations of the load-carrying mechanisms.

Test results showed that the post-punching strength provided by the top reinforcement is small because the concrete cover is thin and spalling of the concrete cover occurs leaving the reinforcement ineffective. In addition, it was observed that integrity reinforcing bars passing through the column significantly improve the post-punching behavior in terms of strength and deformation capacity. The integrity bars behave as a tensile membrane inclined to the plane of the slab and are able to sustain damaged portions from the column. Thus, one possibility to enhance the robustness of the structure against progressive collapse is to provide well-anchored bottom reinforcing bars passing through the column.

A mechanical model capable of predicting the post-punching behavior of slab-column connections without shear reinforcement was developed. The model predicts the contribution of the tensile reinforcement and of the integrity reinforcement to the post-punching strength. The model accounts for possible failure modes including the fracture of the bars and the destruction of the concrete over the integrity bars. The progressive destruction of the concrete within and outside the punching cone is treated by considering the pullout behavior of reinforcement embedded in the concrete.

Finally, a parametric study was performed to evaluate the influence of various parameters and their relative importance in order to develop practical proposals for the estimation of the post-punching strength. It showed that the post-punching strength is not only a function of the cross sectional area and yield strength of the integrity reinforcement as it appears in provisions and codes of practices but also of the diameter of the bars, the effective depth, the ductility, and the type of reinforcement.

Key words:

Flat slab, slab-column connection, progressive collapse, punching failure, post-punching strength, dowel action, integrity reinforcement, punching cone, robustness, ductility, concrete destruction, spalling of concrete cover

Résumé

Les plancher-dalles sont largement utilisés dans la construction d'immeubles et parkings. Leur dimensionnement est gouverné par la flèche à l'état limite de service et par leur résistance au poinçonnement à l'état limite ultime. Lorsque le plancher-dalle est dépourvu d'armatures transversales, la rupture par poinçonnement se produit subitement. Ce type de rupture, également dit fragile, se produit sans signes précurseurs extérieurs, la flèche étant généralement très faible et la fissuration sur la face supérieure de la dalle invisible.

Durant les dernières décennies, plusieurs ruptures par poinçonnement se sont produites conduisant à des pertes humaines et matérielles importantes. Ces accidents ont révélés des faiblesses dans les normes en vigueurs concernant ce phénomène et la nécessité d'améliorer les prescriptions actuelles. L'étude des ces accidents a montré que la rupture c'est produite initialement par poinçonnement au niveau d'une seul colonne puis par propagation progressive à tout la structure. Le terme l'effondrement progressif signifie qu'à partir d'une rupture locale, la rupture se propage à toute la structure par redistribution des charges sur les éléments adjacents. Ces éléments n'étant pas aptes à supporter ces charges excédentaires. L'étude du comportement post-poinçonnement des plancher-dalles peut conduire à l'adoption de solutions constructives permettant d'éviter les ruptures progressives conséquentes au poinçonnement.

Le comportement post-poinçonnement des dalles supportées par des colonnes n'a pas encore été suffisamment traité. Par conséquent, une campagne expérimentale importante a été effectué dans le cadre de cette thèse afin d'étudier le comportement post-poinçonnement de 24 différents schémas d'armatures de dalles. Principalement, l'effet de l'armature flexionnelle, de l'armature d'intégrité, des barres relevées, du type d'armature et des conditions d'ancrage a été étudié. L'efficacité structurelle des différents schémas d'armatures a été analysé afin d'obtenir une interprétation physique du mécanisme de reprise des forces, post-poinçonnement, dans la connexion colonne-dalle.

Les résultats expérimentaux ont montrés que la résistance post-poinçonnement provenant des armatures flexionnelles est faible. Cette incapacité est conséquente au fait que l'éclatement du béton d'enrobage se produit rapidement conduisant à une inefficacité structurelle de cette armature. Au contraire, il a été observé que l'armature d'intégrité, située dans la partie comprimée de la dalle et passant au dessus de la colonne, augmente de manière significative la résistance et la ductilité de la connexion dalle-colonne post-poinçonnement. En effet, cette armature se comporte, post-poinçonnement, comme une membrane tendue et par conséquent est capable de transmettre une partie des charges de la dalle endommagée à la colonne. C'est pourquoi, un ancrage suffisant ainsi qu'un bon choix des dimensions de l'armature d'intégrité augmente l'efficacité structurelle des plancher-dalles pour les ruptures progressives.

Un modèle mécanique capable de prédire le comportement post-poinçonnement des plancher-dalles sans armature transversales a été développé. Le modèle proposé est capable d'estimer la contribution de l'armateur de flexion ainsi que de l'armature d'intégrité. Il considère la rupture possible des armatures et l'endommagement du béton à l'intérieur et à l'extérieur du cône de poinçonnement. Cet endommagement provient de l'arrachement des armatures ancrées dans ces zones.

Finalement, une étude paramétrique a été effectuée pour évaluer l'influence des différents paramètres et leur importance relative. L'objectif de cette étude est le développement d'une approche utilisable dans la pratique permettant l'estimation de la résistance post-poinçonnement des joints colonne-dalle. Il a été démontré que la résistance post-poinçonnement n'est pas uniquement corrélée à la section nominale de la dalle et à la limite d'écoulement des armatures d'intégrité comme cela apparaît dans les normes actuelles. La hauteur effective de la dalle, le

schéma des armatures ainsi que leur diamètre et ductilité influencent également la résistance au post-poinçonnement des joints colonne-dalle.

Mots-clefs:

Plancher-dalle, connexion dalle-colonne, rupture progressive, rupture par poinçonnement, résistance post-poinçonnement, effet goujons, armature d'intégrité, cône de poinçonnement, efficacité structurelle, ductilité, endommagement du béton, éclatement du béton d'enrobage

Zusammenfassung

Die Verwendung von Flachdecken aus Stahlbeton für Gebäude und Parkgaragen ist weitverbreitet. Die Bemessung von Flachdecken wird durch die Durchbiegung im Gebrauchszustand und durch das Durchstanzen im Bruchzustand bestimmt. Falls keine Durchstanzbewehrung vorhanden ist, verhält sich die Flachdecke vergleichsweise spröd. Folglich sind die Durchbiegungen klein und da eventuelle Risse auf der Plattenoberseite üblicherweise nicht sichtbar sind, kann ein Bruch ohne vorhergehende Warnzeichen entstehen.

Während den letzten Jahrzehnten kamen verschiedene Einstürze infolge Durchstanzen von Stützen vor. Dies endete meistens mit grossen Sach- aber auch Personenschaden. Diese Unglücke enthüllten einige Unzulänglichkeiten der aktuellen Normen und die Notwendigkeit die Regelungen bezüglich Durchstanzen zu überarbeiten. Die Untersuchung dieser Unglücke zeigte, dass der Fehler bei einem lokalen Durchstanzversagens anfing und sich danach auf die ganze Tragstruktur ausbreitete und zu einem progressiven Kollaps führte. Der Begriff progressiver Kollaps bezeichnet die Ausbreitung eines lokalen Versagens, beispielsweise durch den Verlust einer oder mehreren Tragstrukturen, bis zum teilweisen oder ganzen Versagens des Bauwerkes. Da ein lokales Durchstanzversagen ein progressiver Kollaps auslösen kann, hilft die Untersuchung vom post-kritischen Verhalten von Flachdecken für neue konstruktive Vorgaben zur Vermeidung eines progressiven Kollapses.

Bislang wurde das post-kritische Verhalten von Flachdecken nicht gründlich erforscht. Deshalb wurde für die Dissertation eine umfangreiche experimentelle Untersuchung durchgeführt. Es wurde das post-kritischem Verhalten von 24 Platten mit unterschiedlicher Bewehrungsanordnung untersucht. Dabei wurde der Einfluss der Biegebewehrung, der unteren Bewehrungslage, von aufgebogenen Stäben, der Stahlqualität und der Verankerung auf das post-kritischem Verhalten von Stützen-Plattenverbindung untersucht. Durch das Verhalten und die Robustheit von den verschiedenen Versuchskörpern konnte das physikalische Verhalten des massgebenden Mechanismus nachvollzogen werden.

Testresultate zeigten, dass die obere Biegebewehrung nur geringen Einfluss auf die post-kritische Festigkeit hat. Dies lässt sich durch die geringe Betonüberdeckung erklären, welche abplatzt und die Bewehrung unwirksam werden lässt. Allerdings wurde beobachtet, dass die untere Bewehrung über der Stütze das post-kritische Verhalten bezüglich Festigkeit und Duktilität erheblich verbessert. Die untere Bewehrung verhält sich wie eine Zugmembrane und hält den beschädigten Teil der Platte. Folglich ist die Verwendung von einer gut verankerten unteren Bewehrung eine Möglichkeit die Robustheit zu erhöhen.

Um das post-kritische Verhalten von Stützen-Plattenverbindungen ohne Schubbewehrung zu berechnen, wurde ein mechanisches Modell entwickelt. Dieses Modell berechnet die Membrankräfte der oberen Biegebewehrung und die Dübelwirkung der unteren Bewehrung. Das Berechnungsmodell berücksichtigt verschiedene Versagensarten, wie Bruch der Bewehrung und die Zerstörung des Betons oberhalb der unteren Bewehrung. Die fortschreitende Zerstörung innerhalb und ausserhalb des Durchstanzkegels wird mittels des Ausziehverhaltens der im Beton liegenden Bewehrung berücksichtigt.

Des Weiteren wurde eine Parameterstudie durchgeführt, um den Einfluss und die Wichtigkeit verschiedener Parametern zu bestimmen. Es wird gezeigt, dass der post-kritische Durchstanzwiderstand nicht nur eine Funktion der Querschnittsfläche und Fliessgrenze der unteren Bewehrung, wie es in den Bestimmungen und Normen geregelt ist, sondern auch eine Funktion des Durchmessers der Bewehrungsstäbe, die statische Höhe, die Duktilität und der Stahlqualität. Anhand dieser Erkenntnisse konnte ein Vorschlag für eine Formel für die Abschätzung des post-kritische Durchstanzwiderstandes entwickelt werden.

Stichwörter:

Flachdecken, Platten-Stützenverbindung, progressive Kollaps, Durchstanzen, post-kritisches Verhalten, Dübelwirkung, Biegebewehrung, Durchstanzkegel, Robustheit, Duktilität, Abplatzen

Table of contents

List of Figures

List of Tables

1 Introduction

1.1 Statement of the problem

Reinforced concrete slabs supported by columns without capital or drop panel are a common structural system for cast-in-place slabs. The benefits of flat slab constructions are widely recognized and this structural system is used for the construction of administrative, commercial, and industrial buildings as well as car parking. Flat slabs can be built relatively rapidly because the absence of drop panels results in simpler formwork arrangements, enabling rapid floor construction, and giving maximum flexibility to the occupants. In addition, flat slab construction places no restrictions on the positioning of horizontal services and partitions and helps minimizing floor-to-floor heights. This provides advantages in terms of lower building height, reduced façade and installation costs. Moreover, flat slab construction offers considerable flexibility to occupants who can easily alter internal layouts to accommodate changes in the use of the structure. This flexibility results from the use of a square or near-square grid and the absence of beams and drop panels that complicate the routing of services and location of partitions. Furthermore, a comprehensive research in this field has been carried out worldwide over the past decades that led to the development of design methods, technical standards, and simple and efficient tools to deal with the design and construction of flat slabs supported by columns.

Punching shear failure, a brittle failure mode, is the major disadvantage of this structural system. Punching shear failure occurs with almost no warning signs because deflections are small and cracks at the top side of the slab are usually not visible. A local punching failure at one column will result in increased shear force at surrounding columns which can trigger the punching failure to the adjacent columns resulting in the progressive collapse of the complete structure.

The term *progressive collapse* has been used to describe the spreading of an initial local failure within a structure, which can lead to partial or total collapse of the structure in a manner analogous to a chain reaction. The local failure is triggered by the loss of one load carrying member. Following the initial failure, the structure seeks alternative load paths to transfer the load originally carried by the damaged portions to the adjacent undamaged members. As the latter may or may not have adequate strength to withstand the additional loads, further redistribution of loads are likely to occur until an equilibrium state is reached. However, due to the magnitude of the loads involved, equilibrium may only be achieved when a substantial part of the structure has already collapsed. Therefore, the main feature of progressive collapse is that the final damage is disproportionately larger than the local damage that initiated the collapse.

Over the past decades, several collapses due to punching shear failure occurred that resulted in human casualties and large damages. Figure 1.1.a shows a shopping center in Morbio Inferiore (TI, Switzerland) at the end of 70’s. The punching failure of one slab during the construction phase led to the progressive collapse of a large part of the structure. The collapse occurred during a break and fortunately nobody was injured. An underground parking collapsed in 1976 in Geneva (GE, Switzerland). An extra loading

due to excavation works in the vicinity of the building was believed to be the cause of the failure (Figure 1.1.b). On December 26, 1981, the collapse of an underground car parking resulted in the death of two children at Bluche (VS, Switzerland). Punching shear failure was believed to have triggered the collapse (Figure 1.1.c). Investigations following this accident concluded that there had been many errors and omissions associated with the structure (Favre *et al.*, 2004, SIA D 0226, 2008).

On December 17, 2004, a tragic accident occurred in Gretzenbach (SO, Switzerland), when firemen were trying to extinguish a fire in an underground car parking (Figure 1.1.d). Seven firemen died after a punching failure of a column instigated a progressive collapse and thus the collapse of a large portion of the structure. The investigation commission painted a picture of a troubled project, with considerable confusion about responsibility for structural safety (Muttoni *et al.*, 2005). It was concluded that not only the applied load had been much larger than the design load but also the design for punching shear had been carried out based on very optimistic assumptions (SIA D 0226, 2008). Moreover, tensile reinforcing bars were misplaced over the column and thus reduced the effective depth of the slab, resulting in a decrease of the punching strength.

a) *b)*

c) *d)*

Figure 1.1: Cases of structural collapse due to punching shear failure

The occurrence of progressive collapse initiated by a punching shear failure is neither rare nor limited to Switzerland and occurred all over the world (Schousboe, 1976; Carino *et al.*, 1983; Kaminetzky, 1991; King and Delatte, 2004). Investigations following these collapses concluded that both design and construction errors contributed to the cause of the collapses. Most failures could have been avoided if better inspections of materials and construction details had been conducted. Historical data indicate that

the risk of progressive collapse in buildings is very low. However, loss of life and severe injuries can be significant when a fully occupied multi-story building experiences a large partial or total collapse (Ellingwood *et al.*, 2007).

These structural collapses show that there are some shortcomings in current codes of practice. As a consequence, there is a question whether flat slabs designed according to current codes of practice really fulfill the basic requirements for structural safety. The failure of reinforced concrete slabs is in most cases ductile, and causes only limited redistribution of loading. Punching failure of flat slabs without shear reinforcement is an exception, and the drop in resistance at failure is considerable and thus leads to a large redistribution of loads, which can trigger failure at adjacent columns and eventually to the progressive collapse of large parts of the structure. To avoid or at least to reduce the likelihood of these failures, it is necessary to provide alternative load paths to transfer the load of a column after it has failed in punching shear. This may be achieved by having some deformation capacity after failure, which can be provided by means of integrity reinforcement passing through the column. Integrity reinforcing bars are placed in the compression zone of the slab over the column, pass through the column core, and are well-anchored in the slab.

In general, the following constructive solutions can be implemented to reduce the likelihood of the progressive collapse:

1. The use of capitals or drop panels to increase the slab thickness so that the punching shear is not determinant.
2. The arrangement of construction and expansion joints to prevent the propagation of a local failure.
3. The reduction of the span lengths.
4. The use of punching shear reinforcement so that a ductile behavior (punching within the shear-reinforced zone) and not a brittle one (crushing of the concrete struts near the column, and punching outside the shear-reinforced zone) is determinant.
5. The use of bent-up bars to increase the strength and deformation capacity of the slab-column connections (Broms, 2000).
6. The use of well-anchored integrity reinforcement passing through the column capable of suspending the damaged portions of the slab from the columns after punching shear failure has occurred (Mitchell and Cook, 1984; Georgopoulos, 1986; Muttoni, 2003).

Solution 1 obviously increases the punching strength of the slab. However, it increases the cost of building on several counts and is in contradiction with architectural criteria in which drop panels are undesirable where the slab itself forms the ceiling. The criteria for sufficient slab thickness are often quite complicated as they are related to a very brittle failure mechanism, which is also influenced by local forces and stresses due to eccentricity, bending and imposed deformations (Knoll and Vogel, 2009).

Solutions 2 and 3 are generally not efficient because of economic problems and functionality limitations.

Solution 4 is interesting given the fact that punching shear reinforcement is increasingly used to enhance the strength and deformation capacity of flat slabs. Various punching shear reinforcement systems are currently available, most of them are proprietary. These systems can be installed in the slab near the columns in the form of studs or stirrups, placed on the top of the columns in the form of steel shearheads or mushrooms, or as a combination of the aforementioned. Experimental results have shown that using shear reinforcement enhances both strength and deformation capacity of slab-column connections. Thus, the slab can be designed for much higher design loads. However, flat slabs with low to moderate applied loads do not need to be reinforced with shear reinforcement. Therefore, using shear reinforcement to enhance the post-punching strength in flat slabs with low to moderate loads may not be a good constructive solution besides practical difficulties of placing such reinforcement.

Solution 5 appears to be an economical solution to prevent progressive collapse by providing a ductile behavior of flat slabs. It has nevertheless been abandoned in Switzerland for practical reasons. Test results have shown that the combination of shear reinforcement with bent-up bars can be efficient in giving the slab a ductile behavior and even in preventing punching failure from happening (Broms, 2000). However, the practical difficulties of placing such reinforcement over the column have not yet been solved as it requires a complicated placing sequence.

Solution 6 was adopted by the Swiss Code SIA 262 (2003), requiring that some reinforcement shall be provided on the compression side and be extended over the column and well anchored on both sides. The proposed empirical formulation is based on the experimental program carried out in Munich in the 80s (Kupfer and Georgopoulos, 1986; Georgopoulos, 1986). Knoll and Vogel confirms that “the bottom reinforcing, which is anchored in the column, or passing through it, will act in a hammock-like fashion, keeping the slab from falling down onto the slab below, triggering the collapse of that one and the ones below it in a progressive collapse as has occurred in some terrifying instances (Knoll and Vogel, 2009). Thus, integrity reinforcement crossing the column and detailed with the intention to provide sufficient post-punching strength can be used as an economical solution to increase the structural robustness and to avoid the propagation of punching to adjacent columns.

1.2 Scope and objective of the work

The goal of the present thesis is to investigate the post-punching behavior of flat slabs and its consequences as

- To gain a better understanding of the post-punching behavior of concrete slab-column connections.
- To provide a substantial body of experimental evidence on the post-punching behavior of slab-column connections.
- To investigate the effect of tensile reinforcement and integrity reinforcement passing through the column.
- To develop a mechanical model capable of predicting the post-punching behavior of slab-column connections.

- To decrease the vulnerability of flat slabs to unforeseen circumstances while preserving their economic advantages and simplicity and to establish the bases for the design of economic solutions that are simple to implement.

1.3 Thesis organization

This thesis is organized as follows:

Chapter 2 is devoted to the literature review on the post-punching behavior of flat slabs supported by columns. The performance of concrete flat slabs after a local failure is described. The post failure shear transfer mechanisms through tensile reinforcement and integrity reinforcement are introduced. An extensive overview on the past research on dowel action is presented. The various design approaches to mitigate the likelihood of progressive collapse are presented. Various available approaches for the robustness of the structure against the progressive collapse are introduced.

Chapter 3 summarizes the experimental investigations on the post-punching behavior of slab-column connection. The post-punching behavior of a total of 24 slab specimens with various flexural reinforcement layouts are introduced and compared to investigate the effects of tensile and integrity reinforcement on the post-punching behavior.

Chapter 4 describes the conceptual bases and applications of the mechanical model developed for studying the post-punching behavior of slab-column connections. The proposed approach based on a physical model predicts the membrane action of the tensile reinforcement as well as the dowel action of the integrity reinforcement passing through the column. The influence of the bar pullout and localized curvature on the ultimate post-punching strength are also investigated. Furthermore, it presents a parametrical study carried out using the model to identify the most important parameters. The geometrical and material parameters are chosen and their influence on the membrane action, dowel action and post-punching strength are described.

Chapter 5 deals with the application of the mechanical model. A parametric study is established to evaluate the influence of various parameters on the post-punching behavior of slab-column connection and to evaluate the relative importance of the parameters. The results of the previous chapters are collected and incorporated in a design proposal for dimensioning slab-column connections. Some recommendations for the practical work as well as constructive solutions are proposed.

Chapter 6 draws conclusions for the present work. Principal results, main conclusions and suggestions for future work are given.

2 State of the art

A comprehensive overview of the post-punching literature is presented in this chapter. First, a general overview on the post-failure load carrying mechanisms in concrete structures is presented including a brief introduction about compressive and tensile membrane actions. Afterwards, post-failure shear transfer mechanism of concrete slabs is explained with the concentration on the post-punching behavior of flat slabs supported by column. Subsequently, an extensive overview on the concept and application of the dowel action is provided. Later, a comprehensive discussion about various modes of failure, and concrete bearing strength and stiffness is presented. Afterwards, various methods proposed by codes of practice dealing with the post-punching behavior of flat slabs are explained. Finally, the concept of robustness is described including different methods to increase the robustness of the structure and to withstand unforeseen circumstances leading to progressive collapse of the structure.

2.1 Performance of concrete slabs after local failure

Figure 2.1 shows the general behavior of a typical square slab fully restrained at its edges under monotonic loading. Three different phases can be characterized for the overall response of the slab. At the beginning of the loading, the behavior is linear elastic. When concrete cracking and reinforcement yielding occur, the behavior turns into the nonlinear phase. This behavior continues up to the initial failure point (point A). This failure can be either the flexural failure or the punching shear failure. Up to this stage, compressive membrane action can be developed due to lateral restraints and enhances the load carrying capacity of the slab (Wood, 1961; Park, 1964; Hopkins and Park, 1971; Mitchell and Cook, 1984).

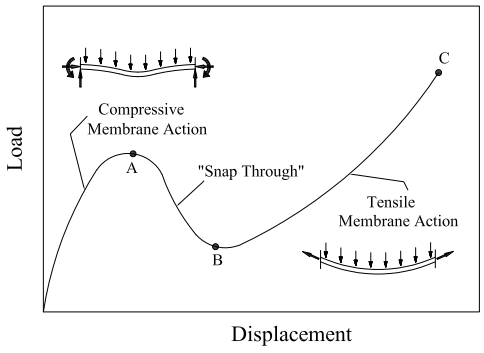

Figure 2.1: Structural response of a fully restrained concrete slab (Mitchell and Cook, 1984)

After the initial failure occurs, the load decreases with the increase of the deflection until a minimum is reached (point B). Beyond this stage, the behavior of the slab will depend strictly on redundancy, continuity, integrity, and deformation capacity of the slab. At this stage, the in-plane membrane forces in the central region of the slab change from compression to tension because the slab restraints begin to resist inward movements of the edges. In addition, due to large tensile strains at the slab surface,

cracks tend to penetrate the whole depth of the slab. Thus, the concrete is fully cracked and the entire load is carried by the reinforcement acting as a tensile membrane (Park, 1964). Finally, the total failure occurs when the axial strain of the reinforcing bars reach the ultimate tensile strain of the reinforcement (Maekawa *et al.*, 2003). In subsequent sections, various post-critical load-carrying mechanisms of concrete structures are presented and discussed.

2.1.1 Compressive membrane action

More than 50 years ago, Ockleston (1955) observed that restrained concrete slabs carried higher loads in relation to those calculated by Johansen's yield line theory (Johansen, 1962). It was believed that compressive membrane action increased the load-carrying capacity. The first attempts to analyze reinforced concrete slabs for the compressive membrane action was due to Wood and Park (Wood, 1961; Park, 1964). Numerous experiments have been performed in the past to investigate the influence of the compressive membrane action on the behavior of reinforced concrete slabs (Kinnunen and Nylander, 1960; Christiansen, 1963; Hopkins and Park, 1971; Hewitt and Batchelor, 1975). Test results confirmed that compressive membrane action can significantly enhance the load carrying capacity of concrete slabs if the edges of the slabs are laterally restrained.

In addition, numerous researchers conducted theoretical study to develop reasonable analytical expressions capable of predicting the effect of the compressive membrane action (Christiansen, 1963; Park, 1964; Kemp, 1967; Morley, 1967; Hayes, 1968; Desayi and Kulkarni, 1977; Braestrup, 1980; Eyre, 1990; Bailey, 2008). Figure 2.2 shows a reinforced concrete strip subjected to ordinary loads. When flexural cracks appear on the most highly stress sections, the neutral axis tends to move toward the compression zone with a corresponding axial extension of the strip. If the axial extension of the middle plane is in any way prevented, in-plane compressive forces will develop in the strip. These forces can increase the load capacity due to its significant role in controlling deflection and crack propagation (Vecchio and Tang, 1990).

With reference to the punching strength, numerous experiments have been carried out to study the enhancement of the punching strength due to the compressive membrane action. Test results showed an increase of the punching strength up to 38% in the presence of the compressive membrane action (Chana and Desai, 1992; Salim and Sebastian, 2003).

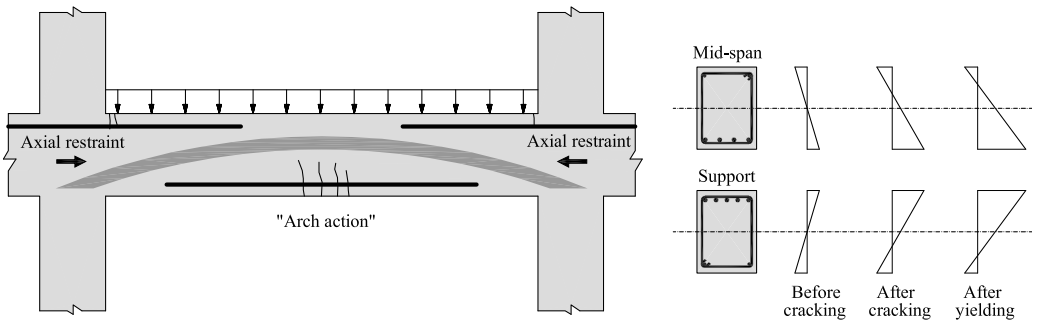

Figure 2.2: Development of compressive membrane action (arch action) and shift of slab neutral axis towards compression zone

2.1.2 Vierendeel action

Reinforced concrete frame structures designed to withstand lateral loads can prevent a local damage from propagating by Vierendeel action. This action relies on the conventional structural behavior and can be implemented without major changes in structural philosophy. With reference to structural deformations by Vierendeel action, beams experience severe double-curvature deformation and columns experience severe flexural loading as can be seen in Figure 2.3.a. Current codes of practice do not address Vierendeel action as a post-failure shear transfer mechanism. However, it was experimentally shown that the development of Vierendeel action can prevent the progressive collapse following a local damage, and limit the maximum vertical deformation of the structure (Sasani and Sagiroglu, 2008; Yi *et al.*, 2008). Nevertheless, Ellingwood argued that in order to resist progressive collapse by this mechanism, it is necessary to strengthen a large portion of the structure (Ellingwood *et al.*, 2007). In terms of existing structures, Ellingwood stated that "…consideration needs to be given to the proximity of the existing moment frames with respect to the locations where initiating events are likely to occur, and to the forces that occur when Vierendeel behavior is activated. However, if beams and columns and their connections can be reinforced to support the applied loads, this method to add robustness can be relatively unobtrusive (Ellingwood *et al.*, 2007).

2.1.3 Secondary trusses

The secondary truss mechanism can occur if the initial damage is the removal of a certain columns at low levels in a building. As Figure 2.3.c shows, it is feasible to add diagonal elements at upper levels to turn two or multiple-story columns and beam systems into trusses. It is apparent that trusses consist of tension and compression elements. Thus, some elements which are originally designed as compression members, e.g. the column above the initial damage, may experience tension forces in the secondary truss system. Particular attention should be paid in the design of such structural elements. In addition, particular consideration needs to be given to the connections between the diagonal elements and the existing structure, the strength of the existing elements to carry new loads, and the ability of originally compression members to carry tension forces.

2.1.4 Tensile membrane action

The concept is the engagement of tensile forces in members that deform into configurations allowing tensile membrane action to be developed. Tensile membrane action is a geometrically nonlinear mechanism whose nature depends highly on boundary conditions and vertical supports. Reinforced concrete slabs that are laterally restrained and have continuous reinforcement can reach a pure state of tension under large deflections. For the tensile membrane action to be activated, it is essential that reinforcing bars are continuous and well-anchored to the slab supports. Tensile membrane action enhances the deformation capacity of the slab and increases the post-failure ultimate strength (Park, 1964).

Provisions made for lateral restraints for the compressive membrane action will satisfy the requirements of the tensile membrane action of internal two-way slab and beam structures. The tensile membrane action can be a useful mechanism to prevent a

catastrophic failure following a local damage. Special attention is needed to be given to originally compression elements that are supposed to carry tension forces at large displacements. Connections are complicated and the initial collapse causes very high forces in tension elements. These forces need to be anchored properly at the supports and transferred to the columns. In addition, a sufficient strength and stiffness in the framing system is needed to resist the horizontal component of anchorage forces.

Park derived an equation to estimate the post-failure load carrying capacity of a uniformly loaded rectangular reinforced slab fully restrained at its edges (Park, 1964). To develop his equation, he assumed that the reinforcing bars are totally in the plastic phase and the concrete has cracked throughout its depth and carries no load. Desayi and Kulkarni (1977) showed that this approach can also be used with some modification for simply supported slabs. Hawkins and Mitchell (1979) developed a simplified iterative method to determine the tensile membrane action of panels having vertical and horizontal restraint at their edges. Assuming that membrane takes a circular deformed shape and concrete carries no tension, the proposed model provides a complete response up to the rupture of the reinforcement.

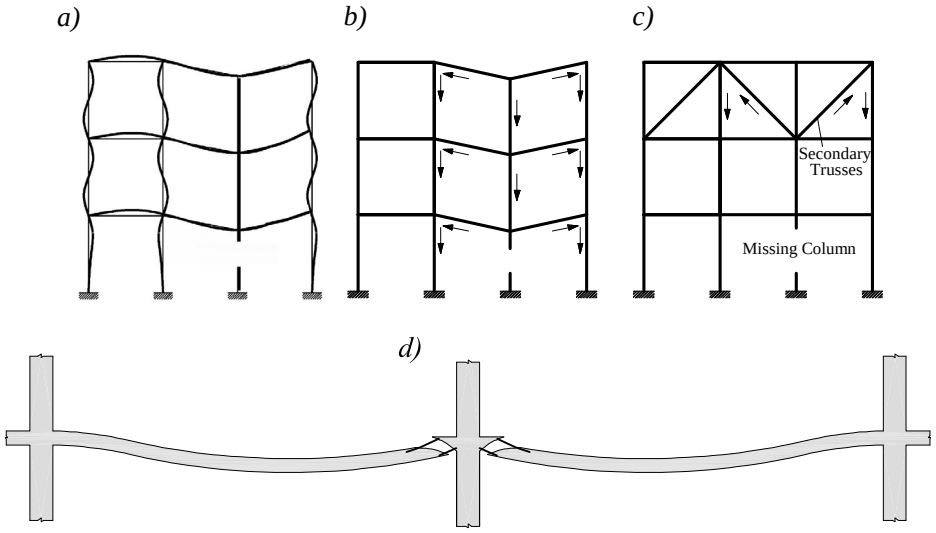

Figure 2.3: Post-failure load-carrying mechanisms in concrete structures: a) Vierendeel action, b) catenary action, c) secondary trussess, and d) membrane action in reinforced concrete slabs (Ellingwood et al., 2007)

With reference to flat slabs, the compressive membrane action can be developed if the provisions proposed by codes and guidelines are satisfied. The tensile membrane action seems less likely as punching of the slab at column connections determine the failure behavior (Regan, 1979, 1986). The development of the tensile membrane action in flat slabs can be very problematic. The large deformations accompanying this phenomenon are likely to damage the compressive zone around the columns and thus to reduce their capacity. Therefore, the presence of integrity reinforcement is essential for an appropriate post-punching behavior (Georgopoulos, 1986; Hawkins and Mitchell, 1979; Melo and Regan, 1998). Mitchell and Cook (1984) reported that well-anchored and effectively continuous integrity reinforcing bars are capable of suspending the damaged slab from the columns.

2.2 Post-failure shear transfer mechanism of flat slabs

Shear resistance in concrete structures is provided by the shear transfer through the compression zone of concrete, the aggregate interaction of the rough faces of cracks, the shear reinforcement, and the longitudinal reinforcement crossing the cracks. As the load increases, cracks open and the aggregate interlocking reduces quickly. Therefore, in the absence of shear reinforcement, longitudinal reinforcing bars play a significant role in transferring shear as other contributions to the shear transfer are fairly small. This is in particular the case when a punching failure occurs. Figure 2.4 shows major mechanisms affecting the stress transfer across a punching crack in a slab-column connection without shear reinforcement. As the only link between the punching cone and the rest of the slab is the longitudinal reinforcement, the contribution of the aggregate interlocking and the compression zone of the concrete can be ignored. The load is thus entirely transferred by the longitudinal reinforcement. The contribution of the longitudinal reinforcement to the shear transfer is the combination of the influence of tensile reinforcement and integrity reinforcement passing through the column.

The contribution of tensile reinforcement to the post-punching strength is small as a result of the spalling of the concrete cover. The main contribution to the post-punching shear transfer is provided by the integrity reinforcement. (Hawkins and Mitchell, 1979; Georgopoulos, 1986; Melo and Regan, 1998). In addition, the likelihood that a local punching failure leads to a progressive collapse can be reduced (Marjanishvili, 2004; Shankar Nair, 2006).

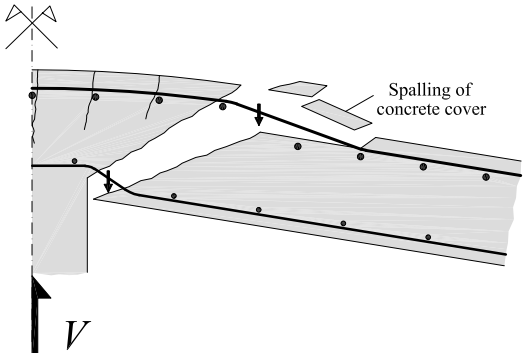

Figure 2.4: Shear transfer through longitudinal reinforcement

2.2.1 Past research on the post-punching behavior

The prediction of the punching strength as well as the development of reliable design rules with an acceptable level of safety have been the main objective of the research on punching shear (Elstner and Hognestad, 1957; Kinnunen and Nylander, 1960; Moe, 1961). However, the behavior of flat slabs after a local punching failure and circumstances in which it can lead to a progressive collapse have not yet been thoroughly studied. Consequently, the literature of post-punching behavior is very limited. Regan investigated the effect of integrity reinforcement on the post-punching behavior (Regan *et al.*, 1979). The tested slabs were 100 mm thick with an effective depth of 79 mm. The column width was 200 mm and the reinforcement ratio was 0.8 %. Due to the presence of three 8 mm integrity reinforcing bars in each direction, the post-

punching strength of the slab reached 71% of the punching strength. Fig 2.5 shows that the specimen comprised of the integrity reinforcement provided an enhanced post-punching strength in relation to the one comprised of only tensile reinforcement.

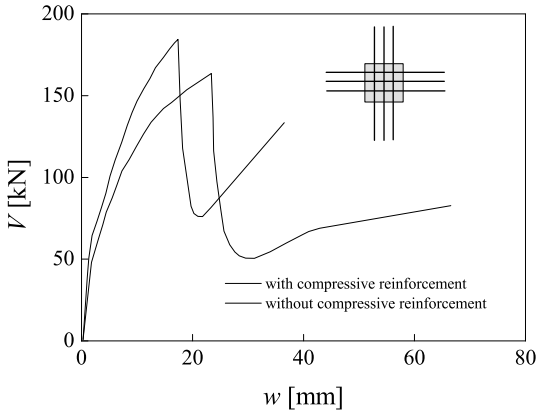

Figure 2.5: Post-punching behavior of specimens tested by Regan (Regan et al., 1979)

On the basis of limited experimental evidence, Regan concluded that the presence of integrity reinforcement is fundamental to enhance the post-punching strength. He observed that the specimens without integrity reinforcement could reach 25% of the punching strength. Therefore, the rest 75% of the punching shear strength should be transferred through the integrity reinforcement. To estimate the post-punching strength of the integrity reinforcement, the following equation was proposed based on Rasmussen's dowel equation (Rasmussen, 1962):

$$V_{pp} = 1.3 \sum Ø^2 \sqrt{f_{sy} f_c} \tag{2.1}$$

where V_{pp} is the post-punching strength, Ø is the bar diameter, f_{sy} is the yielding strength of the reinforcement, and f_c is the concrete compressive strength.

McPeake (1980)performed experiments on thin slabs to investigate the influence of integrity reinforcement on the post-punching behavior of flat slabs. In addition, he investigated the influence of the area of concrete outside the punching cone on the punching strength. It was observed that the area of the concrete outside the line of contraflexture enhanced the punching strength due to the development of compressive membrane action. Moreover, it was observed that considerable advantages can be gained with respect to post-punching capacity from the inclusion of integrity reinforcement. It was also concluded that due to the large deflections encountered in the later stages of the loading, the shear transfer mechanism is the membrane action rather than the dowel action.

Georgopoulos (1986) carried out an analytical and experimental study on the behavior of flat slabs after a local failure. This study was the base of the design formula given by the Swiss Code SIA 262 (2003). He proposed a method to calculate the punching strength as a function of the concrete tensile strength, the punching crack zone, and the compression stress in the vicinity of the column. In addition, he tested a half-scale circular slab with a diameter of 1400 mm including two integrity bars passing through the column in each direction. The effective depth was 109 mm and the column width was 226 mm. The concrete compressive strength was 39.6 MPa and the yielding

strength of the steel reinforcement was 530 MPa. Figure 2.6 shows the reinforcement layout as well as the load versus the central deflection of the slab. The test continued up to failure and the post-punching response was recorded. A promising post-punching behavior was obtained, which was due to the presence of the integrity reinforcement. Furthermore, he observed that the angle of inclination of the integrity reinforcing bars at failure in the vicinity of the column varied from 20 to 22°. Based on his experimental results, using Rasmussen's dowel equation (Rasmussen, 1962), and considering the dowel action as the determinant mechanism, he developed the following equation to estimate the angle of inclination of the reinforcing bars at failure:

$$\sin\psi_u = 1.5\sqrt{\frac{f_{cc}}{f_{sy}}} \tag{2.2}$$

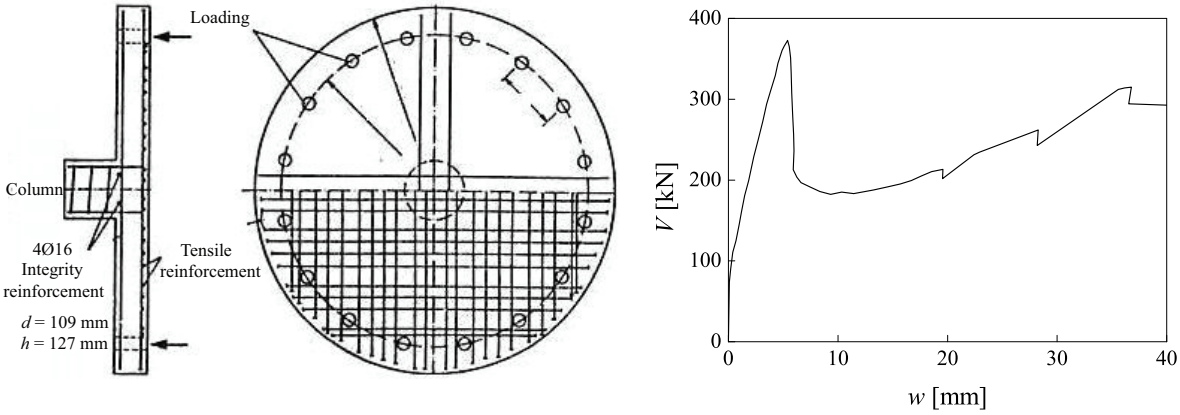

Figure 2.6: Reinforcement layout and structural response of specimen tested by Georgopoulos (1986)

A questionable feature of this approach is the use of the dowel action as the major shear transfer mechanism. Rasmussen's equation was based on the shear behavior of a bar without axial steel stress while integrity reinforcing bars are almost acting at their yield stress. In other words, the approach proposed by Georgopoulos based on Rasmussen's dowel equation seems rather unrealistic in terms of physical modeling. The proposed mechanism does not account for the presence of axial stresses, which significantly affects the post-punching strength of the integrity reinforcement.

Mitchell and Cook (1984) studied the possibility of the development of membrane action in various types of concrete slabs following a local failure. They stated that "the key in preventing progressive collapse may be to design and detail slabs such that they are able to develop secondary load carrying mechanisms after initial failures have occurred". They concluded that tensile membrane action developed by well-anchored reinforcing bars is capable of suspending damaged portions of the structure from the columns. They proposed the following design expression for the integrity reinforcement:

$$A_{sb} = \frac{2q_d \ell_n \ell_2}{\Phi f_{sy}} \tag{2.3}$$

where q_d is the factored uniformly distributed load but not less than twice the slab service dead load, $\Phi = 0.9$ is a shear reduction factor, ℓ_n is the clear span, in the direction being considered, measured face-to-face of supports, and ℓ_2 is the center-to-center span in the direction of the catenary.

Melo and Regan carried out an extensive experimental campaign to investigate the post-punching behavior of reinforced concrete flat slabs (Melo, 1990; Melo and Regan, 1998). Three series of tests were conducted. At the first series, eight quarter scale slab were tested to study the general post-punching behavior. The specimens were 2.5 m square slabs and 75 mm thick with 150 mm square columns at the center of the slabs. The supports were at the column and around the edges of the slab. The loading was applied at 16 points on the slab to simulate a uniformly distributed loading. All of the slabs had the same tensile reinforcement designed according to the minimum requirements of the British Standard (BS 8110, 1989). All the reinforcing bars had a bar diameter of 6 mm.

Slabs 2, 3, and 4 included hot-rolled steel with a yield strength of 759 MPa. Slabs 1, 5, 6, and 7 included hot-rolled steel with a yield strength of 655 MPa. In addition, Slabs 6 and 7 included shear reinforcement. The shear reinforcement consisted of two legs of stirrups made of cold-worked 3 mm soft iron wire with 273 MPa yield strength. The longitudinal reinforcement ratio was 0.75% and the concrete cover was 10 mm for all of the specimens. Figure 2.7 shows the reinforcement layouts as well as the load-deflection responses for the slab specimens. Table 2.1 summarizes the test data and the main test results. It was observed that at the pre-punching phase, there was no significant difference between the slabs with and without integrity reinforcement. However, at the post-punching phase, the slabs containing integrity reinforcement carried much higher loads and did so with smaller deflections. Moreover, it was observed that the failure of the slabs with integrity reinforcement was governed by concrete destruction rather than the fracture of the reinforcing bars.

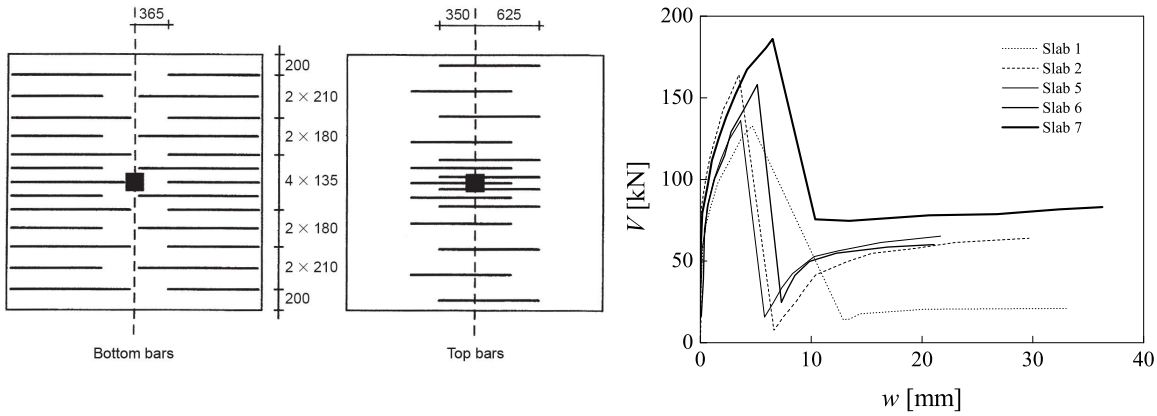

Figure 2.7: Reinforcement layout and response of slabs tested by Melo to study general post-punching behavior (Melo and Regan, 1998)

Melo observed that the original punching loads are relatively high in relation to those predicted by the British Standard. Thus, he stated that "this is probably due primarily to compressive membrane action arising from the considerable area of slab surrounding the failure zone, but may also be partly due to conservatism in the code's depth factor of $(400/d)^{0.25}$ when applied to very shallow slabs".

Table 2.1: Summary of tests to study general post-punching behavior (Melo and Regan, 1998)

Test	d	Tensile reinforcement			Integrity reinforcement					Main results		
		Ø	f_{sy}	f_{su}	A_{sb}	f_{sy}	f_{su}	f_c	f_{ct}	V_p	V_{pp}	w_{pp}
	[mm]	[mm]	[MPa]	[MPa]		[MPa]	[MPa]	[MPa]	[MPa]	[kN]	[kN]	[mm]
1	59	6	655	801	-	-	-	37	3.4	133	21	60
1/1	59	6	655	801	-	-	-	43.1	2.8	160	31	44
2	59	6	759	934	4Ø6	759	934	34.1	3.2	142	64	35
3	59	6	759	934	6Ø6	759	934	42.6	3.5	153	81	21
4	59	6	759	934	4Ø8	529	647	38.3	3.1	148	66	25
5	59	6	655	801	4Ø8	529	647	36	3.1	136	65	38
6	59	6	655	801	-	-	-	37.2	3.1	158	60	38
7	59	6	655	801	4Ø8	529	647	52.1	3.1	186	83	35

To propose a design formula, it was concluded that the post-punching strength is either limited by the destruction of the concrete in the vicinity of the column or by the fracture of the reinforcing bars. For the former case the post-punching strength can be estimated by

$$V_{pp} = 0.33(2n)\sqrt{f_c}\,(\pi d_1^2 / 2) \tag{2.4}$$

where n is the number of the integrity reinforcing bars and d_1 is the depth of the concrete over the integrity reinforcement. For each of two reinforcing bars if $s < 2d_1$

$$V_{pp} = 0.33(2n)\sqrt{f_c}\,(\pi d_1^2 / 2 - A_1) \tag{2.5}$$

$$A_1 = \frac{\theta_j}{360}\pi d_1^2 - \frac{s}{4} d_1 \sin\theta_j$$

where s is the bar spacing and $\theta_j = \cos^{-1}(s / 2d_1)$.

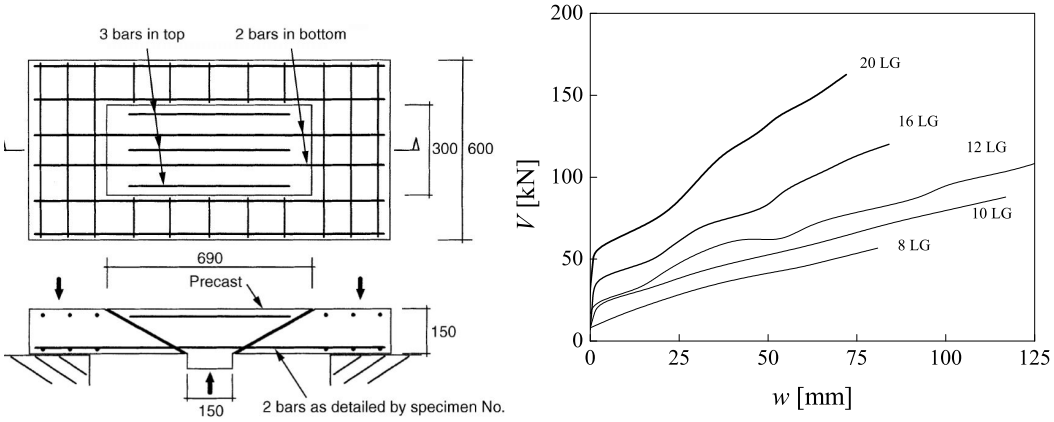

Figure 2.8: Reinforcement layout and response of slabs with discontinuous tensile reinforcement tested by Melo (Melo and Regan, 1998)

As pointed out previously, the failure of the tested slabs occurred by the destruction of concrete rather than the fracture of the integrity bars. Thus, the second test series was carried out to investigate the limit of the post-punching strength associated to the fracture of the integrity reinforcement. The second series consisted of twelve specimens each containing two integrity reinforcing bars. As Figure 2.8 shows, each slab consisted of two parts cast separately and connected by the reinforcing bars: the central part

representing the internal punching cone and the outer part representing the rest of the slab. Table 2.2 presents material properties, anchorage types, types of failure and the ultimate strength of the specimens. Index *cone* refers to the internal punching cone and *slab* refers to the outer part of the slab.

Table 2.2: Summary of specimens with discontinuous tensile reinforcement tested by Melo (Melo and Regan, 1998)

Test	*Type*	A_{sb}	f_{sy} [MPa]	f_c [MPa]	ε_{su} [%]	$f_{c,cone}$ [MPa]	$f_{c,slab}$ [MPa]	$f_{ct,cone}$ [MPa]	$f_{ct,slab}$ [MPa]	Bar fracture	Cone crushing	V_{Du} [kN]
6ST	SHORT	2 Ø 6	655	801	12.9	41.1	30.1	-	-	YES	NO	41
6LG	LONG	2 Ø 6	655	801	12.9	49.2	41.4	-	3.47	YES	NO	41
8ST	SHORT	2 Ø 8	529	647	19.6	41.4	30.1	3.47	-	YES	NO	57
8LG	LONG	2 Ø 8	529	647	19.6	42.6	41.4	-	3.47	YES	NO	57
10ST	SHORT	2 Ø 10	497	620	21.4	28.9	33.4	-	3.06	YES	NO	82
10LG	LONG	2 Ø 10	497	620	21.4	36.9	38.3	-	3.23	YES	NO	90
12ST	SHORT	2 Ø 12	524	649	19.8	25.0	34.3	2.91	3.42	NO	Part	70
12LG	LONG	2 Ø 12	524	649	19.8	30.6	36.9	3.24	-	Yes	Part	123
16ST	SHORT	2 Ø 16	483	599	23.5	41.0	33.4	-	3.45	NO	Part	65
16LG	LONG	2 Ø 16	483	599	23.5	34.6	32.5	3.86	-	NO	Yes	148
20ST	SHORT	2 Ø 20	492	626	24.3	35.4	28.2	3.99	3.06	NO	Part	78
20LG	LONG	2 Ø 20	492	626	24.3	27.3	40.1	-	3.44	NO	Yes	168

Melo observed that the specimens with larger bars and short anchorage length (12ST, 16ST and 20ST) experienced anchorage problems before reaching the ultimate load. However, the other specimens reached the ultimate load without anchorage problems. The failure mode was either crushing of the concrete in the internal punching cone (16LG, 20LG) or by rupture of the reinforcing bars (12LG) as shown in Figure 2.8.

The third series was made to study the fracture of the larger bars and to investigate the possible failure of the column concrete. The test setup shown in Figure 2.9 included a central column with 300 mm square in cross-section and reinforced with eight longitudinal bars. Two reinforcing bars in each direction represented the integrity reinforcement and projected 1.35 m to either side. The outer 850 mm of the bars were encased in cast-in-place concrete on top of large precast concrete blocks. A hydraulic jack under the column was used to apply upward loading. It was observed that the concrete cover at the corners of the column spalled without causing failure. The failure occurred by the fracture of the reinforcing bars at the bends where they entered into the column. It was concluded that failure of the concrete in columns is unlikely to be a problem as long as the integrity reinforcement pass through the cage of the column reinforcement.

In addition, he reported that the angle of inclination of the reinforcing bars at failure in the vicinity of the column face varied from 24° to 26° for the second series and from 22° to 26° for the third series. Finally, the following equation was proposed based on the experimental results for the failure mode associated with the fracture of the reinforcing bars:

$$V_{pp} = \frac{A_{sb} f_{sy}}{2} \tag{2.6}$$

where A_{sb} is the total cross-sectional area of the integrity reinforcement.

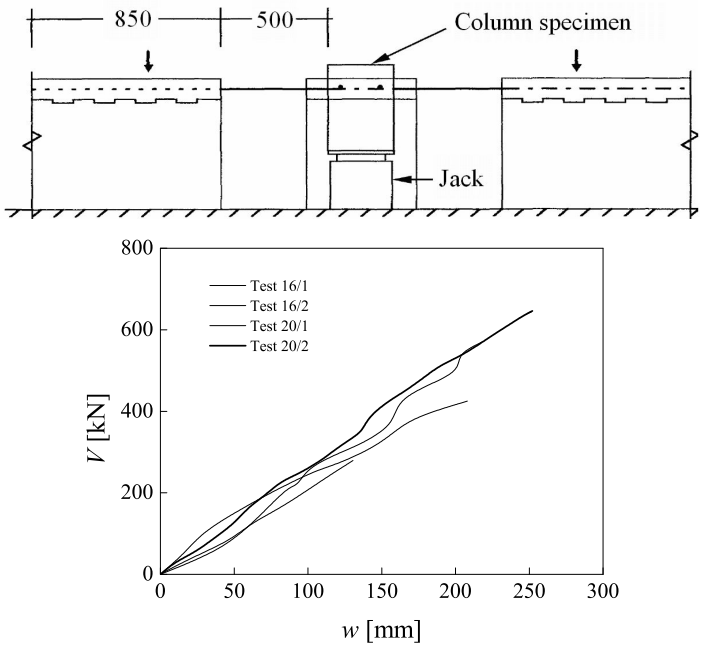

Figure 2.9: Test setup and response of specimens to study reinforcing bars-column interaction tested by Melo (Melo and Regan, 1998)

Broms conducted an experimental work to investigate reinforcement layouts that can provide a ductile behavior of flat slabs as well as sufficient safety against progressive collapse. He tested various reinforcement layouts consisting of flexural reinforcement in combination with shear reinforcement and bent-up bars. It was observed that using only stirrups or so-called stud rails can not provide a ductile behavior because punching failure could occur due to a steep crack around the column leaving such shear reinforcement ineffective. Finally, he concluded that the combination of shear reinforcement with bent-up bars turned out to be very effective in giving the slab the desired ductile behavior without tendency for punching shear failure. Figure 2.10 shows the proposed *ductility reinforcement* that is a combination of flexural reinforcement, stirrups and bent-up bars. Despite the fact that he stated that "all reinforcement bars are placed in a non-interlocking manner with each other", the proposed ductility reinforcement, however, seems to provide difficulties in practice (Broms, 2000, 2006).

With reference to prestressed concrete slabs, researchers (Ritz *et al.*, 1975; Pralong *et al.*, 1979; Freyermuth, 1989) have shown that a high post-punching strength can be achieved by prestressed slabs. Ramos and Lúcio (2008) have recently carried out experimental investigation to study the post-punching behavior of prestressed concrete flat slabs. Six half-scale prestressed concrete slabs were tested and their post-punching behavior was recorded. Figure 2.11 shows the load-deflection response for a tested slab (AR11). It shows that the inclusion of prestressed tendons passing through the column can be highly effective in increasing the post-punching strength and deformation capacity of flat slabs.

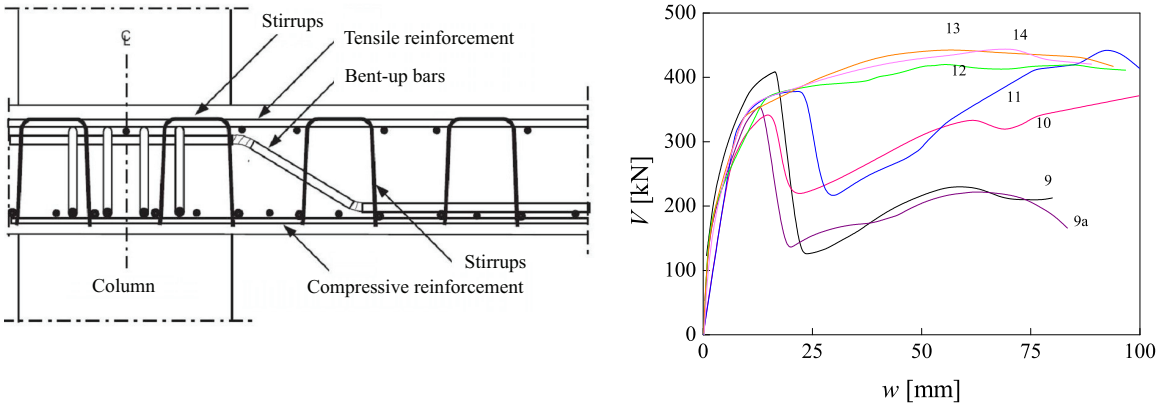

Figure 2.10: Detailing of ductility reinforcement and test results (Broms, 2000)

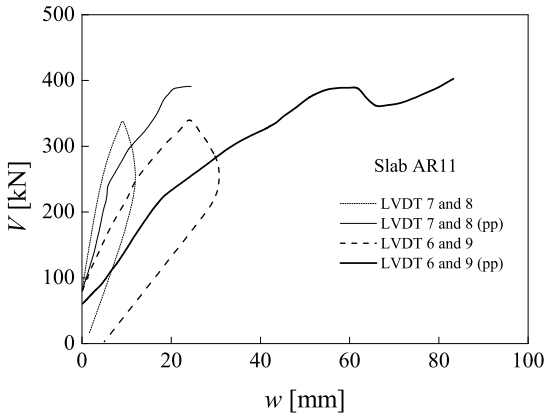

Figure 2.11: Load-deflection response of a prestressed slab: measurement at four different locations (Ramos and Lúcio, 2008)

2.3 Dowel action

Cracks and interfaces in concrete structures significant reduce stiffness and strength. Such interfaces are very common in reinforced concrete structures, e.g. flexural-shear cracks in slabs or beams, construction joints in pavements, interfaces between old and new concrete, interfaces within precast elements connections and so on. The behavior of reinforced concrete structures can be significantly influenced by the behavior of interfaces at critical regions (Marcus, 1951; Krefeld, 1966; Jimenez *et al.*, 1979; Millard and Johnson, 1984; Vintzeleou, 1986; Dei Poli *et al.*, 1993). Figure 2.12 shows major mechanisms affecting the transfer of stresses across cracks in reinforced concrete structures with shear reinforcement.

Although flexural strength of reinforced concrete elements can be well estimated, a precise shear analysis is very complicated due to the complexity of the shear transfer mechanism. The contribution of the compression zone, the aggregate interlocking, and the shear reinforcement to the shear transfer are thoroughly investigated. However, the dowel action of the longitudinal reinforcement has received far less attention.

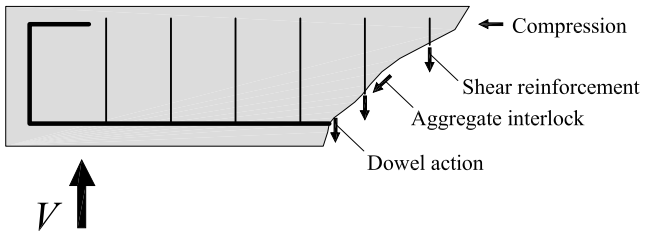

Figure 2.12: Shear transfer mechanisms across a cracks

2.3.1 The mechanism of dowel action

The mechanism of the dowel action is based on the response of the reinforcing bar and the concrete supporting the bar to a lateral bar displacement. Two main modes of failure for dowel action have been proposed by researchers (Vintzeleou and Tassios, 1986; Dei Poli *et al.*, 1992; Jeli *et al.*, 1999):

1. Yielding of the bar and crushing of the concrete supporting the bar simultaneously (failure mode I)
2. Splitting or spalling of concrete (failure mode II).

The concrete thickness is the main parameter upon which the mode of failure depends (Utescher and Hermann, 1983). In fact, experimental results have shown that if the concrete thickness is larger than six to seven times the bar diameter, the former mode of failure is determinant (Soroushian *et al.*, 1986; Dei Poli *et al.*, 1992). The latter mode of failure occurs for smaller concrete thickness. Failure mode II generally occurs in the case of bottom bars in reinforced concrete beams. In addition, it occurs in the post-punching behavior of concrete slab-column connection. With reference to failure mode I, shown in Figure 2.13, three mechanisms can be distinguished according to Paulay, Park, and Philips (Paulay *et al.*, 1974):

1. Bending: the load is transmitted due to bending of the bar and the capacity is limited by the formation of plastic hinges in the bar.
2. Pure shear: the contribution of pure shear to the shear transfer is unlikely due to the concrete deterioration at the vicinity of the bar. In addition, resulting forces at both sides of the crack includes a relatively large eccentricity that leads to yielding of the bar due to bending.
3. Kinking: in the case of large crack openings, the axial bar force has a component parallel to the crack plane. In general, the crack width is relatively small in relation to the bar diameter and the effect of kinking is thus insignificant.

Jelic *et al.*, (1999) stated that "…as the bar size is increased, flexure, rather than kinking or shear, should be the principal mechanism of dowel action because it is proportional to $Ø^3$ ($Ø \cdot A_b$), while kinking and shear are only proportional to $Ø^2$ ($Ø \cdot A_b$), where Ø is the bar diameter".

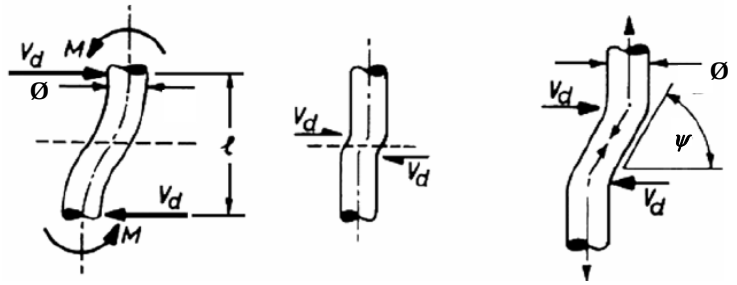

Figure 2.13: Shear transfer mechanisms by dowel action (Paulay et al., 1974)

2.3.2 Dowel action investigations

A large number of experiments have been carried out in the past to investigate the behavior of dowel action. Figure 2.14 shows various test setups that have been used to study the dowel action. Three test configurations were conventionally grouped according to the type of specimens used, namely *direct dowel test*, *divided beam test*, and *beam-end test*. The direct dowel test has been employed by numerous researchers (Mattock, 1969; Mattock, 1974; Eleiott, 1974; Dulacska, 1972; Soroushian *et al.*, 1986; Dei Poli *et al.*, 1992). This configuration allowed researchers to study the influence of the variation of the angle of inclination of the bar on the shear strength of the dowel bars. The divided beam test has been used by other researchers (Taylor, 1961; Krefeld and Thurston, 1966; Baumann, 1968). Houde and Mirza (1974) implemented the beam-end test to investigate the interaction between bond and dowel action.

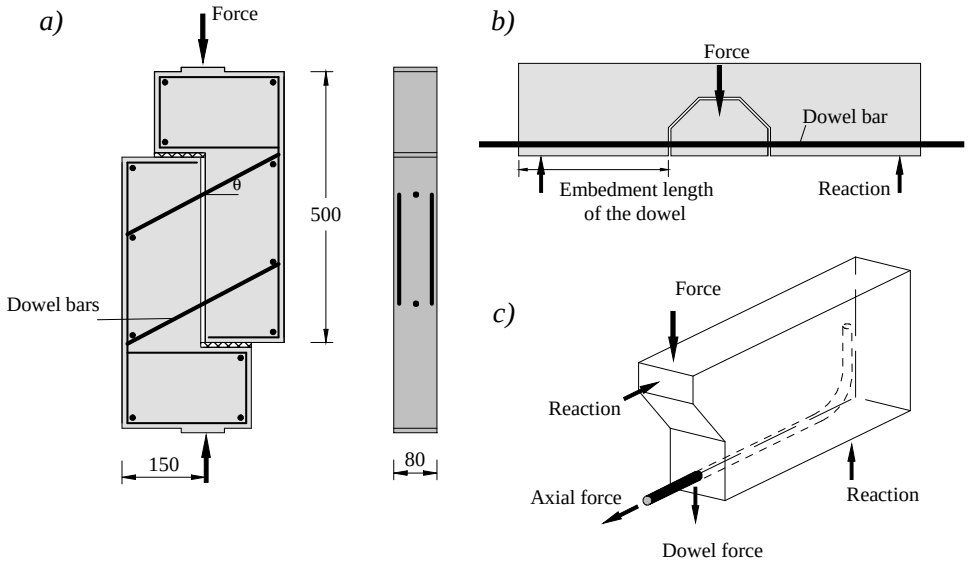

Figure 2.14: Dowel-action test setups: a) direct dowel test, b) divided beam test specimen, and c) beam-end test specimen

The first dowel action tests focused on joints in concrete pavements based on a silt loam subgrade. Teller and Sutherland (1936) showed that the efficiency of a dowel bar depends on the joint width, the slab thickness, the bar spacing, and the applied load with respect to the location of the dowels. Furthermore, a direct relationship between the slab deflection and the magnitude of the load on the slab was observed.

As stated earlier, there are two main failure modes of dowel action: concrete crushing and yielding of the bar simultaneously and spalling of concrete. For the prediction of the dowel strength in the former mode, several theoretical and empirical equations have been proposed. However, for the latter mode of failure, mostly empirical equations are available.

2.3.2.1 Failure mode I

Rasmussen (1962) performed an experimental work to explore the ultimate load carried by dowel bars. Figure 2.15 shows his experimental results. He observed that the failure mode was the formation of the plastic hinges in the dowel bar accompanied by large concrete crushing under the bar. Based on his experimental results the following equation was proposed to estimate the ultimate dowel strength:

$$V_{Du} = B\varnothing^2\sqrt{f_c\ f_{sy}} \tag{2.7}$$

where $B = C(\sqrt{1+(\zeta C)^2} - \zeta C)$

$$\zeta = 3\frac{e}{\varnothing}\sqrt{\frac{f_c}{f_{sy}}}$$

e = eccentricity of the load (see Figure 2.17)

It was found experimentally that C was 1.3 if there was no load eccentricity.

Mills (1975) performed three dowel tests with an angle of inclination of 45°. For a bar with a diameter of 38 mm, f_c = 36 MPa and f_{sy} = 210 MPa, an average of 76 kN for the dowel strength was obtained.

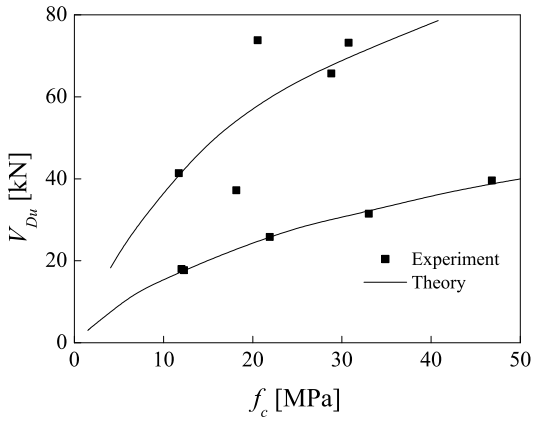

Figure 2.15: Rasmussen's experimental and theoretical results (Rasmussen, 1962)

Utescher and Herrmann (1983) conducted a large number of dowel tests to explore the influence of the bar diameter and the load eccentricity on the ultimate strength of dowel

bars. The variation of the load eccentricity was achieved by applying the load at distances of 5, 10, 20, and 50 mm from the concrete surface. It was observed that the ultimate dowel force was significantly reduced by the load eccentricity.

Reinforcing bars do not always cross cracks perpendicularly. Therefore, Dulacska (1972) studied the effect of the angle of inclination of the dowel bars on the ultimate strength. The specimen used was of a "push-off" type and the aggregate interlock was eliminated by placing two thin lubricated brass sheets at the shear plane. Figure 2.16 shows the experimental results obtained.

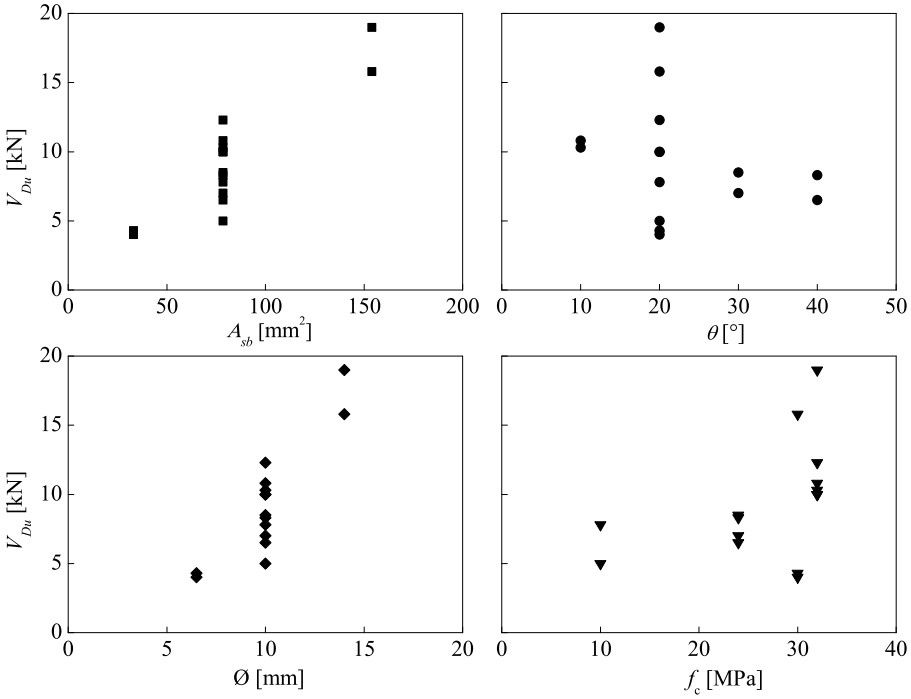

Figure 2.16: Experimental results of Dulacska (1972)

She proposed the following empirical relationship for the estimation of the dowel strength as a function of the angle of inclination of the bar:

$$V_{Du} = 0.2\text{Ø}^2 f_{sy}\eta_s \sin\theta\left(\sqrt{1+\frac{f_{cc}}{0.03\eta_s f_{sy}\sin^2\theta}}-1\right) \qquad (2.8)$$

where η_s =1-(σ_N / f_{sy})^2, σ_N is the axial tensile stress in the bar and f_{cc} is the concrete cube compressive strength. Plotting Equation 2.8 as a function of V_D and σ_N gives an elliptical interaction diagram. It has been reported that if the concrete cover is sufficiently large to prevent the concrete spalling and splitting, failure mode I occurs, and on the contrary for relatively thin concrete covers failure mode II occurs (Vintzeleou and Tassios, 1986; Jeli *et al.*, 1999).

Vintzeleou and Tassios (1986) carried out an analytical approach to predict the ultimate dowel strength for both modes of failure. The theoretical approach was based on a failure criterion used by Broms (1964). Figure 2.17 shows Broms's failure mechanism for a pile embedded in a cohesive soil. It was suggested that the concrete bearing

strength reaches five times the concrete uniaxial compressive strength. Thus, the following expression was developed for the estimation of the dowel strength:

$$V_{Du}^2 + (10\, f_c\, e\varnothing)V_{Du} - \zeta_c \varnothing^4 f_c\ f_{sy} = 0 \tag{2.9}$$

where ζ_c is a factor (<1.3) depending on the available concrete cover of the bar in the direction of the shear force. For zero load eccentricity this expression becomes similar to Rasmussen's formula. Pruijssers (1988) stated that "experimental observations (Dulacska, 1972; Utescher and Hermann, 1983) showed a considerable spalling of the concrete close to the crack plane. Due to this spalling of concrete, Rasmussen's and Brom's descriptions were in closer agreement with the actual stress distribution than Vintzeleou's approach".

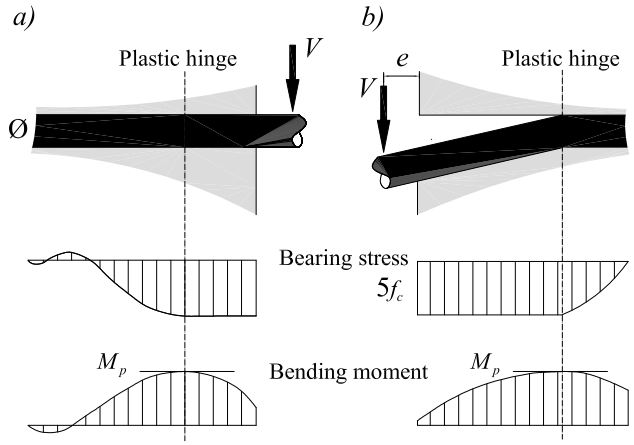

Figure 2.17: a) Failure mechanism of a free-headed pile in cohesive soil (Broms, 1964) and b) failure mechanism for a dowel bar in concrete (Vintzeleou and Tassios, 1986)

Soroushian *et al.* (1986,1987) conducted a series of test to investigate the behavior of dowel action acting against concrete core (failure mode I) and acting against concrete cover (failure mode II). Their test setup and some experimental results are shown in Figure 2.18. They employed the beam on an elastic foundation analogy to establish empirical equations for both modes of failure.

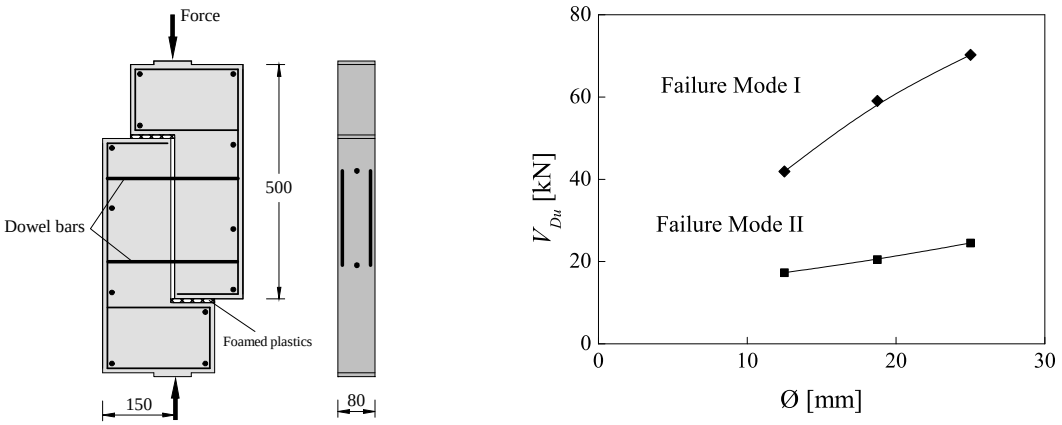

Figure 2.18: Test setup and results of experiments to study dowel bars acting against concrete core and concrete cover (Soroushian et al., 1987)

Millard and Johnson (1984) assumed that flexure rather than shear and kinking is the principal shear transfer mechanism. They employed the beam on elastic foundation theory and proposed the following load-displacement relationship:

$$V(\delta) = V_{Du}[1-\exp(-K_i\delta / V_{Du})]$$
$$V_{Du} = 1.3Ø^2\sqrt{\zeta_s f_c\ f_{sy}} \tag{2.10}$$
$$K_i = 0.166k_c^{0.75}Ø^{1.75}E_s^{0.25}$$

where K_i is the stiffness of the system in the elastic range.

Pruijssers (1988) derived an analytical expression to estimate the ultimate dowel strength. He considered the bond between the bar and the concrete supporting the bar as an axial compressive force with a certain eccentricity from the center of the bar. Therefore, the neutral axis of the bar was shifted due to the bond force and thus the plastic moment of the bar changed. He stated that the change in the plastic moment considerably affected the ultimate dowel strength. Assuming the eccentricity of the bond force equal to 0.465Ø the dowel strength can be calculated by

$$V_{Du} = 1.35Ø^2(\sqrt{1+9\zeta_j^{\ 2}} - 3\zeta_j)\sqrt{f_c\ f_{sy}}$$
$$\zeta_j = \frac{e}{Ø}\sqrt{\frac{f_c}{f_{sy}}} \tag{2.11}$$

Dei Poli, Di Prisco, and Gambarova (Dei Poli *et al.*, 1993) conducted a comprehensive experimental program to investigate the behavior of dowel action. They tested twenty seven specimens to gain further information on the load-displacement response, the curvature along the dowel bar, and the influence of the bar diameter, the concrete cover, and the stirrup position. All specimens were reinforced with a single dowel bar. The load eccentricity from the crack plane was zero (Figure 2.19). Main variables were the concrete cover (c = Ø, 2Ø), the bar diameter (Ø = 14, 18 and 24 mm), the distance of the first stirrup from the crack plane (t = Ø, 3Ø), the shear reinforcement ratio, the direction of the applied shear force (against concrete core or against concrete cover), the angle of the specimen forefront to the crack plane, the bar spacing, the concrete compressive strength (normal and high strength concrete), and the concrete type (normal and FRP).

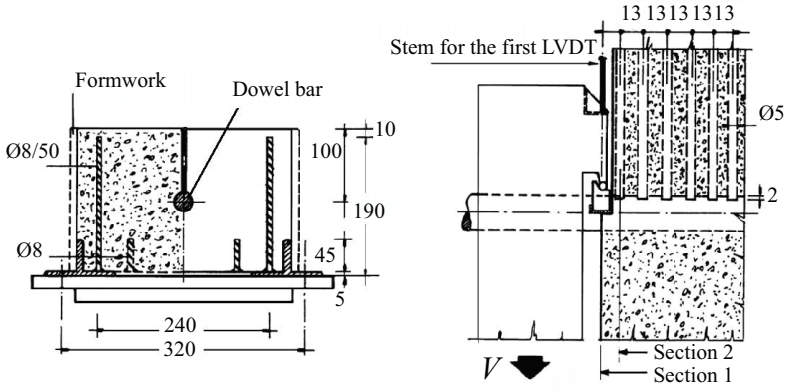

Figure 2.19: Test setup of experiments to study dowel action tested by (Dei Poli et al., 1993)

Test results showed that the behavior of the dowel bar and the concrete supporting the bar is elastic for loads less than 40% of the ultimate load. Therefore, to predict the dowel behavior in this region, they used the beam on elastic foundation analogy. However, this method can not describe the behavior of dowel action for higher loads due to the highly nonlinear behavior of the dowel action. Hence, they used a nonlinear bearing stiffness model to deal with the nonlinear behavior of the dowel action, which will be discussed later (Equation 2.17).

Ince *et al.* (2006) tested 54 push-off specimens to investigate size-dependent response of the dowel action. They employed the fracture mechanic theory and proposed the following equation:

$$V_{Du} = \rho b d \sqrt{f_c f_{sy} \sin\theta}\,(1+\sqrt{\frac{36.6}{d_g}})(1+\frac{d}{19.4 d_g})^{-1/2} \tag{2.12}$$

where d_g is the maximum aggregate size and b is the beam width. Test results showed that the nominal strength at failure decreases as the specimen size increases. In addition, the contribution of the dowel action to the shear capacity increases with the value of ρf_{sy}. Moreover, they stated that although the contribution of dowel action to shear transfer in codes and guidelines is either ignored or limited to 15 to 20%, in the case of beams without shear reinforcement, 50 to 70% of the shear capacity is transferred by dowel action.

Randl (2007) has recently performed an analytical and experimental study to investigate the dowel bars. Figure 2.20 illustrates his test setup and experimental results. His proposed analytical formula was based on the beam on elastic foundation analogy considering the yielding of the reinforcement and the crushing of the concrete simultaneously. He derived the following simplified equation for the range of interest in construction applications ($1.0 \le f_{sy} / f_b \le 10$ and $1.0 \le L_1 / Ø \le 2.5$):

$$V_{Du} = f_b \cdot Ø^2 \left[0.46\frac{L_1}{Ø} + 0.187\frac{f_{sy}}{f_b}\frac{Ø}{L_1} - 0.005\left(\frac{Ø}{L_1}\right)^3\left(\frac{f_{sy}}{f_b}\right)^2 \right] \tag{2.13}$$

where $L_1 = \left(4E_s I_b / k_c Ø\right)^{0.25}$ and f_b is the concrete bearing strength (Equation 2.15).

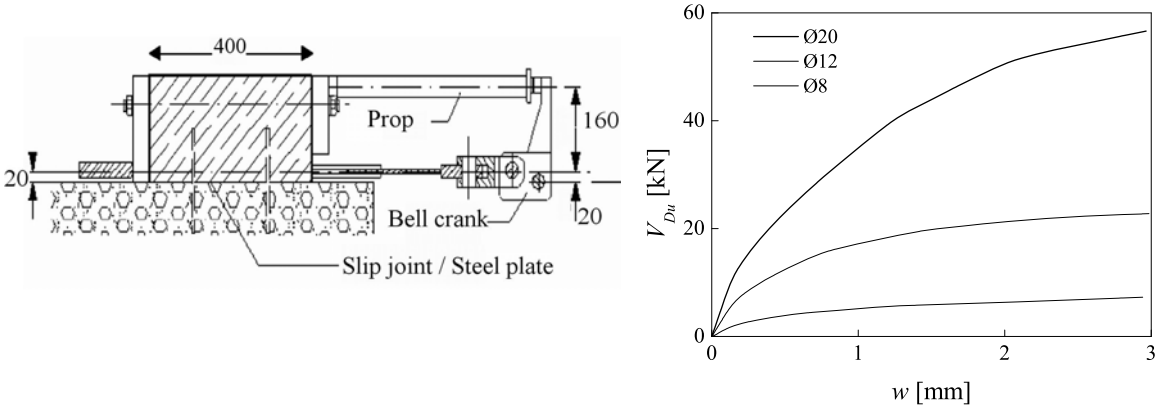

Figure 2.20: Test setup and response of specimens to study dowel action tested (Randl, 2007)

El-Ariss (2007) established an equation showing the relation between the ultimate dowel force and the crack width. He implemented the beam on elastic foundation theory into the experimental results (Dulacska, 1972; Millard and Johnson, 1984; Soroushian *et al.*, 1986). He concluded that the dowel action can significantly affect the ultimate strength and the deformation capacity of the reinforced concrete beams. Davids and Turkiyyah (1997) and He and Kwan (2001) employed finite element methods to investigate the contribution of the dowel action to the shear transfer. Chana (1987) and Reineck (1997) investigated the shear failure mechanism considering the dowel action. Sonnenberg and Al-Mahaidi (2007) investigated the dowel action in reinforced concrete beams using photogrammetry.

2.3.2.2 Failure mode II

Several expressions have been proposed to estimate the dowel strength when the failure mode II is determinant (Taylor, 1961; Krefeld and Thurston, 1966; Baumann, 1968; Houde and Mirza., 1974; Paschen and Schonhoff, 1983; Soroushian *et al.*, 1987). Most of these equations are associated to the dowel action in reinforce concrete beams where the longitudinal reinforcement acts against the concrete cover. It was generally concluded that the ultimate dowel strength in beams without shear reinforcement was limited to 25% of the maximum shear at failure. The ultimate dowel strength was independent from the embedment length and the bar diameter and was proportional to the beam width (Jimenez *et al.*, 1979). In addition, it was observed that the bond splitting was independent from the bar diameter if no shear reinforcement was involved. However, under the confining effect of the shear reinforcement, the bond splitting became dependent on the bar diameter. Moreover, when spalling of concrete cover or splitting of concrete is determinant, the maximum bending moment in the bar is significantly lower than its plastic moment. The experimental results showed that no significant reduction of the spalling or splitting strength occurred for the axial stress less than 80% of the yielding strength of the bar (Vintzeleou and Tassios, 1986).

2.3.3 Bearing strength and bearing stiffness of concrete

Numerous researchers reported that concrete stress under a reinforcing bar exceeds the uniaxial concrete compressive strength. The reason is that the surrounding concrete provides a considerable confining pressure resulting in a triaxial state of stress under the bar. Therefore, the concrete strength can reach several times the concrete uniaxial compressive strength (Dei Poli *et al.*, 1992). ACI 318 (2008) defines the bearing strength f_b as the ultimate stress under concentrated forces, and the bearing stiffness k (subgrade stiffness or foundation modulus) as the slope of the bearing stress-deflection diagram in the elastic region.

The dowel strength depends on the bearing strength and the bearing stiffness of concrete supporting the bar (Marcus, 1951; Jimenez *et al.*, 1979). However, values suggested in the literature are very scattered, ranging from 1.8 to 6.5 f_c and up to 20 f_c for the bearing strength and 200 N/mm^3 to 1250 N/mm^3 for the bearing stiffness (Dulacska, 1972; Soroushian *et al.*, 1987; Lieberum and Reinhardt, 1989; Dei Poli *et al.*, 1992). This dispersion does not allow a realistic evaluation of dowel response at ultimate limit state, in which both concrete and steel show very nonlinear behavior. Dei Poli *et al.* (1992) stated that “an explanation of this scattering is that the measured values for the bearing

strength depend on the actual confinement exerted on the concrete during the test and on the more or less premature splitting of the concrete under a highly localized force".

Vintzeleou and Tassios (1986) proposed an expression for the bearing stiffness assuming that the concrete supporting the bar is deformed by the dowel force up to a distance of two times the bar diameter. Assuming the linear elastic behavior, the bearing stiffness is given by

$$k_c = \frac{E_c}{2Ø} \tag{2.14}$$

Equation 2.14 seemed to be valid for dowel forces less than 50% of the ultimate dowel strength. For very low dowel forces, the deformation depth of the supporting concrete is less than two times the bar diameter and hence, the bearing stiffness is higher than that predicted by this equation. Millard and Johnson (1984) found experimentally the value of 750 N/mm^3 for the bearing stiffness for normal concrete. For high strength concrete, the bearing stiffness is proportional to the square root of the concrete compressive strength.

Soroushian *et al.* (1987) conducted an extensive experimental research to investigate the reasonable values for the bearing strength and the bearing stiffness. They explored the influence of the bar diameter, the concrete compressive strength, the width of the concrete block, the depth of the concrete block , the embedded length of the dowel bar, the number of the dowel bars, and the confinement of the concrete block on the bearing strength and the bearing stiffness. They obtained a bearing strength ranging form 1.2 to 3 f_c and a bearing stiffness between 54 to 163 N/mm^3. Test results showed that both the bearing strength and the bearing stiffness were increased by increasing the concrete compressive strength and by decreasing the bar diameter. Increasing the width of the concrete block or decreasing the embedded length of the dowel bar increased the bearing strength and had no influence on the bearing stiffness. The variation of the depth of the block had no effect on the bearing strength and stiffness. The increase of the number of the dowel bars had no effect on the bearing strength. However, it relatively decreased the bearing stiffness. The confinement provided by the embedded stirrups had favorable effects on the deformation capacity of the concrete under action. It had no influence on the bearing strength and stiffness.

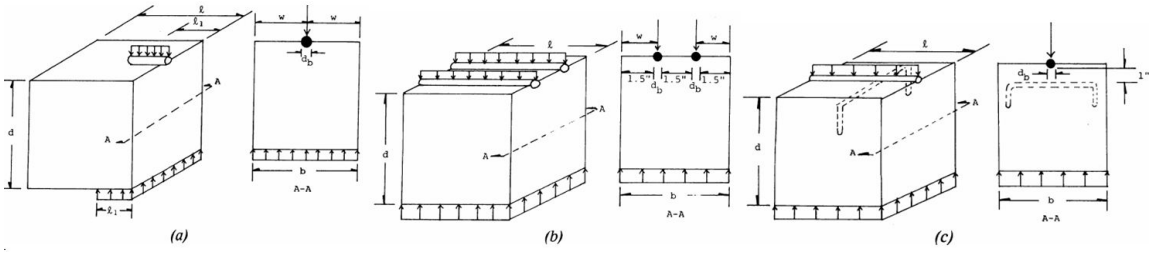

Figure 2.21: Test specimens: a) general geometry, b) multiple-bar specimen, and c) confined specimen (Soroushian et al., 1986)

On the basis of their experimental results, they proposed the following empirical formulas for predicting the bearing strength and stiffness of the concrete supporting the bars:

$$f_b = 37.6\sqrt{f_c} \,/\, \sqrt[3]{Ø} \quad \text{[MPa, mm]} \tag{2.15}$$

$$k_c = 127\zeta_1\sqrt{f_c} \,/\, Ø^{2/3} \quad \text{[MPa, mm]} \tag{2.16}$$

where ζ_1 is a coefficient ranging from 0.6 for a clear bar spacing of 25 mm to 1.0 for large bar spacing. Figure 2.21 shows the geometry of test specimens used in this experimental campaign. In addition, Dei Poli *et al.* (1992) investigated the bearing strength and stiffness of the concrete supporting the dowel bars. They attempt to overcome the nonlinear behavior of concrete supporting the bars by defining a nonlinear bearing stiffness of concrete. They observed that the bearing stiffness can be formulated as a function of "damage" accumulated in the concrete and in the dowel bar. This damage may be represented by means of a suitable "damage index" such as maximum normalized displacement ($w/Ø$) or the load level (V/V_{Du}). They proposed the following nonlinear bearing stiffness to predict the non linear behavior of the dowel action (see Figure 2.22):

$$k = \omega \cdot k_c \tag{2.17}$$

where

$k_c = 127\sqrt{f_c} \,/\, Ø^{2/3}$ [Soroushian *et al.*, 1986]

$$\omega = \begin{cases} 2.12 \quad \text{for} \quad V_D / V_{Du} < 0.4 \\ \{0.544 + .026\cosh[8(V_D / V_{Du} - 0.4)]\}^{-4/3} \quad \text{for} \quad V_D / V_{Du} > 0.4 \end{cases}$$

or

$$k = \omega^* k_c (V_D / V_{Du})$$

$$\omega^* = \begin{cases} 0.85 \quad \text{for} \quad V_D / V_{Du} < 0.4 \\ \{1.104 + .026\cosh[8(V_D / V_{Du} - 0.4)]\}^{-4/3} \quad \text{for} \quad V_D / V_{Du} > 0.4 \end{cases} \tag{2.18}$$

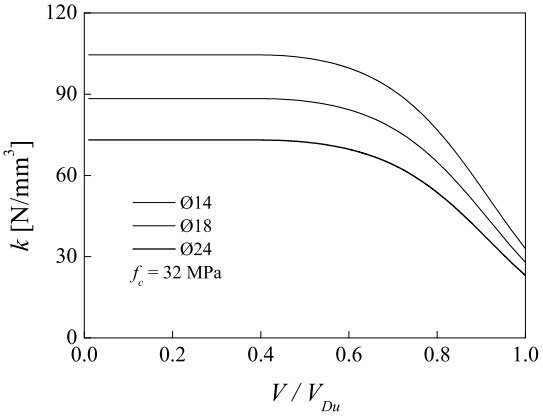

Figure 2.22: Evolution of bearing stiffness of concrete under a dowel bar (Dei Poli et al., 1992)

Brenna, Dei Poli, and Di Prisco (Brenna *et al.*, 1990) proposed the following nonlinear equations for the evolution of the bearing stiffness:

$$k = \omega^* \cdot k_0 \tag{2.19}$$

in which

$$k_0 = 600\, f_c^{0.7} / Ø$$

$$\omega^* = \left[1.5(a_1 + \sqrt{a_4^2(40\delta_e / Ø - a_2)^2 + a_3^2}\right]^{-4/3}$$

$$a_1 = 0.59 - 0.011\, f_c \qquad a_2 = 0.0075\, f_c - 0.23$$

$$a_3 = 0.0038\, f_c + 0.44 \qquad a_4 = 0.0025\, f_c + 0.58$$

where δ_e is the elastic displacement at the face of the crack.

2.4 Post-punching provisions in codes and guidelines

The following codes of practice provide explicit formulation for calculating the cross-sectional area of the integrity reinforcement over slab-column connections. Other codes and guidelines provide only some recommendations to mitigate the likelihood of the progressive collapse following a punching shear failure.

Swiss Code SIA 262-2003

To prevent the slab from totally collapsing after a possible punching, SIA 262 requires that some reinforcement shall be provided on the flexural compression side. The reinforcement shall be extended over the supported area and dimensioned as follows:

$$V_d = A_{sb} \cdot f_{sd} \cdot \sin\psi \tag{2.20}$$

Assuming $\psi = 42°$ leads to:

$$A_{sb} > 1.5 \frac{V_d}{f_{sd}} \tag{2.21}$$

where A_{sb} is the total cross-sectional area of the integrity reinforcement passing through the column, f_{sd} is the dimensioning yield strength of steel reinforcement, V_d is the dimensioning value of the shear transmitted to the column in accidental situation, and ψ is the angle of inclination of the reinforcing bars in the vicinity of the punching shear crack after failure as shown in Figure 2.23.

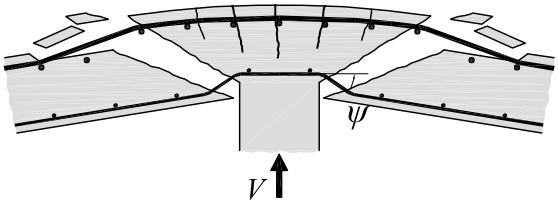

Figure 2.23: Punching failure over a slab-column connection

Canadian Code

The Canadian Code (CSA A23.3, 2004) requires that the summation of the area of integrity reinforcement connecting the slab, drop panel, or slab band to the column or column capital on all faces of the periphery of the column or column capital shall be

$$\sum A_{sb} > 2\frac{V_{se}}{f_{sy}} \tag{2.22}$$

where V_{se} is the shear force transmitted to the column due to specified loads. This reinforcement can be considered effectively continuous if one of the following conditions is satisfied: a) integrity reinforcement is lap spliced within a column or reaction area with the reinforcement in adjacent spans using a class A tension lap splice; b) integrity reinforcement is lap spliced outside of a column or reaction area using a minimum lap splice length of 2 ℓ_d where ℓ_d is the anchorage length of reinforcement; or finally c) at discontinuous edges, integrity reinforcement shall be bent, hooked, or otherwise anchored into the supports such that the yield stress can be developed at the face of the support. This code explains that integrity reinforcement provide a minimum degree of integrity, continuity and redundancy required to prevent flat slabs from totally collapsing due to a local punching failure.

German Code

The German Code (DIN 1045-1, 2005) requires that a particular attention is to be paid to the three-dimensional rigidity of structures and to their stability. If possible, forms of construction in which the failure of one component can lead to the collapse of a series of further components are to be avoided. If it is not clear from the outset that the rigidity and stability of a structure are ensured, evidence is to be produced, by calculation, of the stability of the horizontal and vertical stiffening or bracing components. DIN specifies the following formula to compute the area of the integrity reinforcement passing thorough the column and properly anchored in the slab to enhance the robustness of the structure against unforeseen circumstances:

$$A_{sb} = \frac{V_{Ed}}{f_{yk}} \tag{2.23}$$

where V_{Ed} is the design value of the punching force and f_{yk} is the characteristic value of the yielding strength.

United States Standards

ACI 318 (2008) has no explicit formula for post-punching behavior of concrete flat slabs. Although ACI 318 does not explicitly deal with the progressive collapse, ACI 352.1R (2002) provides recommendations to reduce the likelihood of this phenomenon. ACI 352 recommends that continuous integrity bars passing through the column cage in each principal direction at interior connections should have an area at least equal to

$$A_{sm} = \frac{0.5 q_d \ell_1 \ell_2}{\Phi f_y} \tag{2.24}$$

where A_{sm} is the minimum area of the integrity reinforcement in each principal direction placed over the column, q_d is the factored uniformly distributed load but not less than twice the slab service dead load, f_y is the yielding strength of steel, $\Phi = 0.9$ is a shear reduction factor, and ℓ_1 and ℓ_2 is center-to-center span in each principal direction. The quantity of reinforcement A_{sm} may be reduced to two thirds of that given quantity for edge connections, and to one-half of that for corner connections.

2.4.1 Estimation of the post-punching strength

Various formulas have been proposed by researchers and codes of practice to estimate the post-punching strength of slab-column connection. The predicted post-punching strength is mostly associated with the integrity reinforcement passing through the column. According to Georgopoulos (1986), the post-punching strength of a slab-column connection can be obtained by considering the integrity reinforcing bars as dowel bars embedded in the concrete. He proposed the following equation based on Rasmussen's dowel equation (Rasmussen, 1962):

$$V_{Georg.} = 1.3 \sum Ø^2 \sqrt{f_{sy} f_c} \tag{2.25}$$

Melo and Regan (1998) proposed the following equation based on their experimental results for the failure mode associated with the fracture of the reinforcing bars. The Canadian Code (CSA A23.3, 2004) introduces the same equation as Melo's for predicting the post-punching strength based on the research carried out by Mitchell and Cook (1984).

$$V_{CSA} = \frac{A_{sb} f_{sy}}{2} \tag{2.26}$$

ACI 352.1R (2002) requires the same amount of steel as the Canadian Code but with a shear reduction factor for the yielding strength:

$$V_{ACI} = \frac{A_{sb} \Phi f_{sy}}{2} \tag{2.27}$$

SIA 262 (2003) requires the following equation be satisfied in order to prevent the structure from totally collapsing following a punching failure:

$$V_{SIA} = \frac{A_{sb} f_{sy}}{1.5} \tag{2.28}$$

Table 2.3 presents a comparison of the experimental and the theoretical post-punching strength given by the current provisions.

The post-punching provisions in codes of practice can not account for many influencing parameters such as the ultimate tensile strain of reinforcement, the bar diameter, the effective depth of the slab, the concrete compressive strength, and the concrete cover. The prediction of the post-punching strength based on these provisions is often overestimated as shown in Table 2.3 and Figure 2.24. The reason is that some of the aforementioned parameters, which are not included in the codes of practice, reduce the post-punching strength. The contribution of the integrity reinforcement and the tensile reinforcement to the post-punching shear transfer will be separately calculated by the mechanical model presented in Chapter 4.

Table 2.3: Comparison of the post-punching strength predicted by codes of practice and Georgopoulos' proposition

Test	$V_{pp,test}$ [kN]	$V_{Georg.}$ [kN]	V_{CSA} [kN]	V_{ACI} [kN]	V_{SIA} [kN]	$\frac{V_{pp,test}}{V_{Georg.}}$	$\frac{V_{pp,test}}{V_{CSA}}$	$\frac{V_{pp,test}}{V_{ACI}}$	$\frac{V_{pp,test}}{V_{SIA}}$
PM-9	123	92	124	111	165	1.34	0.99	1.10	0.74
PM-10	159	137	176	158	235	1.16	0.90	1.00	0.68
PM-11	237	199	248	223	331	1.19	0.96	1.06	0.72
PM-12	245	266	325	292	433	0.92	0.76	0.84	0.57
PM-21	185	106	126	113	168	1.75	1.47	1.64	1.10
PM-22	219	162	190	171	253	1.35	1.15	1.28	0.86
PM-25[+]	85	106	126	113	168	-	-	-	-
PM-26[+]	105	162	190	171	253	-	-	-	-
PM-27[+]	94	225	253	228	337	-	-	-	-
PM-28[+]	101	311	356	320	475	-	-	-	-
Melo-2	64	54	86	77	114	1.19	0.75	0.83	0.56
Melo-3	81	120	172	155	229	0.67	0.47	0.52	0.35
Melo-4	70	101	153	137	203	0.65	0.43	0.48	0.32
Melo-5	65	82	106	96	142	0.79	0.61	0.68	0.46
Melo-6LG	32	26	37	33	49	1.22	0.86	0.96	0.65
Melo-6ST	33	31	37	33	49	1.07	0.89	0.99	0.67
Melo-8LG	57	42	53	48	71	1.36	1.07	1.19	0.80
Melo-8ST	57	49	53	48	71	1.16	1.07	1.19	0.80
Melo-10LG	90	67	78	70	104	1.31	1.13	1.25	0.85
Melo-10ST	82	72	78	70	104	1.13	1.04	1.15	0.78
Melo-12LG	123	100	119	107	158	1.12	0.94	1.05	0.71
Melo-12ST[†]	70	104	119	107	158	-	-	-	-
Georgopoulos	312	334	422	380	563	0.87	0.69	0.77	0.52
Broms-9	230	81	111	100	147	2.84	2.08	2.31	1.56
Broms-9a	222	72	111	100	147	3.10	2.01	2.23	1.51
					Ave.	1.31	1.01	1.13	0.76
					COV	0.48	0.42	0.42	0.42

+ : Test terminated due to the risk of falling down of the punching cone
† : Test experienced anchorage failure before reaching the ultimate strength

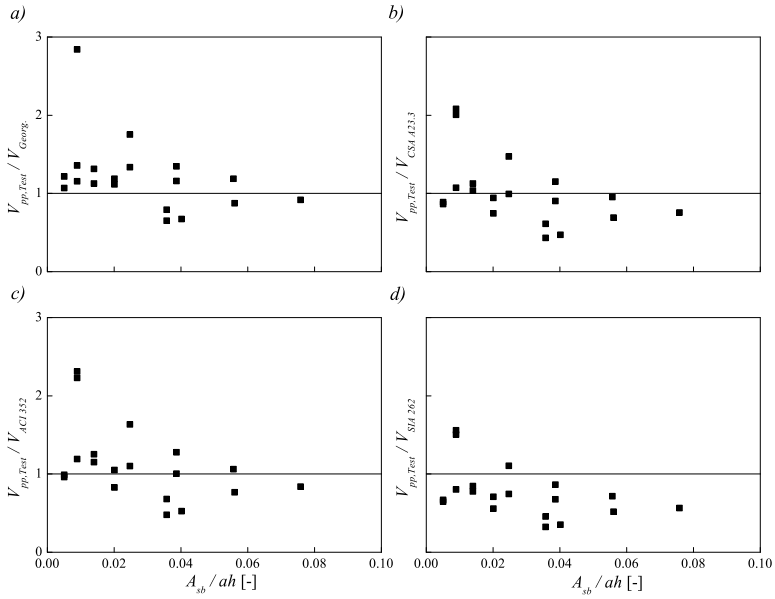

Figure 2.24: Comparison between measured and theoretical post-punching strength: a) model proposed by Georgopoulos, b) CSA A23.3, c) ACI 352.1R, and d) SIA 262

2.5 Progressive collapse of flat slabs

The response of a slab structure following an initial local failure is significantly influenced by parameters such as span, slenderness of the slab, reinforcement ratio, load level, deformation capacity, reinforcement layout, vertical support conditions, and horizontal restraint conditions. The response is dynamic and most likely inelastic. Thus, it is essential to use structural analysis programs that can consider geometric and material nonlinearity, imposed deformations to the slab, time variability of the response, strain-dependent behavior, and system damping. Such dynamic analysis is out of the scope of the present study. The following steps can be suggested for the progressive collapse analysis of flat slabs:

- The design of slab and flexural reinforcement according to codes of practice using ultimate limit state load combinations.
- The design of integrity reinforcement according to codes of practice using accidental load combinations.
- The calculation of the pre-punching behavior using the critical shear crack theory (Muttoni and Fernandez Ruiz, 2008), and the post-punching behavior using the developed mechanical model.
- The implementation of the results into a nonlinear finite element analysis.

Although progressive collapse analysis is out of the scope of this dissertation, a brief overview of general methods for the design and robustness of structures against progressive collapse is presented subsequently.

2.5.1 Concept of robustness

Almost any conventionally designed structure can be susceptible to progressive collapse if it is subjected to sufficiently large and widespread loading. As it is not feasible to foresee all possible sources of collapse initiation, a rational progressive collapse design should aim at localizing damage, rather than preventing damage on the whole structure. This methodology is associated with structural robustness, because the inherent deformation capacity, redundancy, and continuity of a robust structure preclude premature failure modes that can lead to a progressive collapse. The term *robustness* is a widespread notion that in the structural analysis can be defined as the ability of the structure to withstand unforeseen circumstances (Knoll and Vogel, 2009).

The increase of deformation capacity in a structural system involved in a progressive collapse scenario can be beneficial in two ways. Firstly, the ductile response of the members adjacent to the damaged area may limit the sustained damage and prevent the failure in the first place by dissipating more energy than less ductile members. Secondly, deformation capacity in the members adjacent to the failure zone allows alternative load paths to develop and thus facilitates the load redistribution process performed by the distorted structure.

Similar to deformation capacity, redundancy, which is generally associated with the presence of alternative load paths, may limit the effects of a local failure. The lack of alternative load paths can primarily result from lack of frame continuity, connection redundancy, or other load redistribution mechanisms.

The concept of continuity is mainly a way of improving redundancy and local resistance. Studies of numerous recent building collapses have indicated that failure could have been avoided or at least reduced in scale, at fairly small additional cost if structural components had been interconnected more effectively (Shankar Nair, 2006). Hence, the need for continuous systems is emphasized in most recent progressive collapse guidelines (ACI 318, 2008). A comprehensive overview on the principal design approaches currently used for providing resistance to progressive collapse is presented in the subsequent sections.

2.5.2 Hazard scenarios

Regarding possible strategies to improve the structural integrity of buildings and other structures against progressive collapse, much of the required knowledge and technology already exist. However, no building system can be engineered and constructed to be absolutely risk free because of uncertainties associated with the imposed demands on the system, the mechanical properties of materials and the prediction of structural performance using available design software.

To resist the progressive collapse following a local punching failure, it is necessary to consider the nature of initial hazards that can provoke an initial punching failure. Knoll and Vogel (2009) explained that "it is perhaps useful to classify the events in a very general sense since different families of scenarios require different approaches to robustness. We shall call one family the interior flaws or simply flaws where the origin of the event is located within the structural system. The second family will then be exterior causes. Forensic investigation of accidents often finds that a combination of causes relating to both classes is responsible for the mishap, i.e. a weakened structure was subjected to loads that exceeded the design loads. It may be that one or several events would not have been sufficient to cause distress and only their cumulation did". Exterior causes can be categorized as pressure loads (e.g. gas explosion and blast), impact loads (e.g. falling debris, vehicular collision, earthquake), deformation related (e.g. material softening in fire, foundation subsidence), occupant misuse and design and construction errors.

2.5.3 Indirect and direct design approaches

Ellingwood and Leyendecker (1978) first introduce two general approaches used to mitigate the probability of the progressive collapse of a structure, namely, *indirect design approach* and *direct design methods*. The indirect design approach is a prescriptive approach, which is based on providing a minimum connectivity and integrity between various structural elements. Therefore, it can readily be implemented in the structural design with no need for extra structural analyses. In other words, instead of performing a complex structural analysis against progressive collapse, the designer can use implicit design approach that incorporates measures typically related to strength, continuity and deformation capacity to enhance the overall robustness of the structure (Breen and Siess, 1979). Although the indirect design approach can reduce the likelihood of progressive collapse (Corley *et al.*, 1998), an estimation of the post-failure response of structures designed based on such a method is not readily possible (Sasani *et al.*, 2007).

The direct design methods are usually based on sophisticated structural analyses such as nonlinear static or dynamic finite element analysis, which are not commonly used in routine design practice. In this method, the designer should be able to evaluate consequences of an extreme condition that can cause a local failure with the potential to initiate a part or totally collapse of the structure. Hence, the direct design methods seem more rational in relation to the indirect design approach because they can be directly related to the performance-based criteria. A number of structural analyses with different complexity level ranging from linear elastic static analysis to nonlinear dynamic finite element analysis can be used to evaluate the structural performance of a progressive collapse (Vecchio, 2002; Dusenberry and Hamburger, 2006; Seffen, 2008)

2.5.3.1 Indirect design method

As the risk of a progressive collapse for the majority of structures is relatively low, many codes and guidelines prefer to implement the indirect design approach to design structures to reduce their susceptibility to progressive collapse. This approach is used to implicitly increase the robustness of a structure. This can be accomplished by incorporating general structural integrity measures throughout the process of structural system selection, the layout of walls and columns, the member proportioning, and the detailing of connections. Provisions for structural integrity are usual in the form of prescriptive requirements for minimum connection resistance, continuity and tying between structural elements.

As pointed out earlier, the indirect design approach is an easy way to enhance the structural performance against progressive collapse. Although this event independent approach is not based on detailed calculations of the structural response, it results in continuous tied reinforcement for concrete structures. This can enhance the structural performance and allows structural elements to carry more of their capacity when subjected to abnormal loading conditions. This can be attributed to the fact that loads carried originally by damaged portions of the structures will be redistributed to undamaged elements (Mitchell and Cook, 1984, Moore, 2001).

2.5.3.1.1 Tie requirement

To resist progressive collapse, key structural elements of a structure must be tied together so that the load redistribution from damaged portions to undamaged portions of the structure could occur. Ellingwood stated that “If all members are structurally connected by connections capable of transferring the specified capacity in tension, shear, or compression (as appropriate) without reliance on friction due to gravity loads or when additional tie members are provided, then the layout and configuration of the building are deemed to provide adequate protection against progressive collapse under abnormal load (Ellingwood *et al.*, 2007). The ties consist of internal ties, peripheral ties, and vertical ties. Reinforcing bars that are provided to resist normal loading can be regarded as a part of, or the whole of these ties and should be in line with design codes and guidelines. All requirements of lap splicing and anchorage shall be satisfied in order to provide satisfactorily structural integrity. The ties should be effectively continuous over throughout their lengths and should be anchored into the peripheral ties at each end (ACI 318, 2008).

2.5.3.2 Direct design methods

The direct design methods require that the response of a structure subjected to a local failure should be analyzed using highly complex structural analyses. The ability of the structure to bridge damaged and undamaged portions of the structure and the load redistribution across the local failure zone should be evaluated. The direct design methods consist of two approaches commonly referred to as *alternate load path method* and *specific local resistance method* (ASCE 7, 2005).

2.5.3.2.1 Alternate load path method

The alternate load path method is conceptually based on the performance of the structure following a local failure. The structure is required to redistribute the loads and to keep its stability after a local failure. This method provides the assessment of the capability of the structure to resist removal of essential structural elements such as columns or load bearing walls by analyzing the behavior of the remaining structure (Ellingwood *et al.*, 2007). In addition, this method enhances structural properties such as deformation capacity and energy dissipation, which are very desirable to reduce the risk of the progressive collapse (Vlassis, 2007). Moreover, as this approach deals with the performance of the structure after a local failure, it is not sensitive to the initial abnormal loading and thus it is a threat-independent method. However, analysis of a severely damaged structure can be computationally difficult. Thus, the results may not be an accurate representation of the actual results because the actual failure scenario could be completely different from the loss of a single column or a bearing wall.

A number of structural analyses can be used to estimate the response of a damaged structure following a local failure such as *linear static analysis, nonlinear static analysis, linear dynamic analysis,* and *nonlinear dynamic finite element analysis* (Marjanishvili, 2004; Marjanishvili and Agnew, 2006). The last one is the most complex and rigorous method for evaluating the risk of the progressive collapse and provides various level of refinement to account for the large deformation, geometric and material nonlinearities, and time-dependent behavior of the structure following a local failure.

2.5.3.2.2 Specific local resistance method

The specific local resistance method provides supplementary strength for key structural elements, which are essential for overall stability, and are required to remain intact for alternate load paths to develop. The key elements are explicitly designed to withstand a specified level of abnormal loading (ASCE 7, 2005). Thus, unlike the alternate load path method, this approach is threat-specific. This approach provides additional strength at areas that are believed to be prone to accidental loads or in key elements that are necessary for the load redistribution.

In terms of procedure and compared to the alternate load path method, this approach is more similar to current design methods in practice. However, it does not guarantee a desirable performance against threats other than the one specifically considered. In terms of its applicability, this method can be regarded as the only practical approach for retrofitting an existing building because the cost of other approaches can be excessive. Therefore, an engineer can strengthen key elements of the structure to mitigate the risk of a progressive collapse (Ellingwood, 2006).

2.5.4 Progressive collapse provisions in codes and guidelines

Progressive collapse has attracted a lot of attention over the past decades after the Ronan Point collapse and researchers have acknowledged the threat posed to the structural safety by the progressive collapse. Therefore, they have included statements of the required structural performance in provisions and guidelines. The tendency of codes of practice is to increase the redundancy and deformation capacity in structures so that in the event of a local damage to major structural elements, resulting damages may be confined to a relatively small area and should not lead to catastrophic consequences.

Prescriptive code provisions used in conventional structural design require integrity and continuity using continuous integrity reinforcement passing through the column and well-anchored in the slab. Other provisions introduce different methods to reduce the likelihood of a progressive collapse such as specifying minimum tie forces to achieve integrity requirements, introducing the notional removal of load carrying elements, and specifying a level of damage expressed in terms of floor area or volume that the remaining structure is required to sustain following the incident. Moreover, in some countries, the provisions apply to practically all buildings, as opposed to other countries where certain types of construction or buildings below a certain minimum number of stories are excluded. The following sections present an overview of the integrity provisions included in current codes of practice.

2.5.4.1 Canadian Code

The National Building Code of Canada (NBCC, 1995) requires structures to be designed for sufficient structural integrity to withstand all effects that may reasonably be expected to occur during the service life. This code defines structural integrity as "the ability of the structure to absorb local failure without widespread collapse". It also advises engineers to consider a higher probability of occurrence for severe accidents in relation to that proposed by ordinary design codes. However, this code does not provide guidance as to how probabilities should be computed for specific design scenarios. Several general approaches such as local resistance, minimum tie forces, provision of alternate paths of support are suggested. Unlike ASCE 7 (2005), specific load combinations or other prescriptive measures are not presented in this code.

2.5.4.2 European Standard

Eurocode 2 (2004) is a code adopted by many European countries that aims at replacing national standards. Eurocode recommends that at least two compressive reinforcing bars in each orthogonal direction should be provided at internal columns and this reinforcement should pass through the column. In addition to providing general design guidelines to avoid progressive collapse such as selection of a good structural layout, Eurocode requires tying the building together and defines values for tie forces.

2.5.4.3 British Standard

The British Standard (BS 8110, 1997) emphasizes general tying of various structural elements of a building together, to provide continuity and redundancy. Ties enhance the resistance of wall panels to being blown away in the event of a failure, and also the ability of a structure to bridge over a lost support. If effective tying cannot be provided,

an alternative member removal approach should be adopted. This approach requires that each untied member including load bearing vertical members and beams supporting one or more columns should be notionally removed one at a time in each storey. Then, the remaining structure should be checked to verify that it can bridge over the missing member in a substantially deformed condition.

2.5.4.4 United States standards

2.5.4.4.1 ACI 318

ACI 318 (2008) requires that all compressive reinforcement within the column strip shall be continuous. At least two compressive reinforcing bars in each direction shall pass through the column core and shall be anchored at exterior supports. The two continuous compressive bars passing through the column may be termed integrity steel, and are provided to give the slab some residual capacity to prevent a local failure over a column leading to the progressive collapse of a large part of the structure. Therefore, the ACI 318 (2008) standard is an example of indirect design. It defines requirements for structural integrity such as continuity of reinforcement and use of ties in precast concrete construction.

2.5.4.4.2 ASCE 7

The commentary of ASCE 7 (2005) contains an extensive discussion on general structural integrity. It lists the direct design approaches (alternate path method and specific load resistance method) as well as the indirect design approach. It provides design guidelines for general structural integrity, such as good plan layout and use of structural ties. In addition, a recommended set of load combinations for extreme loads to be used with the alternate load path and the specific local resistance design methods. It is suggested that, after an element is notionally removed, the capacity of the remaining structure should be checked using the following load combination:

$$(0.9 \sim 1.2)DL + 0.5LL + 0.2SL + 0.2WL \tag{2.29}$$

where *DL*, *LL*, *SL*, and *WL* are the nominal dead, live, snow, and wind loads. On the other hand, if certain key elements must be designed to withstand the effects of a specific accidental load, the following load combination should be used:

$$(0.9 \sim 1.2)DL + AL + 0.5LL + 0.2WL \tag{2.30}$$

where *AL* is the structural action due to the postulated extreme load. The structural action can be a force, as in the case of explosion or impact, or related to deformation, as in the case of fire or ground subsidence. The partial factor of 0.9 in the above equations is applied when the dead load contributes to the overall building stability. It should be noted that the lateral wind load in both combinations is intended to guarantee that the overall lateral stability of the structural system under gravity loads is not overlooked in a progressive collapse analysis, even if progressive collapse is largely driven by gravity forces.

2.5.4.4.3 General Service Administration (GSA)

Federal buildings in the US are generally designed according to the General Service Administration guidelines (GSA, 2003). These guidelines were developed to provide

minimum requirements for reducing the risk of progressive collapse. They employ the alternate load path method, and, despite the dynamic nature of instantaneous member removal, they promote a simplified equivalent linear static analysis technique. According to this approach, the following load combination is proposed in which the amplification factor of 2.0 is used to consider dynamic effects:

$$2.0(DL + 0.25LL) \tag{2.31}$$

2.5.4.4.4 Department of Defense (DoD)

Progressive collapse guidelines have also been produced by the US Department of Defense for the design of military facilities (DoD, 2005), where protection against progressive collapse is required for new and existing buildings that have three stories or more. Design for resistance to progressive collapse depends on the "level of protection" assigned to the building. For lower levels of protection the indirect design method is used by providing minimum tie forces. For higher levels of protection, the alternate load path method is used if sufficient ties cannot be provided.

With particular reference to the alternate load path method, the following load combination is recommended if nonlinear dynamic analysis is used for structural assessment:

$$(0.9 \text{ or } 1.2)DL + (0.5LL \text{ or } 0.2SL) + 0.2WL \tag{2.32}$$

This equation is similar to that proposed by ASCE 7 (2005) except that the effect of live and snow loads are not concurrent. The following load combination is also suggested for use with both linear and nonlinear static analysis procedures:

$$2.0[(0.9 \text{ or } 1.2)DL + (0.5LL \text{ or } 0.2SL)] + 0.2WL \tag{2.33}$$

where the factor 2.0 accounts for dynamic effects. Finally, to ensure the redistribution of gravity loads after the loss of lateral support in association with local damage at any floor level, the DoD guidelines require all multi-storey vertical load carrying elements, such as columns and walls, to be designed for an unsupported length equal to the total height of two stories.

3 Experimental program

This chapter summarizes an extensive experimental campaign carried out at the Ecole Polytechnique Fédérale de Lausanne. The post-punching behavior of 24 tested slabs with 125 mm thickness and various reinforcement layouts is presented and discussed. The complete test report can be found in Appendix A.

3.1 Overview

The experimental program consisted of three test series. The first series investigated the effects of tensile reinforcement in the negative moment area over the column on the post-punching behavior of flat slabs. The second series investigated the effects of integrity reinforcement on the compression side of the slabs and passing through the column and of bent-up bars acting as shear reinforcement. The third series consisted of twelve specimens: four specimens included bent-up bars with a sufficient anchorage length, two specimens included integrity reinforcement, two had only tensile reinforcement, and the last four included integrity reinforcing bars passing through the column and tensile reinforcement that was cut-off at specified points to ensure that it did not contribute to the shear transfer after punching shear failure. Table 3.1 presents the main parameters and experimental results.

Table 3.1: Summary of experimental parameters and test results

		Tensile reinf.			*Integrity reinf.*						
	Test	ρ [%]	f_{sy} [MPa]	f_c [MPa]	A_{sb}	f_{sy} [MPa]	V_p [kN]	w_p [mm]	V_{pp} [kN]	w_{pp} [mm]	$\frac{V_{pp}}{V_p}$
Series 1	PM-1	0.25	601	36.6	-	-	176	13.6	37	70.5	0.21
	PM-2	0.49	601	36.5	-	-	224	11.0	66	52.7	0.30
	PM-3	0.82	601	37.8	-	-	324	13.1	117	45.3	0.36
	PM-4	1.41	601	36.8	-	-	295	7.4	108	42.6	0.37
Series 2	PM-9	0.82	601	31.0	4Ø8	616	224	7.1	123	36.2	0.55
	PM-10	0.82	601	31.1	4Ø10	560	228	6.7	159	42.9	0.70
	PM-11	0.82	601	32.3	4Ø12	548	241	8.2	237	86.3	0.98
	PM-12	0.82	601	32.4	4Ø14	527	249	8.2	245	116.9	0.98
	PM-13	0.82	601	32.6	4Ø8	616	327	11.4	151	39.9	0.46
	PM-14	0.82	601	32.7	4Ø10	560	356	12.6	188	71.7	0.53
	PM-15	0.84	601	32.7	4Ø12	548	274	9.1	177	66.5	0.64
	PM-16	0.83	601	32.8	4Ø14	527	298	10.1	135	43.4	0.45
Series 3	PM-17	0.82	625	39.7	4Ø8	625	329	15.1	247	50.0	0.75
	PM-18	0.88	625	39.8	4Ø10	605	323	15.7	237	56.5	0.73
	PM-19	0.85	625	39.9	4Ø12	559	417	28.7	315	90.1	0.75
	PM-20	0.82	625	40.0	4Ø14	578	402	19.3	345	95.2	0.86
	PM-21	0.81	625	40.2	4Ø8	625	256	9.7	185	42.9	0.73
	PM-22	0.85	625	40.3	4Ø10	605	288	14.1	219	65.2	0.76
	PM-23	0.88	625	40.4	-	-	227	10.4	82	83.0	0.36
	PM-24	0.86	625	40.4	-	-	272	12.1	101	74.2	0.37
	PM-25	0.85	625	40.4	4Ø8	625	143	7.7	85	69.8	0.60
	PM-26	0.83	625	40.3	4Ø10	605	165	8.5	105	89.3	0.64
	PM-27	0.81	625	40.3	4Ø12	559	211	8.0	94	64.1	0.45
	PM-28	0.85	625	40.3	4Ø14	578	258	11.2	101	57.2	0.39

3.2 Geometry and reinforcement

All twenty four slabs were identical in size and shape. The dimensions of the slabs were 1500×1500 mm and the nominal thickness of the slabs was h = 125 mm. A square steel plate of 130×130 mm was used to simulate a rigid column in all specimens (Figure 3.1). For all specimens, Ø8 was used as the main diameter for the tensile reinforcement. The first four specimens were designed to investigate the influence of various reinforcement ratios on the post-punching behavior. As shown in Figure 3.2.a, for PM-1, PM-2, PM-3, and PM-4, the bar spacing were 200, 100, 60, and 35 mm, respectively (ρ is equal to 0.25%, 0.5%, 0.82%, and 1.41%). For the remaining twenty specimens, the tensile reinforcement ratio was constant (Ø8 at 60 mm).

Slabs PM-9, PM-10, PM-11, and PM-12 had integrity reinforcement with diameters of Ø8, Ø10, Ø12, and Ø14 (Figure 3.2.b). Slabs PM-13, PM-14, PM-15, and PM-16 included bent-up bars with diameters of Ø8, Ø10, Ø12, and Ø14, with an angle of inclination of 30° and bent at a distance of 50 mm from the column face. Their anchorage length turned out to be insufficient during the test and thus for slabs PM-17, PM-18, PM-19, and PM-20, Ø8, Ø10, Ø12, and Ø14 well-anchored bent-up bars were used, respectively (Figure 3.2.c).

a) *b)*

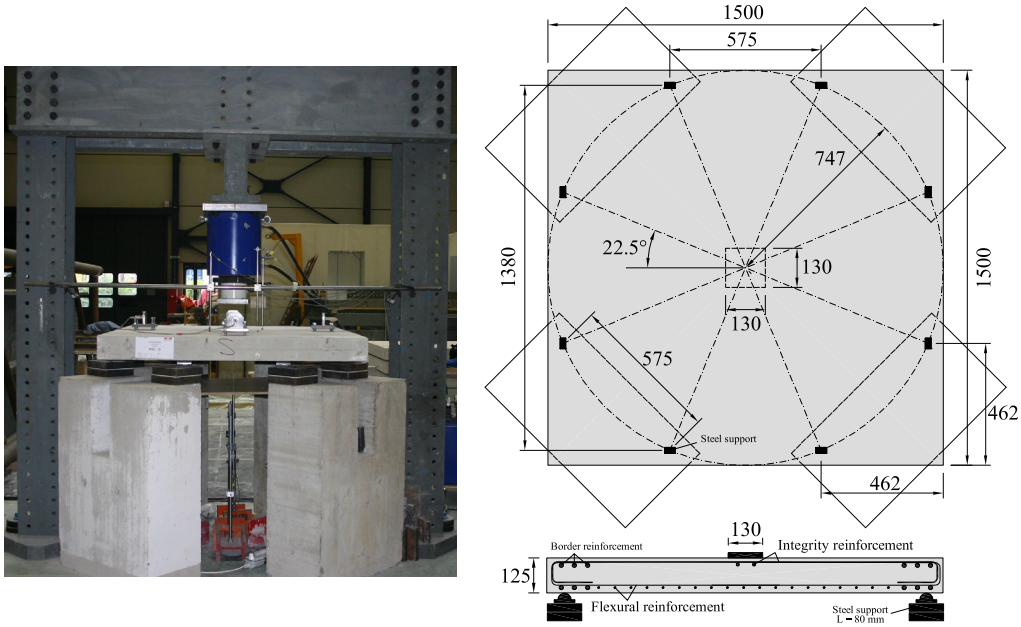

Figure 3.1: a) Test setup and b) typical slab and plan section

Slabs PM-21 and PM-22 were similar to PM-9 and PM-10, respectively. For the former specimens, cold-worked steel and for the latter ones, hot-rolled steel was used. Slabs PM-23 and PM-24 were similar to PM-3. For PM-24, three closed stirrup were placed above the column to investigate the effect of concrete confinement on the post-punching behavior. Slabs PM-25, PM-26, PM-27, and PM-28 included Ø8 at 60 mm as tensile reinforcement, which was cut off at some specified points to investigate the effect of a short anchorage length of the tensile reinforcement. The anchorage length was equal to 2d, 2.5d, 3d, and 3.5d, respectively. In these specimens, Ø8, Ø10, Ø12, and Ø14 were used as the integrity reinforcement, respectively (Figure 3.2.d). In all specimens, very

strong edge reinforcement in both top and bottom layer was provided to avoid unexpected modes of failure. For all slabs, the nominal concrete cover was 15 mm.

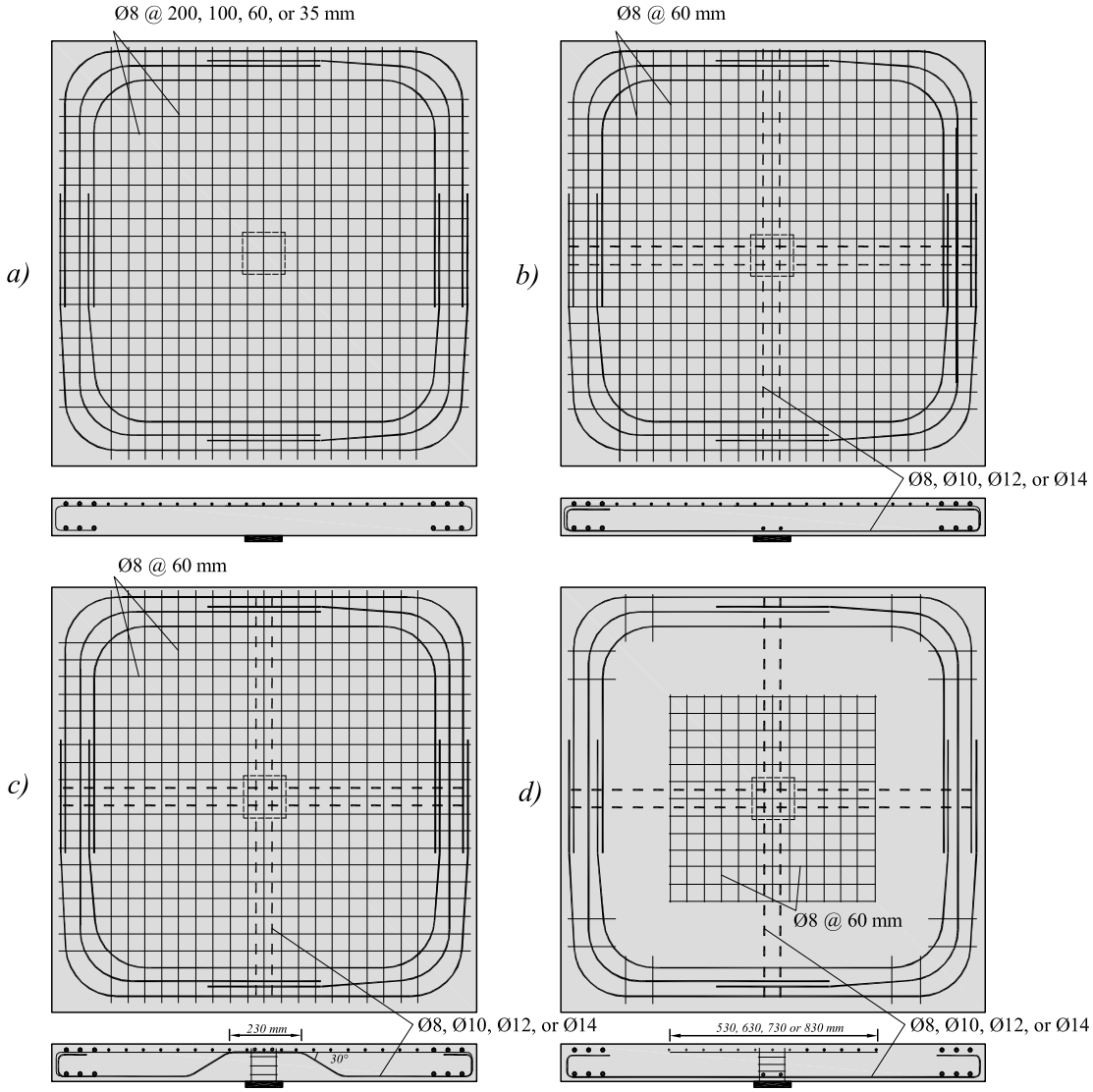

Figure 3.2: Reinforcement layout: a) slabs PM-1, PM-2, PM-3, PM-4, PM-23, and PM-24, b) slabs PM-9, PM-10, PM-11, PM-12, PM-21, and PM-22, c) slabs PM-17, PM-18, PM-19, and PM-20, and d) slabs PM-25, PM-26, PM-27, and PM-28

3.3 Test results and discussion

All tested slabs experienced punching failure and their post-punching responses were recorded up to the point at which no meaningful data were recorded by the measurement instrumentations. It was generally observed that after the punching failure had occurred, the deflection increased and the load decreased rapidly. Afterward, the load started increasing with further deflection in the post-punching phase. The tensile reinforcing bars tend to tear out of concrete by a combination of bond failure and vertical tearing.

Because of the large strains at the tension side of the slab, cracks propagated through the slab and yielding of reinforcement spread throughout the slab. Figure 3.3 shows the load versus the central deflection responses for all slab specimens, which are briefly discussed subsequently.

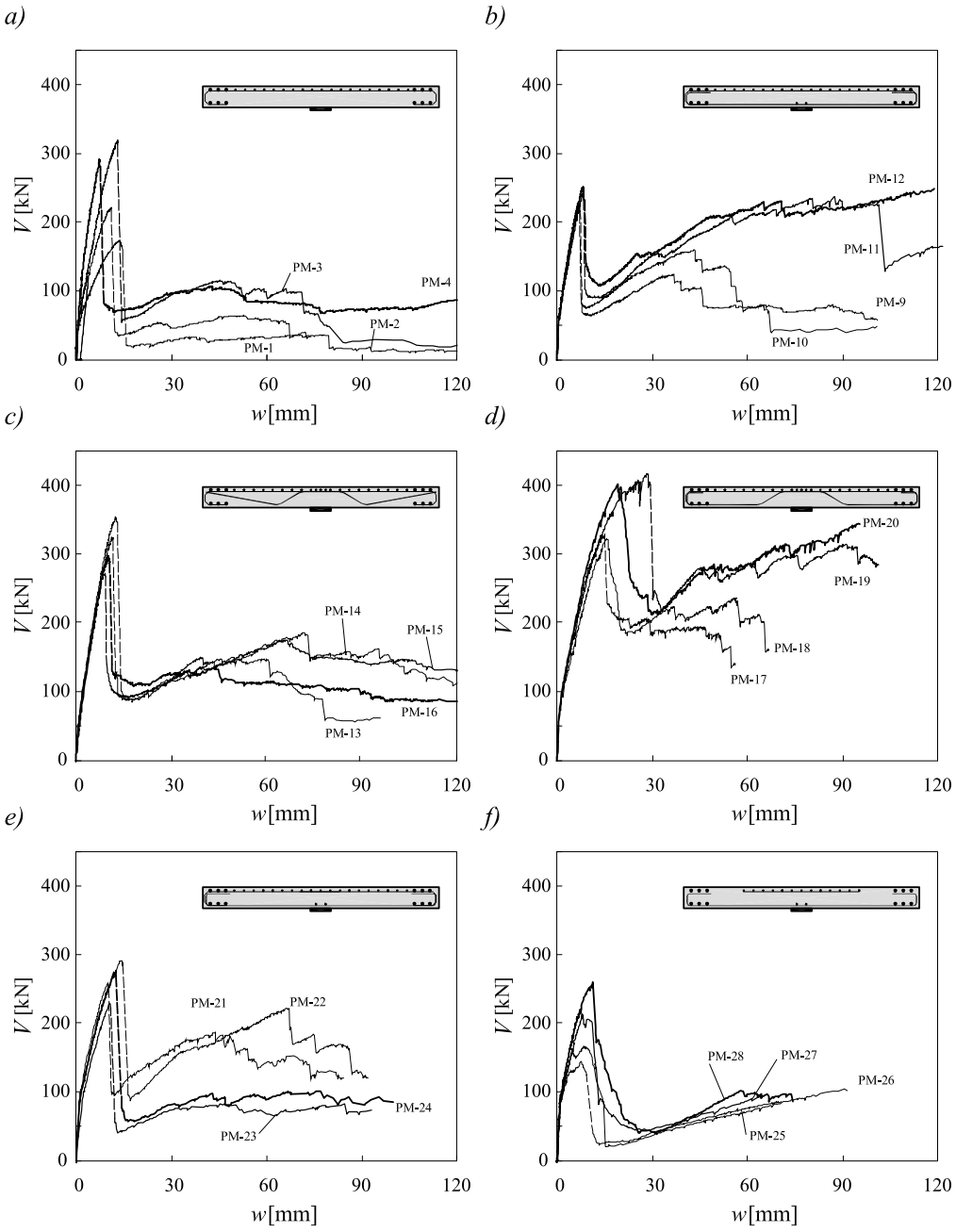

Figure 3.3: Load-deflection response of all test specimens

3.3.1 Tensile reinforcement

Figure 3.3.a shows the load-deflection responses of PM-1, PM-2, PM-3, and PM-4. These specimens had the same geometry but different tensile reinforcement ratios. No integrity reinforcement was included and thus the post-punching response was only influenced by the tensile reinforcement rather than the integrity reinforcement. In other words, the only connection between the punching cone and the rest of the slab after punching failure was the tensile reinforcement. This connection made it possible for slabs to carry load after punching failure. As expected, the increase of the reinforcement ratio resulted in an increase of the punching strength. The ratio of post-punching strength to punching strength was 0.21, 0.30, 0.36, and 0.37 for specimens PM-1, PM-2, PM-3, and PM-4, respectively. The relatively small post-punching strength was attributed to the tensile reinforcing bars that tore out of the concrete surface and became ineffective.

It was observed that after having experienced the punching failure, the slab specimens sustained up to 37% of the punching strength due to the presence of the tensile reinforcement. However, for the higher reinforcement ratios the ratio of post-punching strength to punching shear strength remains almost constant as shown in Figure 3.4. In fact, the increase of the reinforcement ratio results in an increase of the number of reinforcing bars crossing the punching cone. Thus, the overall vertical component of the axial forces developed in the tensile reinforcement increases. The contribution of the tensile reinforcement to the post-punching shear transfer is the vertical component of the axial forces developed in the tensile reinforcement. The increase of the vertical component of the axial forces in the tensile reinforcement results in more destruction of the concrete within and outside of the punching cone. This destruction reduces the angle of inclination of the tensile reinforcing bars resulting in a decrease of the contribution of the tensile reinforcement to the post-punching shear transfer. As the failure process is related to the spalling of the concrete cover, the post-punching strength is mostly related to the concrete cover and not to the reinforcement layout. Regan (1986) also observed this phenomenon and stated that "…large deformations were developed at almost constant loads often as low as 25 to 30% of the peak resistance".

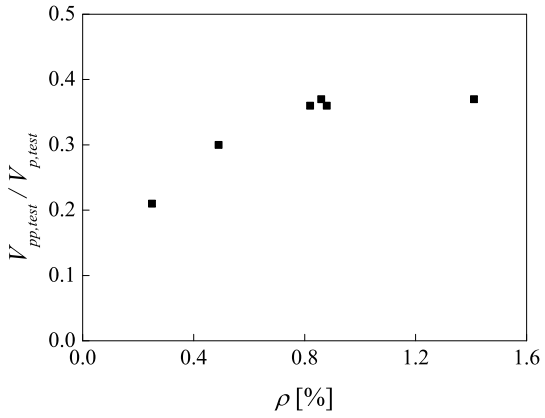

Figure 3.4: Ratio of post-punching strength to punching strength as a function of reinforcement ratio for slabs PM-1, PM-2, PM-3, PM-4, PM-23, and PM-24

3.3.2 Integrity reinforcement

Figure 3.3.b shows the load-deflection responses of slabs PM-9, PM-10, PM-11, and PM-12. In these slabs, Ø8, Ø10, Ø12, and Ø14 integrity bars were used, respectively. The post-punching behavior of these specimens was not only influenced by the tensile reinforcement but also by the integrity reinforcement. It was observed that the post-punching strength of these specimens was clearly higher than that one of the specimens without integrity reinforcement. The ratio of the post-punching strength to the punching strength was 0.55, 0.70, 0.98, and 0.98 for slabs PM-9, PM-10, PM-11, and PM-12, respectively. Although the punching strength was nearly the same for all specimens in this test series, there was a considerable difference in the post-punching behavior of the first two specimens (PM-9 and PM-10), and the last two (PM-11 and PM-12). This can be attributed to the type of steel reinforcement as cold-worked steel was used for the former slabs, while hot-rolled steel was used for the latter slabs. The sudden drops in the graphs are caused by the fracture of the steel bars.

3.3.3 Type of steel and concrete confinement

To study the influence of the type of steel on the post-punching behavior, PM-21 and PM-22 were tested. These test specimens were similar to PM-9 and PM-10, respectively. However, PM-22 had a different steel type. Cold-worked steel was used for PM-10 and hot-rolled steel was used for PM-22. It was observed that hot-rolled steel bars provided a better post-punching behavior and increased the post-punching strength as well as the deformation capacity.

Slab PM-24 was tested to investigate the effects of concrete confinement provided by closed horizontal stirrups over the column (Figure 3.3.e). Slabs PM-24 and PM-23 were identical except PM-24 included three horizontal stirrups above the column. Their punching and post-punching behavior were nearly the same. The ratio of the post-punching to the punching strength was 0.36 and 0.37 for slabs PM-23 and PM-24, respectively. It was observed that placing horizontal stirrups above the column (extension of column stirrups) increased slightly the punching strength as well as the post-punching strength.

3.3.4 Cut-off tensile reinforcement

The load-deflection responses of slabs PM-25, PM-26, PM-27, and PM-28 are shown in Figure 3.3.f. Cutting-off the tensile reinforcing bars localized the critical punching crack at the end of the bars and consequently the tensile reinforcing bars were not activated after the punching failure. Therefore, the only factor affecting the post-punching response was the presence of the integrity reinforcement. It was observed that using improper anchored tensile reinforcement (cut-off tensile reinforcement) reduced significantly the punching strength. The post-punching strength was also influenced by the anchorage failure of the tensile reinforcement. The objective of these experiments was to study the post-punching behavior of slab-column connection in the absence of a well-anchored tensile reinforcement. However, the tests were deliberately terminated because of the risk of falling down of the punching cone and consequently the slabs could not reach their post-punching strength.

3.3.5 Comparison of various reinforcement layouts

Figure 3.5 compares the load-deflection of slabs PM-12, PM-16, PM-20 (one slab for every reinforcement layout, with the same diameter of integrity or bent-up bars, Ø14) and PM-24 (without additional reinforcement) to show the influence of the various reinforcement layouts on the post-punching behavior of flat slabs. To simplify this comparison, both vertical and horizontal axes are normalized. The post-punching strength was 245, 135, 345 and 101 kN and the ratio of post-punching strength to punching strength was 0.98, 0.45, 0.86 and 0.37 for slabs PM-12, PM-16, PM-20, and PM-24, respectively. For PM-16, the punching crack started from the face of the column and went through the slab and then propagated along the bent-up bar, leaving such shear reinforcement ineffective. Compared to PM-16, PM-20 had no anchorage problem and thus had a larger punching strength than the other slabs. However, its ratio of post-punching strength to punching strength was less than that of PM-12. For the specimen PM-12, it was observed that the integrity reinforcement made it possible to reach nearly the punching strength of the slab (98%), which can be considered as a way to mitigate the likelihood of the progressive collapse.

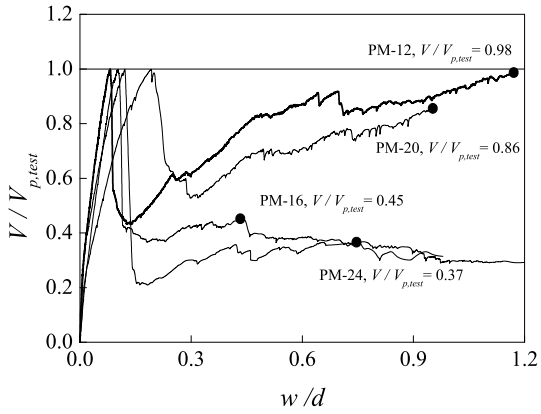

Figure 3.5: Post-punching performance of slabs PM-12, PM-16, PM-20, and PM-24

4 Mechanical model

4.1 Introduction

This chapter deals with the physical understanding of the post-punching shear transfer mechanisms in order to develop a mechanical model capable of predicting the post-punching behavior of flat slab-column connections. Figure 4.1 shows the shear transfer through longitudinal reinforcement in the absence of shear reinforcement after a punching shear failure has occurred. It is obvious that longitudinal reinforcement plays a significant role in transferring shear while other contributions to the shear transfer are fairly small. This is particularly the case with post-punching behavior of flat slabs supported by columns.

The contribution of the longitudinal reinforcement to the post-punching shear transfer is the summation of the contribution of tensile reinforcement and the contribution of integrity reinforcement. Tensile reinforcement provides a little contribution to the post-failure shear strength as the concrete cover is small and spalling of the concrete cover occurs. Hence, the main contribution to the post-punching shear transfer is provided by the integrity reinforcement. To develop a rational model capable of predicting the shear transfer mechanism after a local punching failure, the influence of the tensile reinforcement as well as the integrity reinforcement should be thoroughly investigated.

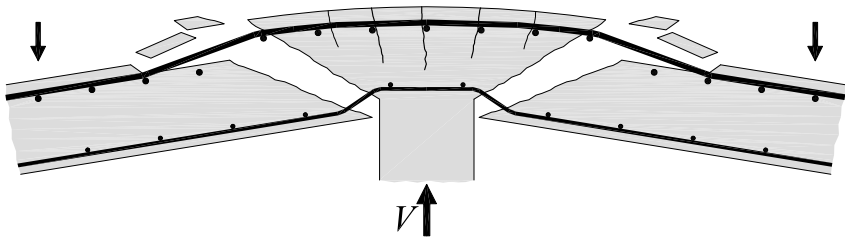

Figure 4.1: Post-punching shear transfer through longitudinal reinforcement

4.2 Material models

4.2.1 Constitutive model for reinforcing steel

Figure 4.2 shows main mechanical properties of steel reinforcement. Cosenza, Greco, and Manfredi (Cosenza *et al.*, 1993) proposed the following relationships for the stress-strain relationships of hot-rolled steel reinforcement:

$$\begin{aligned}
\sigma_s &= E_s \cdot \varepsilon_s && \text{for} \quad \varepsilon_s \le \varepsilon_{sy} \\
\sigma_s &= f_{sy} && \text{for} \quad \varepsilon_{sy} < \varepsilon_s \le \varepsilon_{sh} \\
\sigma_s &= f_{sy} + \left(f_{su} - f_{sy} \right) \cdot k_3 \cdot \left(1 - e^{\frac{\varepsilon_{sh} - \varepsilon_s}{k_4}} \right) && \text{for} \quad \varepsilon_{sh} < \varepsilon_s \le \varepsilon_{su} \qquad (4.1) \\
k_4 &= k_1 \cdot \frac{\varepsilon_{sh} - \varepsilon_{su}}{\varepsilon_{sh} - k_2}
\end{aligned}$$

where k_1 = 0.0245, k_2 = 0.1165, and k_3 = 1.019859. For cold-worked steel as well as prestressed tendons the stress-strain relationship can be obtained by

$$\begin{aligned}
\varepsilon_s &= \frac{\sigma_s}{E_s} + \left(\frac{\sigma_s}{k_3} \right)^{k_4} \\
k_4 &= \frac{\ln\left[\left(\varepsilon_{su} - f_{su}/E_s \right)/k_1 \right]}{\ln\left(f_{su}/f_{sy} \right)} \qquad (4.2) \\
k_3 &= \frac{f_{sy}}{k_2^{\,1/k_4}}
\end{aligned}$$

where $k_1 = k_2 = 0.002$

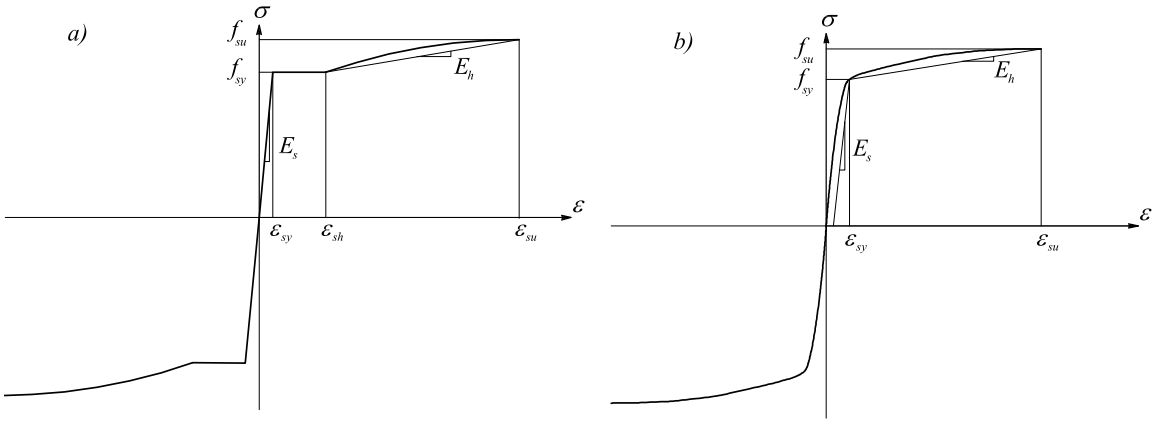

Figure 4.2: Stress-strain relationships of reinforcement: a) hot-rolled and b) cold-worked steel

4.3 Failure modes for concrete

In general, failure of concrete depends on many parameters such as material properties, type of loading, concrete thickness, edge conditions, and the presence of shear reinforcement. Various failure modes exist for concrete as can be seen in Figure 4.3. For thin concrete layers particularly for the concrete cover, spalling of concrete is the controlling mode of failure (Figure 4.3.a). Based on the top, the bottom, and the side cover of concrete, splitting of concrete can be controlling (Figure 4.3.b). For loading acting against the concrete core, crushing of concrete and yielding of the reinforcing bar is the failure mode (Figure 4.3.c). Another failure mode can be considered for relatively

thick concrete layers, which is called concrete breakout (Figure 4.3.d). This failure mode is associated with the performance of anchors embedded in concrete. The concrete breakout strength is defined as the strength corresponding to a volume of concrete surrounding the anchor or the group of anchors separating from the member (ACI 349, 2001).

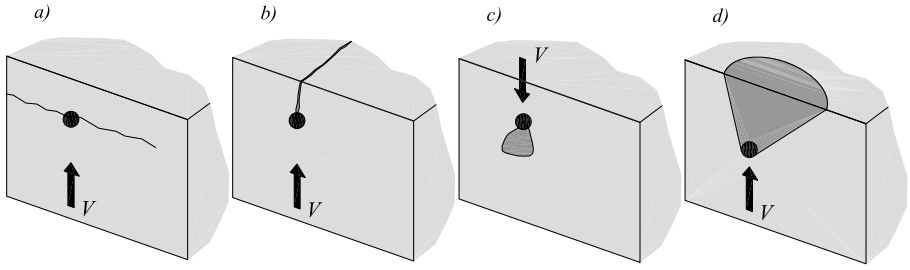

Figure 4.3: Failure of concrete: a) spalling, b) splitting, c) crushing, and d) breakout

Various failure developments can be considered for the interaction between concrete and reinforcing bars in the post-punching phase. These failures are yielding of the bar and crushing of concrete supporting the bar, spalling of concrete cover, and concrete breakout. These modes of failure are illustrated in Figure 4.4. The splitting of concrete is unlikely in the post-punching phase. All of the aforementioned failures can occur in a post-punching test as the loading is continued up to the total failure of the slab.

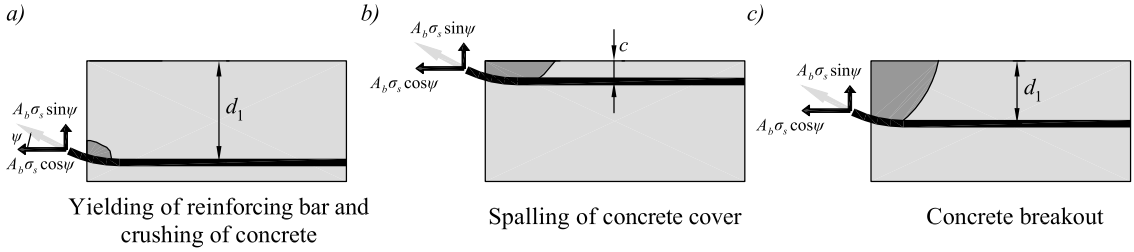

Figure 4.4: Modes of failure due to reinforcing bars acting against concrete

4.4 Interaction between concrete and reinforcement

According to the direction of loading and the thickness of the concrete, four failure zones can be characterized as shown in Figure 4.5. For zone 1, reinforcing bars act against the concrete cover. The concrete cover breaks shortly after the punching failure as the thickness of the cover is small. When the concrete cover crushes, reinforcing bars act against the column face. As reinforced concrete columns are typically reinforced with stirrups, failure of the concrete over the column is unlikely, which has been confirmed experimentally by Melo and Regan (1998).

For zone 2, reinforcing bars seem to act against the concrete core and hence yielding of the bar and crushing of the concrete is expected. However, the thickness of the concrete at the location where the reinforcing bars go into the slab is very small and concrete breakout occurs. It was observed for the specimens including integrity reinforcement (e.g. PM-12) that the failure process was started by the concrete breakout up to a certain point. Beyond this point, the failure changed to yielding of the bar and crushing of the

concrete. This procedure can be explained as follows. The thickness of the concrete over the integrity bars at the beginning of the post-punching phase is small. Therefore, reinforcing bars act against concrete with a small thickness and thus concrete breakout occurs. The progressive destruction of concrete continues up to a certain point at which the thickness of concrete is sufficient to prevent further concrete breakout. Beyond this point, yielding of the bar and crushing of the concrete supporting the bar control the failure process. It has been reported that if the concrete thickness is larger than 6 to 7 times the bar diameter, yielding of the bar and crushing of concrete govern the failure procedure (Vintzeleou and Tassios, 1986; Jeli *et al.*, 1999). It can generally be concluded that using large bar diameters is unfavorable due to the possible change in the failure mode that can reduce the ultimate strength.

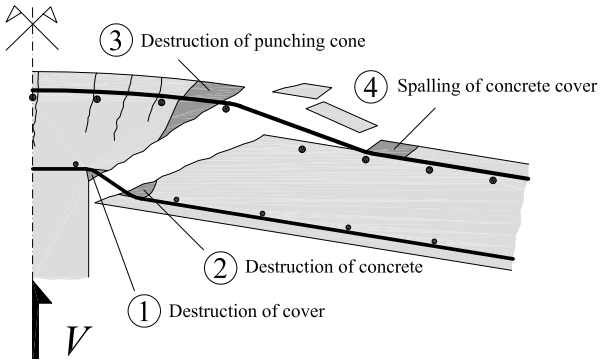

Figure 4.5: Various critical zones due to interaction between concrete and reinforcing bars

For zone 3, which is similar to zone 2, the same scenario happens. The only difference refers to the concrete supporting the bar. Zone 2 is placed on the compression side of the slab and the concrete is barely cracked. However, zone 3 is placed on the tension side of the slab and the concrete is severely cracked due to bending and shear. Thus, the concrete breakout strength is not identical for these zones. For zone 4, reinforcing bars act against the concrete cover. The spalling of the concrete cover is the governing mode of failure. For further deflection, reinforcing bars tend to tear out of concrete and become detached from the concrete surface. As all the aforementioned mechanisms are associated with the behavior of reinforcing bars acting against either concrete core or concrete cover, it is possible to develop a generic model capable of predicting the post-punching behavior for all of the different failure zones.

4.5 Plastic Analysis

The post-punching strength of flat slabs without shear reinforcement is the summation of the shear transfer through tensile reinforcement and integrity reinforcement while other contributions to the shear transfer are negligible:

$$V_{pp} = V_M + V_D = \sum_i^m V_{M,i} + \sum_i^n V_{D,i} \tag{4.3}$$

where V_{pp} is the post-punching strength of the slab-column connection, V_D is the contribution of the integrity reinforcement to the post-punching strength, V_M is the contribution of the tensile reinforcement to the post-punching strength, $V_{D,i}$ is the contribution of an integrity reinforcing bar to the post-punching strength, $V_{M,i}$ is the

contribution of a tensile reinforcing bar to the post-punching strength, *n* is the number of the integrity bars, and *m* is the number of the tensile reinforcing bars crossing the punching cone. To gain a better understanding of the distribution of bending, shear, and axial forces, a simple illustration is given in Figure 4.6. Considering ψ_D and ψ_M as the angles of inclination of the integrity and the tensile reinforcement, the shear transferred through the tensile reinforcement and the integrity reinforcement can be calculated by

$$\begin{aligned} V_{M,i} &= N_I \sin\psi_M + V_I \cos\psi_M \\ V_{D,i} &= N_I \sin\psi_D + V_I \cos\psi_D \end{aligned} \tag{4.4}$$

where N_I and V_I are axial and shear force in an arbitrary section of the bar.

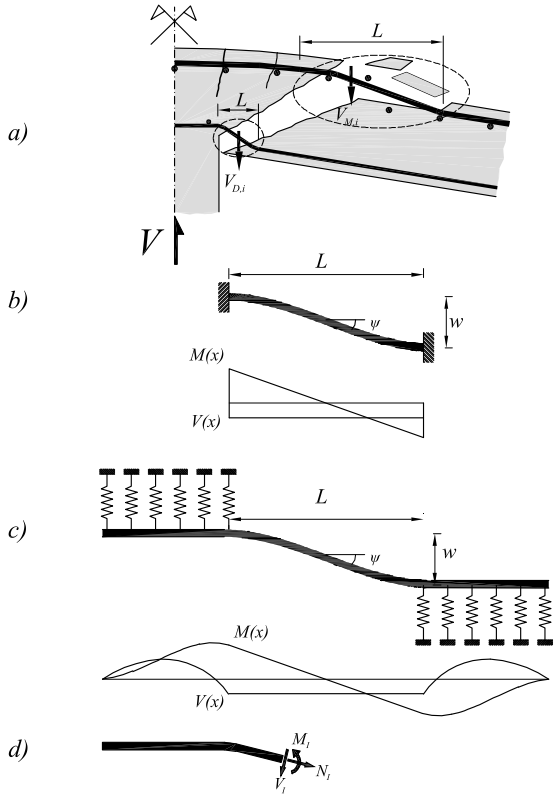

Figure 4.6: a) Shear transfer across a punching crack, b) clamped beam model and bending and shear diagrams, c) beam on elastic foundation analogy and bending and shear diagrams, and d) internal forces at an arbitrary section

It was observed during the experimental campaign that a possible deformation was the formation of plastic hinges in the reinforcing bars at the face of the crack due to combined bending, shear, and axial force, which can be seen in Figure 4.7.

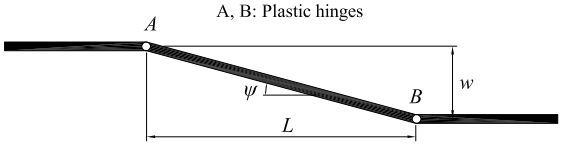

Figure 4.7: Plastic deformation of a reinforcing bar in the post-punching phase

The derivative of the bending moment is the shear force. Thus, one can obtain the shear force at the face of the crack (Figure 4.6)

$$V_I = \frac{2M_p \cos\psi}{L} \tag{4.5}$$

Substituting Equation 4.5 in Equation 4.4 will give

$$V_{D,i} = N_I \sin\psi_D + \frac{2M_p \cos^2\psi_D}{L} \tag{4.6}$$

where V_D can be described as a function of the axial force and geometrical parameters.

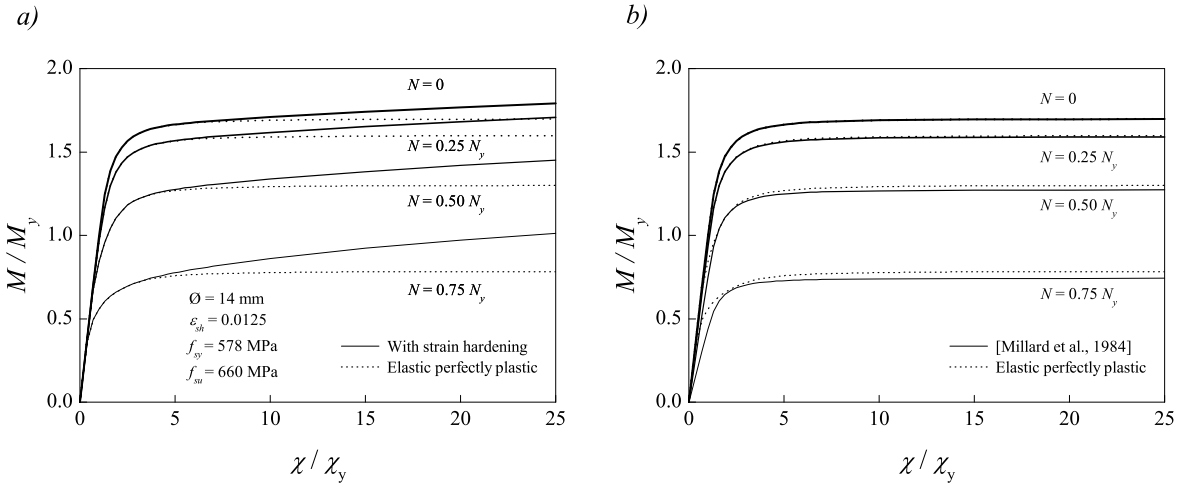

Figure 4.8: Influence of an axial force on the moment–curvature relationship of a reinforcing bar: a) influence of steel strain hardening (hot-rolled steel) and b) comparison between elastic perfectly plastic model and Millard's proposition

It should be noted that the plastic moment of a reinforcing bars is not constant and is a function of the axial force. Figure 4.8 shows the bending moment as a function of the curvature for different axial forces and clearly illustrates that the presence of axial forces significantly influences the plastic moment of a reinforcing bar.

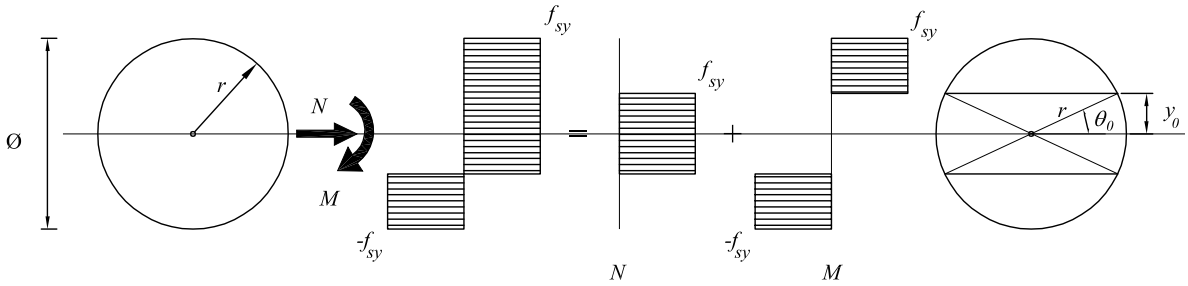

Figure 4.9: Plastic moment calculation of a reinforcing bar based on the theory of plasticity

The plastic moment of a reinforcing bar in the presence of an axial force can be calculated using the theory of plasticity as shown in Figure 4.9. A part of the area of the bar is assumed to carry the axial force and the rest of the area is attributed to the

development of the plastic moment. The plastic moment of the bar in the presence of an axial force can be calculated by

$$M_p = 2\int_{y_0}^{r} 2\sqrt{r^2 - y^2}\, y f_{sy} dy$$
$$M_p = \int_{\theta_0}^{\frac{\pi}{2}} 4r^2 \cos^2\theta \sin\theta f_{sy} d\theta = \frac{Ø^3}{6} f_{sy} \cos^3\theta_0 \tag{4.7}$$

The angle θ_0 can be obtained from the other equilibrium condition:

$$N = 2\int_0^{y_0} 2\sqrt{r^2 - y^2}\, f_{sy} dy = \int_0^{\theta_0} 4r^2 \cos^2\theta f_{sy} d\theta \tag{4.8}$$

The plastic moment can be numerically calculated. Millard and Johnson (1984) proposed a simplified method to estimate the plastic moment in the presence of an axial force:

$$M_p = \frac{Ø^3}{6} f_{sy}\left(1 - \frac{N^2}{N_y^2}\right) \tag{4.9}$$

where N_y is the axial yielding force of the bar. This equation gives a good correlation with the exact solution based on the theory of plasticity as shown in Figure 4.8.b. Substituting Equation 4.9 into Equation 4.6 results in the following equation:

$$V_{D,i} = N_I \sin\psi_D + \frac{Ø^3}{3L} f_{sy}\left(1 - \frac{N_I^2}{N_y^2}\right)\cos^2\psi_D \tag{4.10}$$

This equation describes V_D as a function of the axial force and the distance between two plastic hinges. The distance L is the most controversial parameter in this analysis and its interaction with the yielding of reinforcement and the crushing of the concrete should be considered. For a simplified analysis a rough estimation can be made. Vintzeleou and Tassios (1986) reported that a thickness of at least six to seven times the bar diameter is needed to prevent the splitting of concrete. Therefore, to simplify this plastic analysis, the following assumption is made:

$$L = (c + 8Ø)\cot\alpha \approx 15Ø \tag{4.11}$$

where c is the concrete cover and α is the angle of inclination of the punching cone. Results of this analysis for various bar diameters are shown in Figure 4.10. A comparison between the results of this analysis with available test data (Melo and Regan, 1998) is shown as well. It can be seen that although a rough assumption has been made to estimate the distance between two plastic hinges, the results are in relatively good agreement with the test results. Furthermore, Figure 4.10 shows that at a certain deformation, fracture of reinforcing bars occurs and the load drops rapidly. At this point, reinforcing bars reach their capacity because the axial strain in the reinforcing bars exceeds the ultimate tensile strain. This criterion can be used as a failure criterion for the rupture of the reinforcement and will be discussed later.

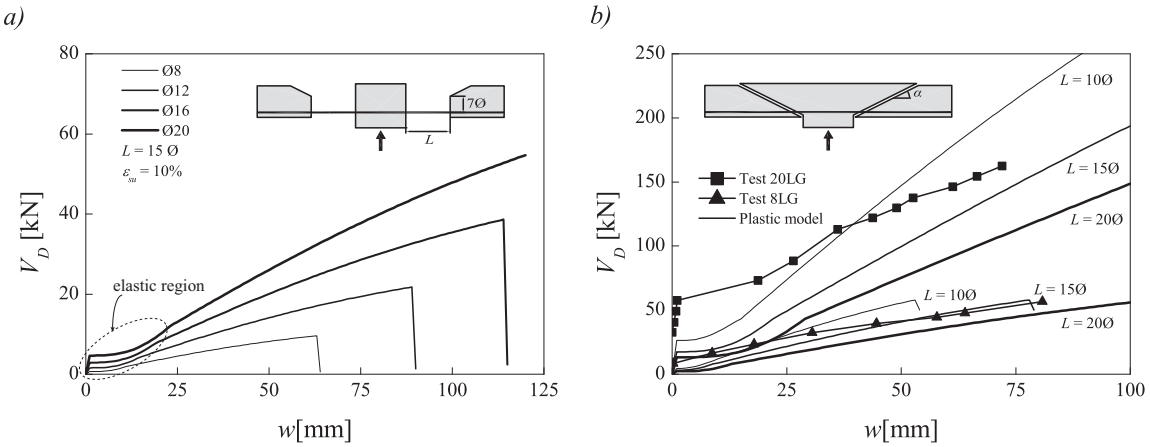

Figure 4.10: Response of reinforcing bars based on the proposed plastic analysis: a) influence of the bar diameter and b) comparison of experimental tests by Melo and theoretical response (Melo and Regan, 1998)

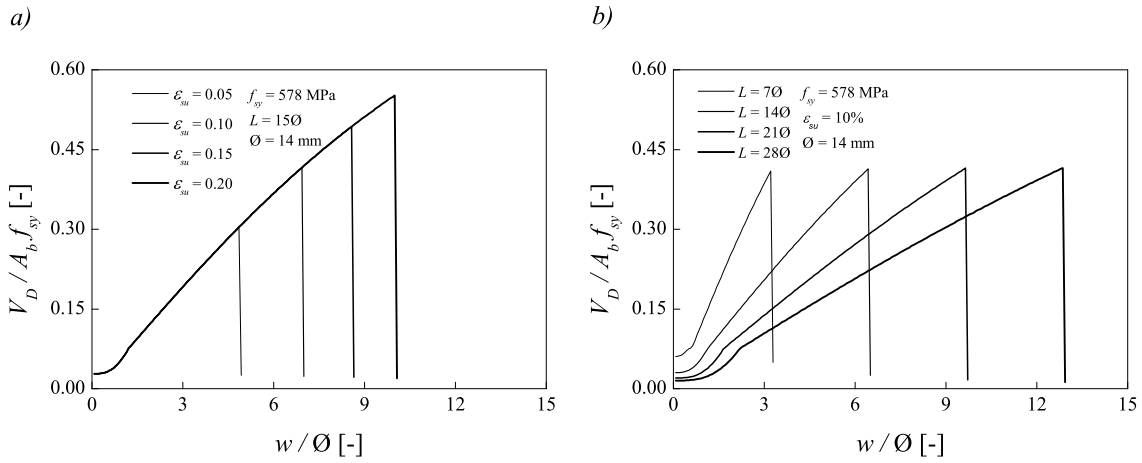

Figure 4.11: Parametric analysis : a) influence of steel ultimate strain and b) influence of distance between two plastic hinges along a reinforcing bar

Figure 4.11 shows the effect of the ultimate tensile strain of the reinforcement as well as the influence of the distance between plastic hinges on the post-punching behavior. It shows that the ultimate tensile strain affects significantly the post-punching behavior. An increase of the ultimate strain results in an increase of strength and deformation capacity. This is attributed to the failure criterion which is based on the maximum strain in reinforcing bars. Figure 4.11.b shows the effect of the distance between plastic hinges on the post-punching strength and deformation capacity. Although it has a significant influence on the stiffness and the deformation capacity, it has almost no effect on the post-punching strength. Considering $N_I = N_y$ and neglecting shearing of the bar with reference to Figure 4.7 and Equation 4.10, the strain in the bar at failure as well as the ultimate strength can be calculated as

$$\varepsilon_{su} = \frac{1}{\cos\psi_{D,max}} - 1$$
$$V_{D,max} = A_{sb} f_{sy} \sin\psi_{D,max} \tag{4.12}$$

where $\psi_{D,max}$ is the angle of inclination of integrity reinforcing bars at failure, and $V_{D,max}$ is the post-punching strength provided by the integrity reinforcement. For a constant ultimate strain ε_{su}, the angle of inclination of the reinforcing bar at failure is constant and thus the post-punching strength remains constant independent from the distance between the plastic hinges. However, the stiffness and the deformation capacity is significantly affected by the increase of the distance between plastic hinges. As shown in Figure 4.7, the deflection at failure can be calculated by

$$\tan\psi_{Du} = \frac{w_u}{L} \tag{4.13}$$

Thus, the maximum deflection is proportional to the distance between plastic hinges as the angle of inclination of the reinforcing bar remains constant for a constant ultimate steel strain. To gain a better understanding of the actual behavior, the influence of concrete crushing, yielding of the reinforcement, curvature localization, interaction of shear and tension, slip, and bar pullout should be considered.

4.6 Destruction of concrete

Figure 4.5 shows the zones that are susceptible to the destruction of concrete. The progressive destruction of the punching cone and the concrete above the integrity reinforcement is predictable. As the distance between the plastic hinges is mainly related to the destruction of concrete, the way how this progressive destruction occurs should be investigated. The loading on the concrete above the integrity reinforcement is comparable to an embedment close to a free edge subjected to shear perpendicular to the plane of the slab. This force is equal to the vertical component of the force developed in the integrity reinforcement. Thus, it is appropriate to deal with the failure process of the integrity reinforcement likewise the pullout resistance of a bar in embedment concrete. The approach is based on assuming a concrete failure cone with an angle γ. Figure 4.12. shows the failure due to reinforcing bars subjected to shear loading.

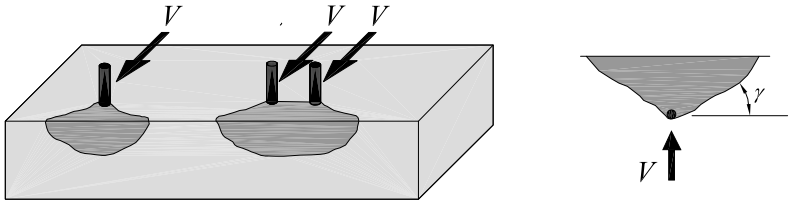

Figure 4.12: Concrete breakout cone due to reinforcing bars acting against concrete

A method for calculating the pullout strength of an embedment reinforcing bar has been given in ACI for nuclear safety related structures (ACI 349, 2001). Based on this method, if the thickness of concrete above the embedment is not sufficient to fully develop the strength of the embedment, failure is entirely controlled by the tensile strength of the concrete. Therefore, the strength can be calculated as the vertical component of the tensile stresses acting on the surface of a concrete cone. The strength of an embedment can thus be calculated by

$$V_{con} = A_{ch} f_{ct,eff} \tag{4.14}$$

where V_{con} is the concrete breakout strength, A_{ch} is the horizontal projection of the conical failure surface and $f_{ct,eff}$ is the effective tensile strength of concrete. The breakout cone angle γ varies from 35°to 45°(ACI 349, 2001), which is assumed to be 45°in the present study. The maximum concrete breakout strength can thus be calculated by

$$V_{con,max} = \frac{\pi}{2} d_1^2 f_{ct,eff} \tag{4.15}$$

where d_1 is the depth of concrete over the reinforcing bar. Figure 4.13 shows the concrete breakout cone for one and two reinforcing bars protruding from the concrete surface. As can be seen, this equation does not depend on material properties of the reinforcement and only deals with the concrete over the integrity reinforcement. For the reinforcing bars close to free edges, the projection area for the conical failure surface is reduced. Moreover, the projection area is further reduced if the bar spacing is less than half the depth of the concrete over the bars. The maximum breakout strength of the concrete above two reinforcing bars can be calculated by

$$\begin{aligned} V_{con,max} &= A_{ch} f_{ct,eff} \\ A_{ch} &= 4\{(\pi - \theta_j) d_1^2 + \frac{1}{2} s d_1 \sin\theta_j\} \end{aligned} \tag{4.16}$$

where $\theta_j = \cos^{-1}(s / 2d_1)$, and s is the bar spacing (Figure 4.13.f). Similar equations can be derived for more than two reinforcing bars (Appendix B).

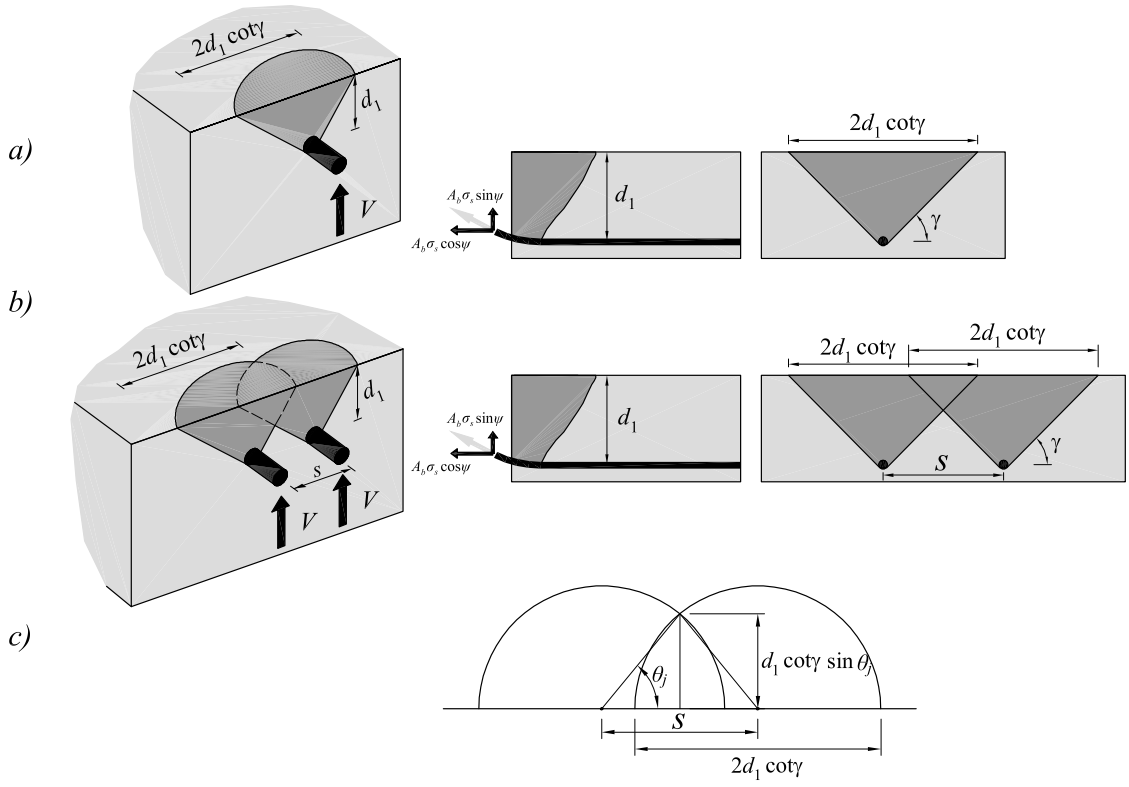

Figure 4.13: ACI model for concrete breakout strength: a) concrete breakout cone for a single reinforcing bar,b) concrete breakout cone for two reinforcing bars, and c) horizontal projection of the conical failure surface

Equation 4.16 gives only an estimation of the maximum concrete breakout strength and provides no information on the progressive destruction of the concrete over the reinforcing bars. Figure 4.14 shows the concept of a modified method that can deal with the progressive destruction of the concrete. The figure shows the failure process of a single bar subjected to shear and tension as well as the horizontal projection area necessary to calculate the concrete breakout strength.

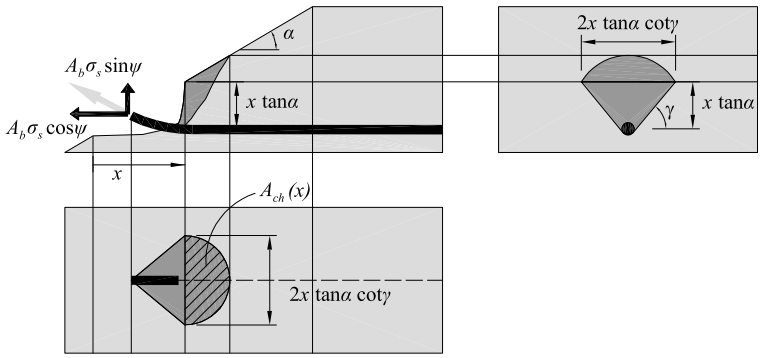

Figure 4.14: Proposed model for the progressive destruction of concrete over reinforcing bars

As can be seen, an arbitrary section along the reinforcing bar at a distance of x from the crack has been selected. At this point, the thickness of the concrete over the bar is equal to $x \cdot \tan\alpha$, and the diameter of the projection area is $2 \cdot x \cdot \tan\alpha \cot\gamma$. Therefore, the concrete breakout strength at this section can be calculated by

$$V_{con}(x) = \frac{\pi}{2}(x \tan\alpha \cot\gamma)^2 f_{ct,eff} \tag{4.17}$$

where α in an angle of inclination of the punching cone and γ is the angle of the breakout cone. The effective concrete tensile strength is expressed as

$$f_{ct,eff} = \eta_D f_{ct} = \eta_D (0.3 f_c^{2/3}) \tag{4.18}$$

where η_D is a reduction factor to consider that the tensile stress is assumed to vary from a maximum at the edge of reinforcing bars to a minimum at the surface of the slab. A good correlation with the experimental results has been found by adopting $\eta_D = 0.6$. Figure 4.15 shows the results of this analysis for various compressive strengths.

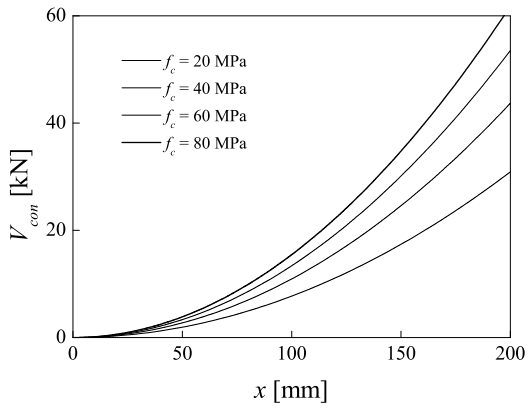

Figure 4.15: Theoretical concrete breakout strength along a reinforcing bar

Figure 4.16 shows the possible failure mode for two reinforcing bars after punching failure if their bar spacing is less than half the depth of the concrete over the bars. Hence, the concrete breakout strength will be a function of the bar spacing and thus of the reinforcement layout.

The horizontal projection of concrete failure cone is reduced in the presence of two reinforcing bars and hence the concrete breakout strength at a distance x from the punching crack can be calculated by

$$V_{con}(x) = A_{ch}(x)\, f_{ct,eff}$$
$$A_{ch}(x) = 4\{(\pi - \theta_j)\left(x \tan\alpha \cot\gamma\right)^2 + \frac{1}{2} s \left(x \tan\alpha \cot\gamma\right) \sin\theta_j\} \tag{4.19}$$

$$\theta_j = \cos^{-1}\left(\frac{s}{2x \tan\alpha \cot\gamma}\right) \tag{4.20}$$

Figure 4.17 shows the influence of different parameters on the concrete breakout strength according to the destruction of the concrete over the reinforcing bars. The effects of the concrete compressive strength, the angle of inclination of the punching cone, the angle of the concrete breakout cone, and the bar spacing are investigated.

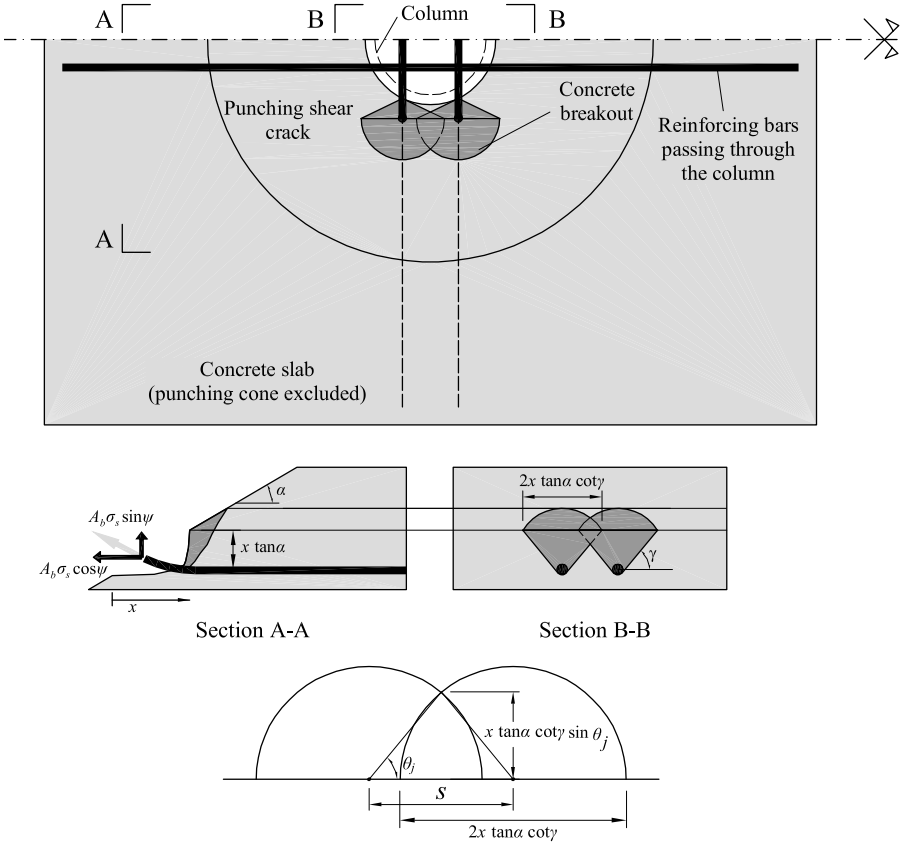

Figure 4.16: Destruction of concrete over reinforcing bars

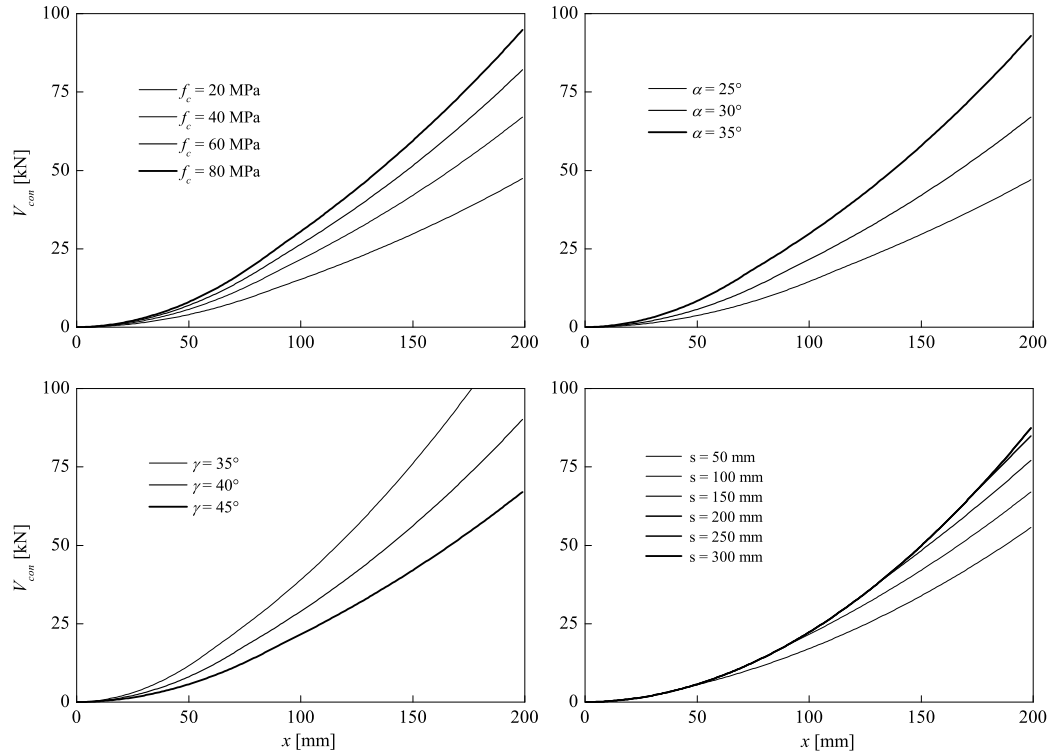

Figure 4.17: Influence of concrete compressive strength, angle of inclination of punching cone, angle of concrete breakout cone, and bar spacing on concrete breakout strength

Figure 4.17 shows that by increasing the concrete compressive strength, an increase of the concrete breakout strength is expected as the concrete tensile strength is directly related to the concrete compressive strength (Equation 4.18). Furthermore, it shows the influence of the angle of inclination of the punching cone. The increase of the angle of inclination of the punching cone increases the concrete breakout strength. Since the projection area is proportionate to this angle (Equation 4.19), an increase of this angle will increase the concrete breakout strength.

Moreover, the effect of the breakout cone angle is negative and the concrete breakout strength decreases when the breakout cone angle increases. This is also related to the projection area. An increase in the breakout cone angle results in a decrease of the projection area and consequently the concrete breakout strength decreases. In addition, the influence of the bar spacing is shown in Figure 4.17. It shows that by increasing the bar spacing, the breakout strength increases. If the bar spacing passes a certain limit, the increase of the bar spacing has no influence on the breakout strength. In fact, if the bar spacing exceeds the diameter of the breakout cone, there is no interaction between the adjacent breakout cones and thus there is no reduction of the projection area (Figure 4.16).

4.6.1 Concrete breakout and spalling of concrete cover

Figure 4.18 shows concrete breakout and spalling of concrete in the post-punching phase. The former occurs for tensile reinforcement acting against the punching cone and the latter occurs for tensile reinforcement acting against the concrete cover.

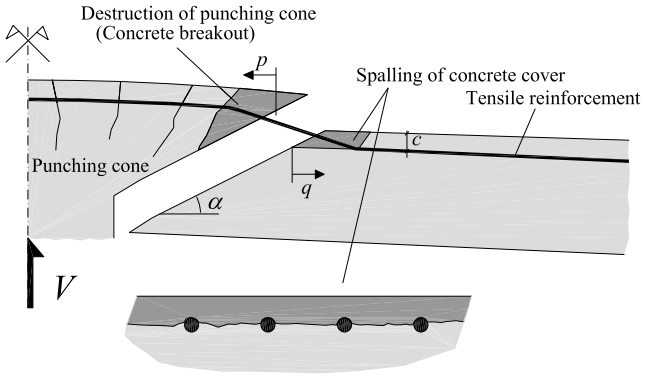

Figure 4.18: Concrete breakout and spalling in the post-punching phase

Concrete breakout failure occurs for relatively large thickness of concrete over reinforcing bars. Whereas, spalling of concrete is very probable for small concrete thicknesses. The mechanism of both failure modes is comparable since the strength can be calculated as the vertical component of tensile stresses acting on the surface of a certain concrete cone. Thus, the spalling strength is the sum of tensile stresses acting on the projection areas of small breakout cones.

It should be noted that even considering breakout failure for concrete cover will lead to the same result as the spalling of concrete. In the presence of the tensile reinforcement, the interaction between projection areas of the breakout cones should be considered. In the case of bar spacing larger than twice the concrete cover, which is a practical range for concrete structure, the projection area will be exactly the same as the area of the spalling of the concrete cover. Figure 4.19 shows the projection area for both the spalling of the concrete cover and the concrete breakout of the punching cone.

As the concrete cover is constant, it seems that the spalling strength should also be constant. This could be legitimate if tensile reinforcing bars act separately on the concrete cover. However, in the present circumstances, tensile reinforcing bars act as a mesh against a circumferential ring of concrete cover outside of the punching cone as can be seen in Figure 4.19. Although the width and the thickness of this ring are equal to the concrete cover and remain constant, its diameter is progressively increasing and thus the spalling strength of the concrete cover is proportionally increasing as well.

The following equations have been derived based on Equation 4.14 to compute the spalling strength of the concrete cover as well as the breakout strength of the punching cone (Figure 4.18):

$$V_{spal}(q) = \begin{cases} \pi q \tan\alpha (D + 2q)(\eta_M f_{ct}) & \text{for} \quad q \le c \cdot \cot\alpha \\ \pi c (D + 2q)(\eta_M f_{ct}) & \text{for} \quad q > c \cdot \cot\alpha \end{cases} \tag{4.21}$$

$$V_{con}(p) = \pi (D - 2p)\, p \tan\alpha (\eta_M f_{ct}) \tag{4.22}$$

where p and q are the distances from the punching crack along the punching cone and spalled zone, respectively, $D = a + 2d \cdot \cot\alpha$ is the diameter of the original punching cone, V_{spal} is the concrete spalling strength, and a is the column width. A reduction factor η_M is adopted to consider the variation of the tensile stress from a maximum at the edge of reinforcing bars to a minimum at the surface of the slab. A good correlation

with the experimental results has been found by adopting η_M = 0.4. Integrity reinforcing bars act against the concrete in the compression zone of the slab and tensile reinforcing bars act against the concrete in the tension side of the slab. Apparently, the state of cracking at the compression and at the tension side of the slab is not the same because of the severe cracking at the tension side due to bending and shear.

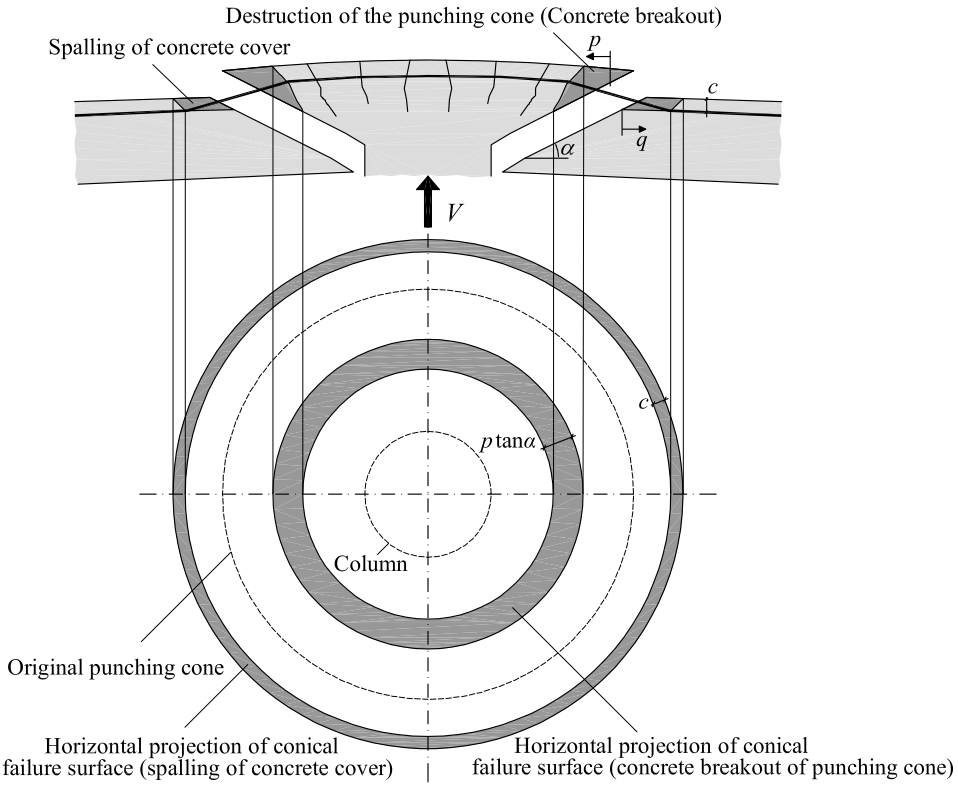

Figure 4.19: Projection area of the concrete breakout of punching cone and projection area of spalled concrete cover

The vertical component of the force exerted to concrete by tensile reinforcing bars is the same for the concrete cover and the punching cone. Thus, the following equations can be derived to relate the rate of progressive destruction of the cover and that one of the punching cone:

$$\begin{cases} (D+2q)q\tan\alpha = (D-2q)\,p\tan\alpha & \text{for} \quad q \le c\cdot\cot\alpha \\ (D+2q)c = (D-2p)\,p\tan\alpha & \text{for} \quad q > c\cdot\cot\alpha \end{cases} \tag{4.23}$$

The aforementioned equations for the spalling strength of the cover and the concrete breakout of the punching cone are compared in Figure 4.20. In addition, it plots the relationship between *p* and *q*, which is in fact, the relationship between the progression of the concrete destruction of the concrete cover and of the punching cone.

The progression of spalling of the cover can continue to the end of the slab if the tensile reinforcement is well anchored. However, the progression of concrete breakout of the punching cone is restricted. As Figure 4.20.a shows, the breakout strength increases to a certain point at which it becomes constant since there is no further progression and the load goes directly to the column. Figure 4.20.b similarly shows the simultaneous

progression of concrete destruction up to a certain limit. Beyond this limit, no further progressive destruction of the concrete of the punching cone occurs.

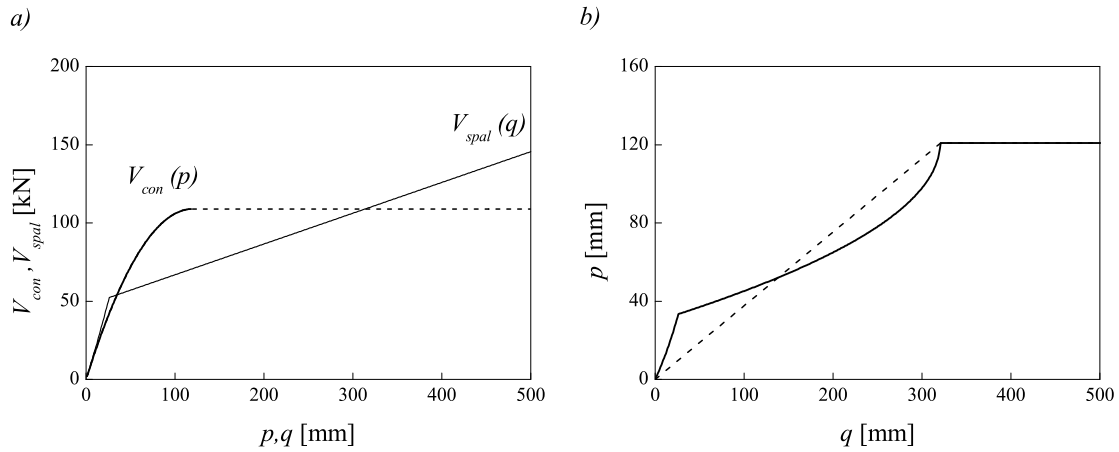

Figure 4.20: Progressive destruction of concrete: a) concrete breakout strength of the punching cone and spalling strength of concrete cover and b) relationship between destruction length along the punching cone (p) and destruction length of concrete cover due to spalling (q)

So far, the behavior of the concrete above integrity bars, possible modes of failure, and the influence of different parameters on the progressive destruction of concrete have been studied. The subsequent sections deal with the role of the reinforcing bars, the force that they induce to the concrete, and the way how they interact with the progressive destruction.

4.7 Shear transfer through reinforcing bars

As pointed out before, the only remaining link between the punching cone and the rest of the slab is the reinforcing bars after punching failure has occurred, and they play a major role in the post-punching shear transfer. Although the behavior of the tensile reinforcement and the integrity reinforcement are different, the mechanisms of shear transfer such as concrete breakout, spalling of concrete cover are quite similar.

Figure 4.21 shows the mechanism proposed for the post-punching shear transfer. The contribution of the tensile reinforcement and the contribution of the integrity reinforcement can be estimated in a similar manner. The elongation of reinforcing bars can be obtained from geometrical considerations. For the elastic phase, the deformed shape of a reinforcing bar can be assumed as a cubic function (Figure 4.21.b):

$$f(x) = C_1 x^3 + C_2 x^2 + C_3 x + C_4 \tag{4.24}$$

To define the shape, four boundary conditions are needed. Considering displacements and rotations at both ends of the curved part define the shape of the deformed reinforcing bar. Because of very large deflections that occur, the deformation of the concrete supporting the bars can be neglected and the following shape function can be described by

$$f(x) = \frac{-2w}{L^3}x^3 + \frac{3w}{L^2}x^2 \tag{4.25}$$

Calculating the elongation of a reinforcing bar, with a deflection of *w*, allows to determine the strain in the bar:

$$\varepsilon_s = \frac{1}{L}\int_0^L \sqrt{1+(df/dx)^2}\,dx - 1 \tag{4.26}$$

Based on the constitutive law for the reinforcement (Cosenza *et al.*, 1993), the following equations can be derived to predict the shear transfer by tensile and integrity reinforcement at the elastic phase:

$$\begin{aligned} V_{M,i} &= A_b E_s \varepsilon_s \sin\psi_M + V_I \cos\psi_M \\ V_{D,i} &= A_b E_s \varepsilon_s \sin\psi_D + V_I \cos\psi_D \end{aligned} \tag{4.27}$$

where V_I can be calculated using the beam on elastic foundation analogy as

$$\begin{aligned} V_I &= w\lambda^3 E_s I_b \\ \lambda &= \left(k_c Ø / 4E_s I_b\right)^{1/4} \end{aligned} \tag{4.28}$$

where $k_c = 127\ \ f_c / Ø^{2/3}$ is the concrete bearing stiffness (Soroushian *et al.*, 1986). When the plastic hinges develop, the abovementioned calculation is no longer valid. Figure 4.21.c shows a suitable deformed shape of a reinforcing bar for the plastic analysis so that the strain in the bar can be calculated by

$$\varepsilon_s = \frac{1}{\cos\psi} - 1 \tag{4.29}$$

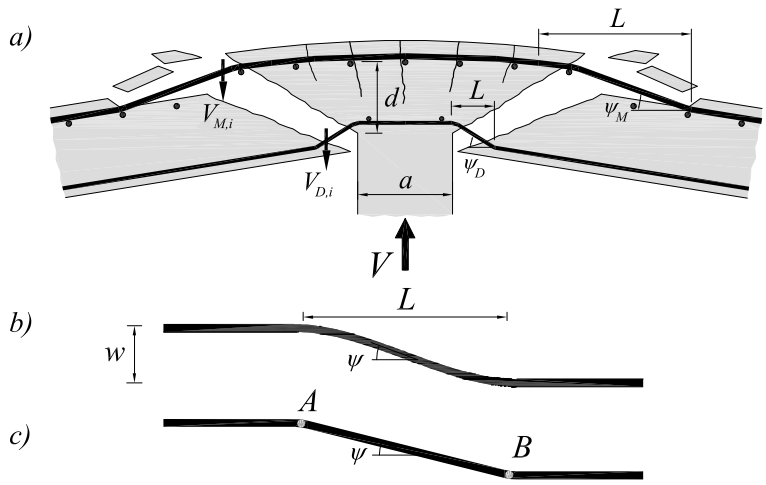

Figure 4.21: Proposed model: a) geometry, b) deformed shape of a reinforcing bar in elastic phase, and c) deformed shape of a reinforcing bar after the development of plastic hinges

Thus, the tensile reinforcement contribution and the integrity reinforcement contribution to the post-punching strength can be calculated by

$$V_{M,i} = N_I \sin\psi_M + \frac{Ø^3}{3L} f_{sy}(1-\frac{N_I^2}{N_y^2})\cos^2\psi_M$$
$$V_{D,i} = N_I \sin\psi_D + \frac{Ø^3}{3L} f_{sy}(1-\frac{N_I^2}{N_y^2})\cos^2\psi_D \quad (4.30)$$
$$N_I = A_b\sigma_s$$

Finally, a summation of the tensile reinforcement contribution and the integrity reinforcement contribution is needed to calculate the post-punching strength:

$$V_{pp} = V_M + V_D = \sum_i^m V_{M,i} + \sum_i^n V_{D,i} \quad (4.3)$$

4.7.1 Distance between two plastic hinges

The distance between the plastic hinges L has not yet been determined. As pointed out earlier, this value is the most controversial parameter in this analysis. To determine this value, it is necessary to consider the interaction between the forces exerted to the concrete by the reinforcing bars and the progressive destruction of the punching cone and the concrete cover. To that aim, the effects of concrete breakout and spalling of concrete cover should also be considered. As can be seen in Figures 4.3, 4.14, and 4.21, the distance between the plastic hinges can be calculated by

$$L = \begin{cases} L(p,q) = p+q & \text{Tensile reinforcement} \\ L(x) = x + c\cdot\cot\alpha & \text{Integrity reinforcement} \end{cases} \quad (4.31)$$

For the tensile reinforcement p and q are interrelated according to Equation 4.23. Thus, for a given q, p is known and the distance between the plastic hinges is known as well. Hence, the force developed in the tensile reinforcement can be calculated directly. Furthermore, q is directly involved in computing the spalling strength of the concrete cover and indirectly in computing the concrete breakout strength of the punching cone. Therefore, to determine L, the force developed in the tensile reinforcement should equate to the spalling strength of the cover or the concrete breakout strength of the punching cone. For this calculation an iterative procedure is proposed as follows.

For a given deflection w, at the beginning of the procedure, q is assumed to be zero. Although tensile stresses are developed in the reinforcement, the spalling strength of the concrete cover and the concrete breakout strength are zero. Consequently, the equilibrium conditions are not satisfied. To satisfy the equilibrium conditions, q is increased so that the calculated spalling strength (Equation 4.21) and the concrete breakout strength (Equation 4.22) are not zero. Hence, they can be compared to the forces developed in the tensile reinforcement (Equations 4.27 and 4.30). This incremental procedure is repeated until the equilibrium conditions are satisfied. At this point, the forces developed in the tensile reinforcement, the concrete breakout strength and the spalling strength of the cover are equal. This procedure leads to the calculation of the contribution of the tensile reinforcement to the post-punching shear transfer.

For the integrity reinforcement L is also given by Equation 4.31. The procedure is similar to that one of the tensile reinforcement and the force developed in the integrity reinforcement (Equations 4.27 and 4.30) is compared to the concrete breakout

strength (Equation 4.19). After the equilibrium conditions are satisfied, the force developed in the integrity reinforcement and the concrete breakout strength are equal. The calculated force is the contribution of the integrity reinforcement to the post-punching shear transfer (Equation 4.3).

4.7.2 Effect of localized curvature

This section presents the influence of induced curvature due to transverse displacement at the faces of the punching crack. As the proposed model is based on computing axial steel strain, the influence of the induced curvature on the strain profile should be thoroughly investigated.

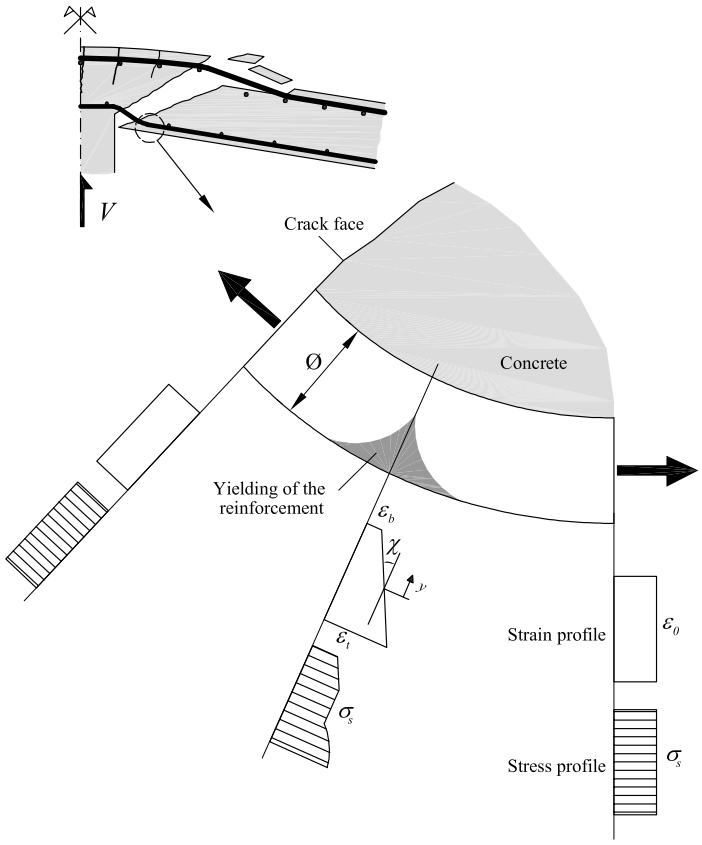

Figure 4.22: Effects of curvature localization

Figure 4.22 shows the profile of the axial strain and the axial stress at three sections in the curvature-influenced zone. The curvature can be computed at any section by

$$\chi = \frac{\varepsilon_t - \varepsilon_b}{\text{Ø}} \tag{4.32}$$

where ε_t denotes the axial strain at the extreme tension fiber of the bar. The axial strain at any fiber can be calculated using the following equation:

$$\varepsilon(y) = \varepsilon_0 + \chi \cdot y \tag{4.33}$$

where ε_0 is the mean axial strain of the bar, and y is the local coordinate measured from the center of the bar as shown in Figure 4.22. The mean stress and the mean strain, which are sectional averaged stress and strain, are computed by assuming that a plane section remains plane. Therefore, they are calculated by the constitutive law of the steel reinforcement:

$$\bar{\sigma} = \frac{1}{A_b} \int_{-\frac{Ø}{2}}^{\frac{Ø}{2}} \sigma(\varepsilon_0 + \chi \cdot y) dA(y) \tag{4.34}$$

$$\bar{\varepsilon} = \frac{1}{A_b} \int_{-\frac{Ø}{2}}^{\frac{Ø}{2}} (\varepsilon_0 + \chi \cdot y)\, dA(y) \tag{4.35}$$

The profile of the axial strain shows that the value of the strain at the extreme tension fiber is more than the mean axial strain of the bar. The source of this increase is the local curvature induced by the transverse displacement. Therefore, the tensile strain at the extreme fiber can be more than the yielding strain while the rest of the reinforcing bar is in the elastic phase. It also can be concluded that the maximum strain can reach the ultimate strain while the mean axial strain is far from the ultimate axial strain. Thus, the influence of the induced local curvature on the strain profile and the strain based failure criterion is significant.

4.7.2.1 Compatibility between displacements and curvature distribution

Using the assumptions of the classical beam theory, the compatibility conditions require that the sum of the double integral of the curvature distribution along the bar axis must equal to the displacement of the bar. In addition, the sum of the integral of the curvature distribution along the bar axis must equal to the rotation of the bar. This geometrical compatibility, which remains true irrespective of bar elastic and plastic behavior is one of the key relations in computational models. Thus, the rotation of the bar can be computed by

$$\psi = \int_0^{\ell_c} \chi(x) dx \tag{4.36}$$

where ℓ_c is the length of the curvature-influenced zone. The rotation of the bar in the developed model can be calculated by geometrical considerations. However, the curvature distribution along the bar and the length of the curvature-influenced zone has not yet been calculated. This calculation of the curvature distribution and its length is treated in the subsequent sections.

4.7.2.2 Curvature-influenced zone

At small deflections when the behavior can be considered elastic, the curvature distribution can be computed using the beam on an elastic foundation analogy. Using the classical beam equation, the following differential equation can be derived:

$$E_s I_b \frac{d^4 w}{dx^4} = -k_c Ø w \tag{4.37}$$

where I_b is the moment of inertia of the bar section. The general solution can be expressed as

$$w(x) = e^{\lambda x}(C_5 \cos \lambda x + C_6 \sin \lambda x) + e^{-\lambda x}(C_7 \cos \lambda x + C_8 \sin \lambda x) \tag{4.38}$$

where $\lambda = \left(k_c Ø / 4E_s I_b\right)^{1/4}$.

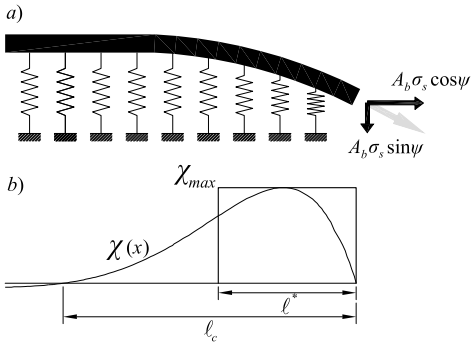

Figure 4.23: Curvature-influenced zone: a) beam on elastic foundation analogy and b) curvature distribution along a reinforcing bar in elastic and plastic phases

Considering trivial assumptions that if $x \to \infty$, then $y \to 0$, and $M \to 0$, it can be concluded that C_5 and C_6 must be zero and hence

$$w(x) = e^{-\lambda x}(C_7 \cos \lambda x + C_8 \sin \lambda x) \tag{4.39}$$

The remaining integration constants, C_7 and C_8, can be determined if $x \to 0$, then $M \to 0$, and $V \to V$. Thus, the curvature along the bar is given by

$$\chi(x) = -\frac{V}{\lambda} e^{-\lambda x} \sin \lambda x \tag{4.40}$$

The curvature is non uniform with zero curvature at, and some distance away from, the crack face as shown in Figure 4.23. Therefore, the length of the curvature-influenced zone can be calculated by

$$\ell_c = \frac{\pi}{\lambda} \approx 6Ø \tag{4.41}$$

This elastic analysis has been basically utilized for computing the length of the curvature-influenced zone since test results of curvature profiles for a wide range of variation of parameters influencing the curvature-influenced zone are not available. However, the beam on elastic foundation analogy can not be considered reliable because of the highly nonlinear behavior of steel and concrete in the post-punching phase.

Figure 4.24 shows the measured curvature distribution along reinforcing bars for both the elastic and the plastic behavior (Dei Poli *et al.*, 1993; Qureshi and Maekawa, 1993). As Figure 4.24 shows, the proposed length equal to six times the bar diameter for curvature-influenced zone is in a good agreement with test results in which loading was

continued up to and slightly above the yielding of steel. As Figure 4.24.b shows, there is a shift of the curvature-influenced zone with increased deflection (Dei Poli *et al.*, 1992). The physical meaning of this shift can be attributed to the plastic relaxation of the reaction springs.

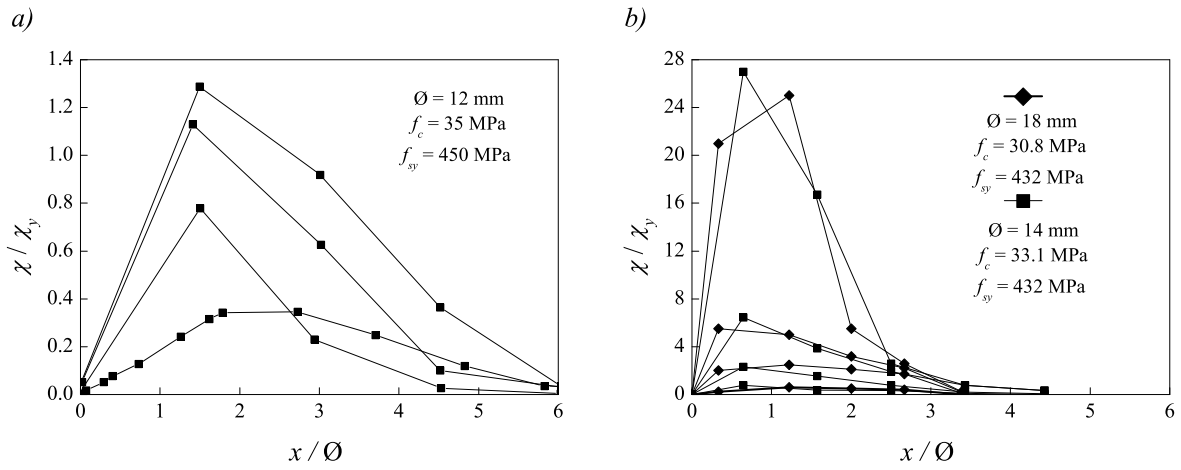

Figure 4.24: Curvature distribution along a reinforcing bar: a) loading up to yielding (Qureshi and Maekawa, 1993) and b) loading up to fracture (Dei Poli et al., 1993)

To simplify the calculation of Equation 4.36, it can be assumed that a full plastic response of concrete occurs in a limited area under the bar according to Figure 4.23.b. In this area, the behavior of concrete is fully plastic and the curvature is constant and equal to the maximum curvature (Figure 4.23.b). It should be noted that the actual reaction stress distribution underneath a bar is not uniform, however, the bearing stresses in the critical region e.g. near the crack faces tend to become uniform, especially as the ultimate condition is approached (Dulacska, 1972; Soroushian *et al.*, 1986). Thus, the rotation of the bar is given by

$$\psi = \int_0^{\ell_c} \chi(x)dx = \int_0^{\ell^*} \chi_{\max} dx = \ell^* \cdot \chi_{\max} \tag{4.42}$$

where ℓ^* is the length of the bar with a fully plastic behavior of the concrete underneath. This length can be calculated by

$$\ell^* = \frac{V_{pp}}{2Ø\sigma_b} \tag{4.43}$$

where σ_b is the bearing stress of the concrete. As discussed in Chapter 2, very scattered values are reported for the bearing stress ranging from 1.8 to 6.5 f_c. Thus, this dispersion does not allow for a realistic evaluation of this length at ultimate limit state at which concrete shows a non-linear behavior. Therefore, according to the experimental results this length is assumed to be half of the length of the curvature-influenced zone in the elastic phase as shown in Figure 4.23. As a result, the maximum curvature is given by

$$\chi_{\max} = \frac{\psi}{3Ø} \tag{4.44}$$

Finally, the maximum tensile strain in the curvature-influenced zone can be calculated by substituting Equation 4.44 into Equation 4.33:

$$\varepsilon_{\max} = \varepsilon_0 + \frac{\psi}{6} \tag{4.45}$$

This value has been used as a failure criterion in the proposed model. The model always calculates the mean strain and the rotation of the bar for any given deflection, and the maximum strain in the reinforcing bar developed in the curvature-influenced zone can be computed by Equation 4.45. The maximum strain is then compared to the ultimate tensile strain. This failure criterion will determine the rupture of the reinforcement.

4.7.3 Effect of bond deterioration and bar slip

A punching shear crack leads to an increase in the axial strain in the longitudinal bars crossing the crack. As a result of the bond deterioration between steel and concrete and an accumulation of axial strains along the reinforcement inside the crack, the extension and the slip of the reinforcing bar at the crack can be significant. The bond performance near the punching crack may easily be deteriorated due to splitting and crushing of the concrete around the bar. The concept of the bond deterioration zone has been considered in the past by considering a linear degradation of the bond stress from somewhere inside the concrete to the crack face. The bond stress distribution, the axial stress, and the axial strain along a reinforcing bar are schematically shown in Figure 4.25. The bond stress decreases gradually to zero representing the locus from which the conical bond micro cracks reach to the surface of the punching crack. The slip resulting from accumulated axial strains in the reinforcing bar can be calculated by integrating the strains over the portion of the bar between the crack face and the location with no axial strain.

Fernandez Ruiz, Muttoni and Gambarova proposed an analytical model that describes the pre and post yielding response of bond in reinforced concrete structures (Fernandez Ruiz *et al.*, 2007). They assumed that bond is locally affected by the lateral expansion and contraction of the bar and bond strength and stiffness are locally controlled by the development of conical cracks close to the crack surface. They stated that "because of the affinity between the bond stress and the bar slip, and between the bond stress and the steel strain, the equation can be integrated for any given bond-stress-slip law". Thus, they employed two bond-stress-slip laws, namely a square-root model and a rigid-plastic model to perform a detailed study of the pre and post yielding behavior of bond in anchored bars and tension ties. According to the square-root model, strain profile and slip along a reinforcing bar can be calculated by

$$\varepsilon_s = \begin{cases} \left(\sqrt{\varepsilon_{sy}} - \dfrac{2\tau_{b,max}(x-\ell_p)}{E_s \varnothing \sqrt{\varepsilon_{sy}}}\right)^2 & \text{for} \quad x > \ell_p \\ \varepsilon_{bu} - (\varepsilon_{bu} - \varepsilon_{sy}) \exp\left[\dfrac{4\tau_{b,max}(x-\ell_p)}{E_h \varnothing (\varepsilon_{bu} - \varepsilon_{sy})}\right] & \text{for} \quad x \le \ell_p \end{cases} \tag{4.46}$$

$$\text{slip} = \begin{cases} \dfrac{E_s \varnothing \sqrt{\varepsilon_{sy}}}{6\tau_{b,max}} \left(\sqrt{\varepsilon_{sy}} - \dfrac{2\tau_{b,max}(x-\ell_p)}{E_h \varnothing \sqrt{\varepsilon_{sy}}} \right)^3 & \text{for} \quad x > \ell_p \\ \dfrac{f_{sy}\varnothing\varepsilon_{sy}}{6\tau_{b,max}} + \varepsilon_{bu}(\ell_p - x) - \dfrac{\varnothing E_h (\varepsilon_{bu}-\varepsilon_{sy})^2}{4\tau_{b,max}} \left(1 - \exp\left[\dfrac{4\tau_{b,max}(x-\ell_p)}{E_h \varnothing (\varepsilon_{bu}-\varepsilon_{sy})} \right] \right) & \text{for} \quad x \le \ell_p \end{cases} \tag{4.47}$$

where $\tau_{b,max}$ is the maximum bond stress equal to $f_c^{2/3}$, E_h is the hardening modulus of steel, and ε_{bu} is a parameter associated to the rib height and the hardening modulus of the bar. There is a good agreement between theoretical and experimental results when $0.07 < \varepsilon_{bu} < 0.12$

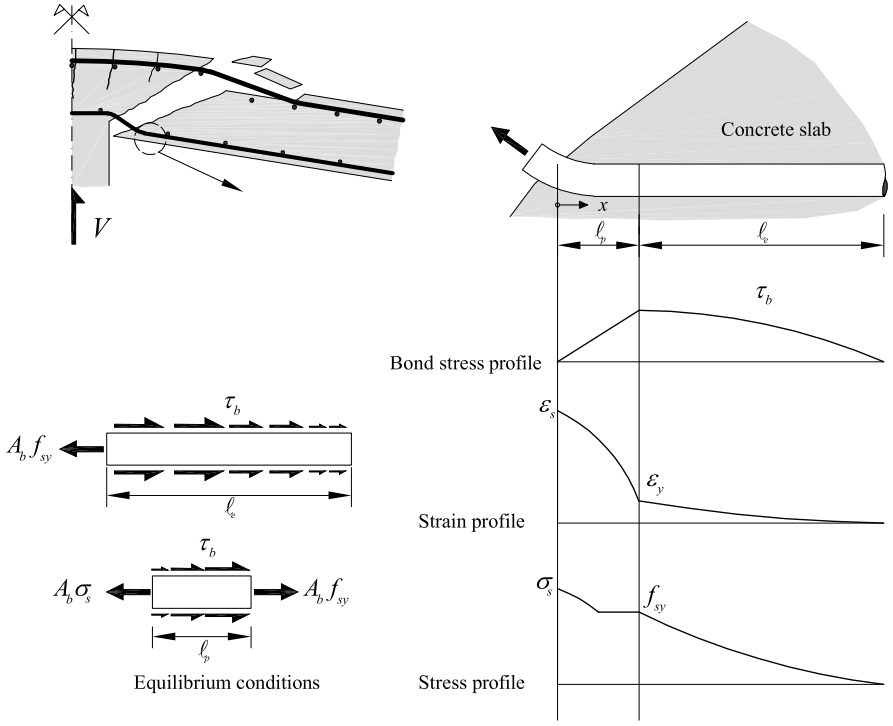

Figure 4.25: Profiles of bond stress, axial stress and strain along a reinforcing bar

Equation 4.47 expressed the strain and the slip along the bar as a function of the plasticized length of the bar. The plasticized length can be obtained from the first part of the proposed equation as

$$\ell_p = \frac{E_h \varnothing (\varepsilon_{bu} - \varepsilon_{sy})}{4\tau_{b,max}} \ln\left[\frac{\varepsilon_{bu} - \varepsilon_{sy}}{\varepsilon_{bu} - \varepsilon_s} \right] \tag{4.48}$$

Substituting Equation 4.48 into Equation 4.47 provides the slip at the crack plane as a function of the strain in the bar. As the developed mechanical model calculates the axial strain in the reinforcing bar, the influence of the bar slip on the post-punching behavior can be considered.

4.8 Bent-up bars

The methodology used to develop the mechanical model can be extended for predicting the post-punching behavior of slabs with bent-up bars. The concept of concrete breakout, maximum concrete breakout strength, and the calculation of the forces in reinforcing bars remain the same. However, the interaction between the progressive destruction within and outside of the punching cone should be reinvestigated in relation to the new geometry of the reinforcement.

Similar to integrity reinforcement, the failure process is related to the concrete breakout. To investigate the progressive destruction of concrete, the thickness of concrete resisting the deformation of the bent-up bars should be calculated as a function of the distance from the punching shear crack. Considering the slab geometry, as shown in Figure 4.26, five various zones can be categorized. The following are the geometrical relationships for calculating the thickness of concrete resisting the deformation of the bent-up bars in each zone:

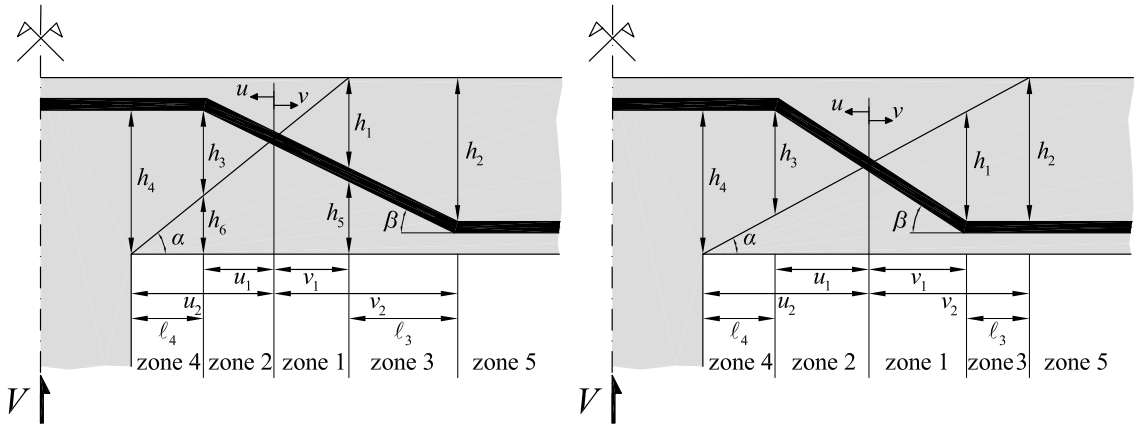

Figure 4.26: Geometry of slab-column connections with bent-up bars

Zone 1:

$$h(v) = v(\tan\alpha + \tan\beta)$$

$$h_1 = \begin{cases} h - \left[\left(\dfrac{d}{2} + \dfrac{h - 2c - Ø}{\tan\beta} - \dfrac{h}{\tan\alpha}\right)\tan\beta + c\right] & \text{if} \quad \alpha > \beta \\ \left(\dfrac{d}{2} + \dfrac{h - 2c - Ø}{\tan\beta}\right)\tan\alpha - c - Ø & \text{if} \quad \alpha \le \beta \end{cases} \tag{4.49}$$

$$v_1 = \frac{h_1}{\tan\alpha + \tan\beta}$$

where u and v are the local coordinates measured from the intersection of bent-up bars and the punching shear crack as illustrated in Figure 4.26.

Zone 2:

$$h(u) = u(\tan\alpha + \tan\beta)$$
$$h_3 = h - c - Ø - \frac{d}{2}\tan\alpha \tag{4.50}$$
$$u_1 = \frac{h_3}{\tan\alpha + \tan\beta}$$

Zone 3:

$$h(v) = \begin{cases} v_1 \tan\alpha + v\tan\beta & \text{if} \quad \alpha > \beta \\ v_1 \tan\beta + v\tan\alpha & \text{if} \quad \alpha \le \beta \end{cases}$$
$$h_2 = h - c - Ø \tag{4.51}$$
$$v_2 = \begin{cases} \frac{1}{\tan\beta}(h_2 - v_1\tan\alpha) & \text{if} \quad \alpha > \beta \\ \frac{1}{\tan\alpha}(h_2 - v_1\tan\beta) & \text{if} \quad \alpha \le \beta \end{cases}$$

Zone 4:

$$h(u) = u_1\tan\beta + u\tan\alpha$$
$$h_4 = h - c - Ø \tag{4.52}$$
$$u_2 = \frac{1}{\tan\alpha}(h_4 - u_1\tan\beta)$$

Therefore, the thickness of concrete resisting the deformation of bent-up bars is calculated as

$$h(v) = \begin{cases} v(\tan\alpha + \tan\beta) & \text{if} \quad v \le v_1 \\ v_1\tan\alpha + v\tan\beta & \text{if} \quad v_1 < v \le v_2 \\ h_2 & \text{if} \quad v_2 < v \end{cases}$$
$$h(u) = \begin{cases} u(\tan\alpha + \tan\beta) & \text{if} \quad u \le u_1 \\ u_1\tan\beta + u\tan\alpha & \text{if} \quad u_1 < u \le u_2 \\ h_4 & \text{if} \quad u_2 < u \end{cases} \tag{4.53}$$

Figure 4.27.a shows the evolution of the concrete thickness resisting the deformation of bent-up bars based on Equation 4.53.

As pointed out previously, accounting equilibrium, the forces exerted by reinforcing bars to the concrete within and outside of the punching cone are equal. Therefore, the progressive destruction of the concrete within the punching cone can be expressed as a function of the progressive destruction of the concrete outside of the punching cone and vice versa. The following relation is derived considering equilibrium conditions between the two sides of the punching crack:

$$\frac{\pi}{2}h(u)^2 f_{ct,eff} = \frac{\pi}{2}h(v)^2 f_{ct,eff} \tag{4.54}$$

Therefore,

$$h(u) = h(v) \tag{4.55}$$

By substituting Equation 4.55 into Equation 4.53, a relationship between u and v can be established. In fact, this is the same as the relationship between the progressive concrete destruction within and outside of the punching cone, which is plotted in Figure 4.27.

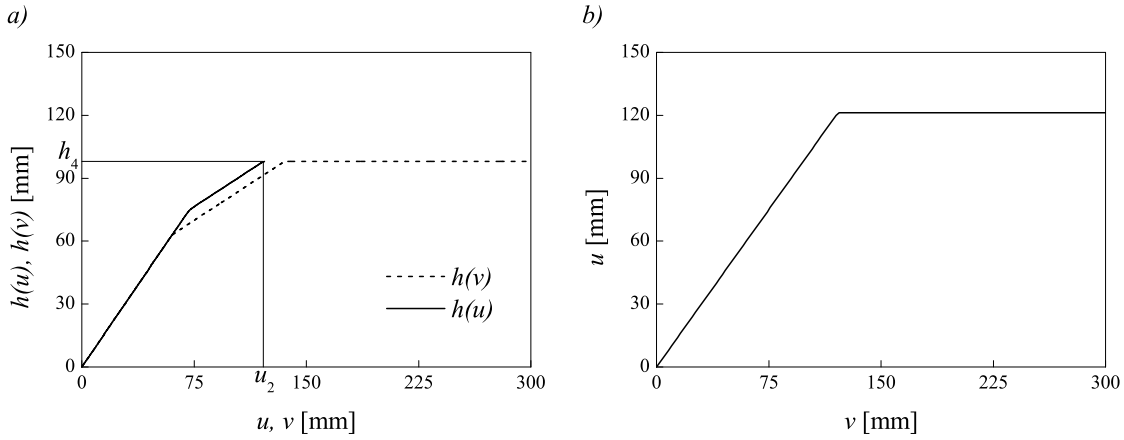

Figure 4.27: Progressive destruction of concrete: a) thickness of concrete resisting the deformation of bent-up bars as a function of distance from the intersection of bent-up bars and the punching shear crack (u and v) and b) relationship between destruction length along the punching cone (u) and destruction length of concrete outside of the punching cone (v)

The geometrical parameters and the progressive concrete destruction relationship for slabs with bent-up bars are investigated previously. In order for the mechanical model to predict the post-punching behavior of these slabs, the developed forces in bent-up bars should be calculated. The following relationships are derived to compute the mean axial strain and stress in bent-up bars. Based on a slab geometry and particularly the angle of inclination of the punching cone, various failure processes, shown in Figure 4.28, can occur. The mean axial strain in each case can be calculated according to the geometrical considerations:

Case I ($v < v_1$ and $u < u_1$):

$$\begin{aligned} \varepsilon_s &= \frac{L_f}{L_i} - 1 \\ L_f &= (u+v)/\cos\psi \\ L_i &= (u+v)/\cos\beta \\ \psi &= \tan^{-1}\left(\tan\beta + \frac{w}{u+v}\right) \end{aligned} \tag{4.56}$$

Case II ($v < v_1$ and $u_1 < u < u_2$):

$$L_i = u - u_1 + (u_1 + v)/\cos\beta$$
$$\psi = \tan^{-1}\left(\frac{w + (u_1 + v)\tan\beta}{u + v}\right) \tag{4.57}$$

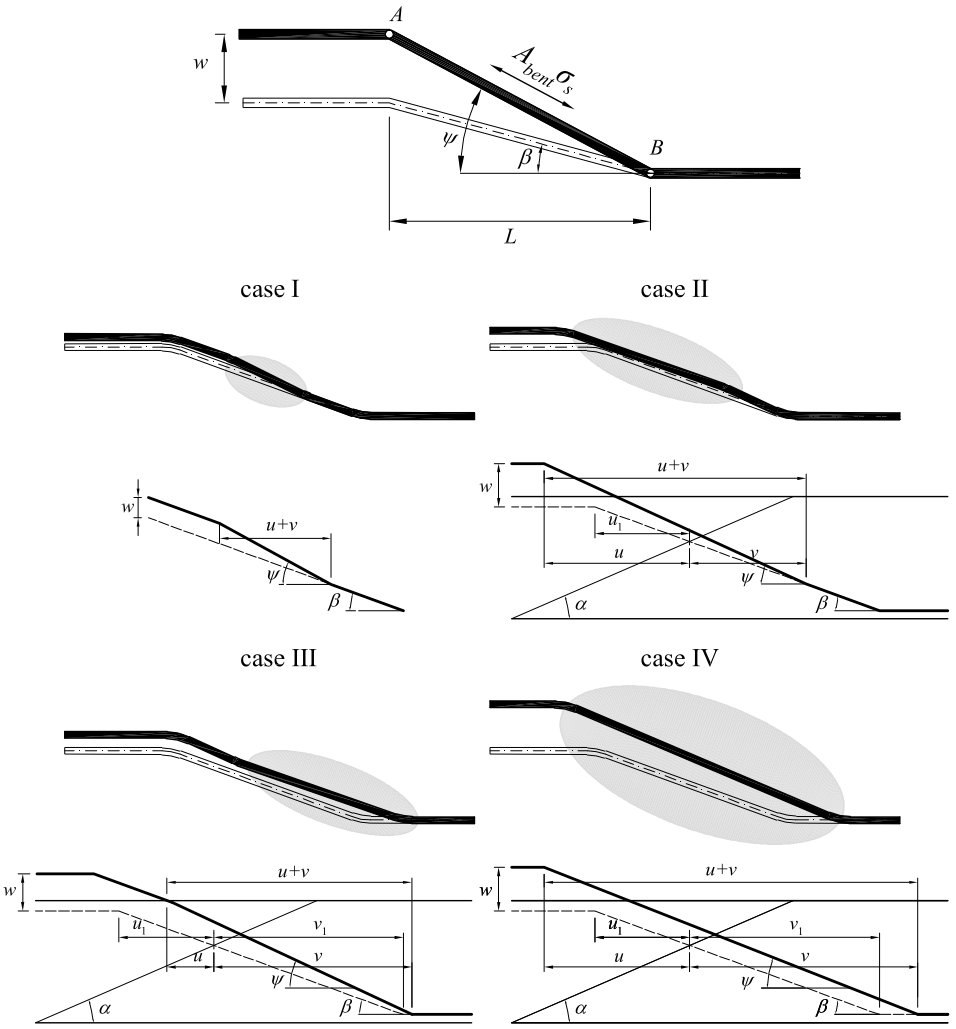

Figure 4.28: Various cases for the calculation of the mean axial strain as a function of angle of inclination of punching cone, angle of inclination of bent-up bars, and distance from the intersection of bent-up bars to the punching shear crack (u and v)

Case III ($v_1 < v < v_2$ and $u < u_1$):

$$L_i = v - v_1 + (u + v_1)/\cos\beta$$
$$\psi = \tan^{-1}\left(\frac{w + (u + v_1)\tan\beta}{u + v}\right) \tag{4.58}$$

Case IV ($v > v_2$ and $u_1 < u < u_2$):

$$L_i = u - u_1 + v - v_1 + (u_1 + v_1)/\cos\beta$$
$$\psi = \tan^{-1}\left(\frac{w + (u_1 + v_1)\tan\beta}{u + v}\right) \tag{4.59}$$

The new geometry, *u*-*v* relationship, and relationships to calculate the mean axial strain and stress are implemented into the mechanical model. The mechanical model is able to predict the post-punching behavior of slabs with bent-up bars.

It should be noted that the pre-punching behavior of slabs with bent-up bars can be predicted according to a simplified model proposed by Muttoni (2008). Equation 4.60 estimates the load-rotation relationship of the slab with bent-up bars:

$$\psi' = 1.5\frac{r_s}{d}\frac{f_{sy}}{E_s}\left(\frac{V}{V_{flex}}\right)^{3/2} \tag{4.60}$$

where r_s is the radius of the equivalent circular slab, which is approximately half of the slab width. The flexural strength V_{flex} of the slab can be estimated according to the yield-line theory (Figure 4.29):

$$V_{flex} = \frac{4m_R b + 8A_{bent} f_{sy} d'}{r_q \cos\frac{\pi}{8} - \frac{a}{2}} \tag{4.61}$$

where m_R is the nominal moment capacity per unit width, A_{bent} is the cross-sectional area of a bent-up bar, and d' is the distance from the extreme compression fiber of the slab over the column area to the centroid of the bent-up bars. As bent-up bars act as shear reinforcement, their influence on the punching strength should be considered. The contribution of bent-up bars to the punching strength has not yet been thoroughly investigated.

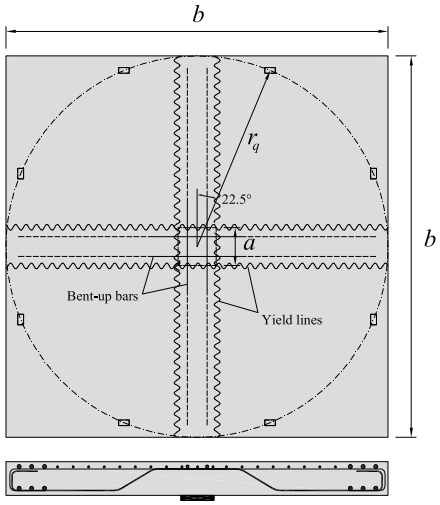

Figure 4.29: Yield line pattern considered for slabs with bent-up bars

Fernandez Ruiz and Muttoni (2009) propose a model based on the critical shear crack theory to estimate the contribution of shear reinforcement to the punching strength. This model can also be used to approximate the contribution of bent-up bars to the punching strength:

$$V_p = V_c + V_s$$
$$V_s = \sum_{i=1}^{n} \sigma_s A_{bent} \sin\beta \tag{4.62}$$

where V_c and V_s are the contribution of concrete and the contribution of shear reinforcement (bent-up bars) to the punching strength. The punching strength is obtained at the intersection of the calculated failure criterion with the load-deflection curve of the slab.

4.9 Verification of mechanical model

The main objective of this research is to predict the post-punching behavior of flat slabs. Hence, a comparison between the developed model and experimental results is presented. As the literature on post-punching behavior is limited, all available experimental data related to post-punching behavior are compared to the model (Georgopoulos, 1986; Melo and Regan, 1998; Broms, 2000). The way that the model calculates the post-punching strength is illustrated as a flow chart in Figure 4.30.

The pre-punching behavior has been modeled using the critical shear crack theory proposed by Muttoni (2008). The critical shear crack theory, which is based on the opening of a critical shear crack, leads to the formulation of a new failure criterion for punching shear as a function of the slab rotation:

$$\frac{V_R}{b_0 \cdot d \cdot \sqrt{f_c}} = \frac{3/4}{1+15\dfrac{\psi' \cdot d}{d_{g0} + d_g}} \tag{4.63}$$

where ψ' is the rotation of the slab, V_R is the resistant punching shear force, and d_g and d_{g0} are the maximum and reference aggregate sizes, respectively. To compute the maximum punching strength, the load-rotation relationship of the slab is also needed for which a mechanical model was proposed based on a quadrilinear moment-curvature relationship for the reinforced concrete section (Muttoni, 2008). Thus, one can use the critical shear crack theory for the pre-punching behavior and the developed model for the post-punching behavior. This allows to acquire the full response of a flat slab before and after punching until the total failure occurs.

Figures 4.31 and 4.32 and Table 4.1 show the comparison between the results obtained by the mechanical model and available test data. The contribution of the tensile reinforcement and the contribution of the integrity reinforcements to the post-punching shear transfer are shown as well. There is a good agreement between the measured post-punching strength and those calculated by the mechanical model with an average ratio of 1.04 (values over 1.0 mean conservative estimates) and a small coefficient of variation (COV = 0.14).

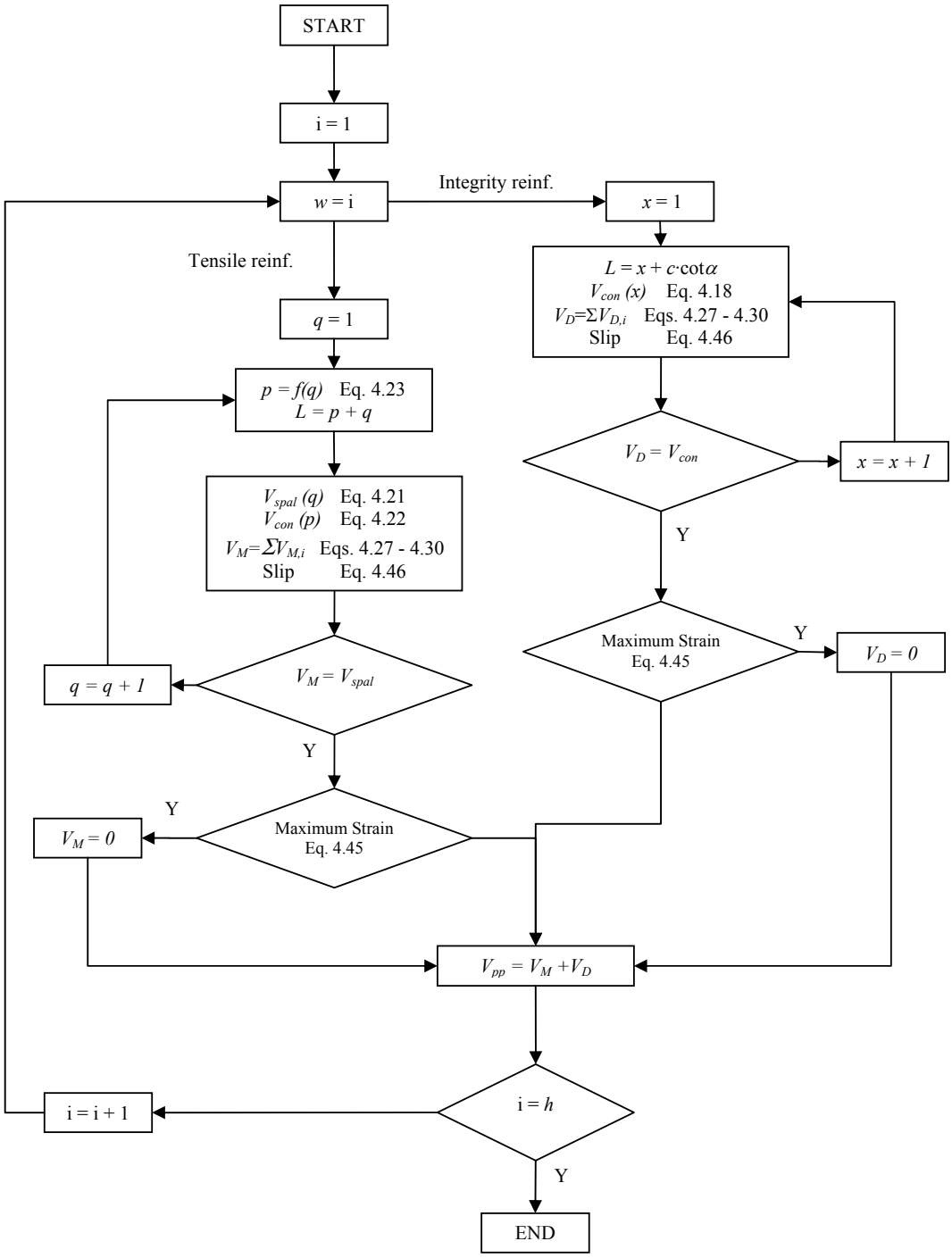

Figure 4.30: Calculation flow chart of the post-punching behavior of slab-column connections

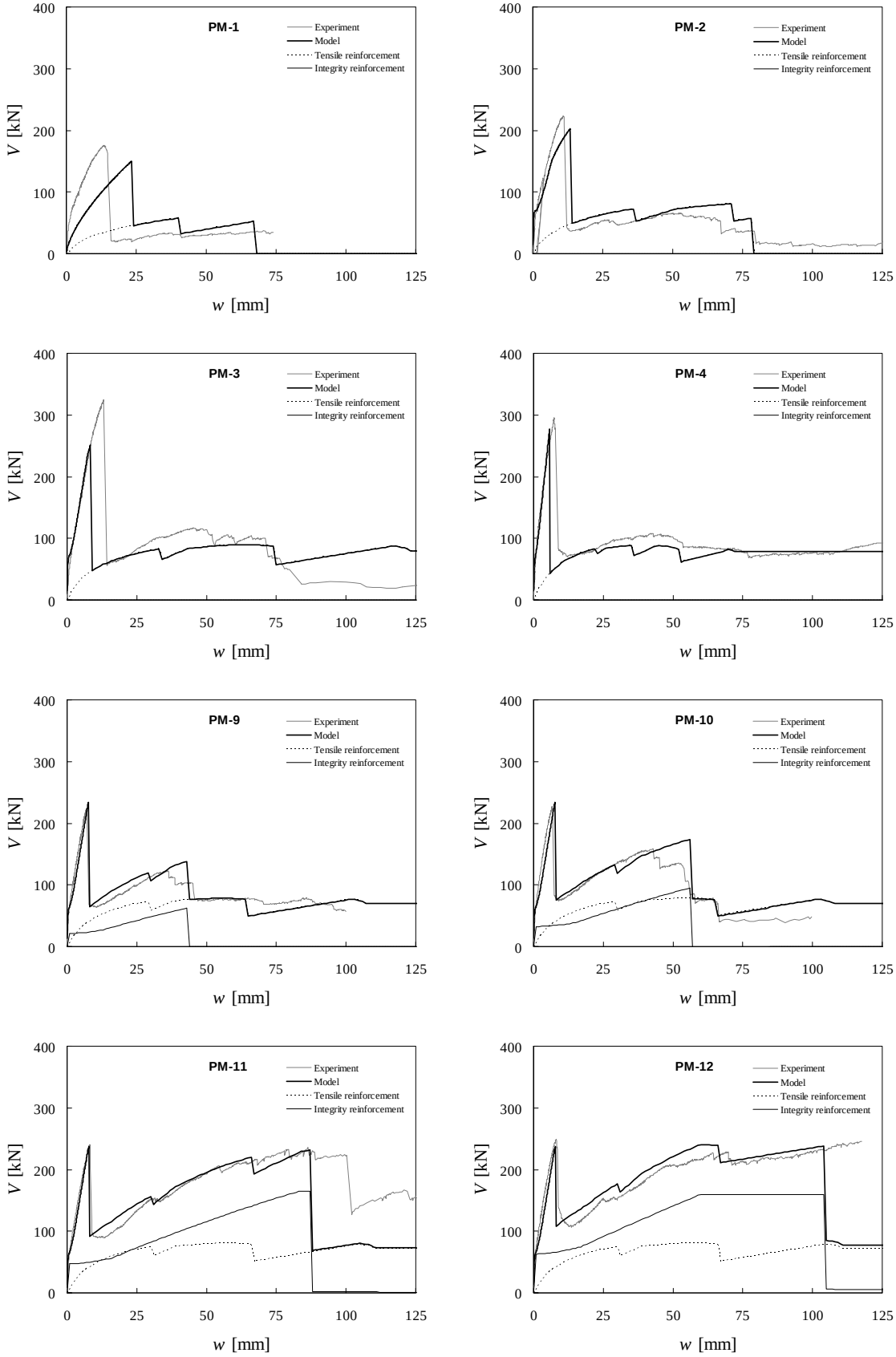

Figure 4.31: Comparison of theoretical and experimental results (continued on next page)

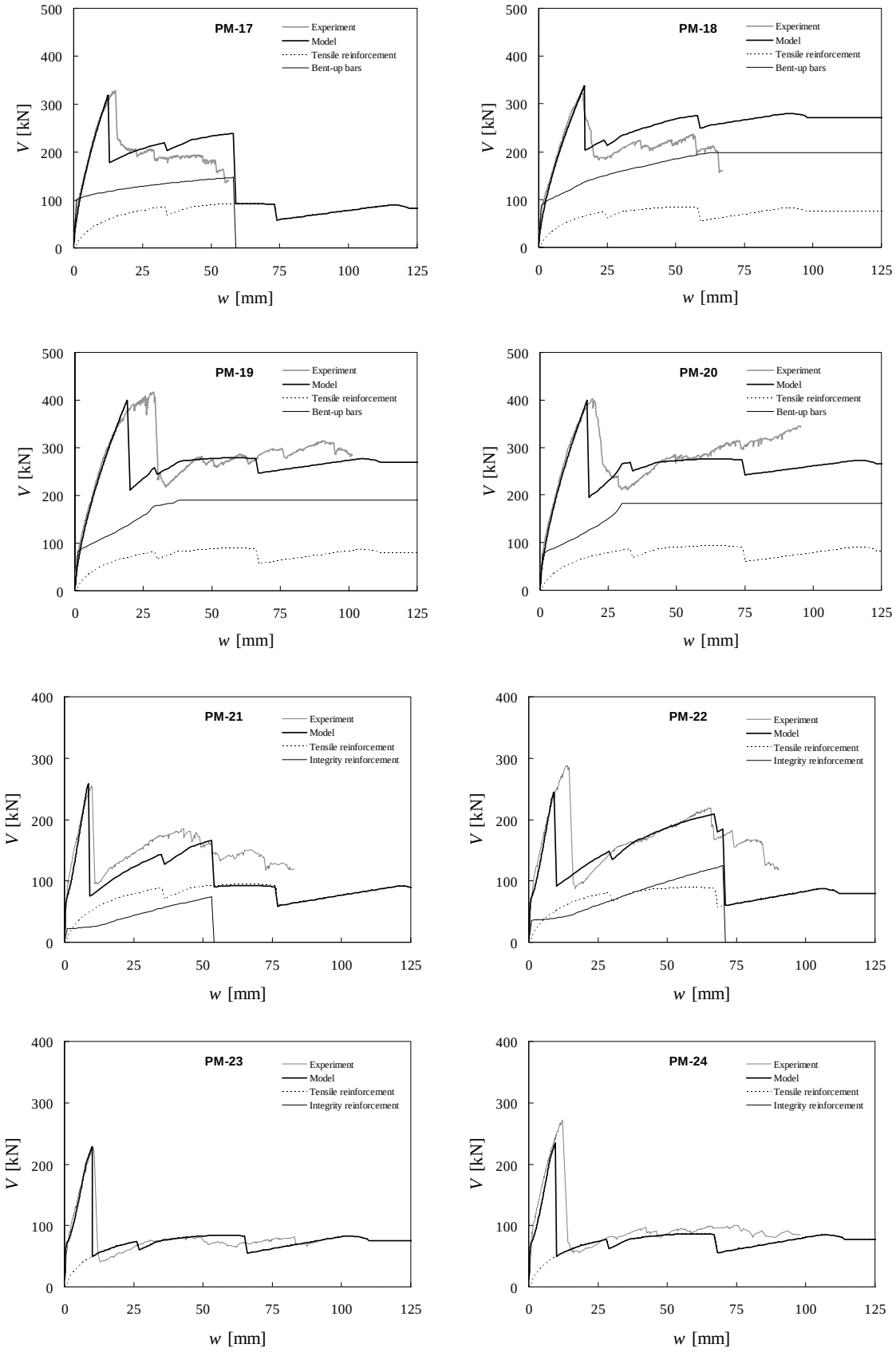

Figure 4.31 (cont.): Comparison of theoretical and experimental results

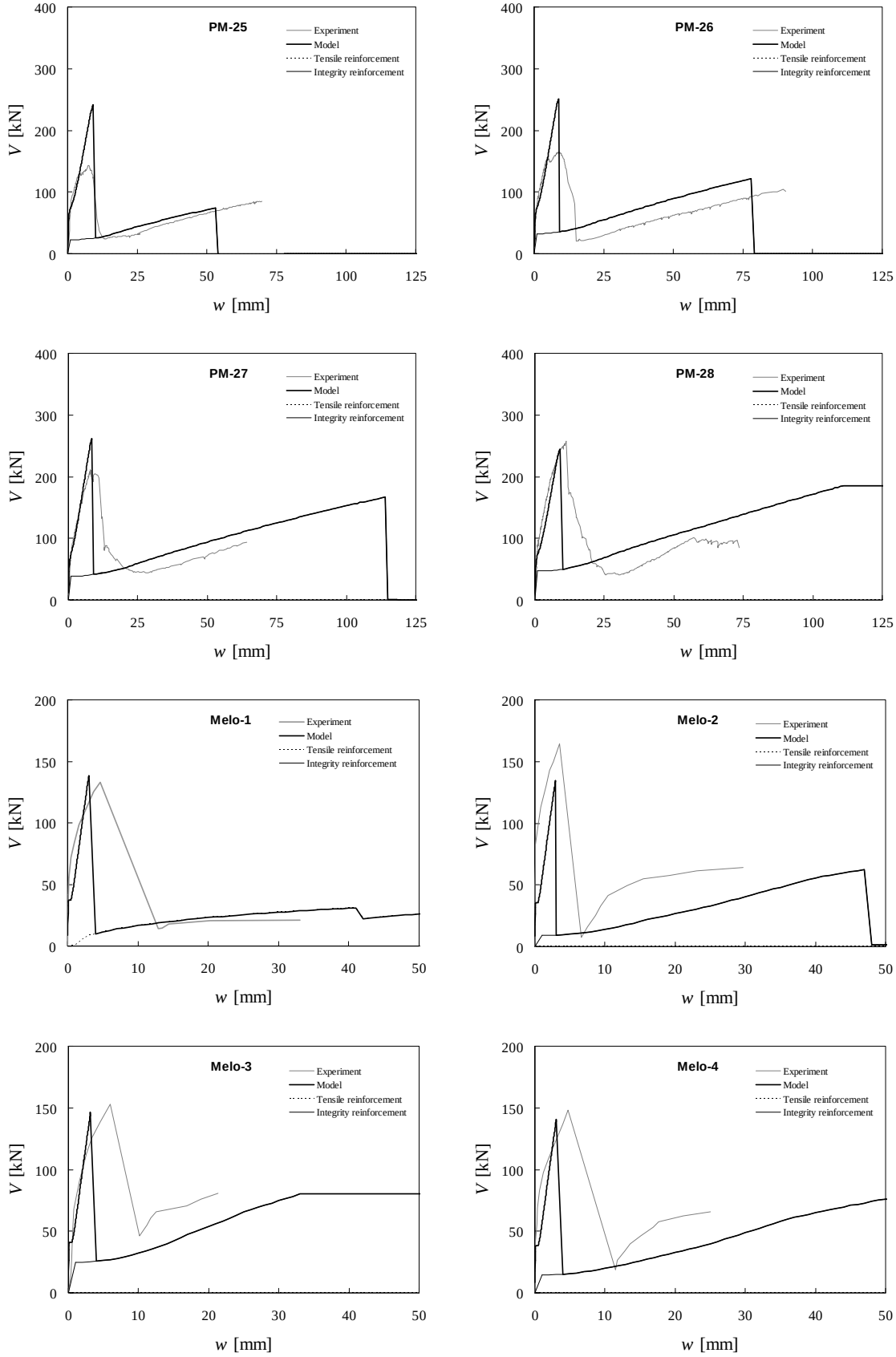

Figure 4.31 (cont.): Comparison of theoretical and experimental results

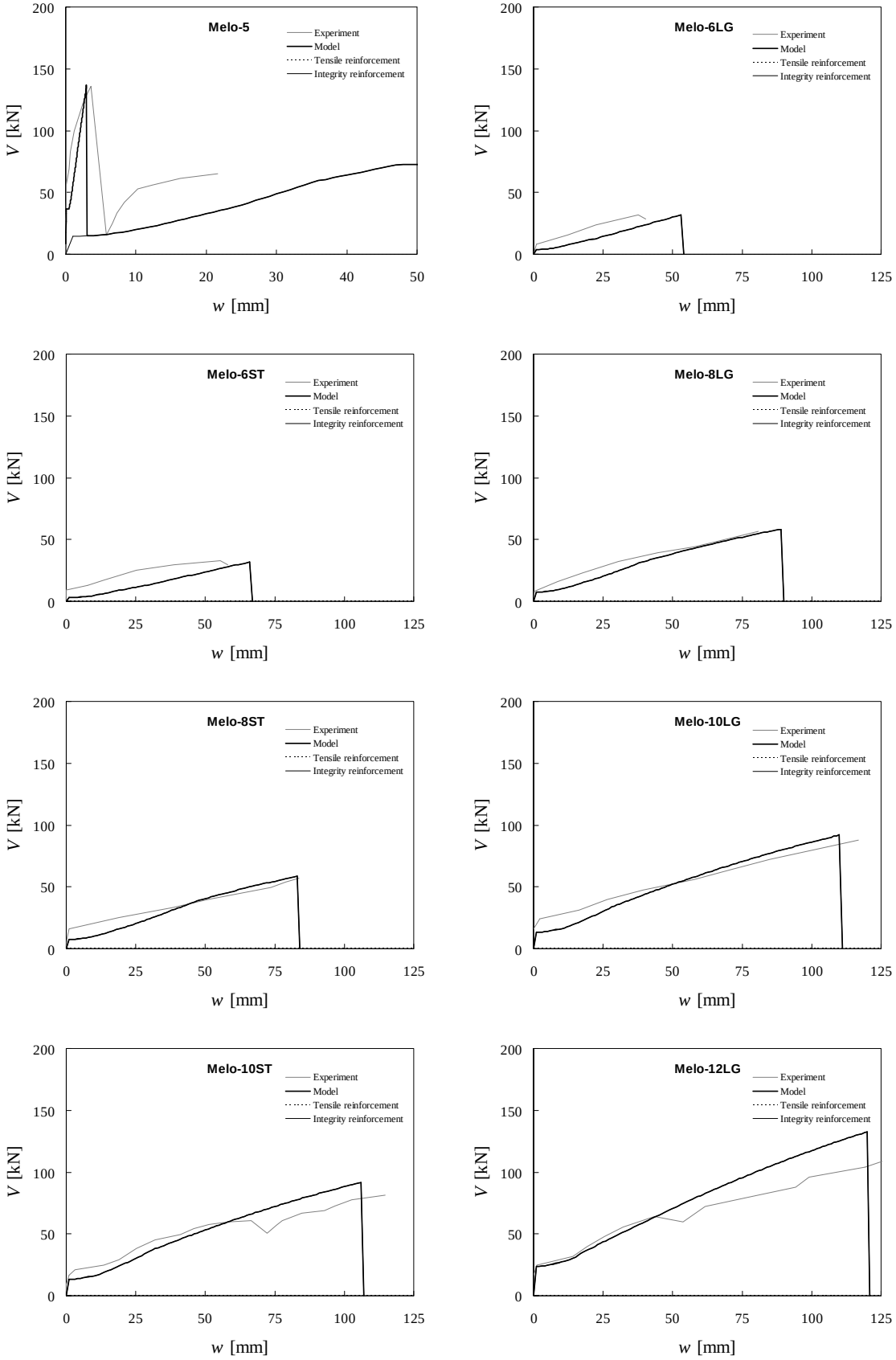

Figure 4.31 (cont.): Comparison of theoretical and experimental results

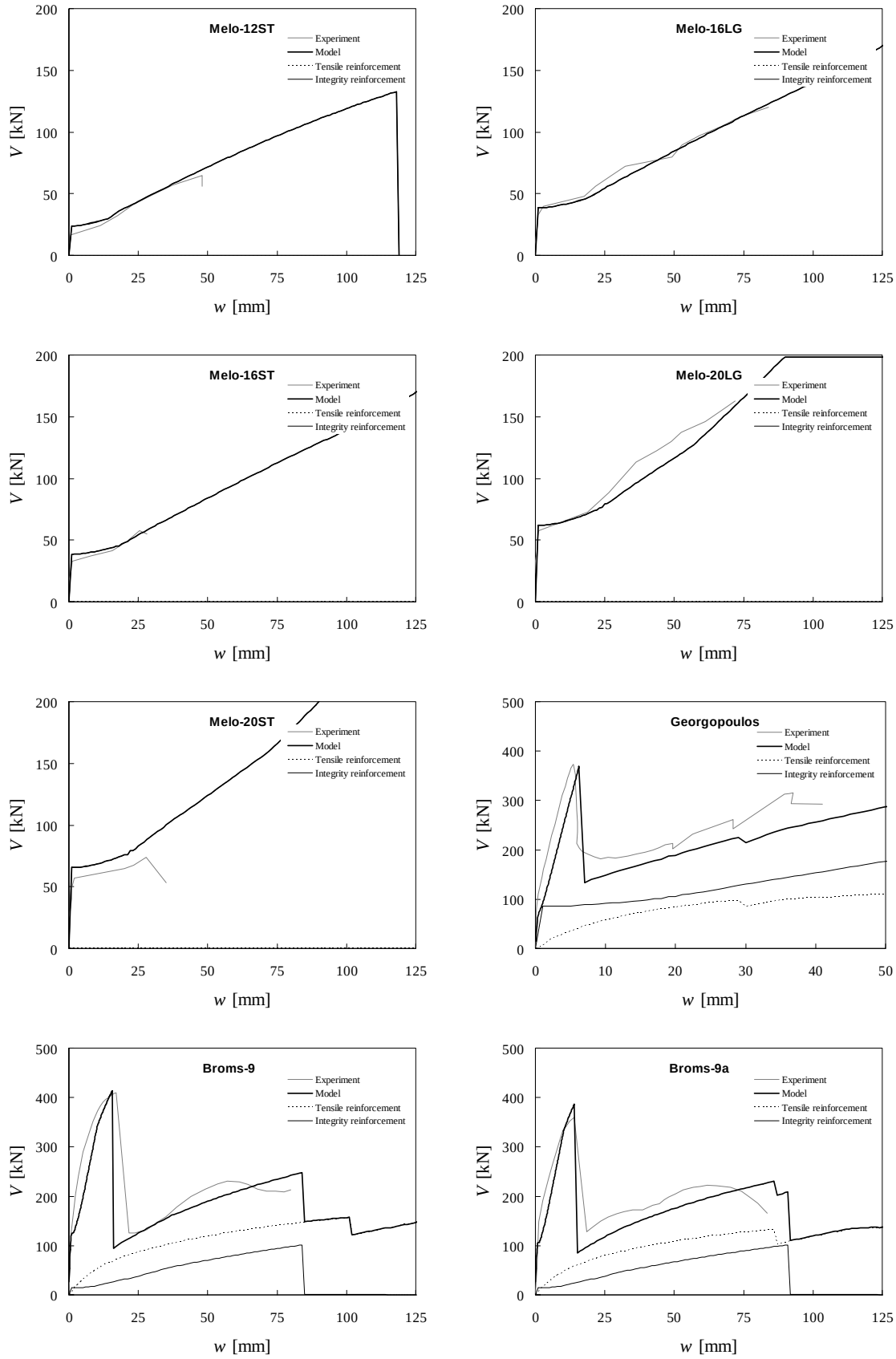

Figure 4.31 (cont.): Comparison of theoretical and experimental results

Table 4.1: Comparison of theoretical and experimental results

Test	Tensile reinf.			Integrity reinf.						
	ρ [%]	f_{sy} [MPa]	f_c [MPa]	A_{sb}	f_{sy} [MPa]	$V_{p,test}$ [kN]	$V_{p,model}$ [kN]	$V_{pp,test}$ [kN]	$V_{pp,model}$ [kN]	$\frac{V_{pp,model}}{V_{pp,test}}$
PM-1	0.25	601	36.6	-	-	176	150	37	58	1.55
PM-2	0.49	601	36.5	-	-	224	203	66	81	1.23
PM-3	0.82	601	37.8	-	-	324	251	117	90	0.76
PM-4	1.41	601	36.8	-	-	295	278	108	88	0.82
PM-9	0.82	601	31.0	2×2Ø8	616	224	234	123	139	1.12
PM-10	0.82	601	31.1	2×2Ø10	560	228	234	159	174	1.09
PM-11	0.82	601	32.3	2×2Ø12	548	241	238	237	231	0.98
PM-12	0.82	601	32.4	2×2Ø14	527	249	241	245	241	0.98
PM-17	0.82	625	39.7	2×2Ø8	625	329	319	204	240	1.18
PM-18	0.88	625	39.8	2×2Ø10	605	323	338	237	284	1.20
PM-19	0.85	625	39.9	2×2Ø12	566	417	400	315	310	0.98
PM-20	0.82	625	40.0	2×2Ø14	578	402	399	345	301	0.87
PM-21	0.81	625	40.2	2×2Ø8	625	256	259	185	166	0.90
PM-22	0.85	625	40.3	2×2Ø10	605	288	244	219	209	0.96
PM-23	0.88	625	40.4	-	-	227	228	82	84	1.03
PM-24	0.86	625	40.4	-	-	272	235	101	87	0.86
PM-25	0.85	625	40.4	2×2Ø8	625	143	242	75	74	-+
PM-26	0.83	625	40.3	2×2Ø10	605	165	252	105	122	-+
PM-27	0.81	625	40.3	2×2Ø12	559	211	262	94	167	-+
PM-28	0.85	625	40.3	2×2Ø14	578	258	245	101	185	-+
Melo-1	2.39	655	29.6	-	-	133	138	21	47	-×
Melo-2	2.39	759	27.3	2×2Ø6	759	164	135	64	63	0.98
Melo-3	2.39	759	34.1	2×4Ø6	759	153	147	81	81	0.99
Melo-4	2.39	759	30.6	2×2Ø8	759	148	141	66	76	1.15
Melo-5	2.39	655	28.8	2×2Ø8	529	136	137	65	73	1.12
Melo-6LG	-	-	30.1	1×2Ø6	655	-	-	32	32	1.00
Melo-6ST	-	-	41.4	1×2Ø6	655	-	-	33	32	0.96
Melo-8LG	-	-	30.1	1×2Ø8	529	-	-	57	58	1.03
Melo-8ST	-	-	41.4	1×2Ø8	529	-	-	57	58	1.02
Melo-10LG	-	-	33.4	1×2Ø10	497	-	-	88	92	1.04
Melo-10ST	-	-	38.3	1×2Ø10	497	-	-	81	92	1.13
Melo-12LG	-	-	34.3	1×2Ø12	524	-	-	112	133	1.18
Melo-12ST	-	-	36.9	1×2Ø12	524	-	-	56	133	-†
Melo-16LG	-	-	33.4	1×2Ø16	483	-	-	120	218	-*
Melo-16ST	-	-	32.5	1×2Ø16	483	-	-	58	214	-†
Melo-20LG	-	-	28.2	1×2Ø20	492	-	-	163	183	-*
Melo-20ST	-	-	40.1	1×2Ø20	492	-	-	74	215	-†
Georgopoulos	1.20	525	30.0	2×2Ø16	525	373	369	292	293	1.00
Broms-9	0.52	550	26.9	2×2Ø8	550	410	414	230	248	1.08
Broms-9a	0.52	550	21.0	2×2Ø8	550	360	387	222	230	1.04
									Ave.	1.04
									COV	0.14

+ : Test terminated due to the risk of falling down of the punching cone
† : Test experienced anchorage failure before reaching the ultimate strength
* : Neither bar fracture nor concrete destruction was reported
× : Neither integrity bar nor well-anchored tensile reinforcement was included

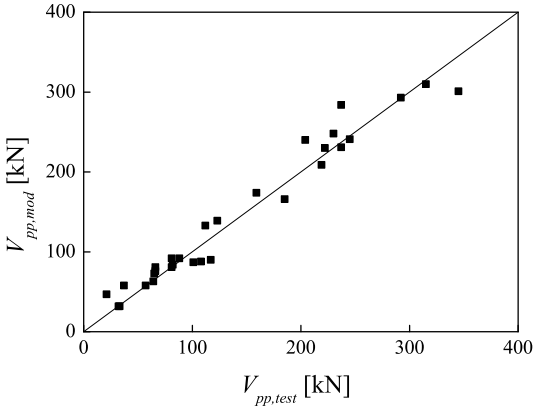

Figure 4.32: Comparison of theoretical results with experimental data

4.10 Influence of various parameters

The developed mechanical model for the prediction of the contribution of the longitudinal reinforcement can be used to study further the influence of various parameters on the post-punching behavior. The influence of a certain parameter on the post-punching behavior can be entirely different for tensile reinforcement and integrity reinforcement. Therefore, the influence of each parameter on integrity and on tensile reinforcement is investigated independently. The influence of each parameter on the post-punching behavior will be investigated separately as well. In the subsequent sections, the base structure is chosen to be PM-3 for studying the tensile reinforcement contribution, and PM-12 for studying the integrity reinforcement contribution to the post-punching shear transfer.

4.10.1 Tensile reinforcement contribution

Effect of the reinforcement ratio:

Figure 4.34.a shows the influence of the reinforcement ratio on the tensile reinforcement contribution. The variation of the reinforcement ratio was achieved by changing the bar spacing and keeping the effective depth constant. Figure 4.34.a shows that the increase of the reinforcement ratio increases the tensile reinforcement contribution for low reinforcement ratios. However, for higher reinforcement ratios, the tensile reinforcement contribution remains almost constant.

In fact, the increase of the reinforcement ratio results in an increase of the forces developed in the tensile reinforcement. The increase of the force in the tensile reinforcement results in more destruction of the concrete (concrete breakout and spalling of the concrete cover). This destruction of concrete reduces the angle of inclination of the tensile reinforcing bars. The contribution of the tensile reinforcement to the post-punching shear transfer is the vertical component of the developed forces in the reinforcing bars. Therefore, the reduction of the angle of inclination of the reinforcing bars decreases the vertical component of the forces in the reinforcing bars. As the spalling of the concrete cover is determinant rather than the fracture of the

reinforcing bars, the post-punching strength is related to the concrete cover and not to the reinforcement layout.

Effect of the ultimate steel strain:

Figure 4.34.b shows the influence of the ultimate strain on the tensile reinforcement contribution. It displays that the ultimate strain has almost no influence even for large deflections. It should be noted that the rupture of the reinforcing bars occur when the maximum strain exceeds the ultimate strain according to the strain-based failure criterion. It was observed during the tests that the axial strain in tensile reinforcing bars barely reached the ultimate strain. The fracture of tensile reinforcing bars was observed only for low reinforcement ratios (PM-1 and PM-2). Figure 4.33 shows the evolution of the axial strain in tensile reinforcing bars obtained by the model.

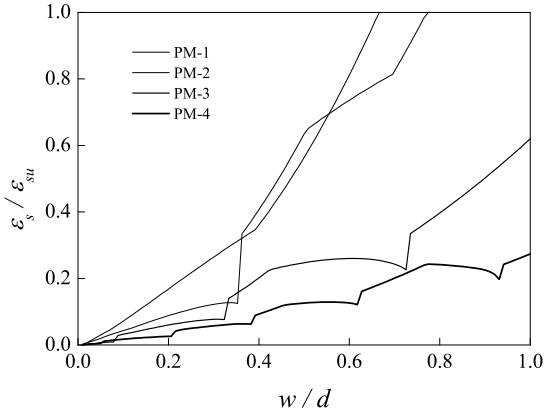

Figure 4.33: Evolution of axial strain in tensile reinforcing bars

Effect of the effective depth:

The influence of the effective depth of the slab on the tensile reinforcement contribution is shown in Figure 4.34.c. The reinforcement ratio is kept constant and the effective depth changes and therefore the cross-sectional area of the reinforcing bars increases. As it can be seen, the increase of the effective depth affects considerably the tensile reinforcement contribution, which can be explained as follows: the diameter of the punching cone is calculated by

$$D = a + 2d \cot \alpha \tag{4.64}$$

Thus, the effective depth has a direct relationship to the diameter of the punching cone. Therefore, the increase of the effective depth increases the diameter of the punching cone and as a result, the number of tensile reinforcing bars crossing the punching cone increases. Hence, the tensile reinforcement contribution increases.

Effect of the angle of inclination of the punching cone:

The influence of the angle of inclination of the punching cone on the tensile reinforcement contribution is shown in Figure 4.34.d. The increase of the angle of inclination of the punching cone results in a slight decrease of the tensile reinforcement contribution, which can be explained by Equation 4.64. The increase of the angle α decreases the diameter of the punching cone as well as the number of tensile reinforcing bars crossing the punching cone. Hence, the tensile reinforcement contribution to the post-punching shear transfer decreases.

Effect of the yielding strength:

Figure 4.34.e shows the effect of the variation of the yielding strength of the tensile reinforcement on the tensile reinforcement contribution. The increase of the tensile reinforcement contribution due to the increase of the yielding strength is not considerable.

Effect of the concrete tensile strength:

Figure 4.34.f shows the effect of the concrete tensile strength on the tensile reinforcement contribution. It shows that the increase of the concrete tensile strength results in an increase of the tensile reinforcement contribution. The concrete breakout strength and the spalling strength of the concrete cover are directly proportional to the concrete tensile strength. Thus, the increase of the concrete tensile strength results in an increase of the concrete breakout strength as well as the spalling strength of the concrete cover. Therefore, the destruction of concrete within and outside of the punching cone decreases and as a result the angle of inclination of the tensile reinforcing bars increases. This will result in an increase of the vertical component of the developed forces in the tensile reinforcement.

The concrete tensile strength and the compressive strength are directly related and thus the effects of the tensile strength and the compressive strength on the post-punching behavior are qualitatively similar.

Effect of the column width:

The effect of the column width on the tensile reinforcement contribution is shown in Figure 4.34.g. The increase of the column width slightly increases the tensile reinforcement contribution, which can be explained as follows: According to Equation 4.64 the increase of the column width increases the diameter of the punching cone as well as the number of tensile reinforcing bars crossing the punching cone. Hence, the tensile reinforcement contribution to the post-punching shear transfer increases.

Effect of the concrete cover:

Figure 4.34.h shows the influence of the variation of the concrete cover on the tensile reinforcement contribution. The increase of the concrete cover results in an increase of the tensile reinforcement contribution. This increase can be justified similar to that one of the effect of the concrete tensile strength. As the spalling strength of the concrete cover is directly related to its value, the increase of the concrete cover increases the spalling strength of the concrete cover, which results in an increase of the tensile reinforcement contribution.

4.10.2 Integrity reinforcement contribution

Effect of the bar diameter:

Figure 4.36.a shows the influence of the bar diameter on the integrity reinforcement contribution. It shows that the increase of the bar diameter increases the integrity reinforcement contribution. However, this increase is limited by the maximum breakout strength of the concrete above the integrity reinforcement.

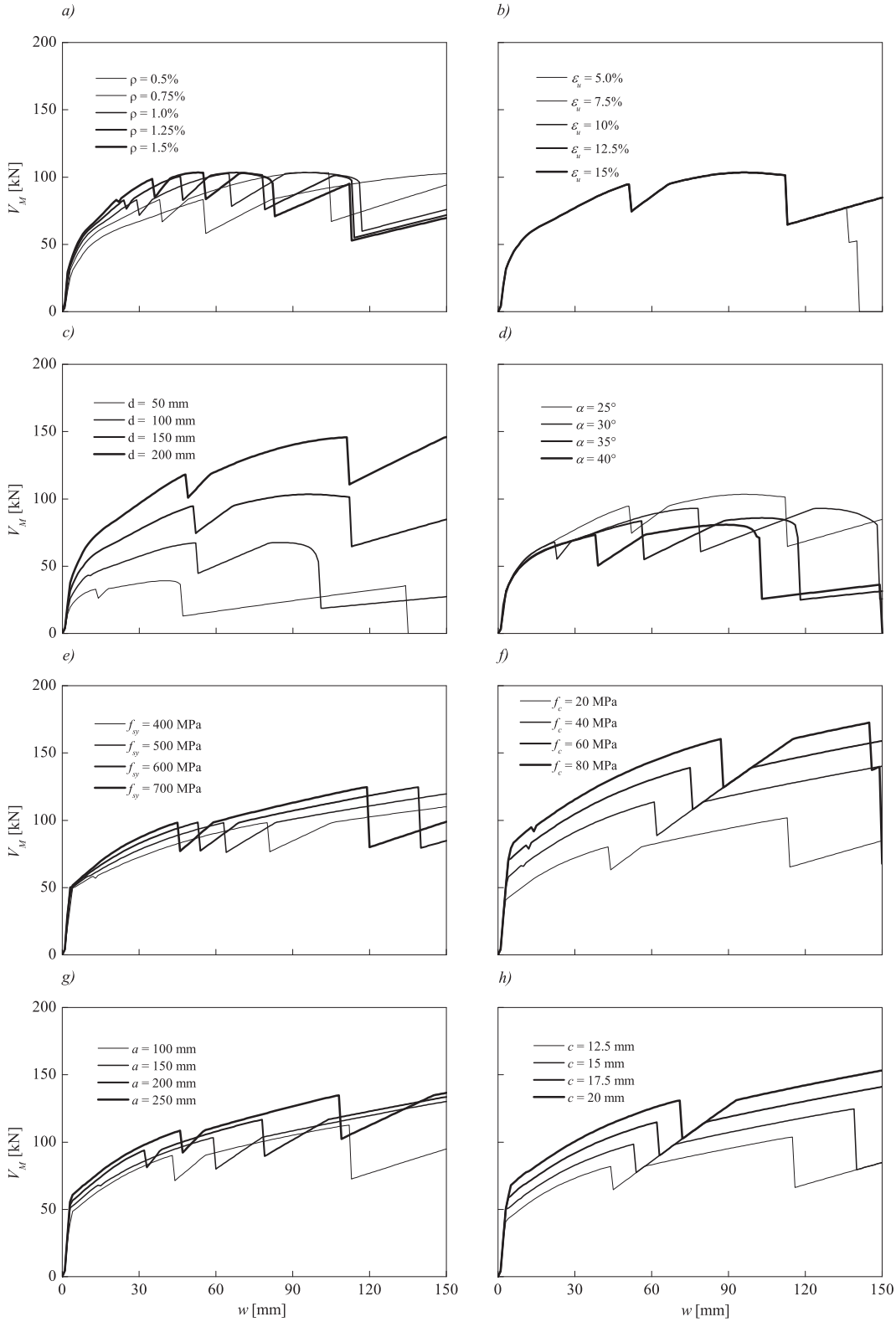

Figure 4.34: Parametric study on tensile reinforcement contribution: a) reinforcement ratio, b) steel ultimate strain, c) effective depth, d) angle of inclination of the punching cone, e) yield strength of tensile reinforcement, f) concrete compressive strength, g) column width, and h) concrete cover

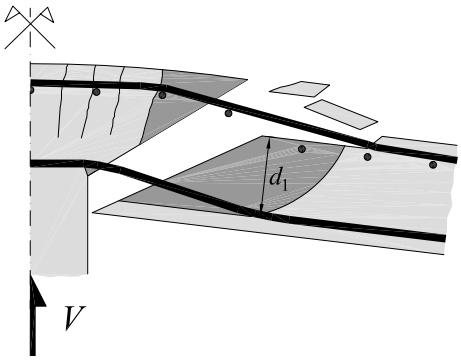

Figure 4.35: Critical zone of concrete breakout over integrity reinforcement

As pointed out previously, the integrity reinforcement contribution is governed either by the maximum breakout strength of the concrete above the bar (Equation 4.19) or by the fracture of the integrity bars (Equation 4.30). Figure 4.35 show the situation at which the maximum concrete breakout strength occurs. For further deflections, the concrete breakout strength remains constant as the thickness of the concrete above the integrity reinforcement remains unchanged. Thus, no further increase of the integrity reinforcement contribution will occur. It is noteworthy to mention that if the integrity reinforcement contribution is governed by the maximum breakout strength, the rupture of the reinforcing bars occur at the same deflection. At such circumstances, the deformed shape of the bar is independent from the bar diameter and thus the reinforcing bars reach their ultimate strain simultaneously as shown in Figure 4.36.a. A small difference in the integrity reinforcement contribution for large bar diameters is attributed to the thickness of the concrete above the integrity reinforcing bars, which is related to the bar diameter as shown in Figure 4.35.

Effect of the ultimate strain:

Figure 4.36.b shows the influence of the ultimate strain on the integrity reinforcement contribution. The increase of the ultimate steel strain results in an increase of the strength and the deformation capacity of the system. This is attributed to the strain-based failure criterion used in the model. The increase of the integrity reinforcement contribution is finally limited by the maximum concrete breakout strength.

Effect of the effective depth:

The influence of the effective depth of the slab on the integrity reinforcement contribution is shown in Figure 4.36.c. The effective depth is proportional to the thickness of the concrete over the integrity reinforcement. It can be seen that the increase of the effective depth increases the strength and the deformation capacity. For low effective depths, the integrity reinforcement contribution is governed by the maximum concrete breakout strength up to a certain depth. Afterwards, the maximum concrete breakout strength is no longer determinant and the integrity reinforcement contribution is governed by the fracture of the reinforcing bars.

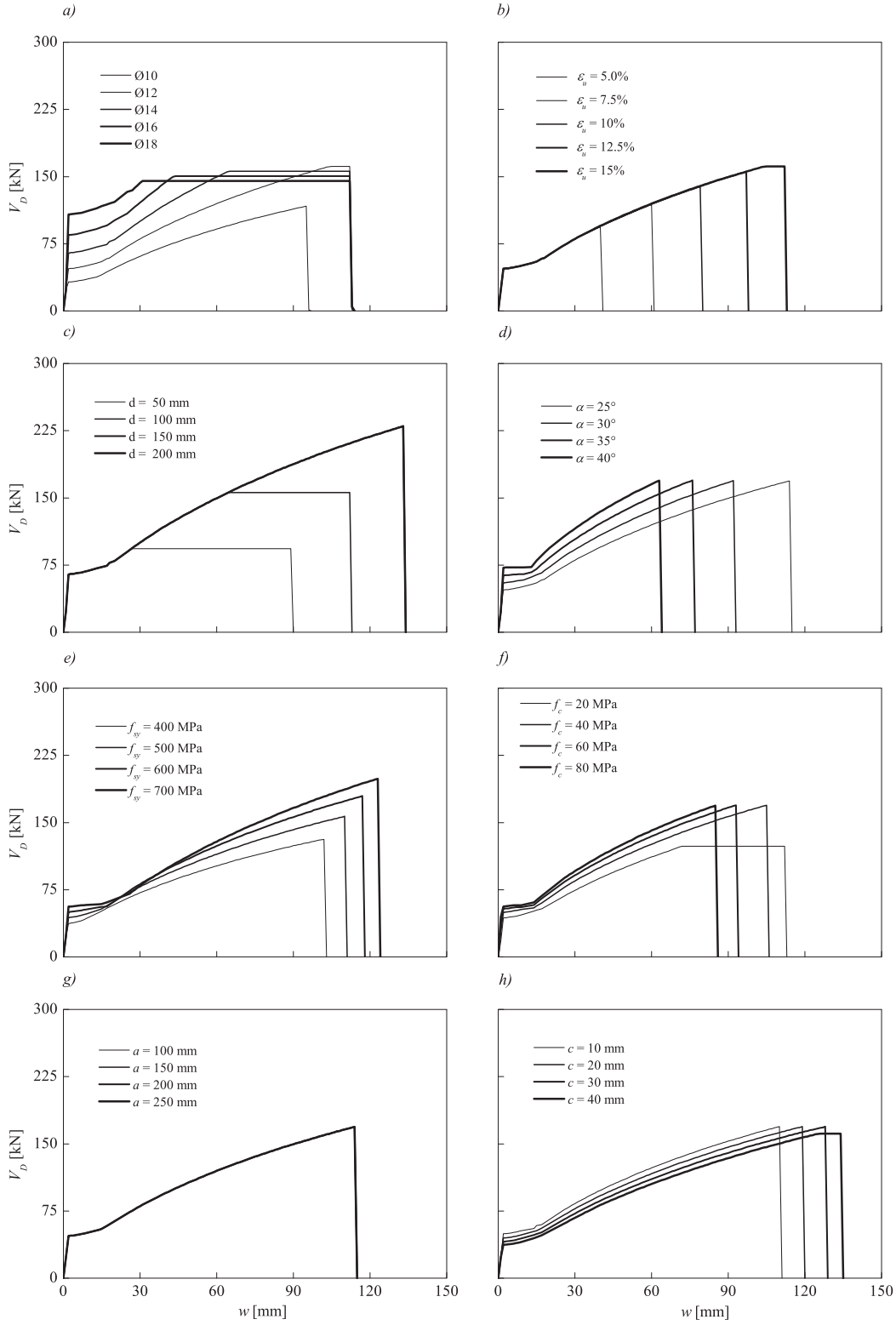

Figure 4.36: Parametric study on integrity reinforcement contribution: a) diameter of integrity reinforcement, b) steel ultimate strain, c) effective depth, d) angle of inclination of the punching cone, e) yield strength of reinforcement, f) concrete compressive strength, g) column width, and h) concrete cover

Effect of the angle of inclination of the punching cone:

Figure 4.36.d shows that the increase of the angle of inclination of the punching cone has almost no influence on the strength. The angle of inclination of the punching cone does not affect the maximum breakout strength as the former parameter is not included in the computation of the latter parameter. The angle of inclination only affects the distance between the plastic hinges. This distance does not influence the strength and only affects the stiffness and deformation capacity (Figure 4.11). The increase of the angle of inclination of the punching cone results in an increase of the depth of the concrete above the integrity reinforcement ($x \cdot \tan\alpha$, see Figure 4.14). Thus, for the same x, the concrete breakout strength increases. To equilibrate this breakout strength, a higher integrity reinforcement contribution is needed. Consequently, the axial strain of the reinforcing bars increases and hence the deformation capacity decreases.

Effect of the yielding strength:

Figure 4.36.e shows the influence of the yielding strength on the integrity reinforcement contribution. The increase of the yielding strength slightly increases both strength and deformation capacity. The strength increases because the integrity reinforcement contribution is directly related to the axial stress in the bars. The increase in deformation capacity can be explained as follows. To equilibrate higher integrity reinforcement contribution due to higher yielding strength, higher concrete breakout strength is needed. To equilibrate this concrete breakout strength, the concrete depth over the integrity reinforcement increases ($x \cdot \tan\alpha$). Therefore, the distance between plastic hinges increases ($L = x + c \cdot \cot\alpha$). Considering the plastic behavior ($\tan\psi = w/L$, Figure 4.21), Equation 4.29 can be rewritten as

$$\frac{w}{L} = \tan\left[\cos^{-1}\left(\frac{1}{1+\varepsilon_{su}}\right)\right] \tag{4.65}$$

This equation clearly shows that the increase of the distance between the plastic hinges results in an increase of the deformation capacity of the slab-column connection. However, if the maximum concrete breakout strength is determinant, the yielding strength will no longer influence the strength and the deformation capacity of the system.

Effect of the concrete tensile strength:

Figure 4.36.f displays the influence of the concrete tensile strength on the integrity reinforcement contribution. The concrete breakout strength is directly proportional to the concrete tensile strength. Thus, the value of concrete tensile strength is very critical in determining the post-punching behavior. Figure 4.36.f shows that the maximum breakout strength is determinant for low concrete tensile strength. However, for higher concrete tensile strength, the failure mode is the fracture of the integrity reinforcing bars. It can be seen that deformation capacity decreases if the concrete tensile strength increases. As the concrete tensile strength increases, the concrete breakout strength increases. To equilibrate the increased concrete breakout strength, the axial strain of the integrity reinforcement increases, indicating that the maximum tensile strain will exceed the ultimate strain earlier and hence the deformation capacity decreases.

Effect of the column width:

The influence of the column width on the integrity reinforcement contribution is shown in Figure 4.36.g. It shows that the increase of the column width has no influence as this parameter is not included in the computation of the integrity reinforcement contribution. This statement is valid only if two integrity reinforcing bars have been placed over the column. However, flat slabs usually include bottom reinforcing bars which can act as integrity reinforcement is the column size sufficiently increases. In such case, the integrity reinforcement contribution to the post-punching shear transfer is significantly increased.

Effect of the concrete cover:

The influence of the concrete cover on the integrity reinforcement contribution is shown in Figure 4.36.h. The concrete cover has almost no influence on the strength. However, the increase of the concrete cover slightly increases the deformation capacity of the slab-column connection. The distance between plastic hinges is increased by increasing the concrete cover (Equation 4.31). Thus, the maximum deflection increases since it has a direct relationship with the distance between the plastic hinges according to Equation 4.65.

4.10.3 Post-punching behavior

The influence of various parameters on the pre and the post-punching behavior is investigated in this section.

Effect of the bar diameter:

Figure 4.37.a displays the influence of the diameter of the integrity reinforcement on the pre and the post-punching behavior. The reinforcement ratio is kept constant (0.82%) and hence the punching strength remains constant according to the critical shear crack theory. The increase of the post-punching strength is attributed to the integrity reinforcement contribution.

Effect of the ultimate strain:

Figure 4.37.b shows the influence of the ultimate steel strain on the pre and the post-punching behavior. As shown previously, the increase of the ultimate strain does not affect the tensile reinforcement contribution. However, its influence on the integrity reinforcement contribution is considerable, particularly in the deformation capacity point of view. The increase of the ultimate strain slightly increases the strength and significantly increases the deformation capacity of the post-punching behavior.

Effect of the effective depth:

Figure 4.37.c shows the influence of the effective depth on the pre and the post-punching behavior. As shown previously, the increase of the effective depth increases the post-punching strength due to the tensile reinforcement contribution as well as the integrity reinforcement contribution. Hence, the post-punching behavior is significantly affected by the effective depth of the slab.

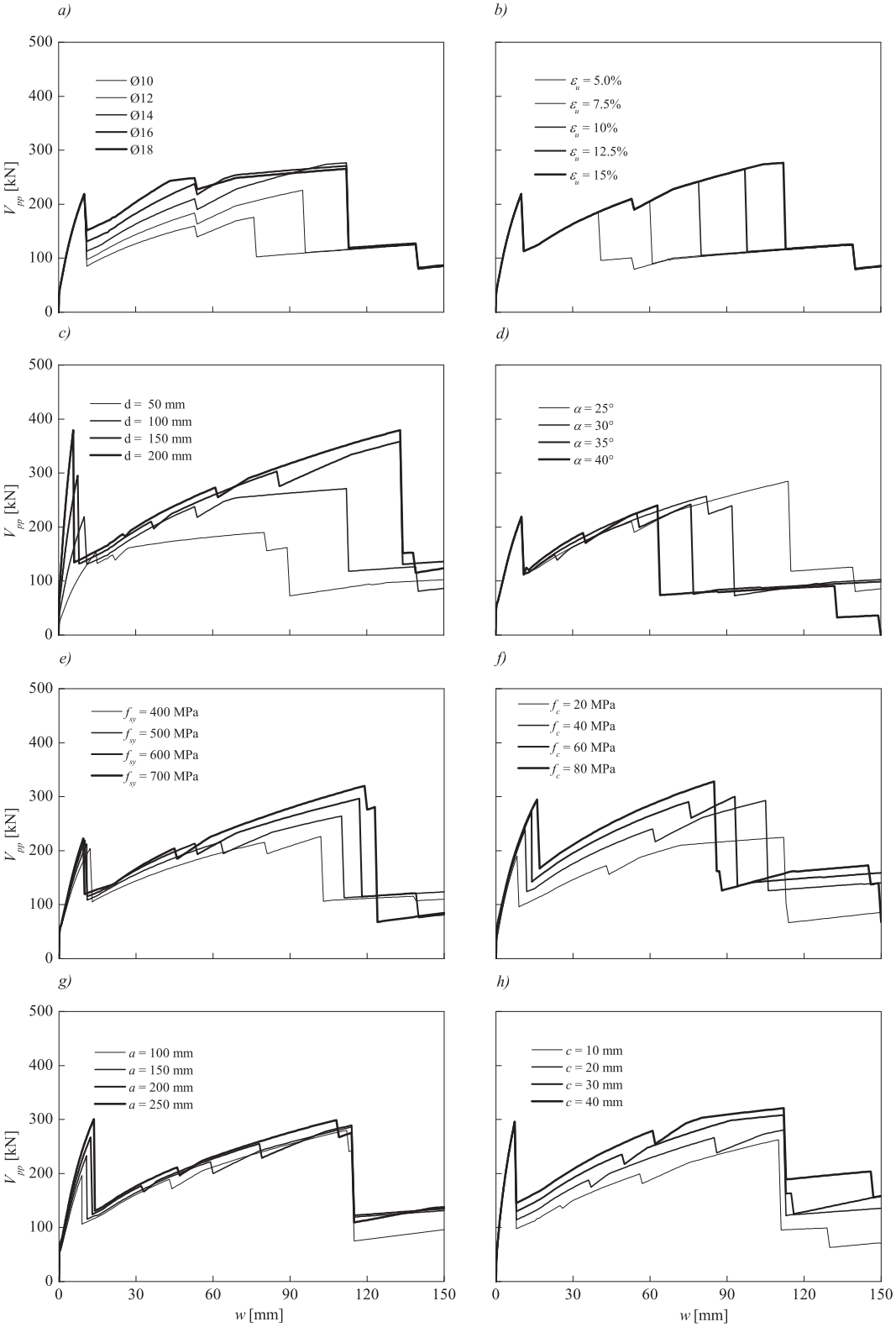

Figure 4.37: Results of parametric study on the post-punching behavior: a) diameter of integrity reinforcing bars, b) steel ultimate strain, c) effective depth, d) angle of inclination of the punching cone, e) yield strength, f) concrete compressive strength, g) column width, and h) concrete cover

Effect of the angle of inclination of the punching cone:

The influence of the angle of inclination of the punching cone on the post-punching behavior is shown in Figure 4.37.d. The change in the tensile reinforcement contribution due to the increase of the angle of inclination is not significant in relation to that of the integrity reinforcement contribution (Figures 4.34.d and 4.36.d).

Effect of the yielding strength:

Figure 4.37.e displays the influence of the yielding strength on the pre and the post-punching behavior, which is not significant. This is attributed to the fact that the influence of the yielding strength on both the integrity reinforcement contribution and the tensile reinforcement contribution is not considerable.

Effect of the compressive strength of concrete:

Figure 4.37.f shows the influence of the concrete compressive strength on the pre and the post-punching behavior. The increase of the concrete compressive strength increases the punching strength according to the critical shear crack theory. Although the concrete compressive strength is not included in the model, it is directly related to the tensile strength of concrete, which is a key parameter in computing the post-punching strength.

Effect of the column width:

The influence of the column width on the punching behavior is shown in Figure 4.37.g. Although it slightly increases the punching strength, its influence on the post-punching behavior is not significant.

Effect of the concrete cover:

The influence of the concrete cover on the post-punching behavior is shown in Figure 4.37.h. It seems that the increase of the concrete cover significantly increases the post-punching behavior. This increase is related to the tensile reinforcement contribution rather than the integrity reinforcement contribution.

5 Applications of the mechanical model

5.1 Introduction

The provisions proposed to estimate the post-punching strength were presented in Chapter 2. The general formulation proposed by codes of practice to estimate the post-punching strength can be expressed as

$$V_{pp} = A_{sb} f_{sy} \sin\psi \tag{5.1}$$

in which ψ is the angle of inclination of the reinforcing bars at failure at the vicinity of the column. This angle is different for different codes of practice. This equation does not account for other parameters influencing the post-punching behavior such as:

- Ultimate strain of integrity reinforcement (ε_{su})
- Effective depth of the slab (d)
- Integrity bar diameter (Ø)
- Initial inclination of the integrity reinforcement (β)

The aforementioned parameters can significantly influence the post-punching behavior and their effects can not be neglected in the computation of the post-punching strength. Other parameters such as the concrete compressive strength, the reinforcement ratio, the bar spacing, the column size, and the slab dimension can affect the post-punching strength. However, as shown in Chapter 4, their influence is not significant.

The study of the experimental and theoretical post-punching behavior of reinforced concrete slab-column connections is presented in Chapters 3 and 4 and Appendix A. A mechanical model capable of predicting the post-punching behavior was developed. The mechanical model is a valuable tool to account for all influencing parameters and will be used for a parametric study in this chapter. A qualitative parametric study was presented in Chapter 4 in which the base structure was similar to the test specimens and far from flat slabs in actual projects. In this chapter, a more realistic base structure is considered to investigate the effects of various parameters. The presented parametric study has the following objectives:

- To evaluate the influence of various parameters on the post-punching behavior of slab-column connections.
- To evaluate the relative importance of the various parameter.
- To acquire information to develop practical proposals for the estimation of the post-punching strength.

These objectives can be achieved by comparing the results obtained by the mechanical model and the Swiss Code proposition.

5.2 Parametric study

The mechanical model accounts for parameters ranging from material properties to geometrical properties. It was shown in Chapter 4 that the effective depth, the concrete compressive strength and the concrete cover considerably affect the tensile reinforcement contribution. On the contrary, the column width, the yielding strength and ultimate strain of steel reinforcement, the reinforcement ratio, and the angle of inclination of the punching cone did not significantly influence the tensile reinforcement contribution. On the other hand, the cross sectional area and the ultimate strain of the integrity reinforcement, and the depth of concrete over the bars can considerably influence the integrity reinforcement contribution. The influence of the other parameters on the integrity reinforcement contribution was not considerable. The influence of each parameter on the post-punching behavior can be expressed as the combination of its influence on the tensile reinforcement contribution and the integrity reinforcement contribution.

To investigate the effects of the influencing parameters on a full-scale slab-column connection, a nine column slab model is considered. Figure 5.1 shows the geometry of this nine column slab model.

The slab in question is 250 mm thick and has 5.5 m square panels. The column width is 260 mm and the effective depth is 204 mm. The applied uniformly distributed loads are

- Self weight : 0.25×25 kN/m^3 = 6.25 kN/m^2
- Dead load : 0.07×20 KN/m^3 = 1.4 kN/m^2
- Live load : 4 kN/m^2 (SIA 261)

To design the tensile reinforcement, the design load is calculated using load factors of the ultimate limit state according to SIA 262 (2003). To design the integrity reinforcement, the design load is calculated using load factors of the accidental situation according to SIA 261 (2003). The design load for dimensioning the tensile reinforcement and integrity reinforcement are 16.33 kN/m^2 and 11.65 kN/m^2, respectively. An elastic analysis is carried out to calculate the central column's reaction. The concrete cross-section is assumed to be fully cracked. The central column's reaction is calculated as 688 kN and 490 kN for the ultimate limit state and the accidental situation, respectively. The integrity reinforcement is designed by the following equation:

$$V_{d,acc} = \frac{A_{sb} f_{sd}}{1.5} \tag{5.2}$$

where f_{sd} is the design value of yielding strength of reinforcing steel. Figure 5.1.b shows the reinforcement arrangement over the central column.

The punching behavior of the slab-column connection has been calculated using the critical shear crack theory (Muttoni, 2008). The post-punching behavior of the slab has been calculated using the mechanical model. Figure 5.1.c shows the pre and post-punching behavior of the central column. The tensile reinforcement and integrity reinforcement are well-anchored in the slab and thus the tensile reinforcement contribution to the post-punching shear transfer is considered.

So far, the design values of material properties have been used for designing the structure. However, likewise the mechanical model, the characteristic values of material properties will be used for the parametric study. Thus, in the subsequent sections, the post-punching strength predicted by SIA 262 (2003) is

$$V_{pp,SIA} = \frac{A_{sb} f_{sk}}{1.5} \tag{5.3}$$

where f_{sk} is the characteristic value of the yielding strength of reinforcing steel. Assuming f_{ck} = 30 MPa, E_c = 32 GPa, f_{sk} = 500 MPa, and E_s = 205 GPa results in a punching strength of 804 kN and a post-punching strength of 701 kN for the central column. The integrity reinforcement contribution to the post-punching strength is 428 kN (61%), and the tensile reinforcement contribution is 273 kN (39%).

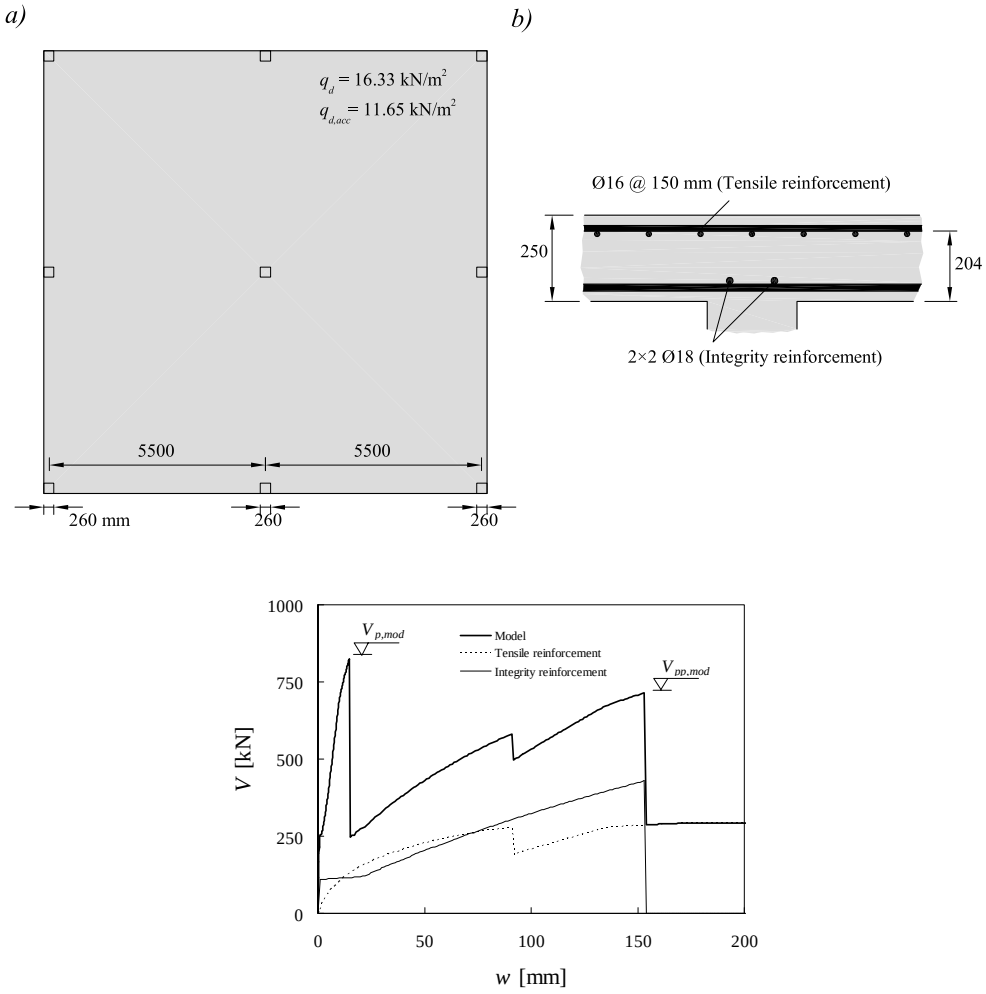

Figure 5.1: Nine column slab model: a) geometry and loading, b) reinforcement arrangement over the colum, and c) pre and post-punching behavior of the internal column

SIA 262 (2003) predicts a post-punching strength of 679 kN for the provided integrity reinforcement (2×2 Ø18) which is slightly lower than that one calculated by the mechanical model. SIA 262 (2003) does not rely on the tensile reinforcement contribution and only considers the contribution of the integrity reinforcement. The

ratio of the integrity reinforcement contribution to the post-punching strength given by the mechanical model (429 kN) to that one predicted by SIA 262 (679 kN) is 0.63. Hence, one can conclude that SIA 262 (2003) overestimates the post-punching strength provided by the integrity reinforcement. This clearly shows the influence of the other parameters on the post-punching strength, which will be discussed later. In subsequent sections, the following notations will be used:

- $V_{pp,mod}$: post-punching strength calculated by the mechanical model
- $V_{p,mod}$: punching strength calculated by the mechanical model
- $V_{pp,SIA}$: post-punching strength calculated in line with SIA 262 (2003)

Following are the influences of various parameters on the post-punching strength ranging from geometrical properties to material properties.

5.2.1 Effective depth

The influence of the effective depth on the post-punching strength in relation to the punching strength and SIA 262 (2003) is shown in Figure 5.2. The effective depth of the base slab is 204 mm and it varies between 154 and 304 mm in this analysis (154, 204, 254, and 304 mm). In the figure, the effective depth is normalized to the integrity bar diameter, which is kept constant in this analysis ($Ø = 18$ mm). According to the critical shear crack theory, the punching strength $V_{p,mod}$ significantly increases by the increase of the effective depth of the slab (47% and 97% for d is equal to 254 mm and 305 mm, respectively). In addition, the increase of the effective depth results in an increase of the tensile reinforcement contribution as discussed in Chapter 4. The increase of the tensile reinforcement contribution obviously results in an increase of the post-punching strength (13% and 23% for d is equal to 254 and 305 mm, respectively). The rate of increase of the punching strength is much higher than that one of the post-punching strength. Therefore, the ratio of $V_{pp,mod}$ to $V_{p,mod}$ decreases in Figure 5.2.a.

Comparison with SIA 262 (2003)

The increase of the effective depth does not influence the post-punching strength predicted by SIA 262 (see Equation 5.3). The increase of the effective depth of the slab results in an increase of the post-punching strength as discussed previously (13% and 23% for d is equal to 254 and 305 mm, respectively). Therefore, the ratio of $V_{pp,mod}$ to $V_{pp,SIA}$ increases as illustrated in Figure 5.2.b.

The post-punching strength without tensile reinforcement contribution remains constant as long as the failure mode is fracture of the integrity bars and not concrete breakout. The failure mode is fracture of the bar as long as the integrity reinforcement contribution (V_D) does not exceed the maximum concrete breakout strength ($V_{con,max}$). It can be concluded that the effective depth has no influence on the integrity reinforcement contribution when fracture of the integrity bars is the determinant mode of failure. However, it can significantly affect the maximum concrete breakout strength because the depth of concrete over the integrity bars plays an important role in the computation of the maximum concrete breakout strength. Moreover, it can be seen that for $d / Ø < 10$ the failure mode is no longer fracture of the bars but concrete breakout over the integrity bars ($V_D > V_{con,max}$).

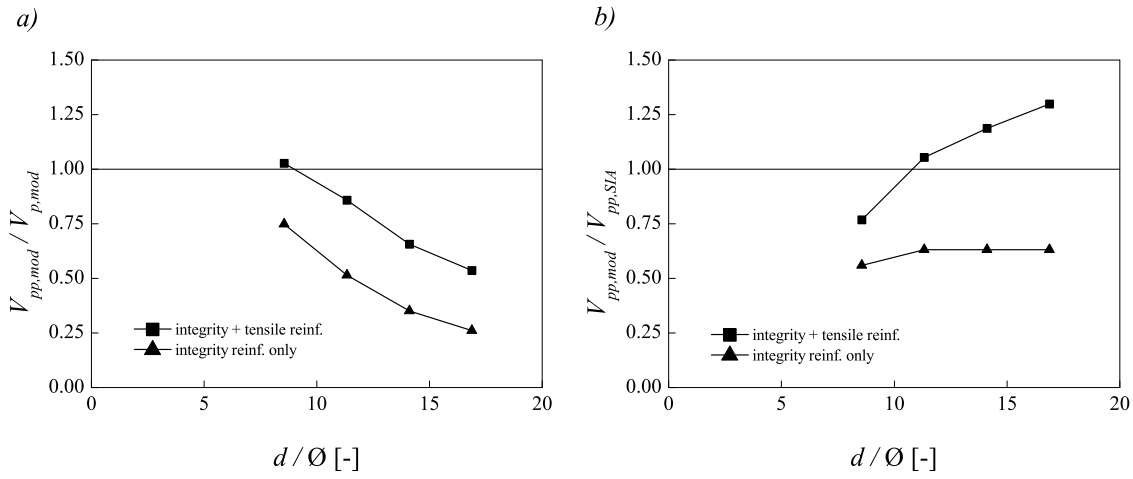

Figure 5.2: Influence of the effective depth on the post-punching strength $V_{pp,mod}$ in relation to $V_{pp,SIA}$ and $V_{p,mod}$

5.2.2 Area of the integrity bars

Figure 5.3 shows the influence of the cross-sectional area of the integrity reinforcement on the post-punching strength. In the base structure, 2×2Ø18 pass through the column as integrity reinforcement. The number of bars passing through the column is increased to investigate the effects of the amount of reinforcement while other parameters remain unchanged (ρ, d and a).

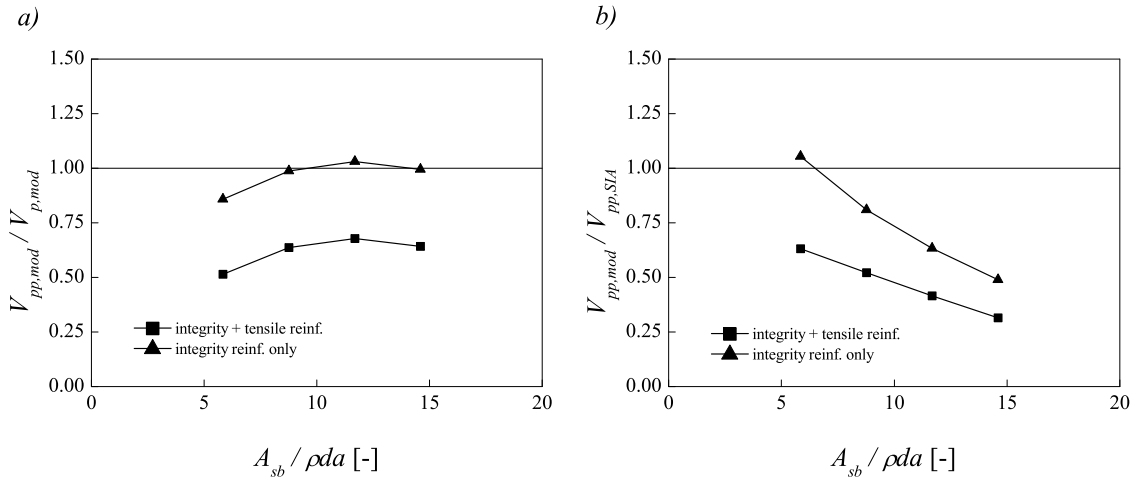

Figure 5.3: Influence of the area of the integrity bars on the post-punching strength $V_{pp,mod}$ in relation to $V_{pp,SIA}$ and $V_{p,mod}$

According to the critical shear crack theory, the increase of the cross-sectional area of the integrity bars (A_{sb}) has no influence on the punching strength and therefore $V_{p,mod}$ remains constant. Obviously, the increase of A_{sb} results in an increase of the post-punching strength and thus the ratio of $V_{pp,mod}$ to $V_{p,mod}$ increases. However, the ratio of $V_{pp,mod}$ to $V_{p,mod}$ increases up to a certain point as Figure 5.3.a shows. Beyond this point, the increase of A_{sb} does not influence the post-punching strength as concrete

breakout is the determinant mode of failure. The increase of A_{sb} can change the mode of failure of the integrity reinforcing bars ($A_{sb} / \rho da > 12$). The increase of A_{sb} increases the post-punching strength to a point at which it exceeds the maximum concrete breakout strength $V_{con,max}$. Beyond this point, the increase of A_{sb} has no influence on the post-punching strength and the ratio of $V_{pp,mod}$ to $V_{p,mod}$ remains constant.

Comparison with SIA 262 (2003)

Equation 5.3 displays that the post-punching strength given by SIA 262 (2003) is directly proportional to the area of the integrity reinforcement. Hence, as the area of the integrity reinforcement increases, the post-punching strength $V_{pp,SIA}$ increases. The post-punching strength calculated by the mechanical model $V_{pp,mod}$ also increases due to the increase of the area of the integrity bars. Although both $V_{pp,mod}$ and $V_{pp,SIA}$ increase, Figure 5.3.a shows that the ratio of $V_{pp,mod}$ to $V_{pp,SIA}$ decreases. The reason is that the rate of increase of $V_{pp,SIA}$ is higher than that one of $V_{pp,mod}$. In fact, $V_{pp,SIA}$ increases proportionally by A_{sb} ,whereas $V_{pp,mod}$ is influenced by other parameters such as the curvature localization. The latter phenomenon increases the maximum strain in the bar and consequently the maximum strain exceeds the ultimate tensile strain earlier and thus the post-punching strength slightly decreases.

5.2.3 Diameter of the integrity bars

The influence of the integrity bar diameter on the post-punching strength is shown in Figure 5.4. The integrity bar diameter of the base structure is 18 mm and it varies between 14 mm and 26 mm in this analysis (14, 18, 22, and 26 mm). In the figure, the diameter is normalized to the depth of concrete over the integrity reinforcement d_1, which remains unchanged.

The punching strength remains constant as it is not influenced by the integrity reinforcement according to the critical shear crack theory. Obviously, the increase of the integrity bar diameter results in an increase of the post-punching strength. Thus, the ratio of $V_{pp,mod}$ to $V_{p,mod}$ increases due to the increase of the post-punching strength as shown in Figure 5.4.a. It can be seen that the mode of failure changes when $d_1 / Ø < 8$. This clearly shows that using large bar diameter in thin slabs increases the possibility of concrete breakout failure.

Comparison with SIA 262 (2003)

The influence of the integrity bar diameter on the post-punching strength predicted by SIA 262 (2003) is similar to that one of the cross-sectional area of the reinforcing bars. The reason is that the increase of the bar diameter automatically increases the cross-sectional area of the integrity reinforcement. In addition, the post-punching strength predicted by the mechanical model is increased by the increase of the integrity bar diameter. However, the rate of this increase is lower than that one of $V_{pp,SIA}$ because of the other parameters influencing the post-punching behavior. Thus, the ratio of $V_{pp,mod}$ to $V_{pp,SIA}$ decreases as shown in Figure 5.4.b. The ratio of $V_{pp,mod}$ to $V_{pp,SIA}$ without tensile reinforcement contribution remains constant as long as fracture of the integrity bars is the determinant mode of failure.

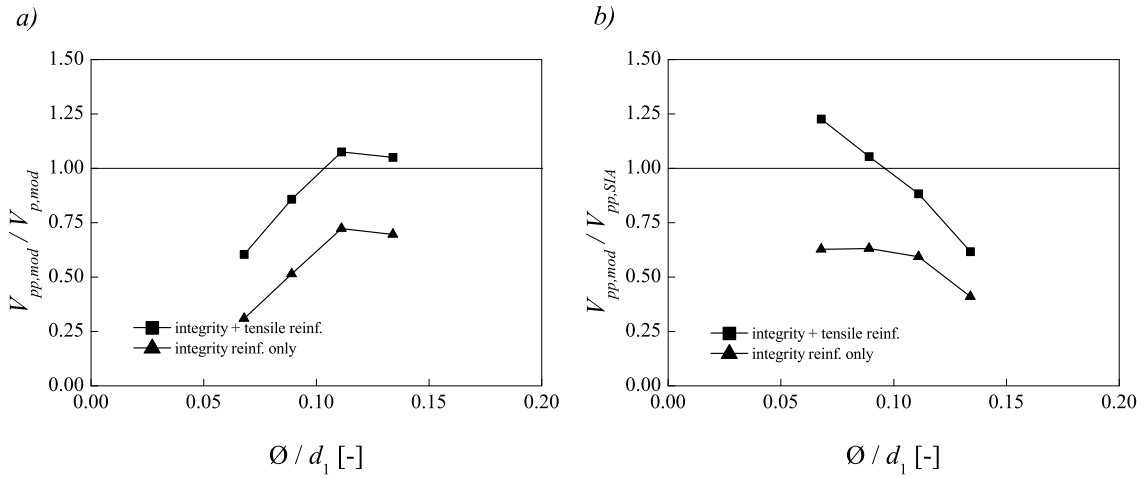

Figure 5.4: Influence of the integrity bar diameter on the post-punching strength $V_{pp,mod}$ in relation to $V_{pp,SIA}$ and $V_{p,mod}$

5.2.4 Yielding strength

Figure 5.5 shows the influence of the yielding strength of the integrity bars on the post-punching strength in relation to the punching strength and the Swiss Code proposition. The base value is 500 MPa and it varies from 400 to 700 MPa in this analysis (400, 500, 600, and 700 MPa). Other parameters remain unchanged and f_c is equal to 33 MPa.

The punching strength remains unchanged as it is not influenced by the integrity reinforcement and its material properties such as yielding strength. However, the post-punching strength is considerably influenced by the integrity reinforcement and its material properties. The increase of the yielding strength results in an increase of the post-punching strength according to the mechanical model. Thus, as shown in Figure 5.5.a, the ratio of $V_{pp,mod}$ to $V_{p,mod}$ increases.

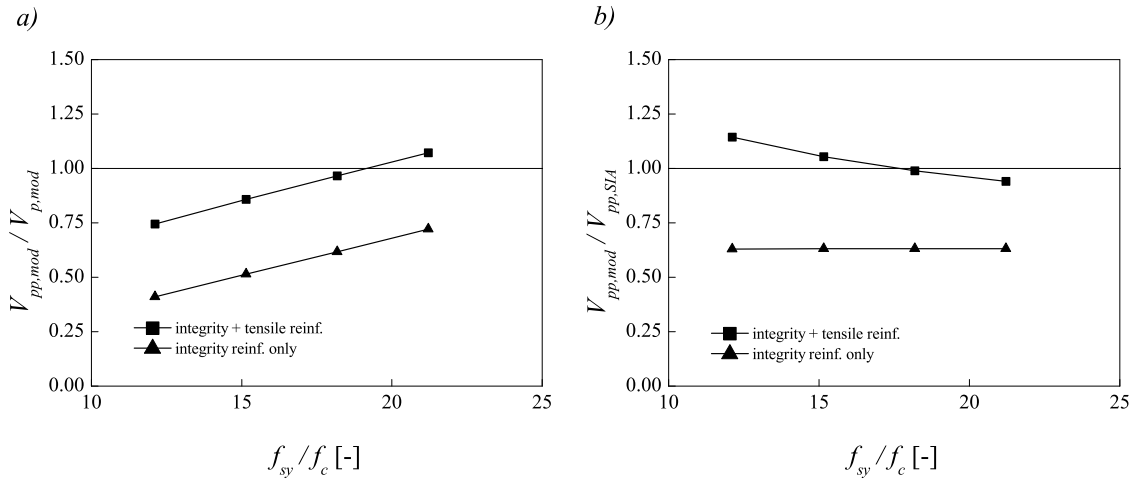

Figure 5.5: Influence of the yielding strength on the post-punching strength $V_{pp,mod}$ in relation to $V_{pp,SIA}$ and $V_{p,mod}$

Comparison with SIA 262 (2003)

The influence of the yielding strength on the post-punching behavior is similar to that one of the area of the integrity reinforcing bars and the bar diameter. The increase of the yielding strength increases the post-punching strength given by SIA 262 (2003) as $V_{pp,SIA}$ is proportional to the yielding strength. The post-punching strength predicted by the mechanical model increases as well but with a lower rate of increase than that one of SIA 262 (2003). This is attributed to the fact that other parameters influence the post-punching strength so that the ratio of $V_{pp,mod}$ to $V_{pp,SIA}$ slightly decreases as shown in Figure 5.5.b.

5.2.5 Ultimate strain

Figure 5.6 shows the influence of the ultimate tensile strain of the integrity reinforcement. In the base structure ε_{su} is equal to 15% and it varies from 5 to 20% in this analysis (5, 10, 15, and 20%). Other parameters remain unchanged.

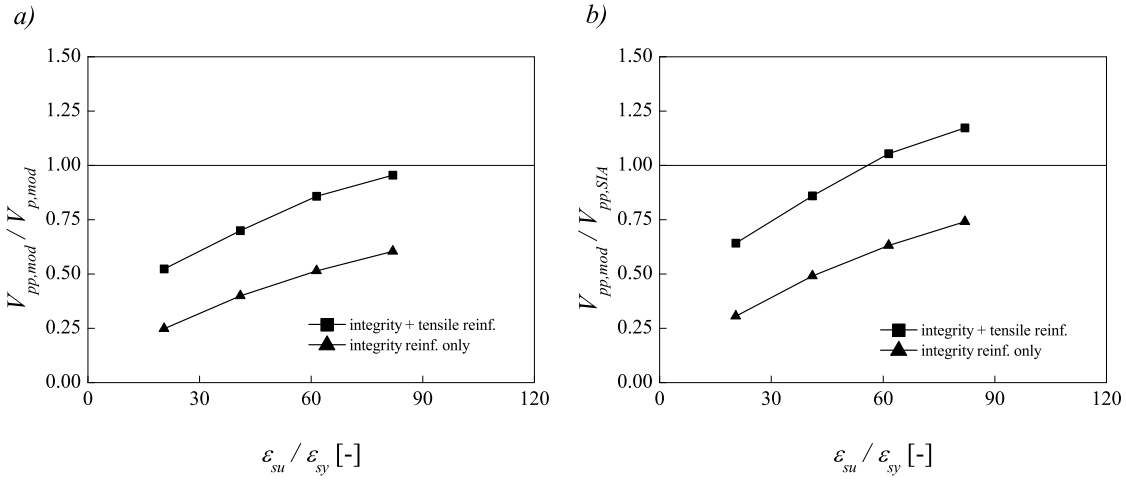

Figure 5.6: Influence of the ultimate steel strain on the post-punching strength $V_{pp,mod}$ in relation to $V_{pp,SIA}$ and $V_{p,mod}$

The punching strength is not influenced by the ultimate tensile strain of the integrity reinforcement according to the critical shear crack theory. However, the post-punching strength is considerably influenced by the material properties associated to the integrity reinforcement such as the ultimate strain. The ultimate strain is a key parameter in determining the angle of inclination of the bars at failure. In addition, it influences the failure criterion as the maximum strain in the bar at the curvature-influenced zone is compared to the ultimate tensile strain of the bar. The increase of the ultimate tensile strain results in an increase of the post-punching strength. Thus, the ratio of $V_{pp,mod}$ to $V_{p,mod}$ increases as shown in Figure 5.6.a.

Comparison with SIA 262 (2003)

The post-punching strength given by SIA 262 (2003) is not influenced by the ultimate strain of the integrity reinforcement and remains unchanged. However, the increase of the ultimate strain has a significant influence on the post-punching strength and deformation capacity. The increase of the ultimate strain decreases the consequences of

the curvature localization and increases the angle of inclination of the bars at failure. As a result, the post-punching strength increases and therefore the ratio of $V_{pp,mod}$ to $V_{pp,SIA}$ increases as shown in Figure 5.6.b.

5.2.6 Compressive strength

Figure 5.7 shows the influence of the concrete compressive strength on the post-punching strength. In the base structure f_c is equal to 33 MPa and varies from 20 MPa to 80 MPa in this analysis while other parameters are constant. The punching strength increases by the increase of the concrete compressive strength according to the critical shear crack theory. The post-punching strength slightly increases as the increase of the concrete compressive strength results in an increase of the tensile reinforcement contribution. It seems that the rate of increase of the punching and the post-punching strength are nearly the same for the increase of the concrete compressive strength. Thus, the ratio of $V_{pp,mod}$ to $V_{p,mod}$ remains almost constant as shown in Figure 5.7.a.

Comparison with SIA 262 (2003)

The post-punching strength given by SIA 262 (2003) is not influenced by the concrete compressive strength and remains constant. As pointed out before, the post-punching strength is increased by the increase of the concrete compressive strength and thus the ratio of $V_{pp,mod}$ to $V_{pp,SIA}$ increases. This ratio remains constant in the absence of a tensile reinforcement contribution as the concrete compressive strength has almost no influence on the integrity reinforcement contribution. This explanation is valid as long as the failure mode is fracture of the bar and not concrete breakout. The latter mode of failure is significantly influenced by the concrete tensile and compressive strengths.

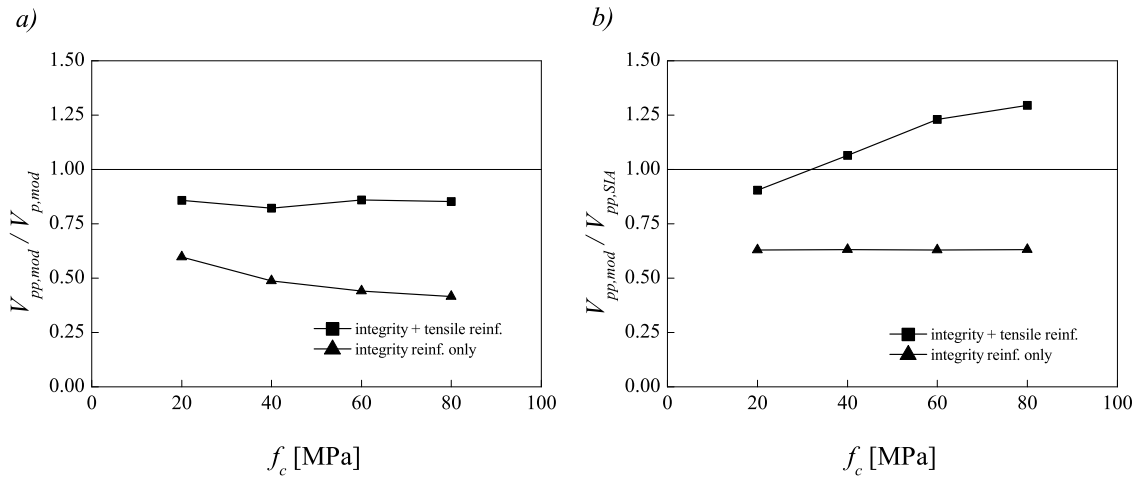

Figure 5.7: Influence of the concrete compressive strength on the post-punching strength $V_{pp,mod}$ in relation to $V_{pp,SIA}$ and $V_{p,mod}$

5.2.7 Concrete cover

The influence of the concrete cover on the post-punching strength is shown in Figure 5.8. In the base structure *c* is equal to 30 mm and varies from 20 to 50 mm in this analysis while other parameters are kept constant.

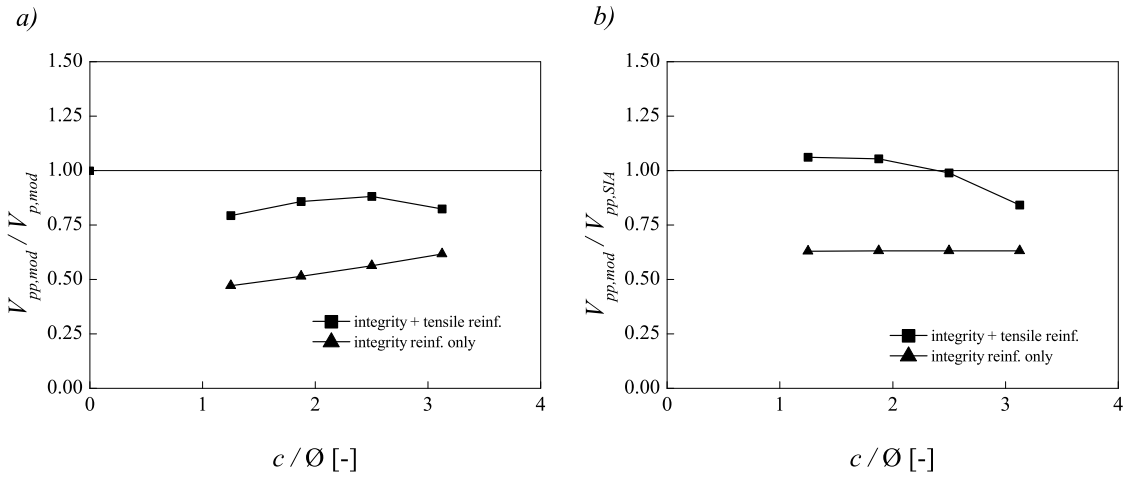

Figure 5.8: Influence of the concrete cover on the post-punching strength $V_{pp,mod}$ in relation to $V_{pp,SIA}$ and $V_{p,mod}$

Figure 5.9 plots the post-punching behavior of the internal column with different concrete covers. It clearly shows that the concrete cover has almost no influence on the integrity reinforcement contribution. However, the influence of the concrete cover on the tensile reinforcement contribution can be significant for very thick covers in terms of deformation capacity. It can be seen that the maximum tensile reinforcement contribution is almost constant for various concrete covers. The punching strength decreases because the increase of the concrete cover results in a decrease of the effective depth of the slab. As the post-punching strength is almost constant, the ratio of $V_{pp,mod}$ to $V_{p,mod}$ slightly increases.

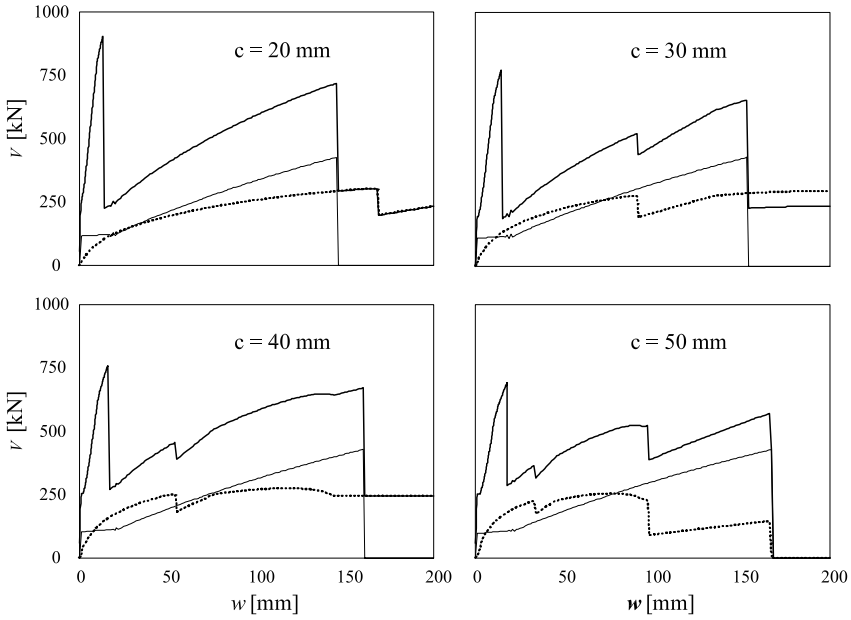

Figure 5.9: Post-punching behavior of the internal column with various concrete covers

Comparison with SIA 262 (2003)

The post-punching strength given by SIA 262 (2003) is not influenced by the concrete cover and remains constant. As discussed before, the concrete cover affects only the tensile reinforcement contribution. That is the reason why the ratio of $V_{pp,mod}$ to $V_{pp,SIA}$ is constant without tensile reinforcement contribution in Figure 5.8.b.

5.3 Influential parameters

The parametric study revealed that several parameters significantly influence the post-punching strength. These parameters are mostly associated with the integrity reinforcement. It was shown that the cross-sectional area, the bar diameter, the yielding strength, and the ultimate strain of the integrity reinforcement significantly affect the post-punching strength. In addition, it was shown that the influence of the effective depth of the slab or the depth of concrete over the integrity bars can be significant in determining the mode of failure which is either fracture of the bars or concrete destruction. It should be noted that the influence of other parameters such as the concrete compressive strength and the concrete cover on the post-punching strength is not considerable.

5.4 Simplified method

A mechanical model based on the plastic analysis and progressive destruction of the concrete over the bars is developed and presented in Chapter 4. This section describes a simplified method based on the results of the mechanical model and the parametric study.

5.4.1 Tensile reinforcement contribution

To estimate the maximum tensile reinforcement contribution to the post-punching strength, a simple model shown in Figure 5.10 is considered. The maximum tensile reinforcement contribution can be expressed as

$$V_M = A_s f_{sy} \sin \psi_M \tag{5.4}$$

where A_s is the cross-sectional area of the bars crossing the reduced punching cone that equals $4\rho d(a + d)$.

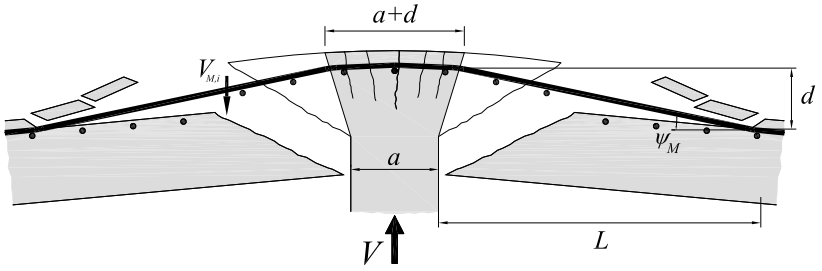

Figure 5.10: Simple model for calculating maximum tensile reinforcement contribution

Several simplifying assumptions have been made:

- The punching cone is almost fully destroyed and its diameter is reduced to $a + d$.
- Spalling of concrete cover occurs to the point of contraflexure of the slab.
- The reinforcement is fully anchored beyond the point of contraflexure.
- The maximum displacement is assumed equal to the effective depth of the slab.

Therefore,

$$V_{M,R} = 4\rho d(a+d) f_{sy} \sin\psi_M \tag{5.5}$$

The angle of inclination of the bars is small and is equal to d/L. Therefore, the maximum tensile reinforcement contribution can be calculated by

$$V_{M,R} = 8\rho d^2 f_{sy} \frac{a+d}{b-a} \tag{5.6}$$

where b is the distance between the points of contraflexure and can be chosen as 0.44 ℓ_n. Figure 5.11 compares the tensile reinforcement contribution given by Equation 5.6 and that predicted by the mechanical model. For various reinforcement ratios and column widths, the ratio of the calculated tensile reinforcement contribution to that one predicted by the mechanical model remains constant. This shows a good consistency between Equation 5.6 and the mechanical model in calculating the tensile reinforcement contribution. However, the results given by Equation 5.6 are generally more conservative than the mechanical model.

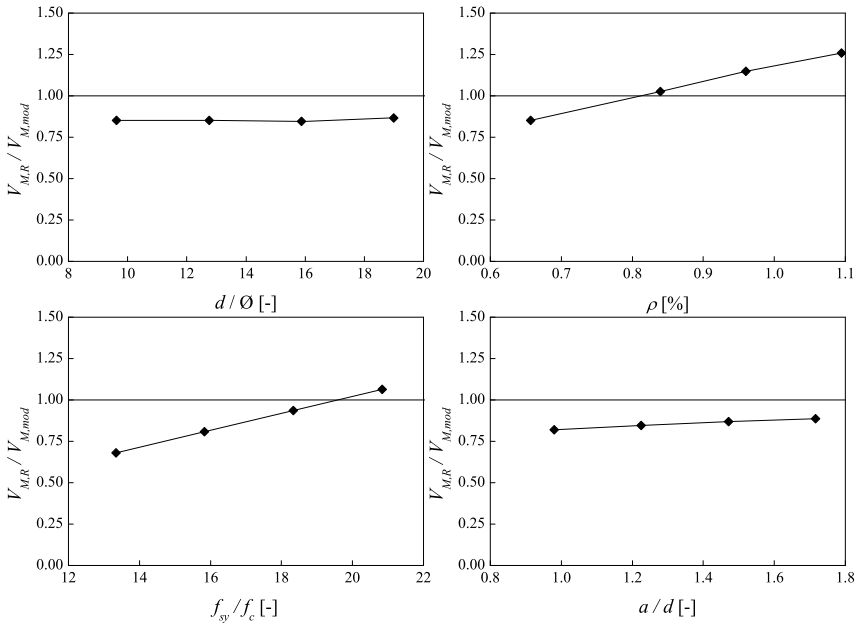

Figure 5.11: Calculated tensile reinforcement contribution of the simplified method versus the prediction of the mechanical model

For slabs with large reinforcement ratios, Equation 5.6 overestimates the calculated tensile reinforcement contribution by almost 30% in relation to the mechanical model. This significant difference is due to the fact that for large reinforcement ratios the

tensile reinforcement contribution remains almost constant. In fact, the maximum tensile reinforcement contribution is in equilibrium with the spalling strength of the concrete cover which is not sensitive to the reinforcement ratio. Figure 5.12 compares of the calculated tensile reinforcement contribution and the experimental results.

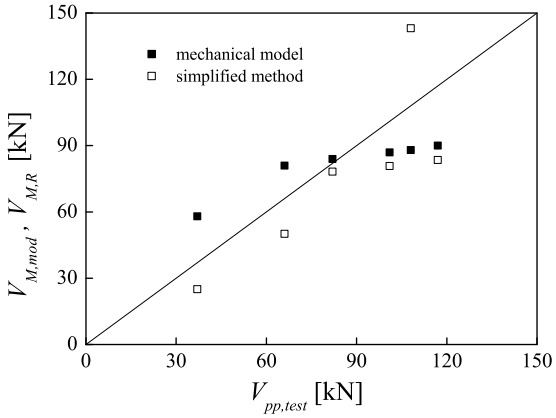

Figure 5.12: Comparison of calculated maximum tensile reinforcement contribution and experimental results

5.4.2 Integrity reinforcement contribution

As pointed out previously, the post-punching strength provided by the integrity reinforcement is limited by either the destruction of the concrete above the integrity bars or the fracture of the reinforcing bars. For relatively thin slabs ($d/Ø < 8$), the destruction of the concrete over the bars is determinant, while the fracture of the integrity reinforcement is the determinant mode of failure for thicker slabs.

5.4.2.1 Maximum concrete breakout strength

The maximum post-punching strength based on the concrete breakout strength can be expressed as

$$V_{con,max} = A_{ch} f_{ct,eff}$$
$$A_{ch} = 4\{[\theta_j + \frac{n}{2}(\pi - 2\theta_j)]d_1^2 + \frac{n-1}{2} s d_1 \sin\theta_j\} \quad (5.7)$$

where $f_{ct,eff}$ is the effective concrete tensile strength ($f_{ct,eff} = 0.6\, f_{ctm}$,see Chapter 4), n is the number of integrity reinforcement bars passing through the column, s is the bar spacing, d_1 is the depth of concrete over the bars, and $\theta_j = \cos^{-1}(s / 2d_1)$. The theoretical and graphical interpretation of this equation is thoroughly described in Chapter 4 and Appendix B. Equation 5.7 is a complex expression that can be further simplified for typical cases. As illustrated in Figure 5.13, the horizontal projection of adjacent conical failure surfaces can be approximated by a rectangle and two quarter circles. Therefore, the total horizontal projection of the conical failure surfaces of integrity bars passing through the column is

$$A_{ch} = 4d_1\left(\frac{\pi}{2}d_1 + b'\right) \tag{5.8}$$

where b' is the distance between the first and the last integrity bar passing through the column and equal to $(n\text{-}1)\cdot s$. Figure 5.14 compares this approximated horizontal projection area of various number of integrity bars with the area calculated by Equation 5.7. There is a good correlation between the two approaches.

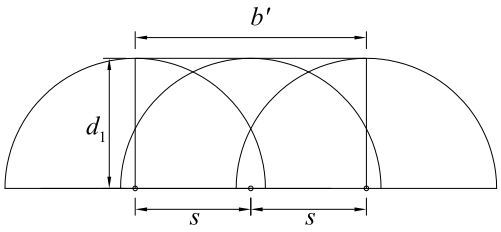

Figure 5.13: Approximated horizontal projection area of adjacent conical failure cones

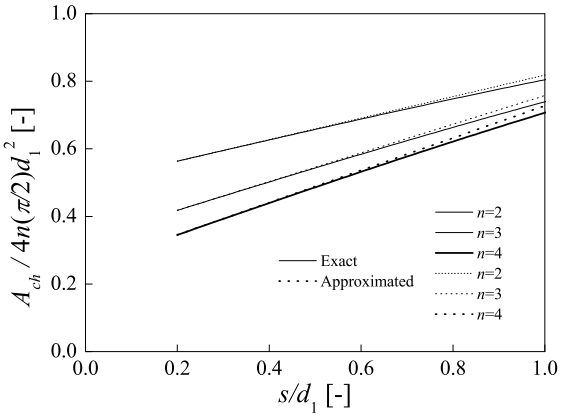

Figure 5.14: Comparison of the results of Equation 5.8 and Equation 5.7 calculating the horizontal projection of conical failure cones

5.4.2.2 Fracture of the integrity reinforcement

For the mode of failure associated with the fracture of the integrity reinforcement, a simple model shown in Figure 5.15 is considered as. The post-punching strength governed by the fracture of the integrity reinforcement can be estimated as

$$V_{D,R} = A_{sb} f_{sy} \sin\psi_u \tag{5.9}$$

where according to Figure 5.15,

$$\psi_u = \cos^{-1}\left(\frac{\cos\beta}{1+\varepsilon_{su}}\right) \tag{5.10}$$

Therefore,

$$V_{D,R} = A_{sb} f_{sy} \sin\left(\cos^{-1}\left(\frac{\cos\beta}{1+\varepsilon_{su}}\right)\right) \tag{5.11}$$

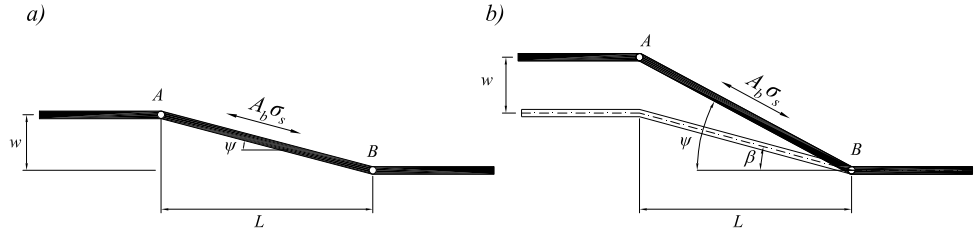

Figure 5.15: Simple model for calculating the maximum integrity reinforcement contribution: a) straight integrity bars and b) bent-up bars

This equation can be simplified using the Taylor series, a representation of a function as an infinite sum of terms calculated from the values of the derivatives at a single point. This series yields to the following equation

$$\sin\left(\cos^{-1}\left(\frac{\cos\beta}{1+\varepsilon_{su}}\right)\right) \approx \sin\beta(1+\varepsilon_{su}\cot^2\beta) \tag{5.12}$$

where β is the initial angle of inclination of bent-up bars. Figure 5.16 plots both sides of Equation 5.12, and reveals that the right-hand side of this equation is a good approximation of the left-hand side for practical range of the ultimate strain and the angle of inclination of bent-up bars ($0.05 < \varepsilon_{su} < 0.125$).

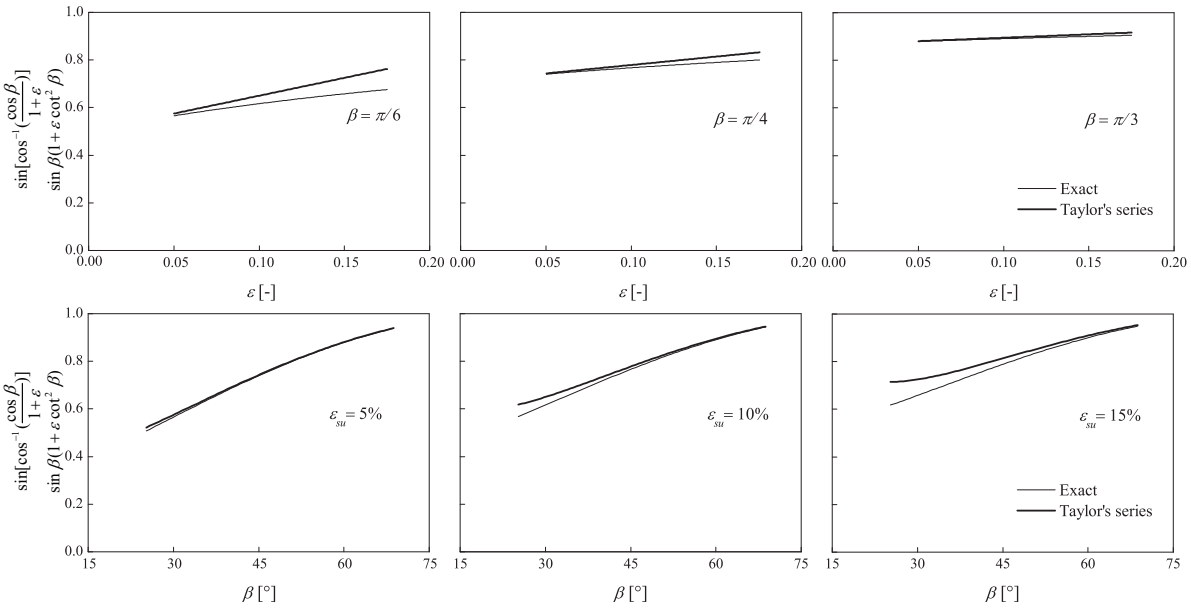

Figure 5.16: Results of the Taylor series in relation to the exact solution for bent-up bars

Equation 5.12 does not apply to integrity reinforcing bars because β is equal to zero. Using the Taylor series for integrity reinforcing bars leads to the following equation:

$$\sin\left(\cos^{-1}\left(\frac{1}{1+\varepsilon_{su}}\right)\right) \approx \sqrt{2\varepsilon_{su}} \tag{5.13}$$

Figure 5.17 shows the satisfactory result of this approximation in relation to the exact solution.

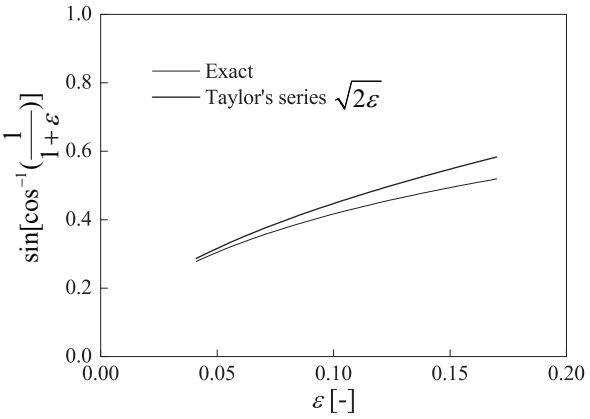

Figure 5.17: Results of the Taylor series in relation to the exact solution for integrity bars

The maximum integrity reinforcement contribution to the post-punching strength can thus be calculated as

$$V_{D,R} = A_{sb} f_{sy} \sqrt{2\varepsilon_{su}} \tag{5.14}$$

In addition, the maximum contribution of bent-up bars to the post-punching shear strength can be calculated as

$$V_{D\beta,R} = A_{sb} f_{sy} \sin\beta(1+\varepsilon_{su}\cot^2\beta) \tag{5.15}$$

where $V_{D\beta,R}$ is the maximum contribution of bent-up bars to the post-punching strength of a slab-column connection. Figures 5.18 and 5.19 compare the post-punching strength given by Equations 5.14 and 5.15 to those predicted by the mechanical model for various parameters. These figures show that there is an offset between the results, which can be adjusted by a constant. This difference is related to the effects of the curvature localization. This phenomenon, which is described in Chapter 4, reduces the angle of inclination of integrity bars, thus decreasing the contribution of the integrity reinforcement. As described in Chapter 4, the angle of inclination of integrity reinforcing bars at failure is

$$\psi_u = \cos^{-1}\left(\frac{1}{1+\varepsilon_{su}-\frac{\psi_u}{6}}\right) \tag{5.16}$$

The influence of the curvature localization is included in Equation 5.16. However, Equation 5.13 does not take into account the influence of the curvature localization. A factor can be added to adjust the results of the simplified method. This factor can be calculated according to the mechanical model. Shown in Figure 5.20, this factor varies from 0.88 to 1.07 for ε_{su} = 5% to 12.5%, respectively. An average value of 1.0 can thus be selected for k_1. Therefore, the maximum integrity reinforcement contribution to the post-punching strength can be estimated as

$$V_{D,R} = k_1 A_{sb} f_{sy} \sqrt{\varepsilon_{su}} \tag{5.17}$$

where k_1 = 1.0.

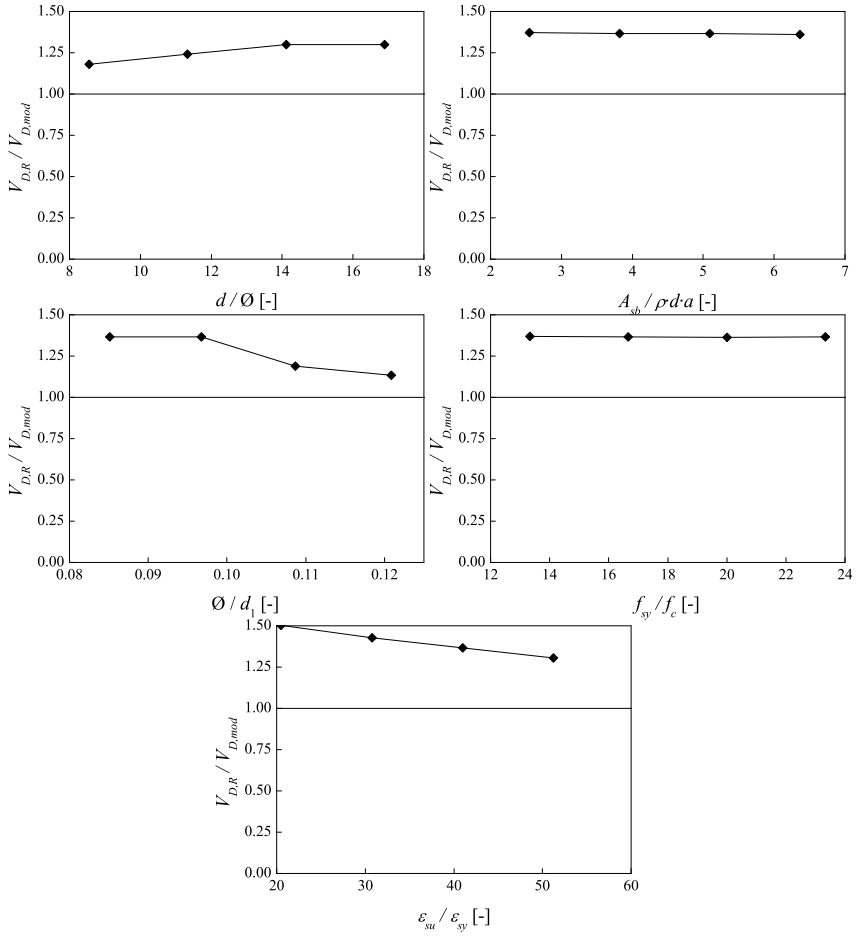

Figure 5.18: Calculated integrity reinforcement contribution of the simplified method versus the prediction of the mechanical model

To adopt a single formulation that applies to both integrity reinforcement and bent-up bars contributing to the post-punching strength, the following equation should be satisfied:

$$k_3 \sin\beta(1+\varepsilon_{su}\cot^2\beta) = k_1\sqrt{\varepsilon_{su}} + k_2 \sin\beta \tag{5.18}$$

The left-hand side of this equation comes form Equation 5.15. Factor k_3 is added to adjust the offset between the results given by Equation 5.15 and that predicted by the mechanical model (Figure 5.19). Factor k_2 can be calculated according to the mechanical model. Figure 5.21 shows the variation of k_2 as a function of the initial angle of inclination of bent-up bars. The variation of k_2 in not significant for the practical range of the ultimate strain (5% < ε_{su} <12.5%). An average value of 0.6 can be chosen for this factor. The maximum contribution of integrity reinforcement and bet-up bars to the post-punching strength can be estimated as

$$V_{D,R} = A_{sb} f_{sy} (\sqrt{\varepsilon_{su}} + 0.6 \sin\beta) \tag{5.19}$$

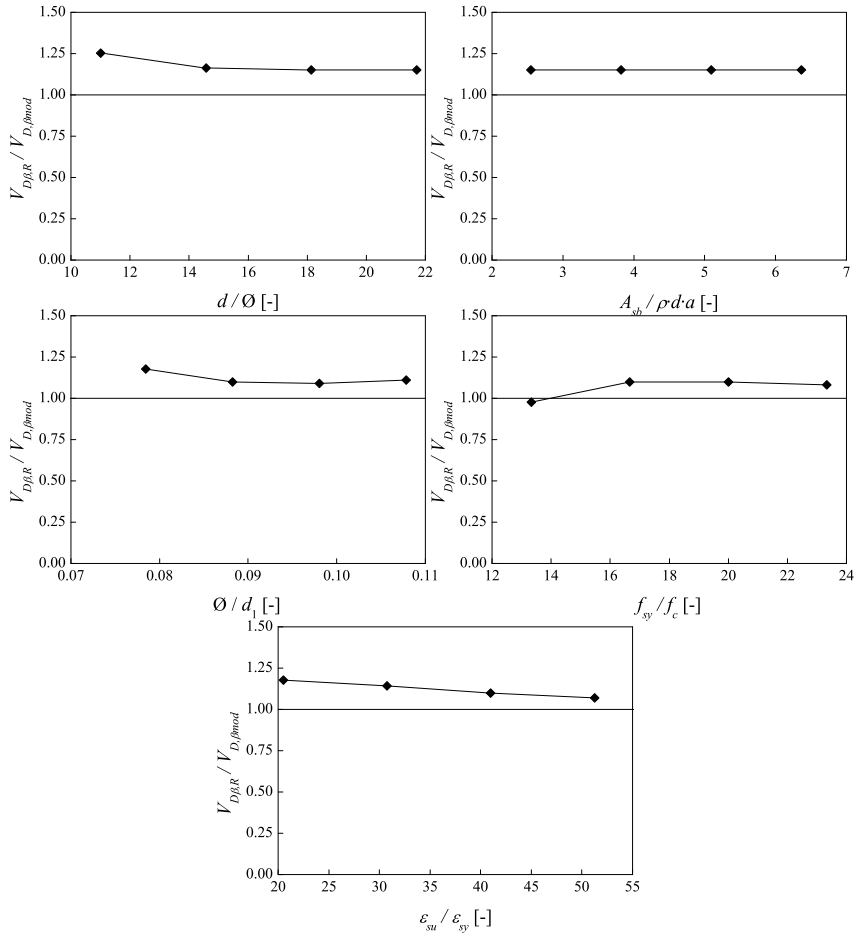

Figure 5.19: Contribution of bent-up bars to the post-punching strength calculated by simplified method versus the prediction of the mechanical model

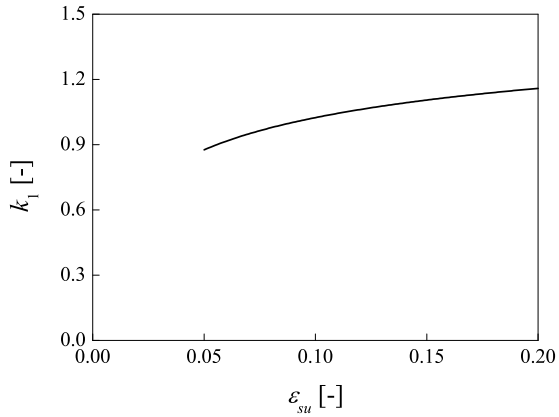

Figure 5.20: Factor k_1 as a function of the ultimate strain of steel

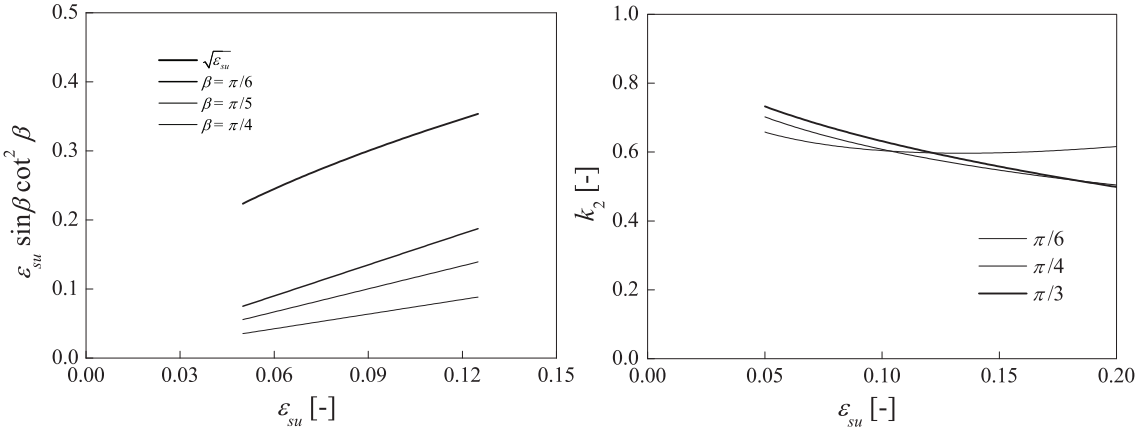

Figure 5.21: Evolution of factor k_2 as a function of the ultimate strain of steel

5.4.3 Post-punching strength

The post-punching strength is the sum of the tensile reinforcement contribution and the integrity reinforcement contribution:

$$V_{pp,R} = V_{M,R} + V_{D,R} \tag{5.20}$$

Thus,

$$V_{pp,R} = A_{sb} f_{sy} (\sqrt{\varepsilon_{su}} + 0.6\sin\beta) + 8\rho d^2 \cdot f_{sy} \cdot \frac{a+d}{b-a} \tag{5.21}$$

Contrary to the current post-punching provisions, the simplified method accounts for the most influential parameters. Figure 5.22 shows the influence of various parameters on the ratio of the post-punching strength calculated by the simplified method in relation to that predicted by the mechanical model.

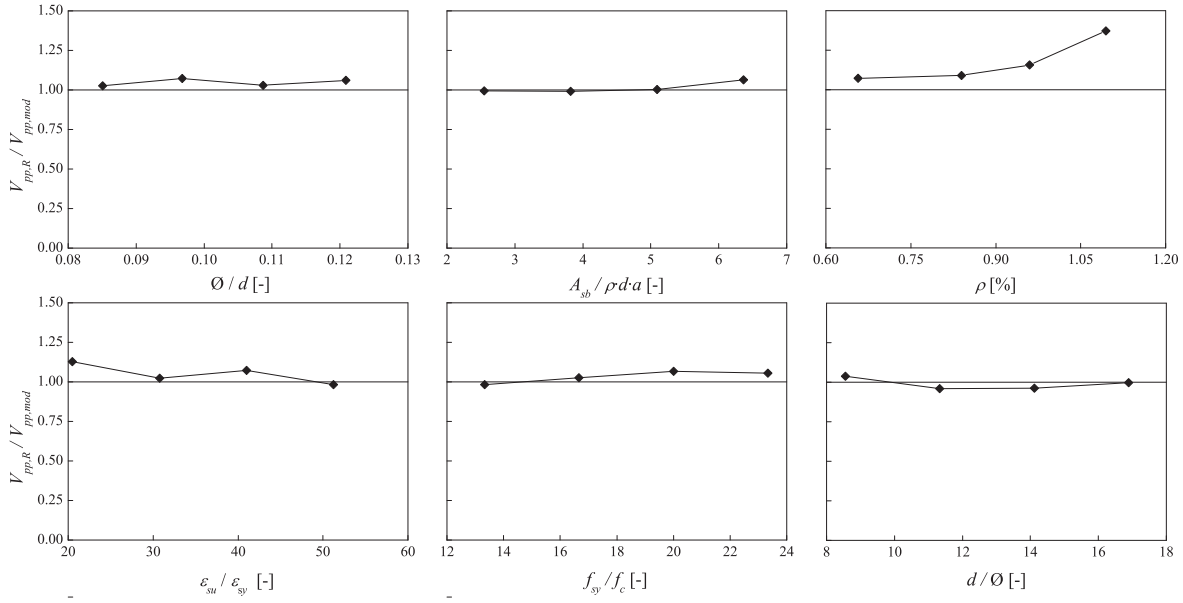

Figure 5.22: Influence of various parameters on the ratio of the post-punching strength based on the simplified method to the strength based on the mechanical model

The ratio of the post-punching strength given by the simplified method to that predicted by the mechanical model ($V_{pp,R} / V_{pp,mod}$) remains almost constant for various parameters. This means that the simplified method can satisfactorily predict the post-punching strength of slab-column connections in relation to the mechanical model. For slabs with large reinforcement ratio, the simplified method overestimates the post-punching strength in relation to the mechanical model. This is because the tensile reinforcement contribution is almost constant for large reinforcement ratios.

As shown in Figure 5.23, a good agreement has been found between the measured post-punching strength and the post-punching strength calculated by the simplified method. The average value of the measured-to-estimated post-punching strength is 0.95 with a coefficient of variation of 0.21.

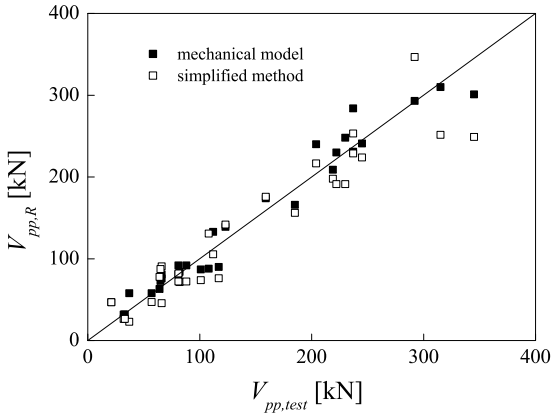

Figure 5.23: Post-punching strength predicted by simplified method and mechanical model versus available experimental data

The simplified method is able to predict the failure mode of slab-column connections. The failure mode in the current provisions is assumed to be the fracture of the bar which is not a necessarily correct assumption. The increase of the cross-sectional area and the bar diameter of the integrity reinforcement can easily change the failure mode because developed force in the integrity reinforcing bars increases and exceeds the maximum concrete breakout strength. It should be noted that other parameters such as the ultimate strain and the yielding strength do not change the failure mode for the practical range of the ultimate strain and yielding strength (ε_{su} < 12.5% and f_{sy} < 600 MPa).

To adopt a design proposal based on the simplified method, only the test specimens that included both tensile reinforcement and integrity reinforcement (bent-up bars) are considered. This is because both tensile reinforcement and integrity reinforcement are present in the case of actual slabs. In order for the design proposal to lead to a satisfactory safety level, the 5% fractile should be larger than 1.0 in the present study (Figure 5.24). The 5% fractile is the value (or score) below which five percent of the observations may be found. Figure 5.24 plots the results of the design proposal in relation to the experimental data. The average value of the measured-to-estimated post-punching strength for these tests is 1.27 with a coefficient of variation of 0.13.

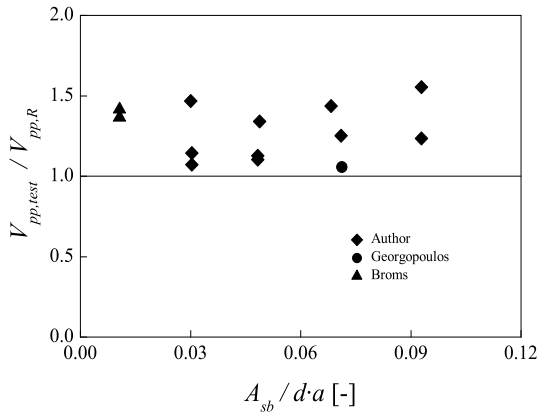

Figure 5.24: Post-punching strength predicted by the simplified method in relation to experimental data

To calculate the 5% fractile, it can be assumed that the test data belongs to a normally distributed population. The normal distribution is often used to describe or approximate any variable that tends to cluster around a mean. Figure 5.25 shows the histogram of the test data, which seems not to be normally distributed. The Kolmogorov–Smirnov test has been used to check the normality of the test data. This test relies on the fact that the value of the sample cumulative density function is asymptotically normally distributed. The Kolmogorov–Smirnov test can be used as a goodness of fit test. In the special case of testing for normality of the distribution, samples are standardized and compared with a standard normal distribution. The results of this analysis show that the test data does belong to a normally distributed population. Therefore, considering the normal distribution for the test data results the value of 1.00 for the 5% fractile according to the following equation:

$$5\%\text{Fractile} = \mu\left(1+\frac{z}{\mu}\sigma\right) \tag{5.22}$$

where μ is the mean value, σ is the standard deviation of the normal distribution, and z equals -1.645, which can be calculated by

$$\Phi(z) = \int_{-\infty}^{z} \phi(x)dx = \frac{1}{\sqrt{2\pi}} \int_{-\infty}^{z} e^{\frac{-x^2}{2}} dx = 0.05 \tag{5.23}$$

where $\Phi(x)$ is the cumulative distribution function and $\phi(x)$ is the probability density function.

The tensile reinforcement contribution to the post-punching strength can be neglected for design purposes because of the unreliable behavior of the tensile reinforcement. This unfavorable behavior is a result of the spalling of the concrete cover and the detachment of the bars from the concrete surface. In addition, uncertainties about the anchorage condition make it difficult to consider the tensile reinforcement contribution to the post-punching strength. Thus, the post-punching design proposal can simply be expressed as

$$V_{pp,R} = A_{sb} f_{sy} (0.86\sqrt{\varepsilon_{su}} + 0.5\sin\beta) \tag{5.24}$$

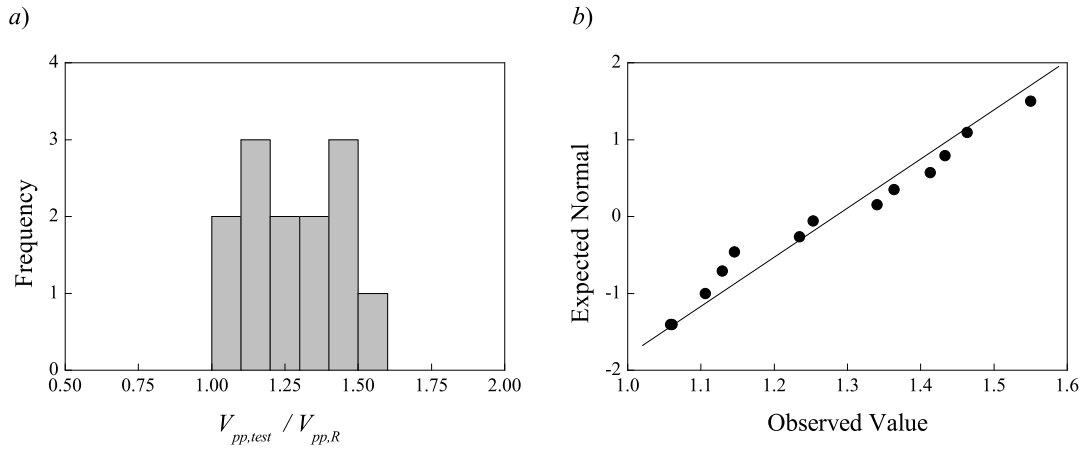

Figure 5.25: Results of the Kolmogorov–Smirnov test: a) histogram and b) normal Q-Q plot

Finally, the following design proposal is proposed to estimate the post-punching strength accounting for the most influential parameters:

$$V_{pp,R} = A_{sb} f_{sy} \frac{2\sqrt{\varepsilon_{su}} + \sin\beta}{2.2} \leq 4d_1 \left(\frac{\pi}{2} d_1 + b' \right) (0.6 f_{ctm}) \tag{5.25}$$

where ε_{su} accounts for the ductility of the reinforcement, β accounts for the initial angle of inclination of bent-up bars, which is zero for straight bars passing through the column. The right-hand side of the equation accounts for the maximum concrete breakout strength, which is the upper bound value of the post-punching strength.

5.4.4 Design example

The central column of the slab shown in Figure 5.1 is designed to carry the accidental load in the post-punching phase. The accidental load transferred to the column is 490 kN according to SIA 260 (2003). A comparison of the required amount of the integrity reinforcement calculated by the design proposal as well as by SIA 262 (2003) is given in Table 5.1.

The required amount of the integrity reinforcement by the design proposal is much higher than that predicted by SIA 262 (2003). For the same integrity reinforcement, the ratio of the post-punching strength calculated by the design proposal and that predicted by SIA 262 is 0.37 (β is equal to zero and ε_{su} is equal to 7.5%). This means that, for the same amount of reinforcement, SIA 262 overestimates the post-punching strength of the slab-column connections. In addition, for the same accidental design load the design proposal requires more reinforcement in relation to that given by SIA 262. As the simplified method and design proposal is in a good agreement with the experimental data, it can be concluded that SIA 262 overestimates the post-punching strength of slab-column connections. Thus, the structural design based on the current provision does not provide a satisfactory safety margin for slab-column connections.

One may argue that the amount of integrity reinforcement required for the post-punching design is too large and using large diameters is inevitable. Using large bar diameters is not common in common projects. It should be noted that the design proposal is very flexible for using various reinforcement arrangement. As Table 5.1

illustrates, one may use 2×3 Ø22 instead of 2×2 Ø30 to reduce the diameter of the integrity bars or reduce the bar diameter even more by using bent-up bars, taking advantage of their initial angle of inclination.

Table 5.1: Example of post-punching design of an interior slab-column connection

	Formulation		Integrity reinforcement
SIA 262	$V_{pp,SIA} = \frac{A_{sb} f_{sd}}{1.5}$		2×2 Ø18
Design proposal	$V_{pp,d} = A_{sb} f_{sd} \frac{2\sqrt{\varepsilon_{su}} + \sin\beta}{2.2} \leq V_{con,max}$		2×2 Ø30
		or	2×3 Ø22
		or	2×2 Ø20 bent-up bars (β = 30°)
		or	2×2 Ø18 bent-up bars (β = 45°)

5.5 Minimum integrity reinforcement

Continuous integrity reinforcing bars are used to give residual capacity to slab and prevent its local failure leading to a progressive collapse of the large part of the structure. The integrity reinforcement ratio is defined as

$$\rho_{int} = \frac{A_{sb}}{u_0 d} \tag{5.26}$$

where u_0 is the perimeter of the column. In the absence of the integrity reinforcement (ρ_{int} = 0), the post-punching strength is small and insufficient for the load redistribution after a punching failure. According to the experimental results presented in Chapter 3, for low reinforcement ratios (ρ_{int} < 1.2%), the contribution of the tensile reinforcement and the contribution of the integrity reinforcement contribution to the post-punching strength are almost the same and insufficient for the load redistribution after a punching failure. However, for high reinforcement ratios (ρ_{int} > 1.2%), the integrity reinforcement contribution increases considerably. Thus, a minimum reinforcement ratio can be defined as equal to 1.2%. This minimum reinforcement ratio results in 2×2 Ø20 for a slab similar to the one analyzed in this chapter.

5.6 Design recommendations

The following are several recommendations to improve the post-punching strength of slab-column connections and to increase the robustness of the structure against the possibility of a progressive collapse:

- The flexural reinforcement should be continuous over the column area to take advantage of the tensile reinforcement contribution. A minimum length of 3*d* plus the full anchorage length of the reinforcement from the column face should be provided.

- At least two integrity reinforcing bars in each direction must pass through the column core. These must be anchored in the slab. The minimum integrity reinforcement ratio should be provided to protect the system against unforeseen circumstances.
- The post-punching design proposal is expressed as

$$V_{d,acc} \le V_{pp,d} = A_{sb} f_{sd} \frac{2\sqrt{\varepsilon_{su}} + \sin\beta}{2.2} \le 4d_1 \left(\frac{\pi}{2} d_1 + b' \right) (0.6 f_{ctd}) \qquad (5.27)$$

- A very ductile type of steel shall be chosen for the integrity reinforcement to enhance the post-punching strength. Therefore, the use of hot-rolled steel with a high ultimate strain is strongly recommended.
- Using well-anchored bent-up bars is recommended to decrease the required amount of reinforcement by taking advantage of the initial angle of inclination of the bent-up bars.

6 Conclusions

This chapter summarizes the results obtained within this thesis. The summary and principal results related to the objectives of the thesis are given, and suggestions for future work are proposed.

6.1 Results and concluding remarks

Particular attention should be paid to the design and detailing of concrete slab-column connections. Otherwise, these connections can be "weak links", the failure of which can initiate progressive collapse leading to partial or complete collapse of the structure. As it is not feasible to foresee all possible sources of collapse initiation, a rational progressive collapse design should aim at localizing damage, rather than preventing damage on the whole structure. This is related to structural robustness because the inherent redundancy and continuity of a robust structure prevent local failure from propagating throughout the structure. To localize the consequences of a possible local punching failure, it is necessary for the slab-column connection to possess a significant post-punching strength.

Although large scientific efforts have been devoted to punching shear failure, post-punching behavior of flat slabs has received far less attention. The post-punching behavior of flat slabs, particularly the effects of various parameters and reinforcement layouts, have not yet been thoroughly investigated. Hence, an extensive experimental campaign was carried out to extend the knowledge of post-punching behavior of slab-column connections. A total of 24 slab specimens with various reinforcement layouts were tested, and their post-punching behavior was recorded. The effects of tensile reinforcement, integrity reinforcement passing through the column, bent-up-bars, and anchorage details were investigated.

The test results showed that the reinforcing bars play an important role in post-punching behavior as they are the only remaining link between the punching cone and the rest of the slab. Therefore, the load-carrying mechanisms that take place after punching failure are related to the well-anchored tensile reinforcement and to the integrity reinforcement passing through the column.

The post-punching strength provided by the tensile reinforcement is small because the concrete cover is thin and susceptible to spalling. Tensile reinforcing bars tear out of concrete at an almost constant load until the remaining anchorages are inadequate and the reinforcing bars are detached from the concrete surface. On the contrary, integrity reinforcing bars can carry load by developing high tensile stresses ($> f_{sy}$) accompanied by a significant inclination. It was observed that the inclusion of integrity reinforcement made it possible for PM-12 to reach nearly the punching strength of the slab (98%), which can be considered as a way to mitigate the likelihood of a progressive collapse.

A mechanical model capable of predicting the post-punching behavior of slab-column connections without shear reinforcement was formulated. Following are the conclusions drawn in relation with the proposed model:

- The performance of reinforcing bars acting against the concrete cover and against the punching cone is fundamentally different. However, a generic procedure was developed capable of predicting the behavior of all possible mechanisms. Within this scope, the concept of concrete breakout strength, maximum concrete breakout strength, spalling strength of concrete cover, and strain-based failure criterion were introduced.
- Various approaches were proposed to consider both the elastic and the plastic behavior of reinforcing bars crossing the punching cone. However, the plastic behavior is mostly determinant as the axial strain exceeds the yielding strain at the beginning of the post-punching phase.
- Based on experimental results and by utilizing the concept of the curvature-influenced zone coupled with compatibility relations to predict the maximum curvature at the face of crack, the maximum strain at the extreme tension fiber of the bar can be calculated. A failure criterion was developed in which the maximum strain in the reinforcing bars is compared with the ultimate tensile strain.
- The post-punching strength is the summation of the contribution of the tensile reinforcement and the contribution of the integrity reinforcement to the post-punching shear transfer. A comparison between the proposed model and the experimental results was presented and the predicted post-punching behavior was in a good agreement with the experimental data.
- It was shown by a parametric study that the effective depth of the slab, the concrete tensile strength and the concrete cover significantly affect the contribution of the tensile reinforcement to the post-punching strength. On the other hand, the ultimate tensile strain and the cross-sectional area of the integrity reinforcement and, the depth of the concrete over the integrity reinforcement considerably influence the contribution of the integrity reinforcement to the post-punching shear transfer.

The post-punching strength provided by the integrity reinforcement is limited either by the destruction of the concrete above the integrity reinforcing bars or by the fracture of the reinforcing bars. It was shown by the proposed model and experimental evidence that the maximum concrete breakout governs the post-punching strength when the depth of the concrete over the integrity reinforcement is smaller than eight times the bar diameter. At such circumstances, the maximum concrete breakout strength remains constant for further deflection as the thickness of the concrete above the integrity reinforcement is constant. Thus, no further increase of the post-punching strength will occur. The maximum post-punching strength based on this mode of failure can be expressed as

$$V_{con,max} = A_{ch} f_{ct,eff}$$

$$A_{ch} = 4d_1\left(\frac{\pi}{2}d_1 + b'\right)$$

where A_{ch} is the horizontal projection of the conical failure surface, $f_{ct,eff}$ is the effective tensile strength of concrete.

The post-punching strength as limited by the fracture of the integrity reinforcement can be estimated as

$$V_{pp,R} = A_{sb} f_{sy} \frac{2\sqrt{\varepsilon_{su}} + \sin\beta}{2.2}$$

The upper bound value of the post-punching strength of a slab-column connection should be the maximum concrete breakout strength

$$V_{pp,R} \leq 4d_1 \left(\frac{\pi}{2} d_1 + b' \right) f_{ct,eff}$$

The post-punching design proposal can be expressed as

$$V_{pp,d} = A_{sb} f_{sd} \frac{2\sqrt{\varepsilon_{su}} + \sin\beta}{2.2} \leq 4d_1 \left(\frac{\pi}{2} d_1 + b' \right) (0.6 f_{ctd})$$

It should be mentioned that the integrity reinforcement must be well-anchored in the slab in order for the abovementioned post-punching strength to be achieved. A total length from the column face equal to 3*d* plus the full anchorage length should be adequate.

The way that a punching shear failure of a slab-column connection can lead to progressive collapse depends not only on the post-punching behavior of the connection but also on the overall behavior and flexural characteristics of the region of the slab surrounding the damaged connection and the punching strength of adjacent slab-column connections.

The experimental investigation and the proposed model have principally considered only interior slab-column connections as the regions of initial punching failure. However, the initial damage can initiate from edge or corner columns. In the event of punching failure at an edge column, reliance can be placed on the post-punching strength provided by the integrity reinforcement parallel to the slab edge. Reinforcing bars perpendicular to the edge might not be very useful because they tend to pull the column inward. In the event of punching failure at a corner column, the integrity reinforcement would probably be of relatively little use. Although punching failure of a corner column slightly increases the edge column's reaction, large deflection of the damaged area with a hyperbolic-parabolic behavior will be beneficial to the load carrying capacity of the slab.

6.2 Future work

Due to the complexity of post-punching behavior of slab-column connections and progressive collapse of flat slabs, this thesis could not have analyzed all the typologies and issues related to progressive collapse following a punching failure. However, in order to build on the above presented results, some suggestions for future work can be outlined as follows:

- Using nonlinear dynamic finite element analysis to simulate the progressive collapse of flat slabs following a punching shear failure of a slab-column connection.

- Post-punching behavior of flat slabs considering the dynamic nature of initial failures.
- The effects of impact, seismic loading and imposed deformations on the progressive collapse of flat slabs supported by columns.
- Post-punching behavior of flat slabs with shear reinforcement.
- Post-punching behavior of flat slabs with shear reinforcement in combination with bent-up bars.
- Non-symmetric post-punching behavior of flat slabs.
- Full scale test of slab-column connections with integrity reinforcement passing through the column.
- Full scale test of complete flat slabs, e.g. a sixteen column flat slab with the columns detailed with various reinforcement layouts.
- Post-punching behavior of edge or corner columns.

Bibliographic references

ACI, *Code Requirements for Nuclear Safety Related Concrete Structures,* ACI 349-01, American Concrete Institute, 134 p., USA, **2001**.

ACI, *Recommendations for Design of Beam-Column Connections in Monolithic Reinforced Concrete Structures*, ACI 352R-02, ACI-ASCE Committee 352, American Concrete Institute, 37 p., USA, **2002**.

ACI, *Building Code Requirements for Structural Concrete,* ACI 318-08, American Concrete Institute, ACI Committee 318, 368 p., Detroit, **2008**.

ASCE 7, *Minimum Design Loads for Buildings and Other Structures*, American Society of Civil Engineers, SEI/ASCE 7-05, Reston, VA, USA, **2005**.

Bailey C. G., *Efficient arrangement of reinforcement for membrane behavior of composite floor slabs in fire conditions*, Journal of Constructional Steel Research, Vol. 59, No. 7, pp. 931-949, July, **2003**.

Bailey C. G., Toh W. S., Chan B. M., *Simplified and Advanced Analysis of Membrane Action of Concrete Slabs*, ACI Structural Journal, Vol. 105, No.1, pp. 30-40, January, **2008**.

Baumann T., *Versuche zum Studium der Verdubelungswirkung der Biegezugbewehrung eines Stahlbetonbalken*, Material Prüfungsamt Für Das Bauwesen Der Technischen Hochschule, München, Bericht, No.77, **1968**.

Bazant Z. P., Verdure M., *Mechanics of Progressive Collapse: Learning from World Trade Center and Building Demolitions*, Journal of Engineering Mechanics, Vol. 133, pp. 308-319, No. 3, March, **2007**.

Bennett E. W., Banerjee S., *Strength of beam-column connections with dowel reinforcement*, The strutcural engineer, Vol. 51, No.4, pp. 133-139, April, **1976**.

Braestrup M. W., *Dome Effect in RC Slabs: Rigid-Plastic Analysis*, Journal of the Structural Division - ASCE, ST6, pp. 1237-1253, USA, June, **1980**.

Breen J. E., Siess C. P., *Progressive Collapse-Symposium Summary*, ACI Journal, Vol. 76 No.9, pp. 997-1004, USA, September, **1979**.

Brenna A., Dei Poli S., di Prisco M., *Dowel action: some experimental and theoretical results regarding special concrete*, Studi e Ricerche, School for the design of R/C structures, Milan University of Technology, pp. 321-380, **1990**.

Broms B. B., *Lateral resistance of piles in cohesive soils*, ASCE Journal of Soil Mechanics, Vol. 90, No.2, pp. 27-59, **1964**.

Broms C. E., *Elimination of Flat Plate Punching Failure Mode*, ACI Structural Journal, V. 97, No. 1, pp. 94-101, Jan./Feb., **2000**.

Broms C. E., *Punching of Flat Plates - A Question of Concrete Properties in Biaxial Compression and Size Effect*, ACI Structural Journal, V. 87 No 3, pp. 292-304, may, **1990**.

BS 8110, *Structural use of Concrete, Part 1: Code of Practice for Design and Construction*, British Standards Institution, London, UK, **1997**.

Carino N. J., Woodward K. A., Leyendecker E. V., Fattal S. G., *A review of the Skyline Plaza collapse*, Concrete International, pp. 35-42, USA, July, **1983**.

Cesare M.A., Archilla J.C., *A Model for Progressive Collapse of Conventional Framed Buildings*, Proceedings of the 17th Analysis and Computation Specialty Conference, May, **2006**.

Chana P. S., *Investigation of the mechanism of shear failure of reinforced concrete beams*, Magazine of Concrete Research, Volume 39, No. 141, pp. 196-204, December, **1987**.

Chana P. S., Desai S. B., *membrane action, and design against punching shear*, The Structural engineer, Vol. 70, No. 19, pp. 339-343, October, **1992**.

Chen W. F., *Plasticity in reinforced concrete*, McGraw-Hill., 474 p., **1982**.

Christiansen K. P., *The effect of membrane stresses on the ultimate strength of the interior panel in a reinforced concrete slab*, structural engineer journal, Vol. 41, No. 8, pp. 261-265, **1963**.

Collins M. P., Bentz E. C., Sherwood E. G., Xie L., *An adequate theory for the shear strength of reinforced concrete structures*, Magazine of Concrete Research, Vol. 60, pp. 635–650, No. 9, November, **2008**.

Corley W. G., Mlakar P. F., Sozen M. A., Thornton C. H., *The Oklahoma City Bombing: Summary and Recommendations for Multihazard Mitigation*, Journal of Performance of Constructed Facilities, Vol. 12 No. 3, pp. 100-112, **1998**.

Cosenza E., Greco C., Manfredi G., *The Concept of Equivalent Steel*, Comité Euro-International du Béton (CEB), Bulletin d'Information No. 218, pp. 163-183, Lausanne, **1993**.

CSA Standard A23.3:, *Canadian Standard Association*, 232 p., December, **2004**.

Davids W. G., Turkiyyah M., *Development of Embedded Bending Member to Model Dowel Action*, Journal of Structural Engineering, Vol. 123, No.10, pp. 1312-1320, October, **1997**.

Dei Poli S., di Prisco M., Gambarova P., *Cover and Stirrup Effects on the Shear Response of Dowel Bar Embedded in Concrete*, ACI Structural Journal, Volume 90, No. 4, pp. 441-450, July-August, **1993**.

Dei Poli S., di Prisco M., Gambarova P., *Shear Response, Deformations, and Subgrade Stiffness of a Dowel Bar Embedded in Concrete*, ACI Structural Journal, Vol. 89, No.6, pp. 665-675, November, **1992**.

Dei Poli S., di Prisco M., Gambarova P., *Stress Field in Web of RC Thin-Webbed Beams Failing in Shear*, ASCE, Journal of Structural Engineering, 116 n°9, pp. 2496-2515, Reston, USA, September, **1990**.

Denton D., Morley C. T., *Accounting for biaxial bending in yield-line analysis of reinforced concrete slabs*, Magazine of Concrete Research, Vol. 60, pp. 597–607, No. 8, October, **2008**.

Desayi P., Kulkarni A.B., *Membrane action, deflections and cracking of two-way reinforced concrete slabs*, Materials and Structures,, Vol. 10, No. 59, pp. 303-312, **1977**.

Dilger W. H., *Flat slab column connections*, Progress in Structural Engineering and Materials, Vol. 2, pp. 386-399, **2000**.

DIN, *DIN 1045-1 Tragwerke aus Beton und Stahlbeton*, DIN 1045-1, Deutsches Institut für Normung, 2nd Edition, 148 p., Berlin, Germany, January, **2005**.

DoD, *Unified Facilities Criteria, Design of Buildings to Resist Progressive Collapse*, Washington (DC): US Department of Defense, USA, **2005**.

Dulacska H., *Dowel Action of Reinforcement Crossing Cracks in Concrete*, ACI Structural Journal, Vol. 69, No.12, pp. 754-757, December, **1972**.

Dusenberry D., Hamburger R., *Practical Means for Energy-Based Analyses of Disproportionate Collapse Potential*, Journal of Performance of Constructed Facilities, Vol. 20, No. 4, pp. 336-348, November, **2006**.

El-Ariss B., *Behavior of beams with dowel action*, Engineering structures, Vol. 29, No.6, pp. 899-903, June, **2007**.

Eleiott A. F., *An experimental investigation of shear transfer across cracks in reinforced concrete.*, M.S. Thesis, Cornell University, Ithaca, June, **1974**.

Ellingwood B., *Mitigating Risk from Abnormal Loads and Progressive Collapse*, Journal of Performance of Constructed Facilities, Vol. 20, No. 4, pp. 315-323, November, **2006**.

Ellingwood B., Leyendecker E. V., *Approaches for design against progressive collapse*, Journal of the Structural Division, Proceedings of the American Society of Civil Engineers, 104, pp. 413-423, **1978**.

Ellingwood B., Smilowitz R., Dusenberry D., Duthinh D., Carino J. N., *Best Practices for Reducing the Potential for Progressive Collapse in Buildings*, National Institute of Standards and Technology, Technology Administration, U.S. Department of Commerce, 216 p., February, **2007**.

Elstner R. C., Hognestad E., *Laboratory Investigation of Rigid Frame Failure*, Journal of ACI, Vol. 29, pp. 637-668, USA, January, **1957**.

Ettouney M., Smilowitz R., Tang M., Hapij A., *Global System Considerations for Progressive Collapse with Extensions to Other Natural and Man-Made Hazards*, Journal of Performance of Constructed Facilities, Vol. 20, pp. 403-417, No. 4, **2006**.

Eurocode 2, *Design of concrete structures - Part 1-1: General rules and rules for buildings*, CEN, EN 1992-1-1, 225 p., Brussels, Belgium, April, **2004**.

Favre R., Jaccoud J.-P., Burdet O., Charif H., *Dimensionnement des structures en béton - Aptitude au service et éléments de structures*, Presse Polytechnique et Universitaires Romandes, Traité de Génie Civil, Vol. 8, 3è éd., 612 p., Lausanne, Switzerland, **2004**.

Fernández Ruiz M., Muttoni A., *Applications of the critical shear crack theory to punching of R/C slabs with transverse reinforcement*, ACI Structural Journal, Vol. 106 N° 4, pp. 485-494, USA, **2009**.

Fernández Ruiz M., Muttoni A., Gambarova P., *Analytical modelling of the pre- and post-yield behaviour of bond in reinforced concrete*, ASCE Journal of Structural Engineering, Vol. 133, N° 10, pp. 1364-1372, Reston, USA, October, **2007**.

Fernández Ruiz M., Muttoni A., Gambarova P., *Relationship between nonlinear creep and cracking of concrete under uniaxial compression*, Journal of Advanced Concrete Technology, Vol. 5, No 3, pp. 383-393, Japan, **2007**.

Foster S. J., Bailey C. G., Burgess I.W., Plank R.J., *Experimental behaviour of concrete floor slabs at large displacements*, Engineering Structures, Vol. 26, pp. 1231-1247, **2004**.

Freyermuth C. L., *Structural integrity of buildings constructed with unbounded tendons*, Concrete International, pp. 56-63, March, **1989**.

Georgopoulos T., *Durchstanzlast und Durchstanzwinkel über Innenstützen punktförmig gestützter Stahlbetonplatten und deren Sicherung gegen progressiven Kollaps*, Dissertation, 197 p., Munich, Germany, **1986**.

Ghali A., Tadros G., *Bridge progressive collapse vulnerability*, Journal of Structural Engineering, Vol. 123, No. 2, pp. 227-231, **1997**.

GSA, *Progressive Collapse Analysis and Design Guidelines for New Federal Office Buildings and Major Modernization Projects*, General Services Administration, USA, **2003**.

Guandalini S., *Poinçonnement symétrique des dalles en béton armé*, Thèse de doctorat, N. 3380 (2005), 289 p., Lausanne, Switzerland, December, **2005**.

Guandalini S., Muttoni A., *Analyse structurale et évaluation*, Documentation SIA, D 0226 : Sécurité structurale des parkings couverts, pp. 45-62, Zürich, Switzerland, June, **2008**.

Hawkins N. M., Mitchell D., *Progressive collapse of flat plate structures*, ACI Journal, Vol. 76 No.10, pp. 775-808, USA, July, **1979**.

Hayes B., *Allowing for membrane action in the plastic analysis of rectangular reinforced concrete slabs*, Magazine of Concrete Research, Vol. 20, No. 65, pp. 205-212, December, **1968**.

He X.G., Kwan A. K. H., *Modeling dowel action of reinforcement bars for finite element analysis of concrete structures*, Computers & Structures, Vol. 79, No.6, pp. 595-604, February, **2001**.

Hegemier G. A., Murakami H., *On global shear transfer across a crack or joint plane penetrated by continuous fiber reinforcement with application to reinforced concrete*, International Journal of Solids and Structures, 26, pp. 1115-1131, 9, **1990**.

Hess U., Jensen B. C., Braestrup M. W., Nielsen M. P., Bach F., *Punching shear in reinforced concrete slabs*, Technical University of Denmark (DTU) Rapport, R 90, 63 p., Copenhagen, Denmark, **1978**.

Hewitt B. E., Batchelor B., *Punching shear strength of restrained slabs*, Proceedings of the ASCE Convention, V. 101, ST9, pp. 1837-1853, September, **1975**.

Heyman J., *The plasticity of unreinforced concrete*, Magazine of Concrete Research, Vol. 60, pp. 555–559, No. 8, October, **2008**.

Hopkins D. C., Park R., *Test on a reinforced concrete slab and beam floor designed with allowance for membrane action*, Cracking, Deflection and Ultimate Load of Concrete Slab Systems, ACI, SP. 30, pp. 223-250, **1971**.

Houde J., Mirza M. S., *A finite element analysis of shear strength of reinforced concrete beams*, ACI, Special Publication 42, pp. 103-128, **1974**.

Ince R., Arici E., *Size effect in bearing strength of concrete cubes*, Construction and Building Materials, Vol. 18, pp. 603-609, **2004**.

Ince R., Yalcin E., Arsan A., *Size-dependent response of dowel action in R.C. members*, Engineering structures, Vol. 29, No.6, pp. 955-961, September, **2006**.

Jaafar K., *Shear behaviour of reinforced concrete beams with confinement near plastic hinges*, Magazine of Concrete Research, Vol. 60, pp. 665–672, No. 9, November, **2008**.

Jelic I., Pavlovic M. N., Kotsovos M. D., *A study of dowel action in reinforced concrete beams*, Magazine of Concrete Research, Volume 2, No. 2, pp. 131-141, April, **1999**.

Jimenez R., White R. N., Gergely P., *Bond and Dowel Capacities of Reinforced Concrete*, Vol. 76, No.1, pp. 73-92, January, **1979**.

Johansen K.W., *Yield-line Theory*, Cement and Concrete Association, 181 p., **1962**.

Johnston D. W., Zia P., *Analysis of dowel action*, ASCE Journal of the Structural Division, Vol 97, No ST5, pp. 1611-1630, USA, May, **1971**.

Kaewkulchai G., Williamson E. B., *Modeling the Impact of Failed Members for Progressive Collapse Analysis of Frame Structures*, Journal of Performance of Constructed Facilities, Vol. 20, pp. 375-383, No. 4, November, **2006**.

Kaminetzky D., *Design and Construction Failures, Lessons from Forensic Investigations*, McGraw-Hill., New York, 600 p., **1991**.

Kemp K. O., *Yield of a square reinforced concrete slab on simple supports allowing for membrane action*, structural engineer journal, Vol. 45, No. 7, pp. 235-240, **1967**.

Khandelwal K., Kunnath S.K, El-Tawil Sh., Lew H. S., *Macromodel-Based Simulation of Progressive Collapse:Steel Frame Structures*, Journal of Structural Engineering, Vol. 134, pp. 1070-1078, No. 7, July, **2008**.

King S., Delatte N. J., *Collapse of 2000 Commonwealth Avenue: Punching Shear Case Study*, ASCE Journal of Performance of Constructed Facilities, Vol. 18 No 1, pp. 54-61, Reston, USA, February, **2004**.

Kinnunen S., Nylander H., *Punching of Concrete Slabs Without Shear Reinforcement*, Transactions of the Royal Institute of Technology, N° 158, 112 p., Stockholm, Sweden, **1960**.

Klingner R. E., Mendonca J. A., *Tensile capacity of short anchor bolts and welded studs: a literature review*, Vol. 79, No. 4, pp. 270-279, **1982**.

Knoll F., Vogel T., *Design for Robustness*, Structural Engineering Documents 11, 99 p., ISBN 978-3-85748-120-8, **2009**.

Kollegger J., Mehlhorn G., *Material model for the analysis of reinforced concrete surface structures*, Computational Mechanics, Vol. 6, pp. 341-357, **1990**.

Krefeld W., Thurston Charles W., *Contribution of Longitudinal Steel to Shear Resistance of Reinforced Concrete Beams*, ACI Structural Journal, Vol. 63, No.3, pp. 325-344, March, **1966**.

Kupfer H., Georgopoulos T., *Eine kostengünstige Massnahme zur Vermeidung des fortschreitenden Einsturzes punktgestützter Stahlbetonplatten infolge Durchstanzens*, Bauingenieur, Heft 61, pp. 561-562, **1986**.

Lee Y. M., Mitchell D., Harris P. J., *Lessons from structural performance – Slabs containing improperly placed reinforcing*, Concrete International, Vol. 1, pp. 45-53, No. 6, June, **1979**.

Lew H. S., Carino N. J., Fattal S. G., *Cause of the condominuim collapse in Cocoa Beach, Florida*, Concrete International, pp. 64-73, USA, August, **1982**.

Lieberum K. H., Reinhardt H. W., *Strength of Concrete on an Extremely Small Bearing Area*, ACI Structural Journal, Vol. 86, No.1, pp. 67-75, January, **1989**.

Loizeaux M., Osborn A. E. N., *Progressive Collapse—An Implosion Contractor's Stock in Trade*, Journal of Performance of Constructed Facilities, Vol. 20, pp. 391-402, No. 4, November, **2006**.

Maekawa K., Pimanmas A., Okamura H., *Nonlinear Mechanics of Reinforced Concrete*, Spon Press, 768 p., ISBN: 0415271266, **2003**.

Maekawa K., Qureshi J., *Stress transfer across interfaces in reinforced concrete due to aggregate interlock and dowel action*, J. Materials, Conc. Struct., Pavements, JSCE, 34, pp. 159-172, 557, February, **1997**.

Maekawa K., Qureshi J., *Embedded bar behavior in concrete under combined axial pullout and transverse displacement*, J. Materials, Conc. Struct., Pavements, 30, pp. 183-195, 532, February, **1996**.

Mannava S. S., Bush T.D., Kukerti A.R., *Load-Deflection Behavior of Smooth Dowels*, ACI Structural Journal, Vol. 96, No.2, pp. 891-898, November, **1999**.

Marcus H., *Load Carrying Capacity of Dowels at Transverse Pavement Joints*, ACI Structural Journal, Vol. 48, No.10, pp. 169-184, October, **1951**.

Marjanishvili Sh., *Progressive Analysis Procedure for Progressive Collapse*, Journal of Performance of Constructed Facilities, Vol. 18, No. 2, pp. 79-85, May, **2004**.

Marjanishvili Sh., Agnew E., *Comparison of Various Procedures for Progressive Collapse Analysis*, Journal of Performance of Constructed Facilities, Vol. 20, No. 4, pp. 365-374, November, **2006**.

Marti P., Pralong J., Thürlimann B., *Schubversuche an Stahlbeton-Platten*, Institut für Baustatik und Konstruktion, Nr. 7305-2, 123 p., Zurich, Switzerland, September, **1977**.

Martin-Pérez B., Pantazopoulou S. J., *Effect of bond, aggregate interlock and dowel action on the shear strength degradation of reinforced concrete*, Engineering structures, Vol. 23, No.2, pp. 214-227, February, **2001**.

Mattock A. H., *Shear transfer in reinforced concrete*, ACI Journal, Vol. 66, pp. 119-128, No. 2, **1969**.

Mattock A. H., *Shear Transfer in Concrete Having Reinforcement at an Angle to the Shear Plane*, ACI, Special Publication, 42, pp. 17-42, Farmington Hills, USA, August, **1974**.

Mattock A. H., *Diagonal Tension Cracking in Concrete Beams with Axial Forces*, ASCE Journal of the Structural Division, September, **1969**.

McPeake F. A., *Post-punching resistance of internal slab-column connection*, Department of Civil Engineering, Queen's University of Belfast, B.Sc. Honours Project, 107 p., May, **1980**.

Melo G. S., *Behaviour of Reinforced Concrete Flat Slabs after Local Failure*, PhD thesis, Polytechnic of Central London, 214 p., **1990**.

Melo G. S., Regan P. E., *Post-punching resistance of connections between flat slabs and interior columns*, Magazine of Concrete Research, Vol. 50 No 4, pp. 319-327, UK, December, **1998**.

Millard S. G., Johnson R. P., *Shear transfer across cracks in reinforced concrete due to aggregate interlock and to dowel action*, Magazine of Concrete Research, Vol. 36, No.126, March, **1984**.

Mills G. M., *A partial kinking yield criterion for reinforced concrete slabs*, Magazine of Concrete Research, Vol. 27, No.90, pp. 13-22, March, **1975**.

Mirza M. S., Houde J., *Study of bond stress-slip relationship in reinforced concrete*, ACI Journal, 76-2, pp. 19-46, Detroit, USA, January, **1979**.

Mirzaei Y., *Post punching behaviour of reinforced concrete slab-column connections*, 7th International FIB PhD Symposium, Stuttgart, Germany, September, **2008**.

Mirzaei Y., Muttoni A., *Tests of the post-punching behavior of the reinforced concrete flat slabs*, IS-BETON, Switzerland, October, **2008**.

Mishima T., Suzuki A., Shinoda Y., Maekawa K., *Nonelastic Behavior of Axial Reinforcement Subjected to Axial and Slip Deformation at the Crack Surface*, ACI Structural Journal, 92, pp. 380-385, 3, May, **1995**.

Mitchell D., Cook W. D., *Preventing Progressive Collapse of Slab Structures*, Journal of Structural Engineering, Vol. 110 No.7, pp. 1513-1532, USA, July, **1984**.

Moe J., *Shearing Strength of Reinforced Concrete Slabs and Footings under Concentrated Loads*, PCA, Vol. D47, Illinois, USA, April, **1961**.

Mohamed O.A., *Progressive Collapse of Structures: Annotated Bibliography and Comparison of Codes and Standards*, Journal of Performance of Constructed Facilities, Vol. 20, No. 4, pp. 418-425, November, **2006**.

Moore D.B., *The UK and European Regulations for Accidental Actions*, National Workshop on Prevention of Progressive Collapse, NIST/NIBS Multi-hazard Mitigation Council, National Institute of Building Sciences, Chicago, USA, **2002**.

Morley C. T., *Yield-line theory for reinforced concrete slabs at moderately large deflections*, Magazine of Concrete Research, Vol. 19, No. 61, pp. 211-222, **1967**

Müllers I., Vogel T., *Evaluating Phenomena Related to Robustness of Structures*, JCSS and IABSE Workshop on Robustness of Structures, Garston, Watford, UK, November, **2005**.

Müllers I., Vogel T., *Vulnerability of Flat Slab Structures*, Proceedings of the 2005 Structures Congress and the 2005 Forensic Engineering Symposium, ASCE, **2005**.

Muttoni A., *Sécurité structurale des parkings couverts*, Documentation SIA, A. Muttoni, Editor, 105 p., Zürich, Switzerland, June, **2008**.

Muttoni A., *Punching shear strength of reinforced concrete slabs without transverse reinforcement*, ACI Structural Journal, V. 105, N° 4, pp. 440-450, USA, July-August, **2008**.

Muttoni A., *Introduction à la norme SIA 262*, Documentation SIA, D 0182 Introduction à la norme SIA 262, pp. 5-9, Zürich, Switzerland, **2003**.

Muttoni A., Fernández Ruiz M., *Shear strength of members without transverse reinforcement as function of critical shear crack width*, ACI Structural Journal, V. 105, No 2, pp. 163-172, Farmington Hills, USA, March-April, **2008**.

Muttoni A., Fernández Ruiz M., *Exemples de renforcement contre le poinçonnement*, Documentation SIA, D 0226: Sécurité structurale des parkings couverts, pp. 67-74, Zürich, Switzerland, June, **2008**.

Muttoni A., Fernández Ruiz M., *Shear strength in one- and two-way slabs according to the critical shear crack theory*, fib Symposium, Amsterdam 2008, Amsterdam, Netherlands, **2008**.

Muttoni A., Fernández Ruiz M., Burdet O., *Poinçonnement des planchers-dalles : nouveaux acquis et applications pratiques*, Journée d'étude EPFL, 10 septembre 2008, 102 p., Lausanne, Switzerland, September, **2008**.

Muttoni A., Fernández Ruiz M., Guandalini S., *Poinçonnement des ponts-dalles*, Documentation SIA, 4. FBH/ASTRA Studientagung 'Neues aus der Brückenforschung', D0223, pp. 85-94, Bern, Switzerland, November, **2007**.

Muttoni A., Fürst A., Hunkeler F., *Deckeneinsturz der Tiefgarage am Staldenacker in Gretzenbach*, Medieninformation vom 15.11.2005, 14 p., Solothurn, Switzerland, November, **2005**.

Muttoni A., Schwartz J., Thürlimann B., *Dimensionamiento y concepción de estructuras en hormigón armado mediante campos de tensiones*, IS-BETON, 110 p., Lausanne, Switzerland, **2006**.

Ockleston A. J., *Arching Action In Reinforced Concrete Slabs*, The Structural Engineer, 36, pp. 197-201, London, **1958**.

Oswald C. J., *Prediction of injuries to building occupants from column failure and progressive collapse with the BICADS computer program*, Conference Proceeding, Paper Part of Metropolis & Beyond 2005, **2005**.

Park R., *Tensile membrane behaviour of uniformly loaded rectangular reinforced concrete slabs with fully restrained edges*, Magazine of Concrete Research, Vol. 16, No. 40, pp. 39-44, March, **1964**.

Park R., *The ultimate strength and long-term behaviour of uniformy loaded, two-way concrete slabs with partial lateral restraint at all edges*, Magazine of Concrete Research, 16, pp. 139-152, UK, September, **1964**.

Paschen H., Schonhoff T., *Untersuchungen uber in Beton eingelassene Scherbolzen aus Betonstahl*, In Deutscher Ausschuss fur Stahlbeton. Wilhelm Ernst und Sohn, Berlin, vol. 346, pp. 105-149, **1983**.

Paulay T., Park R., Philips M. H., *Horizontal construction joints in cast in place reinforced concrete*, ACI-Special Publication SP-42, pp. 599-616, **1974**.

Pearson C., Delatte N., *Lessons from the Progressive Collapse of the Ronan Point Apartment Tower*, Proceedings of the Third Forensic Engineering Congress, pp. 190-200, October, **2003**.

Polak M. A., Vecchio F. J., *Reinforced Concrete Shell Elements Subjected to Bending and Membrane Loads*, ACI Structural Journal, Vol. 91, No. 3, pp. 261-268, May, **1994**.

Prakhya G., *Plasticity applications in reinforced concrete and prestressed concrete structures*, Magazine of Concrete Research, Vol. 69, pp. 691–699, No. 9, November, **2008**.

Pralong J., Brändli W., Thürlimann B., *Durchstanzersuche an Stahlbeton und Spannbetonplatten*, Birkhäuser Verlag, Institut für Baustatik und Konstruktion ETH Zürich, Nr. 7305-3, Switzerland, **1979**.

Pruijessers A. F., *Aggregate Interlock and Dowel Action Under Monotonic and Cyclic Loading*, PhD thesis, 165 p., Delft University, Netherland, **1988**.

Qureshi J., Maekawa K., *Computational model for steel embedded in concrete under combined axial pullout and transverse shear displacement*, Proceeding of JSCE, 15, pp. 1249-1254, 2, **1993**.

Ramos A.P., Lucio V. J. G., *Post-punching behaviour of prestressed concrete flat slabs*, Magazine of Concrete Research, Vol. 60, No. 4, pp. 245-251, May, **2008**.

Randl N., *Load Bearing Behaviour of Cast-in Shear Dowels*, Beton- und Stahlbetonbau, Vol. 102, No. S1, pp. 31-37, **2007**.

Rasmussen B. H., *Strength of transversely loaded bolts and dowels cast into concrete*, Laboratoriet for Bugningastatik, Denmark Technical University, Meddelelse, Vol. 34, No.2, **1962**.

Regan P. E., *Shear Combs, Reinforcement against Punching*, The Structural Engineering, Vol. 63B, No. 4, pp. 76-84, December, **1985**.

Regan P. E., *Symmetric Punching of Reinforced Concrete Slabs*, Magazine of Concrete Research, Vol. 38, pp. 115-128, England, **1986**.

Regan P. E., Khan M.H., *Bent-Up Bars as Shear Reinforcement*, ACI Special Publication SP42-11, Vol. 42, January, **1974**.

Regan P. E., Walker P. R., Zakaria K. A. A., *Tests of Reinforced Concrete Flat Slabs*, School of the Environment, Polytechnic of Central, CIRIA Project RP 220, 217 p., London, UK, **1979**.

Reineck K.-H., *Simplified Shear Design of*, Comité Euro-International du Béton (CEB), No.237, pp. 185-197, **1997**.

Ritz P., Marti P., Thürlimann B., *Versuche über das Biegeverhalten von Vrgesppannten Platten Ohne Verbund*, Zurich, **1975**.

Salim W., Sebastian W. M., *Punching Shear Failure in Reinforced Concrete Slabs with Compressive Membrane Action*, ACI Structural Journal, Vol. 100, pp. 471-479, july, **2003**.

Sasani M., Bazan M., Sagiroglu S., *Experimental and analytical progressive collapse evaluation of actual reinforced concrete structure*, ACI Structural Journal, Vol. 104, pp. 731-739, No. 6, **2007**.

Sasani M., Bazan M., Sagiroglu S., *Experimental and Analytical Progressive Collapse Evaluation of Actual Reinforced Concrete Structure*, ACI Structural Journal, Vol. 104, No.6, pp. 731-739, November, **2007**.

Sasani M., Kropelnicki J., *Progressive collapse analysis of an RC structure*, The Structural Design of Tall and Special Buildings, Vol. 17, pp. 757–771, **2008**.

Sasani M., Sagiroglu S., *Progressive Collapse of Reinforced Concrete Structures: A Multihazard Perspective*, ACI Structural Journal, Vol. 105, No.1, pp. 96-103, January, **2008**.

Sasani M., Sagiroglu S., *Progressive Collapse Resistance of Hotel San Diego*, Journal of Structural Engineering, Vol. 134, No. 3, pp. 478-488, March, **2008**.

Schousboe I., *Bailey's Crossroads Collapse reviewed*, Journal of the Engineering Mechanics Division, Vol. 102, pp. 365-378, No. CO2, June, **1976**.

Seffen K.A., *Progressive Collapse of the World Trade Center: Simple Analysis*, JOURNAL OF ENGINEERING MECHANICS, Vol. 134, No. 2, pp. 125-132, February, **2008**.

Shankar Nair R., *Preventing Disproportionate Collapse*, Journal of Performance of Constructed Facilities, Vol. 20, No. 4, pp. 309-314, **2006**.

SIA, *SIA 261/1 Actions sur les structures porteuses – Spécifications complémentaires*, 32 p., Zurich, Switzerland, **2003**.

SIA, *SIA 261 - Actions sur les structures porteuses*, 114 p., Zurich, Switzerland, **2003**.

SIA, *SIA 260 - Bases pour l'élaboration des projets de structures porteuses*, 44 p., Zurich, Switzerland, **2003**.

SIA, *SIA 262 - Construction en béton*, 94 p., Zurich, Switzerland, **2003**.

SIA, *Documentation SIA, D 0226: Sécurité structurale des parkings couverts*, Zurich, 105 p., Switzerland, **2008**.

Sonnenberg A. M. C., Al-Mahaidi R., *Investigation of dowel shear in RC beams using photogrammetry*, Magazine of Concrete Research, 59, pp. 621-626, November, **2007**.

Soroushian P., Obaseki K., Baiyasi M. I., El-Sweidan B., Choi Ki-Bong, *Inelastic Cyclic Behavior of Dowel Bars*, ACI Structural Journal, Vol. 85, No.1, pp. 23-29, January, **1986**.

Soroushian P., Obaseki K., Rojas M., *Bearing Strength and Stiffness of Concrete Under Reinforcing Bars*, ACI Structural Journal, Vol. 84, No.3, pp. 179-184, November, **1987**.

Soroushian P., Obaseki K., Rojas M., Najm H. S., *Behavior of Bars in Dowel Action Against Concrete Cover*, ACI Structural Journal, Vol. 84, No.2, pp. 170-176, March-April, **1987**.

Soroushian P., Obaseki K., Rojas M., Sim Jongsung, *Analysis of Dowel Bars Acting Against Concrete Core*, ACI Structural Journal, Vol. 83, No.4, pp. 642-649, July, **1986**.

Stanton J. F., *An investigation of dowel action of the reinforcement of nuclear containment vessels and their nonlinear dynamic response to earthquake loads*, M.Sc. dissertation, Cornell University, Ithaca, **1977**.

Starossek U., *Progressive Collapse of Structures: Nomenclature and Procedures*, Structural Engineering International, pp. 113-117, **2006**.

Taylor H. P. J., *Investigation of the Dowel Shear Forces Carried by the Tensile Steel in Reinforced Concrete Beams*, Cement and Concrete Association Report No. TRA 431, **1961**.

Teller L. W., Sutherland E. J., *A study of structural action of several types of transverse and longitudinal joint design*, Public Roads, Vol. 17, No.7, September, **1936**.

Utescher G., Hermann M., *Versuche zur Ermittlung der Tragfähigkeit in Beton eingespannter Rundstahldollen aus nichtrostendem austenitischem Stahl*, Deutscher Ausschuss für Stahlbeton, Heft 346, pp. 49-104, Berlin, Germany, **1983**.

Vecchio F. J., *Contribution of Nonlinear Finite-Element Analysis to Evaluation of Two Structural Concrete Failures*, Journal of Performance of Constructed Facilities, Vol. 16, No. 3, pp. 110-115, August, **2002**.

Vecchio F. J., Tang K., *Membrane action in reinforced concrete slabs*, Canadian Journal of Civil Engineering, Vol.17, pp. 686-697, Toronto, Canada, **1990**.

Vintzeleou E., Tassios T.P., *Mathematical models for dowel action under monotonic and cyclic conditions*, Magazine of Concrete Research, Vol. 38, No.134, pp. 13-22, March, **1986**.

Vintzeleou E., Tassios T.P., *Behavior of Dowels Under Cyclic Deformations*, ACI Structural Journal, Vol. 84, No.1, pp. 18-30, January, **1987**.

Vlassis A.G., *Progressive Collapse Assessment of Tall Buildings*, Ph.D. Thesis, Department of Civil and Environmental Engineering, Imperial College London, 320 p., **2007**.

Vlassis A.G., Izzuddin B.A., Elghazouli A.Y., Nethercot D. A., *Progressive collapse of multi-storey buildings due to sudden column loss—Part II: Application*, Engineering Structures, Vol. 30, pp. 1424–1438, **2008**.

Wood R. H., *Plastic and elastic design pf slabs and plates*, Thames and Hudson, **1961**.

Yagust V. I., Yankelevsky D. Z., *On Potential Progressive Failure of Large-Panel Buildings*, Journal of Structural Engineering, Vol. 133, pp. 1591-1603, No. 11, November, **2007**.

Yang K-H, Ashour A.F., *Mechanism Analysis for Concrete Breakout Capacity of Single Anchors in Tension*, ACI Structural Journal, V. 105, No. 5, pp. 609-616, September, **2008**.

Yi W-J, He Q.-F., Xiao Y., Kunnath S.K, *Experimental Study on Progressive Collapse-Resistant Behavior of Reinforced Concrete Frame Structures*, ACI Structural Journal, V. 105, No. 4, pp. 433-439, July, **2008.**

List of notations

Capital Roman letters

A	Area
A_b	Cross-sectional area of a reinforcing bar
A_{bent}	Cross-sectional area of a bent-up bar
A_s	Cross-sectional area of tensile reinforcing bars crossing punching cone
A_{sm}	Minimum cross-sectional area of integrity reinforcement in each principal direction
A_{sb}	Cross-sectional area of integrity reinforcing bars
A_{ch}	Horizontal projection are of conical failure cones
$C_1 \ldots C_8$	Integration constants
D	Diameter of punching cone
E_c	Modules of elasticity of concrete
E_h	Hardening modulus of steel reinforcement
E_s	Modulus of elasticity of steel reinforcement
I_b	Moment of inertia for a reinforcing bar
K_i	Elastic stiffness of a dowel bar
L	Distance between two plastic hinges
L_i	Initial length of bent-up bars in critical zone
L_f	Length of deformed bent-up bars in critical zone
M	Bending moment
M_I	Bending moment in section I
M_p	Plastic moment
N	Axial force
N_I	Axial force in section I
N_y	Axial yielding force of a reinforcing bar
V	Shear force
V_{ACI}	Post-punching strength according to ACI 352.1R
V_c	Concrete contribution to punching shear strength
V_{con}	Concrete breakout strength
$V_{con,max}$	Maximum concrete breakout strength
V_{CSA}	Post-punching strength according to CSA A23.3
V_D	Integrity reinforcement contribution to post-punching shear transfer
V_d, V_{Ed}	Dimensioning value of punching force
$V_{D,i}$	Contribution of an integrity reinforcing bar to post-punching shear transfer
$V_{D,mod}$	Integrity reinforcement contribution calculated by mechanical model
$V_{D\beta,mod}$	Contribution of bent-up bars to post-punching shear calculated by mechanical model
$V_{D,R}$	Maximum integrity reinforcement contribution to post-punching shear strength
$V_{D\beta,R}$	Maximum contribution of bent-up bars to post-punching shear strength
V_{Du}	Ultimate dowel strength
V_{flex}	Shear force associated with flexural capacity of slab
$V_{Georg.}$	Post-punching strength according to Georgopoulos' proposition
V_I	Shear force in section I
V_M	Tensile reinforcement contribution to post-punching shear transfer
$V_{M,i}$	Contribution of a tensile reinforcing bar to post-punching shear transfer
$V_{M,mod}$	Tensile reinforcement contribution calculated by mechanical model
$V_{M,R}$	Maximum tensile reinforcement contribution to post-punching shear strength
V_p	Punching strength
V_{pp}	Post-punching strength
$V_{pp,d}$	Design value of post-punching strength
$V_{pp,test}$	Post-punching strength of tested specimens
$V_{pp,R}$	Post-punching strength calculated by simplified method
$V_{pp,SIA}$	Post-punching strength according to SIA 262
$V_{p,mod}$	Punching strength calculated by mechanical model
$V_{pp,mod}$	Post-punching strength calculated by mechanical model

V_R	Resistance punching shear force
V_s	Contribution of shear reinforcement to punching shear strength
V_{se}	Shear force transmitted to column
V_{SIA}	Post-punching strength according to SIA 262
V_{spal}	Spalling strength of concrete cover

Small Roman letters

a	Column width
b	Slab width or beam width
$b´$	Distance between the first and the last integrity bars passing through column
b_n	Net width of reinforced concrete section
c	Concrete cover
c_b	Bottom cover of reinforced concrete section
c_m	Minimum cover of a concrete specimen
c_s	Side cover of reinforced concrete section
c_t	Top cover of reinforced concrete section
d	Effective depth of reinforced concrete flat slab
$d´$	Distance from extreme compression fiber of slab to centroid of bent-up bars
d_1	Distance from extreme tension fiber to centroid of an integrity reinforcing bar
d_g	Maximum aggregate size
d_{g0}	Reference aggregate size
e	Eccentricity of dowel force
f_b	Bearing strength of concrete
f_c	Cylinder compressive strength of concrete
$f_{c,28}$	Cylinder compressive strength of concrete at age of 28 days
f_{cc}	Cube compressive strength of concrete
f_{ck}	Characteristic value of cylinder compressive strength (5% fractile)
f_{ct}	Tensile strength of concrete
$f_{c,cone}$	Compressive strength of concrete of punching cone
$f_{c,slab}$	Compressive strength of concrete of slab
f_{ct}	Concrete tensile strength
f_{ctd}	Design value of concrete tensile strength
f_{ctm}	Mean value of concrete tensile strength
$f_{ct,cone}$	Tensile strength of concrete of punching cone
$f_{ct,slab}$	Tensile strength of concrete of slab
$f_{ct,eff}$	Effective tensile strength of concrete
f_{su}	Ultimate tensile strength of reinforcement
f_{sy}, f_y	Yielding strength of steel reinforcement
f_{sd}	Design value of yielding strength of steel reinforcement
f_{yk}	Characteristic value of yield strength of steel reinforcement
h	Slab thickness
$h_1 \ldots h_6$	Thickness of concrete resisting against bent-up bar at specific location
$h(u)$, $h(v)$	Thickness of concrete resisting against bent-up bar
k	Nonlinear bearing stiffness of concrete
k_1	Factor to adjust results of the Taylor series with that predicted by mechanical model
k_2	Factor to account for angle of inclination of bent-up bars in simplified method
k_3	Factor to adjust results of the Taylor series with that predicted by mechanical model
k_c, k_0	Bearing stiffness of concrete
ℓ	Length
ℓ_1, ℓ_2	Center-to-center span in each principal direction
ℓ_c	Length of curvature-influenced zone
ℓ_d	Development length of reinforcement
ℓ_e	Elastic length of a bonded bar
ℓ_n	Clear span in each direction
ℓ_p	Plastified length of a bonded bar
ℓ^*	Length of a reinforcing bar with a fully plastic behavior of concrete underneath
m	Number of bending reinforcement crossing punching cone

m_R	nominal moment capacity per unit width
n	Number of integrity reinforcement passing through column
n_b	Number of bars in one layer
p, q	Local coordinates associated to concrete breakout and spalling of concrete cover
q_d	Uniformly distributed design load
$q_{d,acc}$	Uniformly distributed design load according to accidental situations (SIA 261)
r_s	Radius of equivalent circular slab, approximately half of the slab width
r_q	Radius of the load introduction at the perimeter
s	Bar spacing
s_i	Distance between two consecutive dowel bars
u_0	Perimeter of column
u, v	Local coordinates measured from intersection of bent-up bars and punching crack
u_1, u_2,	Parameters defined to calculate mean axial strain in bent-up bars
v_1, v_2	Parameters defined to calculate mean axial strain in bent-up bars
w	Deflection
w_p	Deflection corresponding to punching shear strength
w_{pp}	Deflection corresponding to maximum post-punching strength
w_u	Maximum deflection of slab
x_1	Distance of diagonal crack from support
y	Local coordinate measured from center of a reinforcing bar section

Capital Greek letters

Φ	Shear reduction factor
$\Phi(x)$	Cumulative distribution function

Small Greek letters

α	Angle of inclination of punching cone
β	Angle of inclination of bent-up bars
γ	Angle of concrete breakout cone
δ	Dowel displacement
δ_e	Elastic displacement of dowel bar at face of crack
ε	Strain
ε_0	Mean axial strain in reinforcing bars
ε_b	Minimum axial strain at curvature-influenced zone
ε_{bu}	Parameter associated to rib height and hardening modulus of bar
ε_c	Concrete strain
ε_{cu}	Ultimate concrete compressive strain
ε_{max}	Maximum tensile strain in reinforcing bars
ε_s	Steel strain
ε_t	Axial tensile strain at extreme tension fiber of a reinforcing bar
ε_{sh}	Initial strain of steel hardening
ε_{su}	Ultimate strain of steel reinforcement
ε_{sy}	Yielding strain of steel reinforcement
η_D, η_M	Factor to account for non-uniform tensile stresses across breakout cone
θ	Initial angle of inclination of dowel bar
μ	Mean value of normal distribution
ν	Poisson's ratio
ρ	Reinforcement ratio
ρ_{int}	Integrity reinforcement ratio
$\rho_{int,min}$	Minimum integrity reinforcement ratio
σ	Standard deviation of normal distribution
σ_N	Axial tensile stress in reinforcing bars
σ_c	Concrete stress
σ_r	Radial stress in concrete underneath bar

σ_s	Steel stress
σ_x	Stress in *x* direction
σ_y	Yielding stress
$\tau,\ \tau_{xy}$	Shear stress
$\tau_{b,max}$	Maximum bond stress
$\phi\,(x)$	Probability density function
χ	Curvature
χ_{max}	Maximum curvature of reinforcing bars in curvature-influenced zone
ψ	Angle of inclination of bars in vicinity of punching crack
ψ'	Slab rotation
ψ_D	Angle of inclination of integrity reinforcing bars
ψ_M	Angle of inclination of bending reinforcing bars
ψ_u	Angle of inclination of reinforcing bars at failure

Other symbols

Ø	Diameter of reinforcing bar

List of Abbreviations

ACI	American Concrete Institute
AL	Accidental Load
ASCE	American Society of Civil Engineers
CSCT	Critical shear crack theory
COV	Coefficient of variation
DL	Dead Load
DoD	Department of Defense
GSA	General Service Administration
ISC	Interagency Security Committee
LL	Live Load
NBCC	National Building Code of Canada
RC	Reinforces Concrete
SL	Snow Load
SLS	Serviceability Limit State
ULS	Ultimate Limit State
WL	Wind Load

Appendices

Appendix A: Test on the post-punching behavior of reinforced concrete flat slabs

Appendix B: Estimation of the projected area A_{ch}

Appendix C: Summary of experimental results

Tests on the Post-Punching Behavior of Reinforced Concrete Flat Slabs

Essais sur le comportement post-critique des planchers-dalles en béton armé

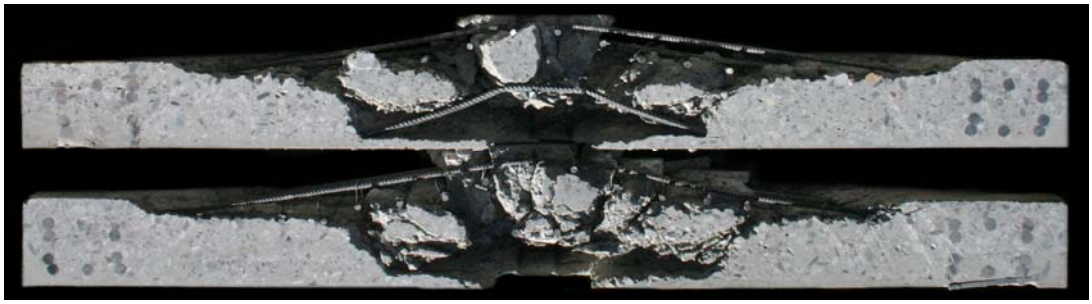

Ecole Polytechnique Fédérale de Lausanne
Institut de Structures
Laboratoire de Construction en Béton

Yaser Mirzaei
Prof. Dr. Aurelio Muttoni

October 2008

This research is funded by the Swiss association of the cement industry (CEMSUISSE)

Table of contents

A-1 Introduction

This report presents the results of an extensive experimental campaign carried out at the Ecole Polytechnique Fédérale de Lausanne. The post-punching behavior of 24 tested slabs, with 125 mm thickness and various reinforcement layouts are presented and discussed. The performance and robustness of the various solutions is investigated to obtain physical explanations of the load-carrying mechanisms after punching shear failure.

A-1.1 Scope

Flat plates are a very common and competitive structural system for cast in place slabs in buildings. Using flat slabs as structural elements decreases the time of construction and thus makes it very economical. Due to the highly complex tri-axial state of stress over the columns, brittle punching failure is the major disadvantage of reinforced concrete flat slabs supported by columns. Punching shear failure occurs with almost no warning signs since deflections are small and cracks at the top side of the slab are usually not visible. A local punching failure at one column will result in increased curvatures of the slab at surrounding columns which can trigger the punching failure to the adjacent columns resulting in the progressive collapse of the entire structure. Over the past decades, several collapses due to punching shear failures have occurred resulted in human casualties and large damages showing some shortcomings in the codes of practice as can be seen in Fig. A-1.1.

a) Shopping center, Serfontana, Switzerland, 70's

b) Underground parking garage, Bluche, Switzerland, 1981

c) Underground parking garage, Switzerland, 2004

Figure A-1.1: Structural collapses due to the punching shear failure

Integrity reinforcement crossing the column and detailed with the intent to provide sufficient post-punching strength can be used to avoid the propagation of punching to adjacent column. To that aim, the Swiss Standard 262 [1] requires that some reinforcement shall be provided on the compression side and be extended over the column and well anchored on both sides (Fig. A-1.2 a). Besides this solution, bent-up bars also appear to be a solution to prevent the progressive collapse by providing a ductile behavior [6] (Fig. A-1.2 b). This study investigates the post-punching behavior of the various types of integrity reinforcement.

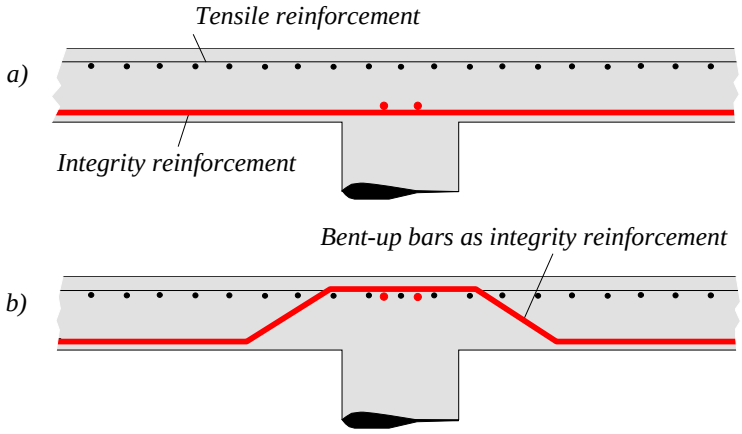

Figure A-1.2: Integrity reinforcement: a) compressive reinforcement passing through the column, and b) bent-up bars

A-2 Description of the slabs

A-2.1 Overview

Three test series on a total of 24 flat plates were carried out at the Structural Concrete Laboratory of the Ecole Polytechnique Fédérale de Lausanne to investigate the post-punching behavior of flat slabs supported by columns. The first series investigated the effect of tensile reinforcement in the negative moment area over the column on the post-punching behavior of flat slabs. The second series investigated the effect of additional straight bars on the compression side of the slabs and passing through the column and of bent-up bars acting as shear reinforcement. The third series consisted of twelve specimens: four specimens included bent-up bars with a sufficient anchorage length, two specimens included straight integrity reinforcement, two had only tensile reinforcement, and the last four included both tensile reinforcement and straight reinforcing bars passing through the column on the compression side of the slab. The tensile reinforcement was cut-off at specified points to ensure that it did not contribute to the shear transfer after punching failure. In this case, the only link between the punching cone and the rest of the slab is the integrity reinforcement and its influence on the post-punching behavior is investigated. Table A-2.1 presents the main parameters and mechanical properties of the specimens.

Table A-2.1: Reinforcement detail and mechanical properties of materials for all test specimens

			Tensile reinforcement				*Integrity reinforcement*						
	Test	d [mm]	ρ [%]	f_{sy} [MPa]	f_{su} [MPa]	E_s [GPa]	A_{sb}	f_{sy} [MPa]	f_{su} [MPa]	E_s [GPa]	f_c [MPa]	f_{ct} [MPa]	E_c [GPa]
Series 1	PM-1	102	0.25	601	664	201	-	-	-	-	36.6	2.9	36.9
	PM-2	102	0.49	601	664	201	-	-	-	-	36.5	2.8	36.7
	PM-3	102	0.82	601	664	201	-	-	-	-	37.8	3.4	37.9
	PM-4	102	1.41	601	664	201	-	-	-	-	36.8	3.0	37.1
Series 2	PM-9	102	0.82	601	664	201	4Ø8	616	680	202	31.0	2.3	33.3
	PM-10	102	0.82	601	664	201	4Ø10	560	599	195	31.1	2.3	33.3
	PM-11	102	0.82	601	664	201	4Ø12	548	625	201	32.3	2.5	33.7
	PM-12	102	0.82	601	664	201	4Ø14	527	629	199	32.4	2.6	33.7
	PM-13	102	0.82	601	664	201	4Ø8	616	680	202	32.6	2.6	33.8
	PM-14	102	0.82	601	664	201	4Ø10	560	599	195	32.7	2.6	33.8
	PM-15	100	0.84	601	664	201	4Ø12	548	625	201	32.7	2.6	33.8
	PM-16	101	0.83	601	664	201	4Ø14	527	629	199	32.8	2.6	33.9
Series 3	PM-17	102	0.82	625	641	200	4Ø8	625	641	200	39.7	2.8	28.7
	PM-18	95	0.88	625	641	200	4Ø10	605	658	194	39.8	2.8	28.8
	PM-19	99	0.85	625	641	200	4Ø12	559	618	197	39.9	2.8	28.8
	PM-20	102	0.82	625	641	200	4Ø14	578	695	203	40.0	2.9	29.0
	PM-21	103	0.81	625	641	200	4Ø8	625	641	200	40.2	2.9	29.3
	PM-22	99	0.85	625	641	200	4Ø10	605	658	194	40.3	2.9	29.5
	PM-23	95	0.88	625	641	200	-	-	-	-	40.4	2.9	29.7
	PM-24	97	0.86	625	641	200	-	-	-	-	40.4	3.0	29.9
	PM-25	98	0.85	625	641	200	4Ø8	625	641	200	40.4	3.0	30.1
	PM-26	101	0.83	625	641	200	4Ø10	605	658	194	40.3	3.0	30.1
	PM-27	104	0.81	625	641	200	4Ø12	559	618	197	40.3	3.0	30.2
	PM-28	99	0.85	625	641	200	4Ø14	578	695	203	40.3	3.0	30.3

A-2.2 Geometry and reinforcement

The twenty four square slab elements tested in this experimental program were identical in size and shape. The total width of the slabs was 1500 mm and nominal total thickness of the slabs was 125 mm. The square steel plate of 130×130 mm was used to simulate a rigid column in all tests. Fig. A-2.1 shows the general dimensions and geometry of the slabs.

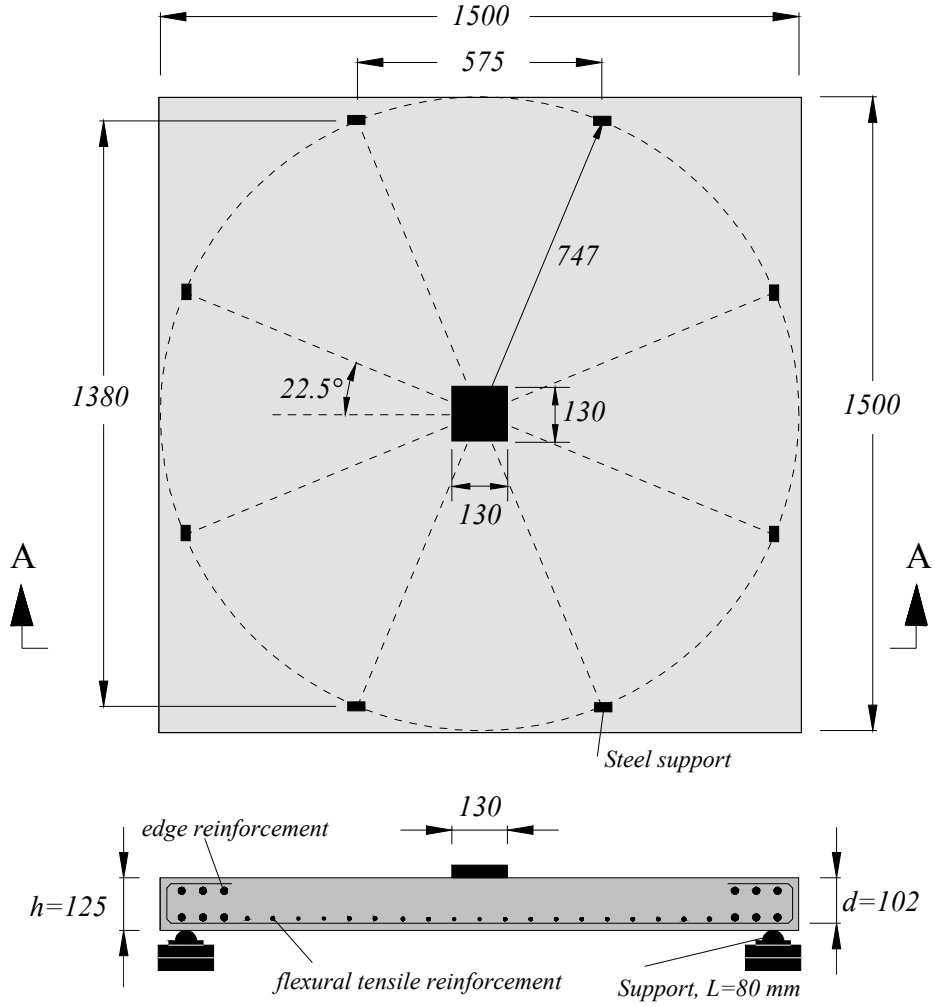

Figure A-2.1: Typical slab dimensions, plan and section [mm]

For all specimens, Ø8 was used as the main diameter for the tensile reinforcement. The first four specimens, PM-1 to PM-4, were designed to investigate the effect of various reinforcement ratios on the post-punching behavior of flat slabs. The variation of the reinforcement ratio was achieved by changing the bar spacing, see Fig. A-2.2. For the remaining twenty specimens, the tensile reinforcement ratio was the same and equal to 0.82% (Ø8 at 60 mm). For all slabs, the nominal concrete cover was 15 mm and Ø8 was used as the main tensile reinforcing bar, therefore the nominal effective depth (the average effective distance from the extreme compression fiber to the centroid of the tensile reinforcing bars) was 102 mm. The simulated column consisted of a stack of three square steel plates with the dimension of 130×130×30 mm. No vertical shear reinforcement was provided.

As can be seen in Fig. A-2.2.e, for slabs PM-9, PM-10, PM-11 and PM-12, Ø8, Ø10, Ø12 and Ø14 were used as integrity reinforcement in the compression zone of the slab. The full anchorage condition for this reinforcement (50Ø for Ø14, according to SIA 262) was provided, and thus the results should not be influenced by the anchorage condition.

Fig. A-2.2.f shows that for slabs PM-13, PM-14, PM-15 and PM-16, Ø8, Ø10, Ø12 and Ø14 bent-up bars were used as integrity reinforcement with an angle of inclination of 30° and bent at a distance of 50 mm from the column face. In addition, with these specimens, the full anchorage length for the bent-up bars was not provided, thus the results were influenced by the anchorage condition.

Fig. A-2.3.a shows slabs PM-17, PM-18, PM-19 and PM-20 in which Ø8, Ø10, Ø12 and Ø14 bent-up bars were used as integrity reinforcement respectively. In these tests, the full anchorage length for bent-up bars was provided; in consequence, the results were not affected by the anchorage condition.

PM-21 and PM-22 were similar to PM-9 and PM-10 respectively. PM-23 and PM-24 were similar to PM-3 as well, see Fig. A-2.3.b. This series of tests was about to investigate the influence of using various types of reinforcing steel and the effect of the concrete confinement over the column on the post-punching behavior of concrete slab-column connection. It should be noted that cold-worked Ø8 as well as hot-rolled Ø14 were used for all tested slabs. For slab PM-22 hot-rolled Ø10 was used and cold-worked Ø10 was used for the other test specimens. For slabs PM-11 and PM-15 hot-rolled Ø12 was used and cold-worked Ø12 was used for the other test specimens.

Fig. A-2.3 shows reinforcement layouts for slabs PM-25, PM-26, PM-27 and PM-28. They had Ø8 at 60 mm as their tensile reinforcement. Their tensile reinforcement was cut off at some specified points to investigate the effect of short anchorage length of tensile reinforcement on the post-punching behavior of flat slabs: PM-25 (cut-off at 2d from the column face); PM-26 (cut-off at 2.5d from the column face); PM-27 (cut-off at 3d from the column face); PM-28 (cut-off at 3.5d from the column face). In addition, Ø8, Ø10, Ø12 and Ø14 were used as integrity reinforcement in the compression zone of the slabs PM-25 to PM-28, respectively.

In all specimens, very strong edge reinforcement in both the top and bottom layer was provided to avoid unexpected modes of failure.

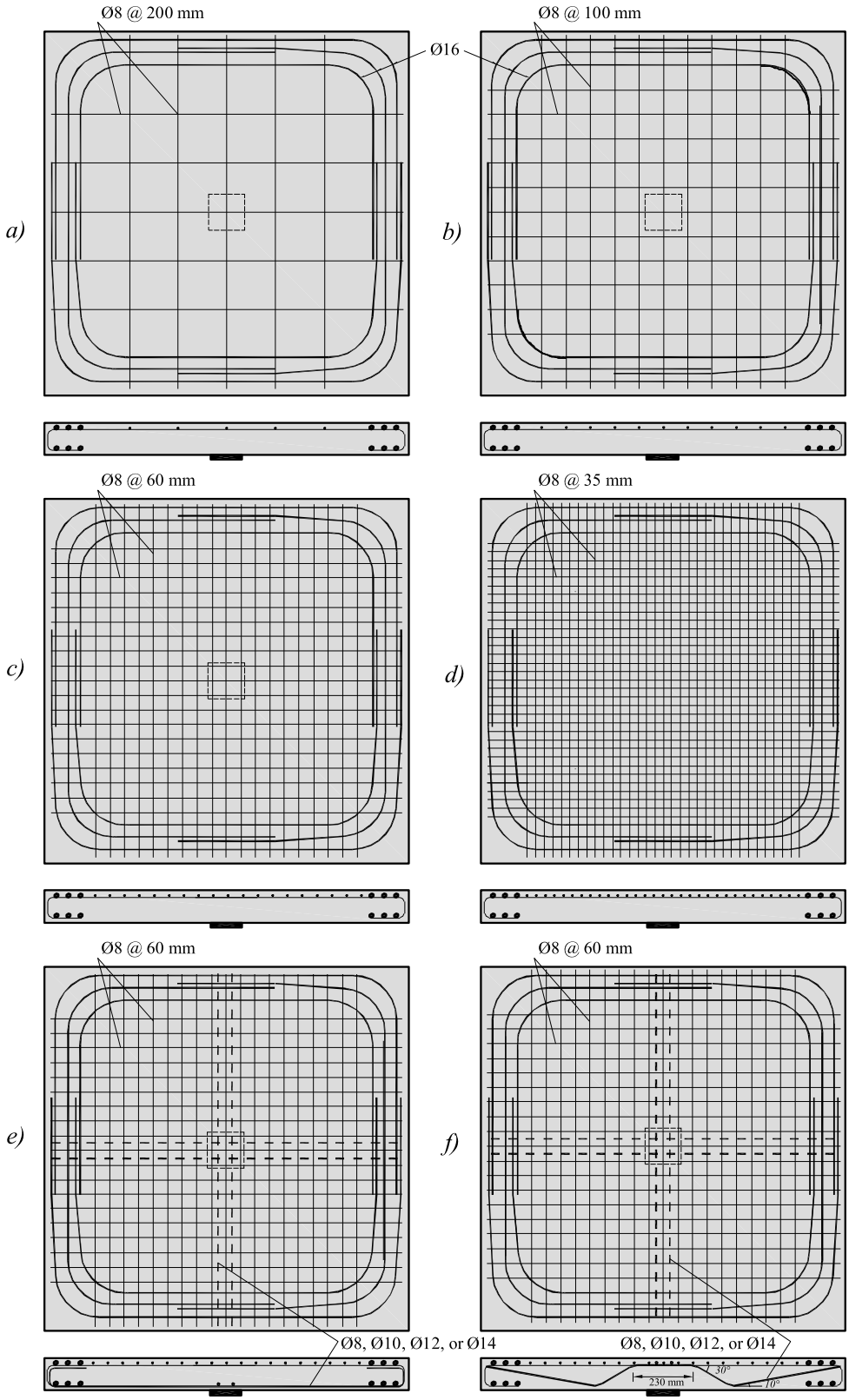

Figure A-2.2: Reinforcement layout: a) PM-1, b) PM-2, c) PM-3 and PM-23 d) PM-4, e) PM-9, PM-10, PM-11, and PM-12 (Ø8, Ø10, Ø12 and Ø14), and f) PM-13, PM-14, PM-15, and PM-16 (Ø8, Ø10, Ø12 and Ø14)

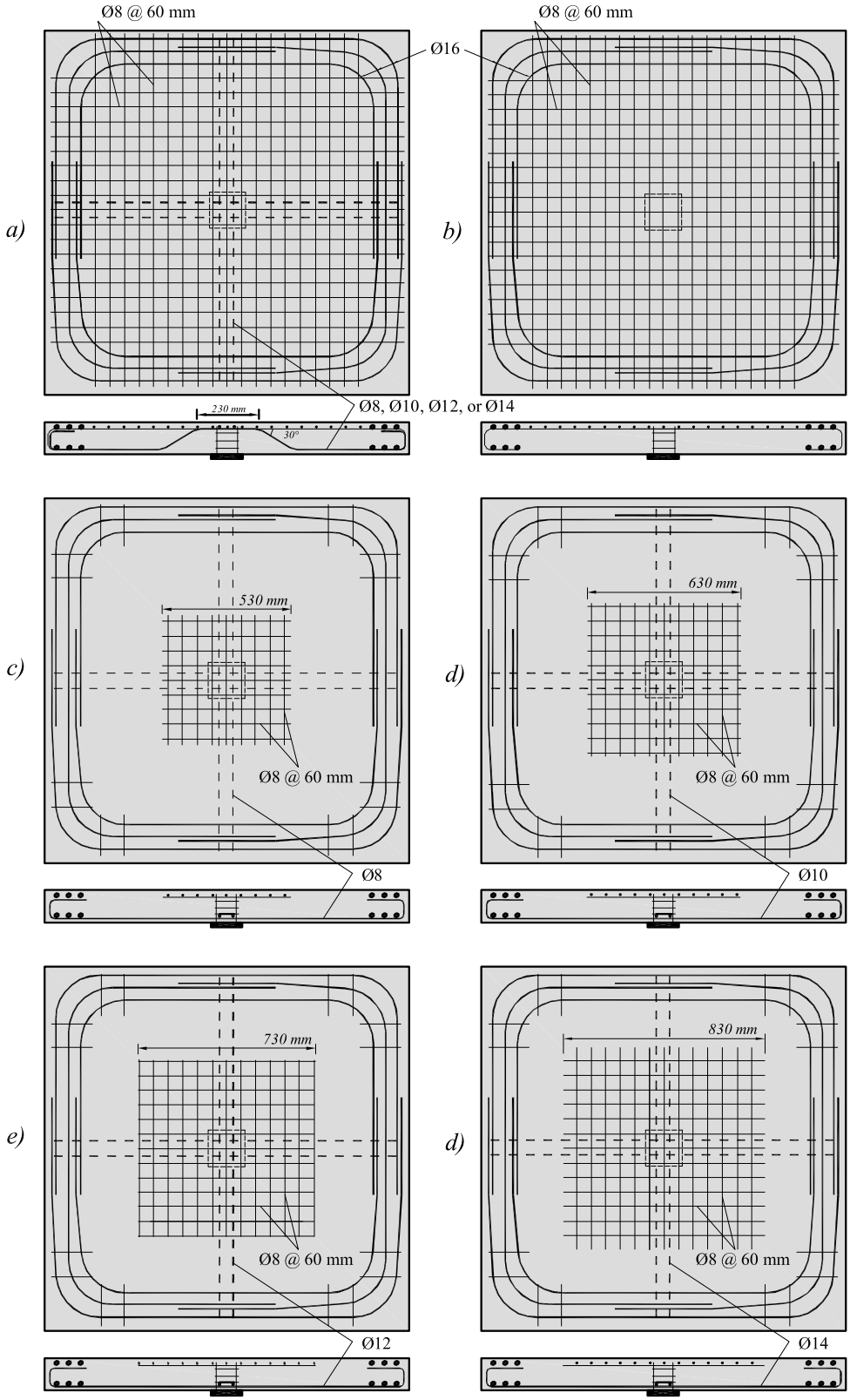

Figure A-2.3: Reinforcement layout: a) PM-17, PM-18, PM-19, and PM-20 (Ø8, Ø10, Ø12 and Ø14), b) PM-24, c) PM-25, d) PM-26, e) PM-27, and f) PM-28

A-2.3 Concrete casting and slab preparation

The first and two series were cast at the Laboratory of Structures of the Ecole Polytechnique Fédérale de Lausanne, while the third series was cast by GENETTI, a company located in Riddes, Valais, Switzerland.

Fig. A-2.4 shows the main steps of casting and preparation of the slabs. The formwork surface in contact with concrete was impregnated with mould oil before putting in the reinforcement. The concrete was prepared in a batching plant and delivered to the Laboratory of Structures by a concrete mixer truck. The first series of this campaign was cast on 31st March, 2006, the second one on 26th June, 2006 and the last one on 14th May, 2007. The slab surface was levelled and smoothed with the help of a ruler and a mason's mortar board. After casting, the slab was covered with a plastic sheet to maintain a moist environment. Water was sprayed onto the slab during the period of curing. The slump and flow table tests were performed before the casting of the slab. Table A-2.2 shows the results of the slump and flow table tests. Three concrete cylinders were cast and tested for each slab using the same batch of concrete.

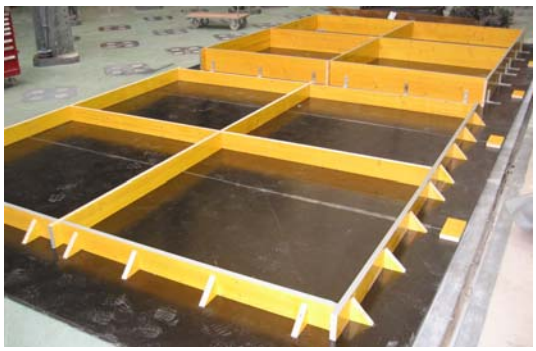

a) Formwork

b) Formwork and reinforcement

c) Reinforcement layout (PM-12)

d) Bent-up bars

Figure A-2.4: Formwork and reinforcing bars

A-2.4 Material properties

A-2.4.1 Concrete

Concrete of type C30/37 was chosen as it is representative for slabs cast in Switzerland. The concrete for the first and the second series was provided by Bétonfrais + Pompages SA Company, while for the third series, concrete was provided by GENETTI. The composition of concrete used for the slabs is shown in Table A-2.2. The water-cement ratio was about 0.54 for the first two series and 0.49 for the last one. The maximum aggregate size was 16 mm in all test series.

a) Concrete casting

b) Slump test

c) Flow table test

d) Cylinders

e) Slabs PM-9 to PM-16

f) Slabs PM-17 to PM-28

Figure A-2.5: Casting of the slabs

The measured mechanical properties were the concrete compressive strength, the Young's modulus, the apparent density and the tensile strength of the concrete. For this purpose, three cylinders were cast using the same concrete for each slab. Each concrete cylinder had a diameter of 160 mm and height of 320 mm. The tests were performed at the Laboratoire de Matériaux de Construction (LMC) of the Ecole Polytechnique Fédérale de Lausanne.

The mechanical properties at the time of testing were measured individually or calculated using the following fitted equation of logarithmic form proposed by CEB-FIP Model Code 90 [14]:

$$f_c(t) = f_{c,28} \exp\{s(1 - \sqrt{\frac{28}{t}})\} \tag{2.1}$$

where s is assumed to be 0.2.

Table A-2.2: Concrete composition and results of tests on fresh concrete

Slab	Sand 0-4 [kg]	Gravel 4-8 [kg]	Gravel 8-16 [kg]	Cement [kg]	Water [kg]	Slump [mm]	Flow table [mm]
Series 1 & 2	753 30%	604 24%	661 26%	325	174 W/C = 0.54	15	350
Series 3	820 35%	432 18%	621 26%	325	159 W/C = 0.54	12	320

Table A-2.3: Main concrete properties for the tested slabs

	Test	Date	age	Compressive Strength		Tensile Strength	Young's Modulus	Density
			[day]	$f_{c,28}$[MPa]	f_c [MPa]	f_{ct} [MPa]	E_c [GPa]	[t/m^3]
Series 1	PM-1	05.05.2006	33	36	36.6	2.9	36.9	2.45
	PM-2	02.05.2006	30	36	36.5	2.8	36.7	2.45
	PM-3	12.06.2006	71	36	39.5	3.4	37.9	2.45
	PM-4	10.05.2006	38	36	36.8	3.0	37.1	2.44
Series 2	PM-9	31.08.2006	35	30	31.0	2.3	33.3	2.42
	PM-10	01.09.2006	37	30	31.1	2.3	33.3	2.42
	PM-11	20.09.2006	56	30	32.3	2.5	33.7	2.41
	PM-12	22.09.2006	58	30	32.4	2.6	33.7	2.42
	PM-13	26.09.2006	62	30	32.6	2.6	33.8	2.42
	PM-14	28.09.2006	64	30	32.7	2.6	33.8	2.42
	PM-15	29.09.2006	65	30	32.7	2.6	33.8	2.42
	PM-16	02.10.2006	68	30	32.8	2.6	33.9	2.41
Series 3	PM-17	18.06.2007	35	37	39.7	2.8	28.7	2.42
	PM-18	19.06.2007	36	37	39.8	2.8	28.8	2.42
	PM-19	20.06.2007	37	37	39.9	2.8	28.8	2.43
	PM-20	22.06.2007	39	37	40.0	2.9	29.0	2.43
	PM-21	26.06.2007	43	37	40.2	2.9	29.3	2.40
	PM-22	29.06.2007	46	37	40.3	2.9	29.5	2.41
	PM-23	03.07.2007	50	37	40.4	2.9	29.7	2.44
	PM-24	06.07.2007	53	37	40.4	3.0	29.9	2.41
	PM-25	09.07.2007	56	37	40.4	3.0	30.1	2.41
	PM-26	10.07.2007	57	37	40.3	3.0	30.1	2.41
	PM-27	11.07.2007	58	37	40.3	3.0	30.2	2.42
	PM-28	13.07.2007	60	37	40.3	3.0	30.3	2.42

Table A-2.3 presents the average value of the mechanical properties at the time of failure. Tables A-2.4, A-2.5 and A-2.6 show the results of tests on concrete cylinders for series 1, 2 and 3 respectively. Fig. A-2.6 shows the evolution over time of concrete compressive strength, tensile strength and the modulus of elasticity. Fig. A-2.7 shows the stress-strain curve in compression for concrete for the first series.

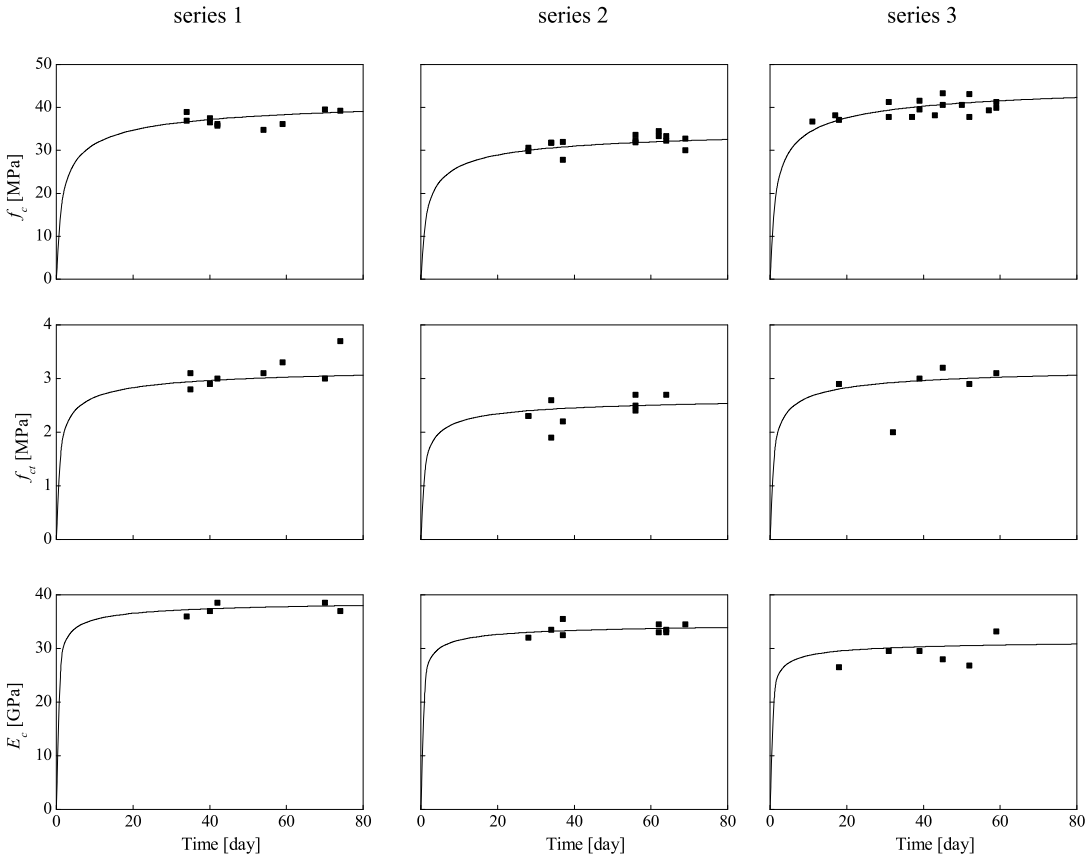

Figure A-2.6: Evolution of mechanical properties of concrete over time

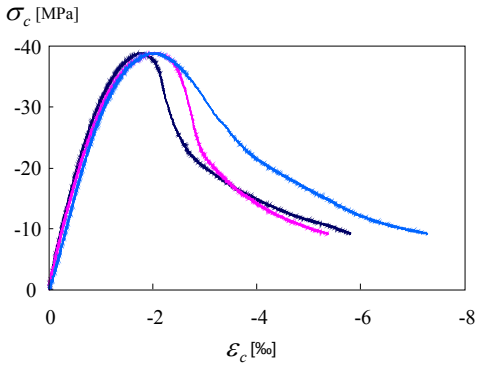

Figure A-2.7: Stress-strain curve of concrete in compression

Table A-2.4: Results of tests on concrete cylinders for the first series (PM-1 to PM-4)

Date of test	Age	Compressive Strength f_c [MPa]	Tensile Strength f_{ct} [MPa]	Young's Modulus E_c [GPa]	Density [t/m^3]
04.05.2006	34	39.0	-	36.0	2.45
04.05.2006	34	36.9	-	-	2.45
05.05.2006	35	-	3.1	-	2.44
05.05.2006	35	-	2.8	-	2.44
10.05.2006	40	37.5	2.9	37.0	2.44
10.05.2006	40	36.5	-	-	2.44
12.05.2006	42	36.1	3.0	38.5	2.45
12.05.2006	42	35.8	-	-	2.45
24.05.2006	54	34.8	3.1	-	2.44
29.05.2006	59	36.1	3.3	-	2.45
09.06.2006	70	39.5	3.0	38.5	2.44
09.06.2006	70	39.5	3.0	38.5	2.44
13.06.2006	74	39.2	3.7	37.0	2.44
13.06.2006	74	39.2	3.7	37.0	2.44

Table A-2.5: Results of tests on concrete cylinders for the second series (PM-9 to PM-16)

Date of test	Age	Compressive Strength f_c [MPa]	Tensile Strength f_{ct} [MPa]	Young's Modulus E_c [GPa]	Density [t/m^3]
23.08.2006	28	30.6	2.3	32	2.42
23.08.2006	28	29.8	-	-	2.42
29.08.2006	34	31.8	1.9	33.5	2.42
29.08.2006	34	31.8	-	-	2.42
01.09.2006	37	32	2.2	32.5	2.42
01.09.2006	37	27.8	-	-	2.42
20.09.2006	56	33.6	-	35.5	2.42
20.09.2006	56	31.9	-	33	2.41
20.09.2006	56	32.4	-	33	2.41
22.09.2006	58	-	2.5	-	2.42
22.09.2006	58	-	2.4	-	2.41
22.09.2006	58	-	2.3	-	2.42
26.09.2006	62	33.3	-	34.5	2.42
26.09.2006	62	34.5	-	-	2.42
27.09.2006	63	-	2.7	-	2.42
28.09.2006	64	33.3	2.7	33.5	2.42
28.09.2006	64	32.3	-	-	2.42
03.10.2006	69	32.8	-	34.5	2.41
03.10.2006	69	30	-	-	2.41
04.10.2006	70	-	2.6	-	2.41

Table A-2.6: Results of tests on concrete cylinders for the third series (PM-17 to PM-28)

Date of test	Age	Compressive Strength f_c [MPa]	Tensile Strength f_{ct} [MPa]	Young's Modulus E_c [GPa]	Density [t/m^3]
25.05.2007	11	36.7	-	-	2.44
31.05.2007	17	38.2	-	-	2.42
01.06.2007	18	37.1	2.9	26.5	2.43
14.06.2007	31	37.8	-	29.5	2.43
14.06.2007	31	41.3	-	-	2.43
15.06.2007	32	-	2	-	2.41
20.06.2007	37	37.8	-	-	2.42
22.06.2007	39	39.5	3	29.5	2.43
22.06.2007	39	41.6	-	-	2.43
26.06.2007	43	38.2	-	-	2.40
28.06.2007	45	43.3	3.2	28	2.41
28.06.2007	45	40.6	-	-	2.41
03.07.2007	50	40.6	-	-	2.44
05.07.2007	52	43.1	2.9	26.8	2.41
05.07.2007	52	37.8	-	-	2.41
10.07.2007	57	39.3	-	-	2.41
12.07.2007	59	41.3	3.1	33.2	2.42
12.07.2007	59	39.9	-	-	2.42

A-2.4.2 Steel

Fig. A-2.8 shows the stress-strain relationship for the reinforcing bars used for these test series. All of the reinforcing bars were of the type of B500B according to the Swiss concrete construction code SIA 262 (2003). Table A-2.7 presents the average value of the mechanical properties of tensile reinforcement as well as integrity reinforcement for all of the tested slabs. Table A-2.8 shows the detailed results for each tensile test. The strains were measured using an extensometer at the centre of the specimen with a measurement length of 100 mm. The loading speed was 10 MPa/s and ℓ is the length of the reinforcement measured between the clamps of the tension testing machine.

Table A-2.7: Average mechanical properties of the reinforcement

Test	Tensile reinf.					Integrity reinf.				
	Ø [mm]	f_{sy} [MPa]	f_{su} [MPa]	ε_{su} [%]	E_s [GPa]	Ø [mm]	f_{sy} [MPa]	f_{su} [MPa]	ε_{su} [%]	E_s [GPa]
PM-1	8	601	664	7.39	201	-	-	-	-	-
PM-2	8	601	664	7.39	201	-	-	-	-	-
PM-3	8	601	664	7.39	201	-	-	-	-	-
PM-4	8	601	664	7.39	201	-	-	-	-	-
PM-9	8	601	664	7.39	201	8	616	680	7.4	202
PM-10	8	601	664	7.39	201	10	560	599	7.9	195
PM-11	8	601	664	7.39	201	12	548	625	10.5	201
PM-12	8	601	664	7.39	201	14	527	629	13.5	199
PM-13	8	601	664	7.39	201	8	616	680	7.4	202
PM-14	8	601	664	7.39	201	10	560	599	7.9	195
PM-15	8	601	664	7.39	201	12	548	625	10.5	201
PM-16	8	601	664	7.39	201	14	527	629	13.5	199
PM-17	8	625	641	6.07	200	8	625	641	6.1	200
PM-18	8	625	641	6.07	200	10	605	658	7.8	194
PM-19	8	625	641	6.07	200	12	559	618	7.9	197
PM-20	8	625	641	6.07	200	14	578	695	12.0	203
PM-21	8	625	641	6.07	200	8	625	641	8.9	200
PM-22	8	625	641	6.07	200	10	605	658	10.3	194
PM-23	8	625	641	6.07	200	-	-	-	-	-
PM-24	8	625	641	6.07	200	-	-	-	-	-
PM-25	8	625	641	6.07	200	8	625	641	6.1	200
PM-26	8	625	641	6.07	200	10	605	658	7.8	194
PM-27	8	625	641	6.07	200	12	559	618	7.9	197
PM-28	8	625	641	6.07	200	14	578	695	12.0	203

Table A-2.8: Detailed results of tests on the reinforcement

Series	Ø [mm]	f_{sy} [MPa]	f_{su} [MPa]	ε_{su} [%]	f_{su}/f_{sy}	E_s [GPa]	ℓ [mm]
1,2	8	633	691	7.68	1.09	200	634
1,2	8	581	641	-	1.10	198	601
1,2	8	594	657	-	1.11	202	641
1,2	8	598	668	7.10	1.12	204	652
1,2	10	561	584	5.21	1.04	195	578
1,2	10	555	619	8.68	1.12	195	579
1,2	10	566	585	5.19	1.03	194	584
1,2	10	557	608	5.47	1.09	197	592
1,2	12	556	616	7.01	1.11	195	541
1,2	12	539	633	13.90	1.17	207	592
1,2	14	531	630	14.57	1.19	201	550
1,2	14	523	627	12.46	1.20	196	557
3	8	619	635	6.68	1.03	199	620
3	8	633	651	-	1.03	201	621
3	8	623	637	5.46	1.02	200	627
3	10	619	665	5.41	1.07	191	613
3	10	627	673	5.16	1.07	197	622
3	10	596	642	10.72	1.08	192	605
3	10	579	653	9.88	1.13	194	628
3	12	541	600	7.84	1.11	193	664
3	12	576	632	8.43	1.10	199	649
3	12	581	639	8.75	1.10	194	652
3	12	539	601	6.41	1.12	200	659
3	14	578	697	11.96	1.21	200	674
3	14	583	697	12.23	1.20	206	684
3	14	573	690	11.73	1.20	202	701

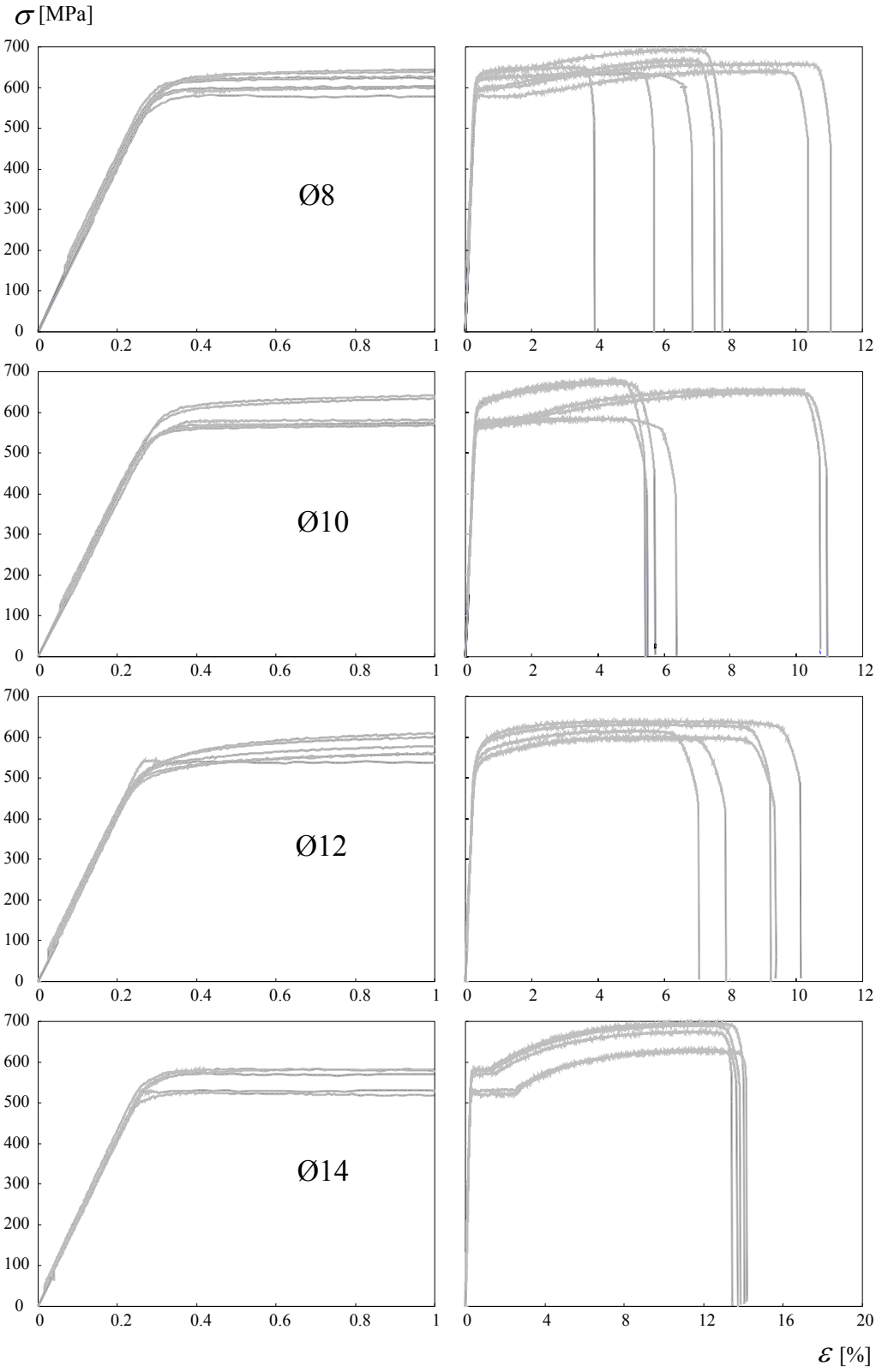

Figure A-2.8: Stress-strain curves for steel bars

A-3 Test setup and instrumentation

A-3.1 Framework and loading procedure

Fig. A-3.1 shows the test setup and the main dimensions of a typical tested slab. The test frame is mainly composed of two principal columns, a strong girder, a hydraulic jack, a load cell, four concrete blocks, steel plates, and also measurement instruments. The columns were fixed to the reaction floor by pre-stressing bars to ensure an adequate rigidity in the system. The load cell and the hydraulic jack were connected to the girder by a steel transfer beam.

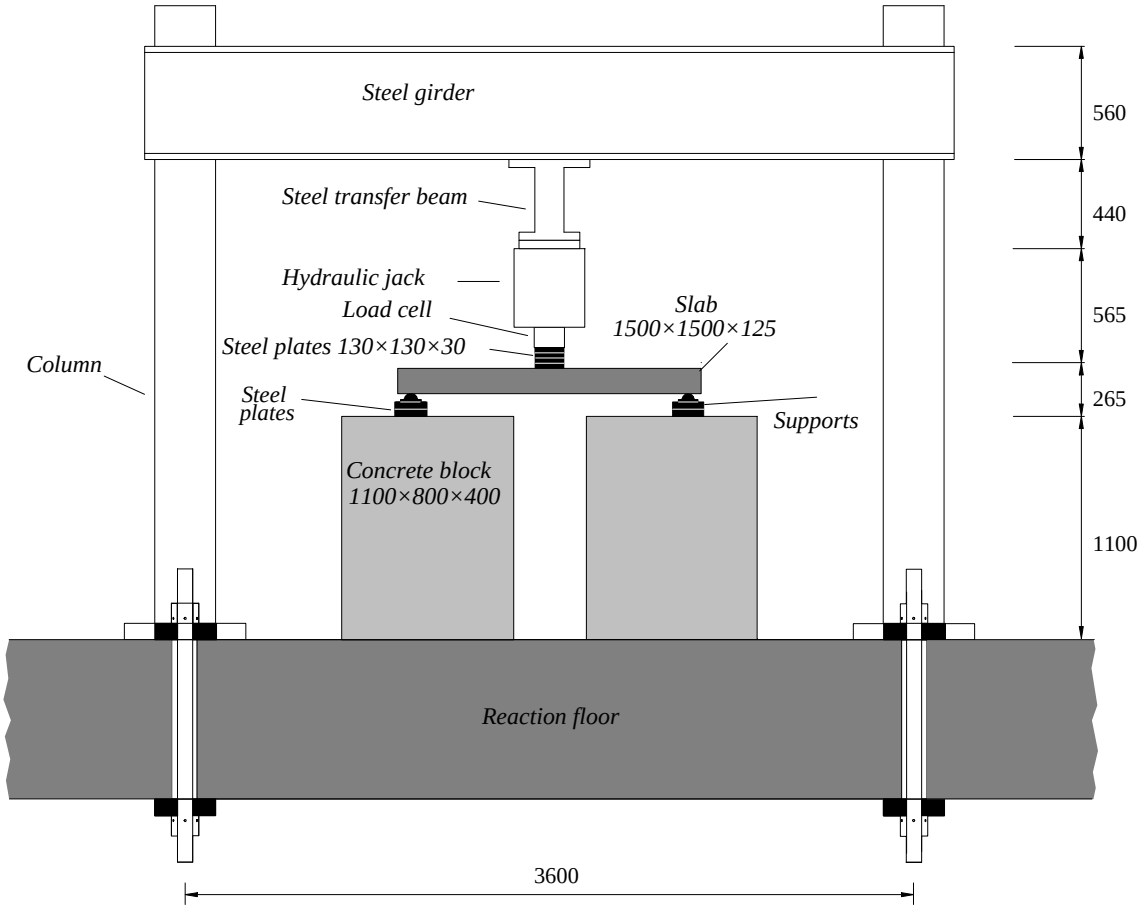

Figure A-3.1: Test setup [mm]

The slab was simply supported on eight metallic supports in a circular pattern along the edge of the slab at the distance of 60 mm from the edge. The metallic supports were placed on four concrete blocks with the dimension of 1100×800×400 mm and the distance between consecutive supports was 575 mm. The slabs were free to undergo very large deformations after the punching failure, consequently, to allow the slabs to

rotate and move without restraints, aluminum and teflon plates were placed between the support steel plates. Fig. A-3.2 shows the locations and arrangement of the supports.

The concentrated load was applied on the center of the slab through a stack of three square steel plates with the dimension of 130×130×30 mm. The load was applied by the hydraulic jack with the maximum capacity of 2000 kN. The test was displacement controlled and the value of the applied force was measured by the load cell at defined time intervals. A 2 to 5 mm thick layer of plaster was placed between the slab and the steel plates to regularize the load introduction surfaces.

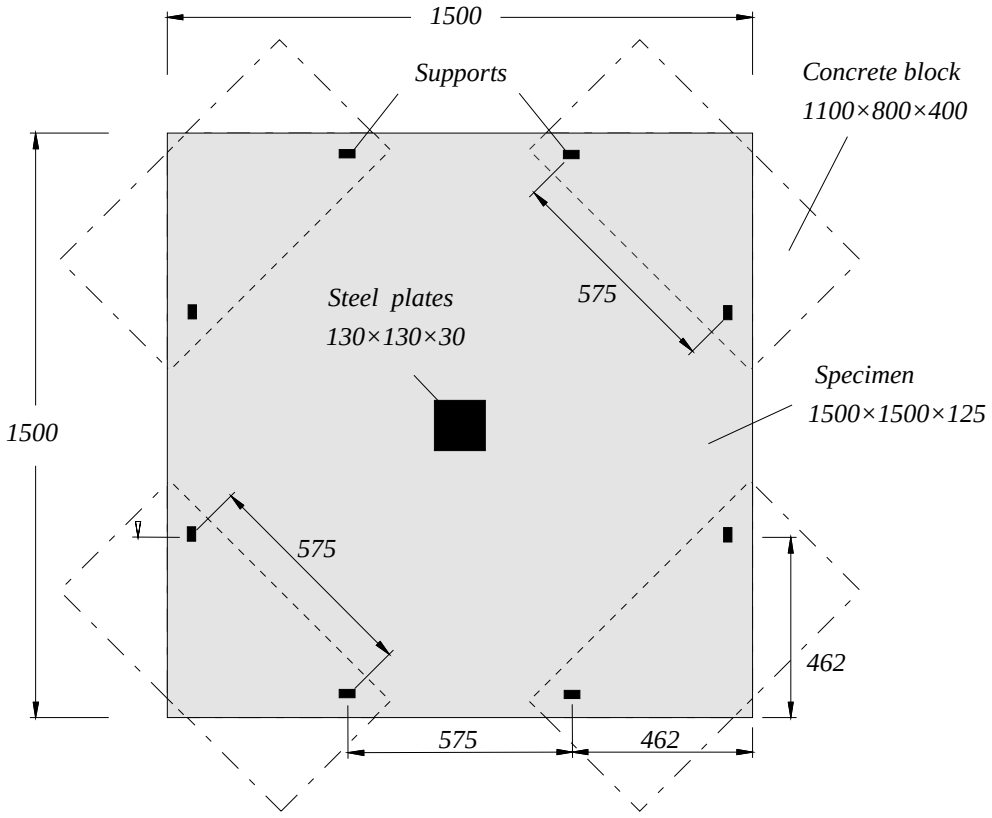

Figure A-3.2 Test setup, plan view [mm]

A-3.2 Measurement instrumentation

Three different kind of measurement devices were used in these experiments. The force was measured using the load cell, the deflections were measured using LVDTs (linear variable displacement transducer), the variation of the thickness of the slab was measured using LVDTs, and the rotation of the slabs was measured using inclinometers. The time interval of the inclinometers measurements was about 10 seconds and for the other devices it was between 2 to 4 seconds. Fig. A-3.3 shows the instrument setup at the bottom of a typical slab with the dimension of 1500×1500×125 mm. V1 measured the central displacement of the slab. Furthermore, V2 to V4 measured the deflection of the truncated punching cone symmetrically. In series 3, the number of LVDTs was increased to record the evolution of the slab displacement from support to the center of the slab, as shown in Fig. A-3.3b. For the first and second test series, V2 to V5 were placed at a distance of 250 mm from the center of the slab. For the third series V2 to V4

were at the same position as in the two first series, V5 was placed at the distance of 125 mm from the center of the slab, and the additional transducers, V10 to V13, were placed in one single line with the distance of 125 mm from each other.

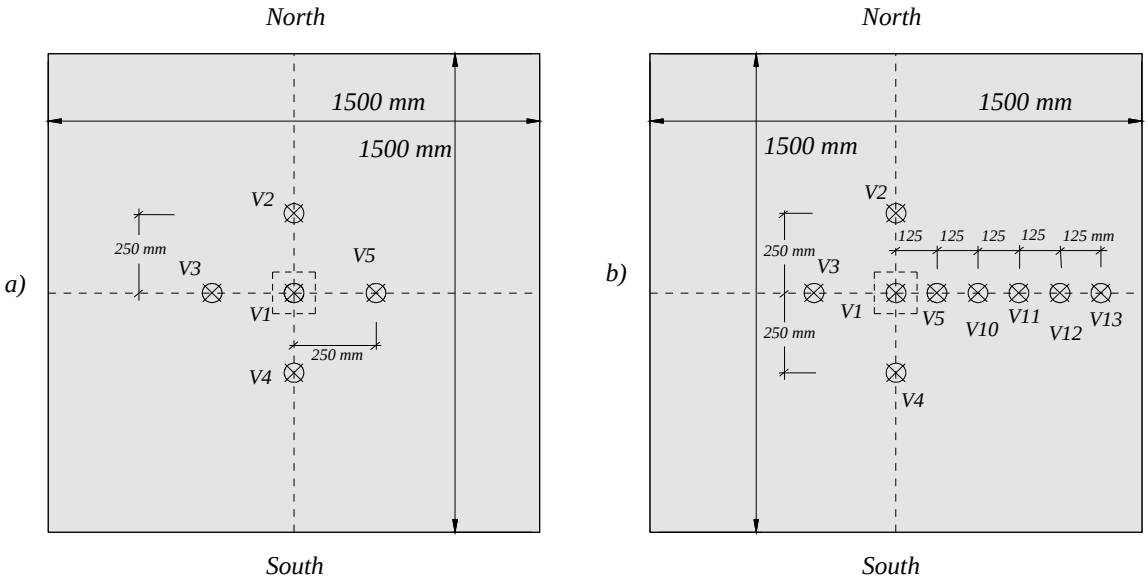

Figure A-3.3: Instrument setup at the bottom of the slab for test series 1 and 2 (a), and for series 3 (b)

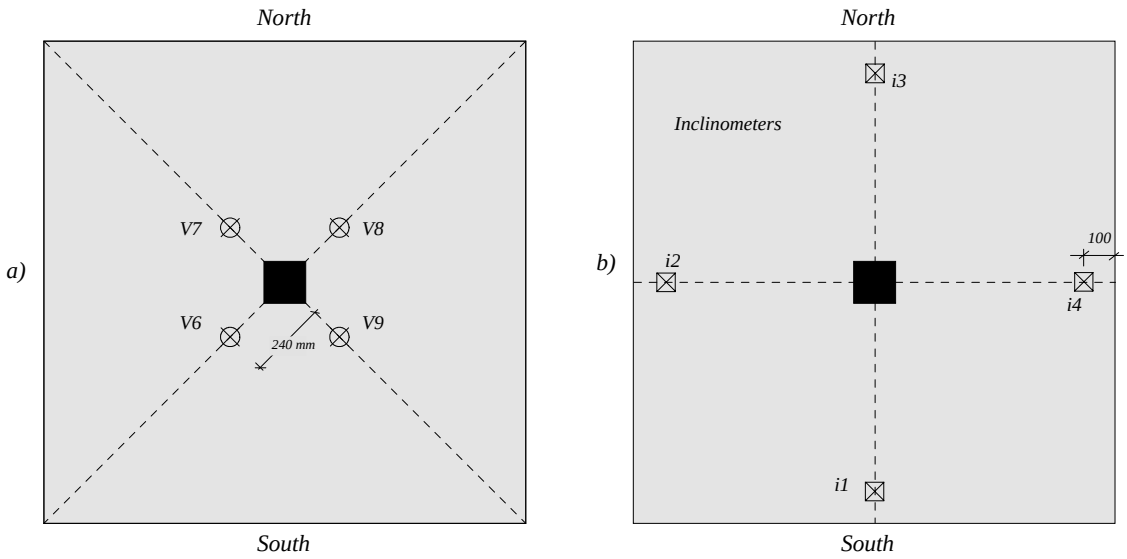

Figure A-3.4: Instrument setup at the top of the slab for all test series

Fig. A-3.4 shows the instrument layout at the top of the slab for all test series. V6 to V9 measured top surface displacement. V6 to V9 were placed at a distance of 240 mm from the center of the slab, whereas the inclinometers were placed at a distance of the 100 mm from the edge of the slab specimen.

One of the main objects of this experiment was to investigate the effect of the integrity reinforcement on the post-punching behavior of concrete flat slabs supported by columns. The effect of the integrity reinforcement is related to the relative displacement between the punching cone and the rest of the slab. This relative penetration displacement was obtained as the difference between two transducers V14 and V15 as shown in Fig. A-3.5.

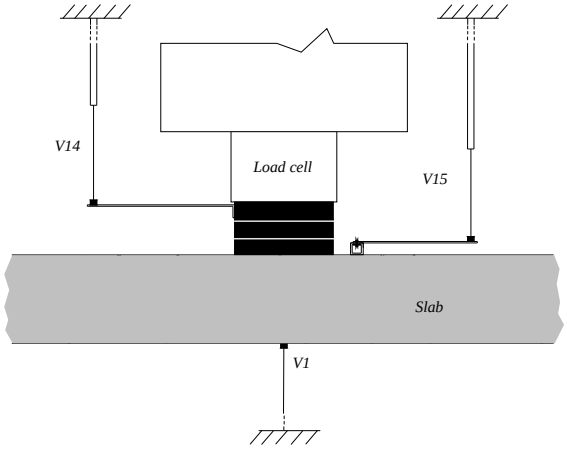

Figure A-3.5: Instrument arrangement to measure the penetration displacement (V14 – V15)

Reinforcing bars play a great role in the post-punching behaviour of flat slabs supported by columns, because they are the only remaining link between the truncated punching cone and the rest of the slab. Thus the load carrying capacity of flat slabs after punching is significantly influenced by the amount and strength of reinforcing steel. To gain a better understanding of the behaviour of the tensile reinforcement during and after punching failure, strain gauges were used to measure the elongation of the steel bars of the slabs PM-1 to PM-4. Fig. A-3.6 shows the position of the strain gages.

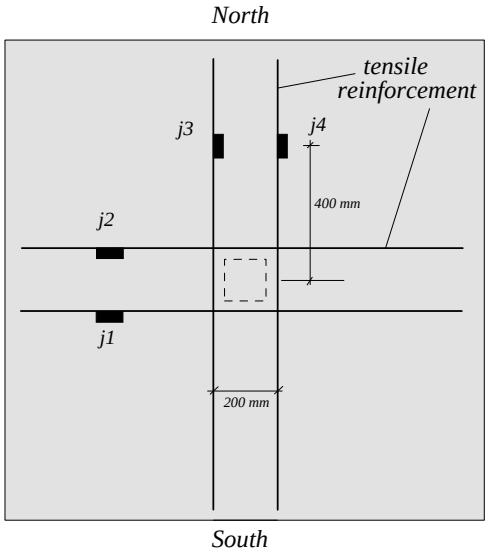

Figure A-3.6: Layout of the strain gauges on the tensile reinforcement

A-4 Experimental results

Table A-4.1 summarizes the main experimental results of this experimental campaign. The most important parameters are:

- V_p: Maximum load at punching failure
- w_p: Deflection corresponding to V_p
- V_{pp}: Maximum post-punching strength
- w_{pp}: Deflection corresponding to V_{pp}

Table A-4.1: Summary of results for all the slabs

Test	ρ [%]	A_{sb}	V_p [kN]	w_p [mm]	V_{pp} [kN]	w_{pp} [mm]	$\frac{V_{pp}}{V_p}$
PM-1	0.25	-	175.8	13.6	37.2	70.5	0.21
PM-2	0.49	-	223.7	11.0	66.0	52.7	0.30
PM-3	0.82	-	324.3	13.1	117.4	45.3	0.36
PM-4	1.41	-	295.2	7.4	107.8	42.6	0.37
PM-9	0.82	4Ø8	224.2	7.1	123.4	36.2	0.55
PM-10	0.82	4Ø10	227.5	6.7	158.6	42.9	0.70
PM-11	0.82	4Ø12	240.6	8.2	236.5	86.3	0.98
PM-12	0.82	4Ø14	249.0	8.2	245.0	116.9	0.98
PM-13	0.82	4Ø8*	326.7	11.4	150.6	39.9	0.46
PM-14	0.82	4Ø10*	355.8	12.6	187.5	71.7	0.53
PM-15	0.84	4Ø12*	274.0	9.1	176.7	66.5	0.64
PM-16	0.83	4Ø14*	298.4	10.1	134.8	43.4	0.45
PM-17	0.82	4Ø8**	329.1	15.1	246.6	50.0	0.75
PM-18	0.88	4Ø10**	322.7	15.7	236.7	56.5	0.73
PM-19	0.85	4Ø12**	417.3	28.7	315.0	90.1	0.75
PM-20	0.82	4Ø14**	402.1	19.3	344.9	95.2	0.86
PM-21	0.81	4Ø8	255.7	9.7	185.4	42.9	0.73
PM-22	0.85	4Ø10	288.2	14.1	218.7	65.2	0.76
PM-23	0.88	-	227.0	10.4	82.2	83.0	0.36
PM-24	0.86	-	271.5	12.1	100.6	74.2	0.37
PM-25+	0.85	4Ø8	143.0	7.7	85.4	69.8	0.60
PM-26+	0.83	4Ø10	164.7	8.5	104.6	89.3	0.64
PM-27+	0.81	4Ø12	211.2	8.0	94.1	64.1	0.45
PM-28+	0.85	4Ø14	257.6	11.2	101.4	57.2	0.39

* Bent-up bars with insufficient anchorage length

** Well-anchored bent-up bars

+ Test was terminated due to the risk of falling down the punching cone

In this chapter the experimental results are shown for each slab specimen including the following parts:

- Graph (a): Load versus central slab deflection (V1).
- Graph (b): Load versus rotation of the slab, measured with the inclinometers, i1, i2, i3 and i4. This curve is shown up to the initial punching failure due to the fact that the experimental results obtained beyond this point were rather random: N – S: average of i1 and i3, E – O: average of i2 and i4.
- Graph (c): Load versus relative penetration displacement δ between the truncated punching cone and the rest of the slab specimen. This relative displacement was measured using V14 and V15.
- Graph (d): Load versus average deflection of the compression side of the slab at the distance of 240 mm from the center, expressed as the average of V6, V7, V8 and V9. This curve is truncated after the initial punching shear failure as for graph (b).
- Graph (e): For PM-1 to PM-16 is slab plan view after testing. For PM-17 to PM-28 is slab section after testing accompanied by the evolution of the slab deflection at representative load levels.

$\rho = 0.25\%$ $f_c = 36.6$ MPa

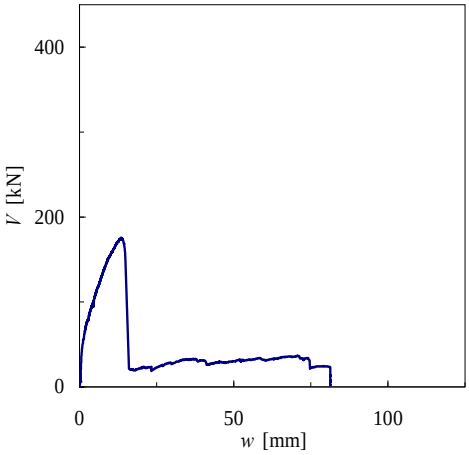

(a) *Load - central deflection*

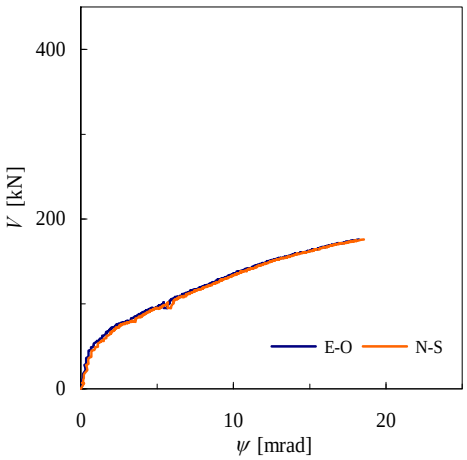

(b) *Load - rotation up to punching*

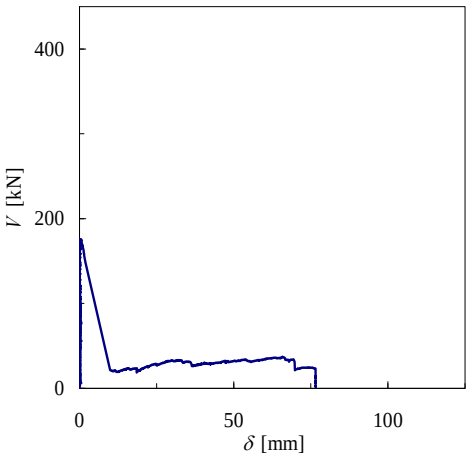

(c) *Load - penetration displacement*

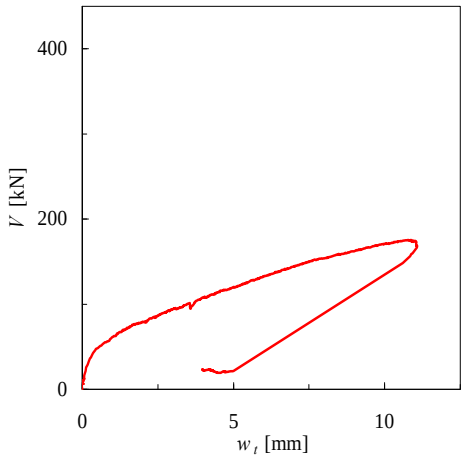

(d) *Load - compression side deflection*

(e) *Slab plan view after testing*

Figure A-4.1: Slab PM-1, ρ = 0.25 %

$\rho = 0.49\%$ $f_c = 36.5\ MPa$

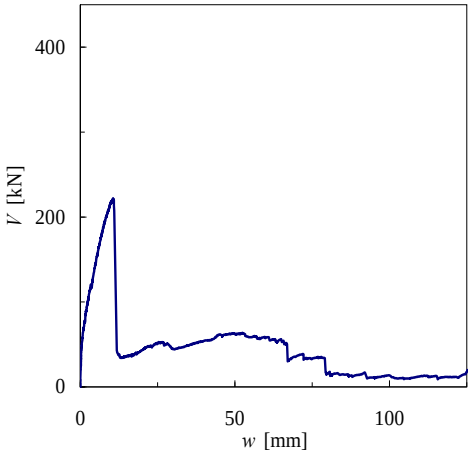

(a) *Load - central deflection*

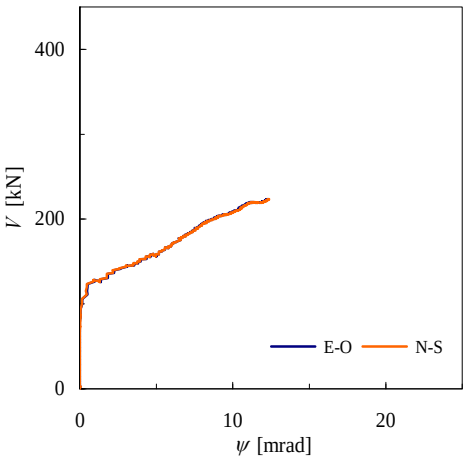

(b) *Load - rotation up to punching*

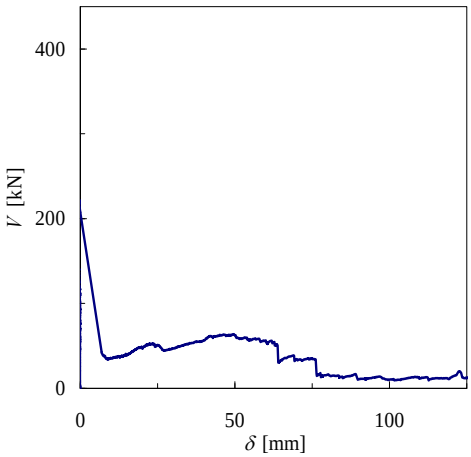

(c) *Load - penetration displacement*

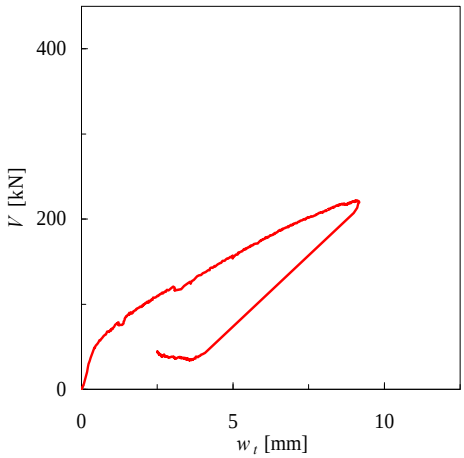

(d) *Load - compression side deflection*

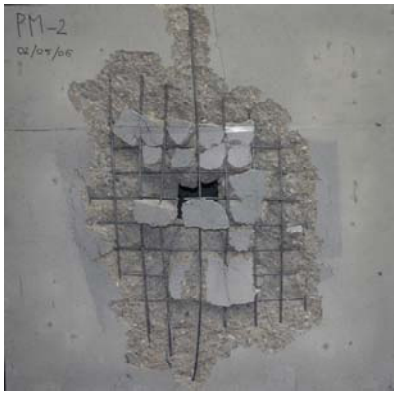

(e) *Slab plan view after testing*

Figure A-4.2: Slab PM-2, ρ = 0.49 %

$\rho = 0.82\%$ $f_c = 37.8$ MPa

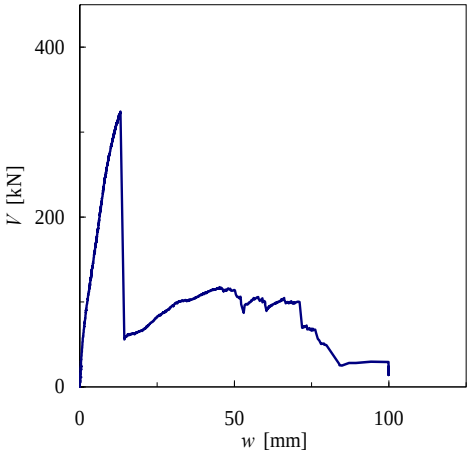

(a) *Load - central deflection*

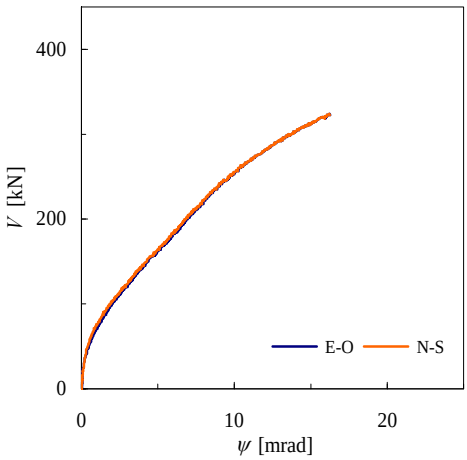

(b) *Load - rotation up to punching*

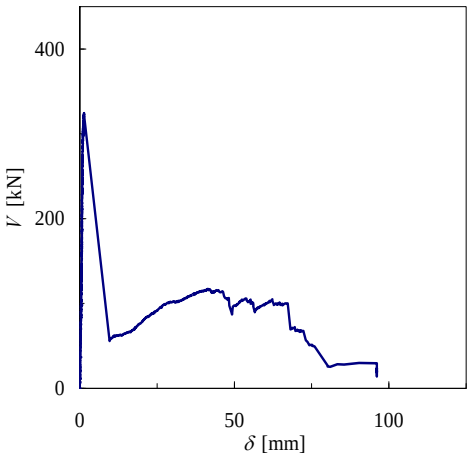

(c) *Load - penetration displacement*

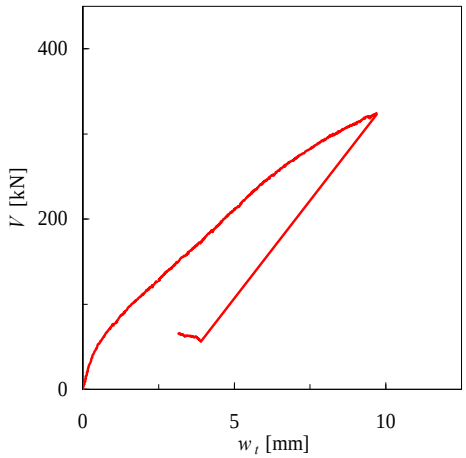

(d) *Load - compression side deflection*

(e) *Slab plan view after testing*

Figure A-4.3: Slab PM-3, ρ = 0.82 %

$\rho = 1.41\%$ $f_c = 36.8\ MPa$

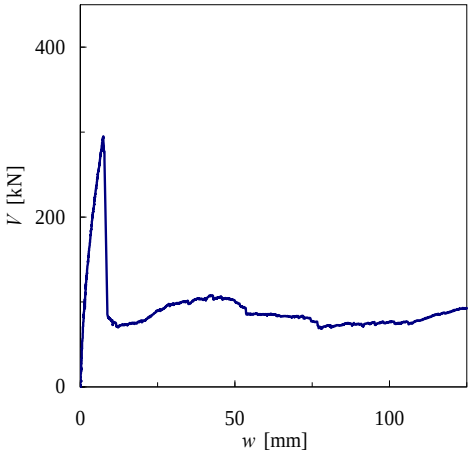

(a) *Load - central deflection*

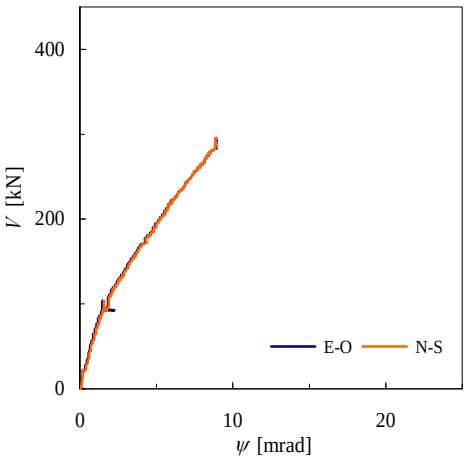

(b) *Load - rotation up to punching*

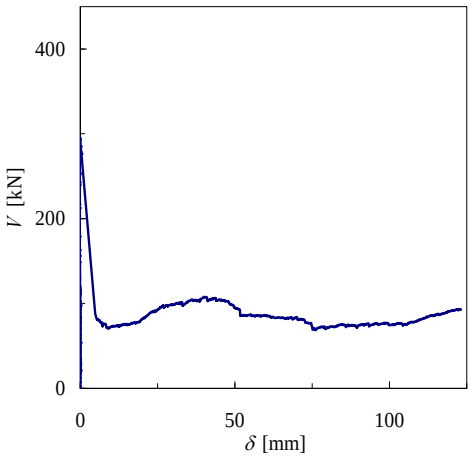

(c) *Load - penetration displacement*

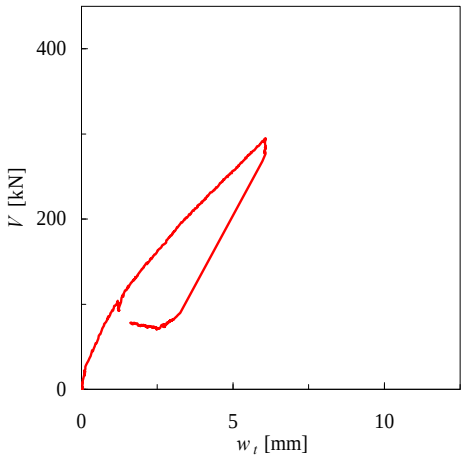

(d) *Load - compression side deflection*

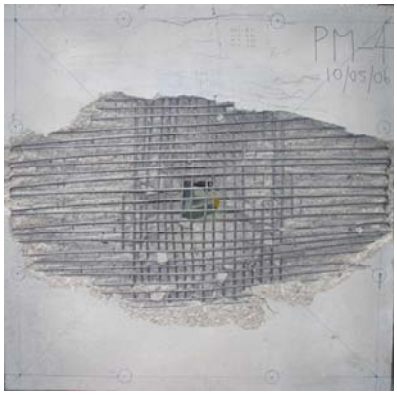

(e) *Slab plan view after testing*

Figure A-4.4: Slab PM-4, ρ = 1.41 %

$\rho = 0.82\%$ $f_c = 31$ MPa

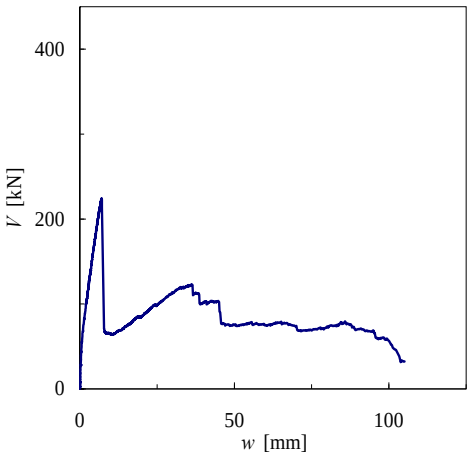

(a) *Load - central deflection*

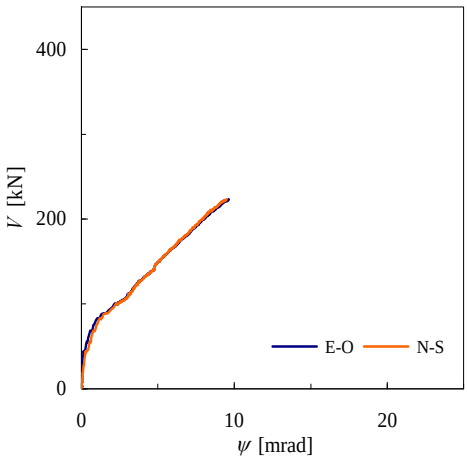

(b) *Load - rotation up to punching*

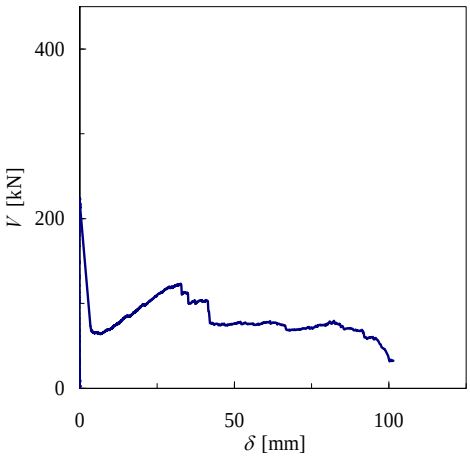

(c) *Load - penetration displacement*

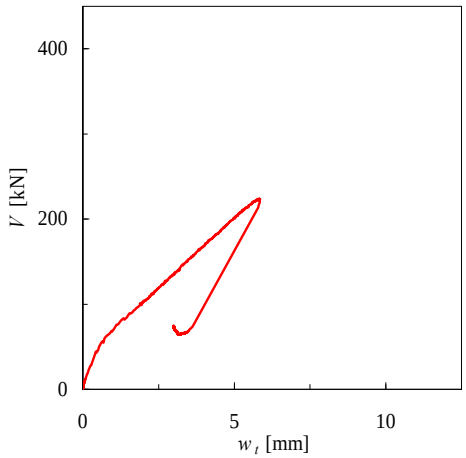

(d) *Load - compression side deflection*

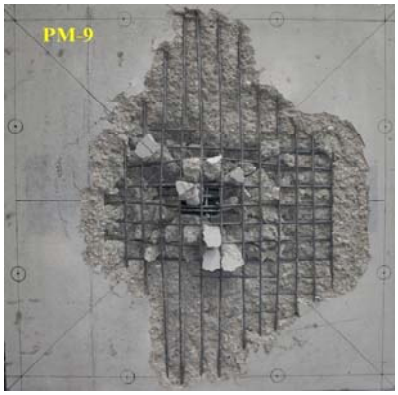

(e) *Slab plan view after testing*

Figure A-4.5: Slab PM-9: straight integrity bars Ø8

$\rho = 0.82\%$ $f_c = 31.1\ MPa$

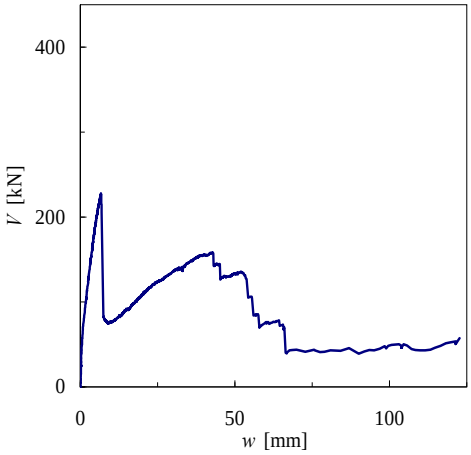

(a) *Load - central deflection*

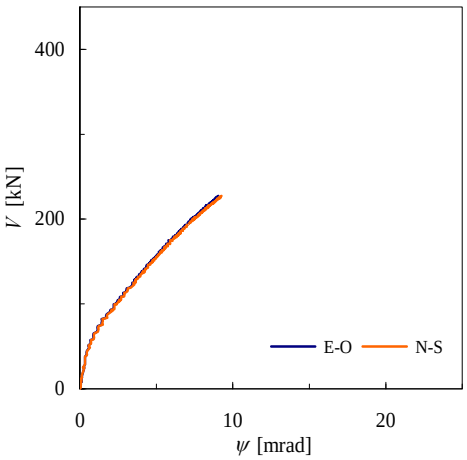

(b) *Load - rotation up to punching*

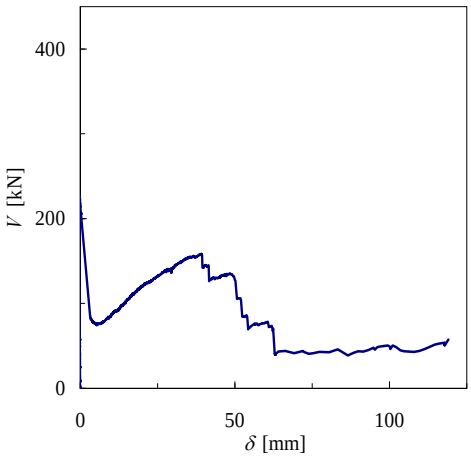

(c) *Load - penetration displacement*

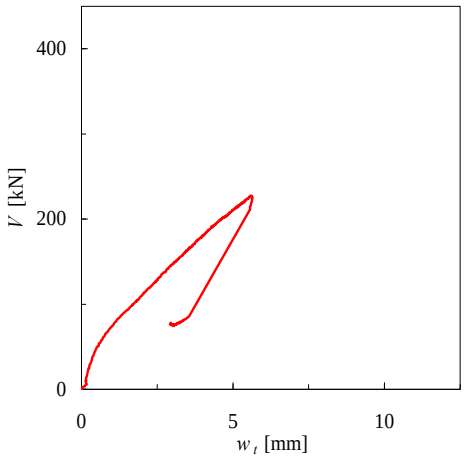

(d) *Load - compression side deflection*

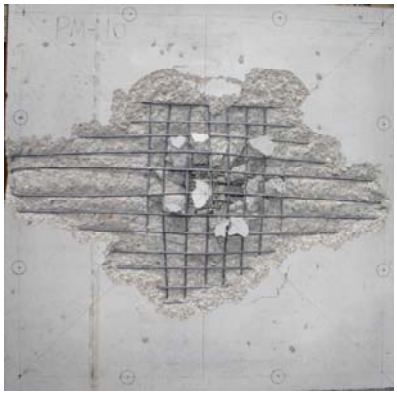

(e) *Slab plan view after testing*

Figure A-4.6: Slab PM-10: straight integrity bars Ø10

$\rho = 0.82\%$ $f_c = 32.3$ MPa

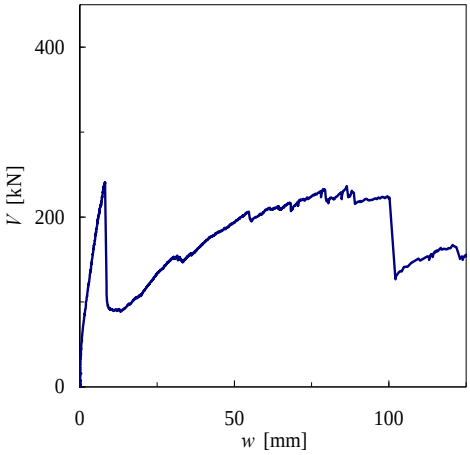

(a) *Load - central deflection*

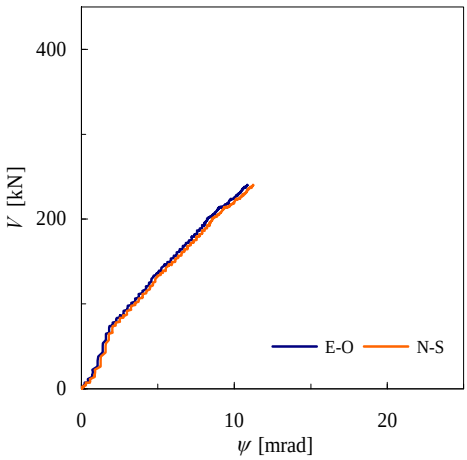

(b) *Load - rotation up to punching*

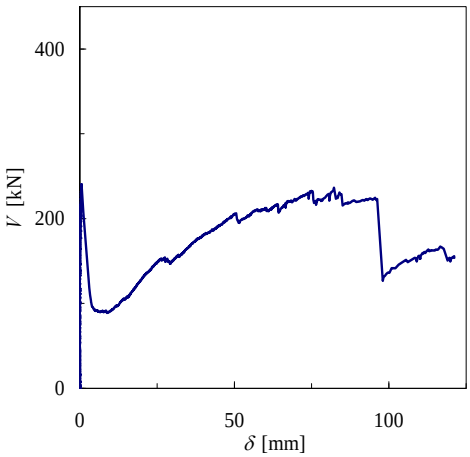

(c) *Load - penetration displacement*

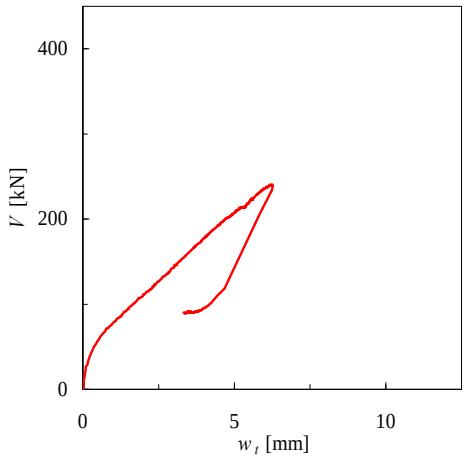

(d) *Load - compression side deflection*

(e) *Slab plan view after testing*

Figure A-4.7: Slab PM-11: straight integrity bars Ø12

$\rho = 0.82\%$ $f_c = 32.4\ MPa$

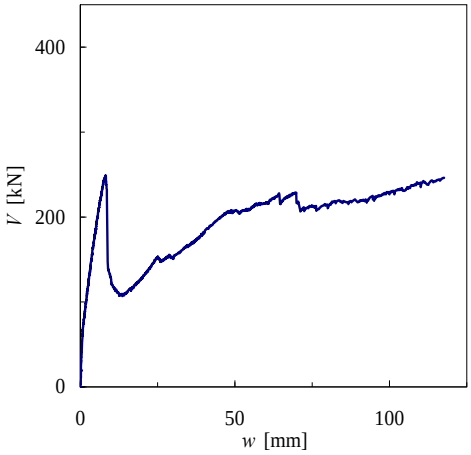

(a) *Load - central deflection*

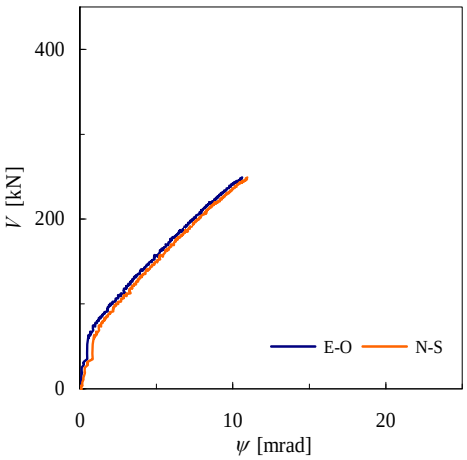

(b) *Load - rotation up to punching*

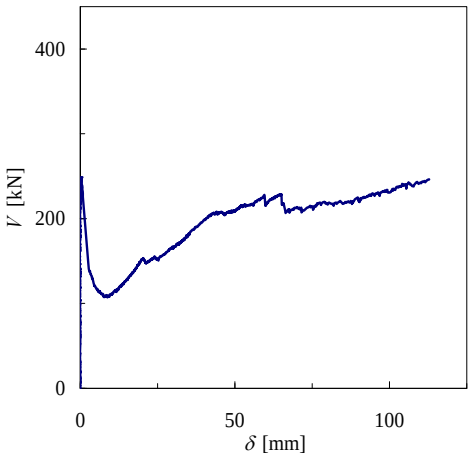

(c) *Load - penetration displacement*

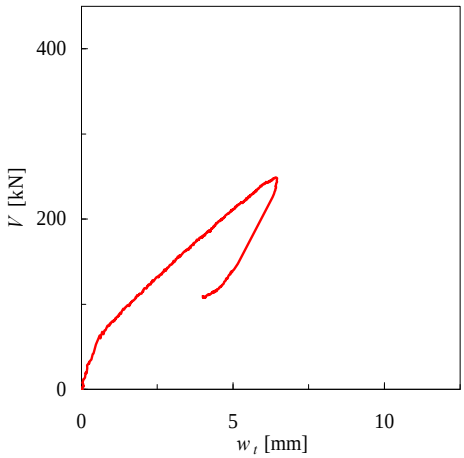

(d) *Load - compression side deflection*

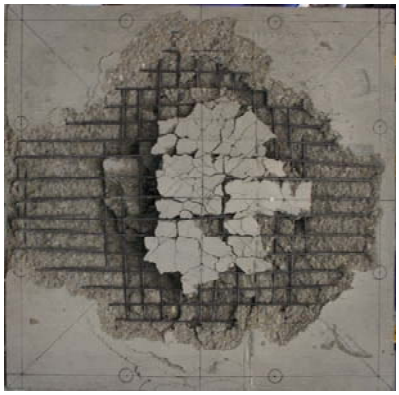

(e) *Slab plan view after testing*

Figure A-4.8: Slab PM-12: straight integrity bars Ø14

$\rho = 0.82\%$ $f_c = 32.6$ MPa

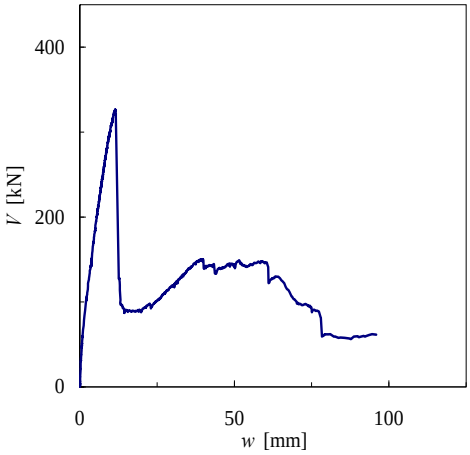

(a) *Load - central deflection*

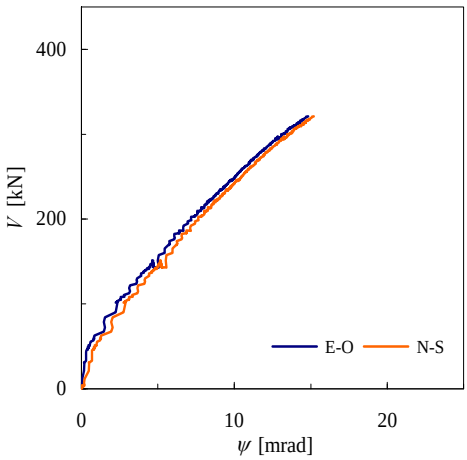

(b) *Load - rotation up to punching*

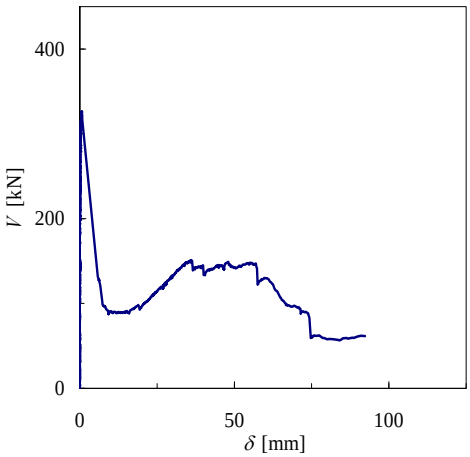

(c) *Load - penetration displacement*

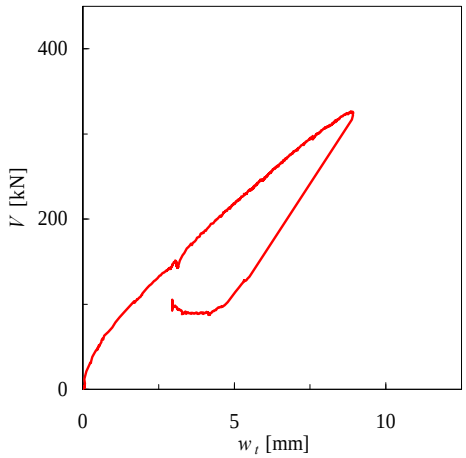

(d) *Load - compression side deflection*

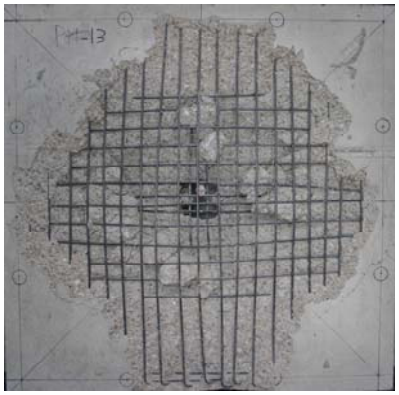

(e) *Slab plan view after testing*

Figure A-4.9: Slab PM-13: bent-up-bars Ø8, insufficient anchorage

$\rho = 0.82\%$ $f_c = 32.7\ MPa$

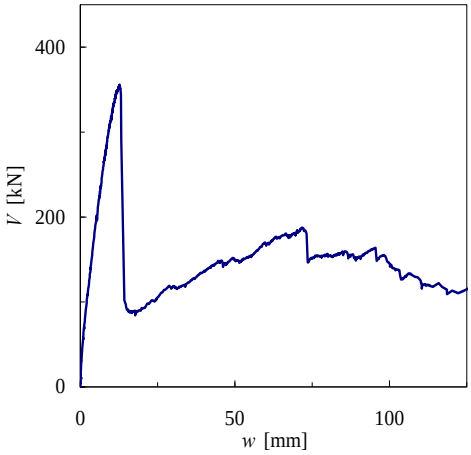

(a) *Load - central deflection*

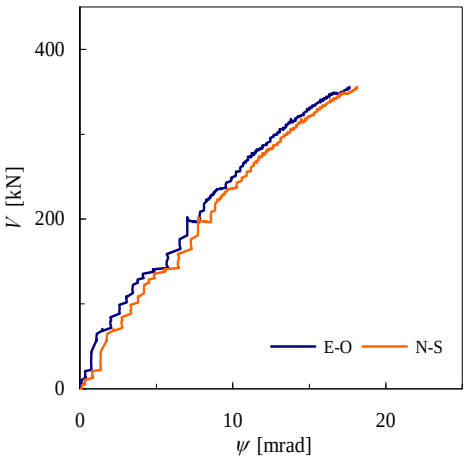

(b) *Load - rotation up to punching*

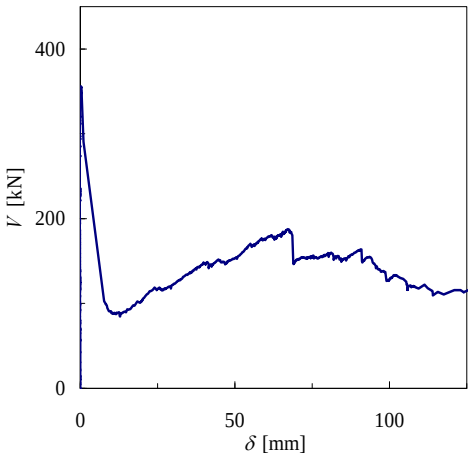

(c) *Load - penetration displacement*

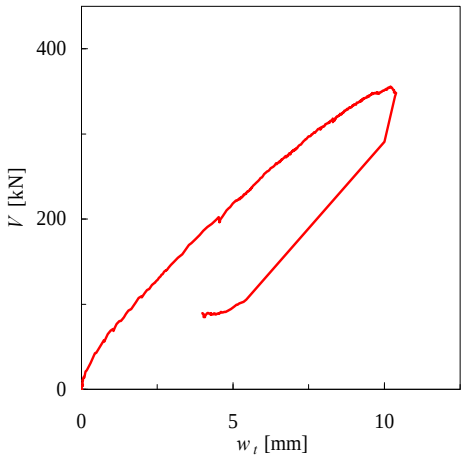

(d) *Load - compression side deflection*

(e) *Slab plan view after testing*

Figure A-4.10: Slab PM-14: bent-up-bars Ø10, insufficient anchorage

$\rho = 0.84\%$ $f_c = 32.7\ MPa$

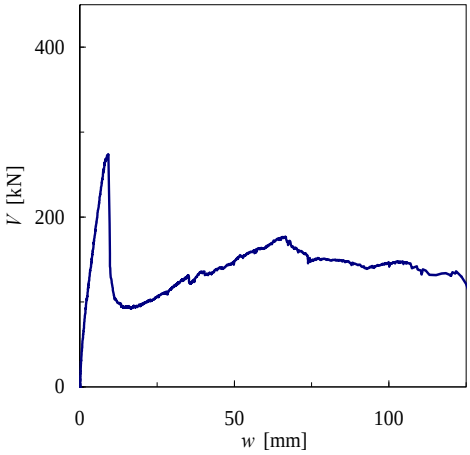

(a) *Load - central deflection*

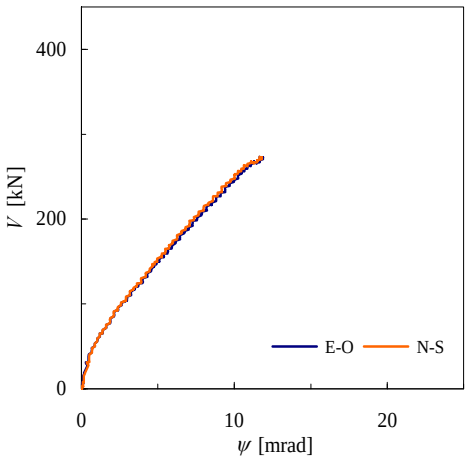

(b) *Load - rotation up to punching*

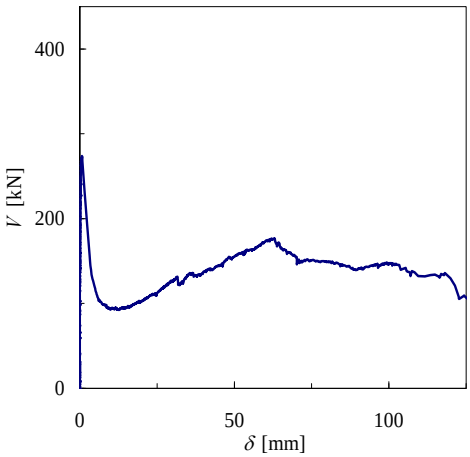

(c) *Load - penetration displacement*

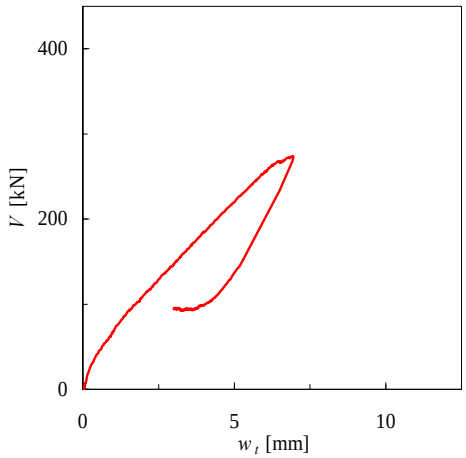

(d) *Load - compression side deflection*

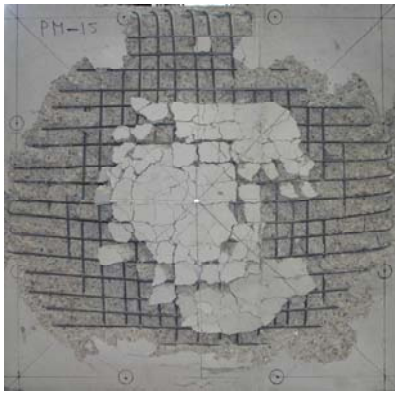

(e) *Slab plan view after testing*

Figure A-4.11: Slab PM-15: bent-up-bars Ø12, insufficient anchorage

$\rho = 0.83\%$ $f_c = 32.8$ MPa

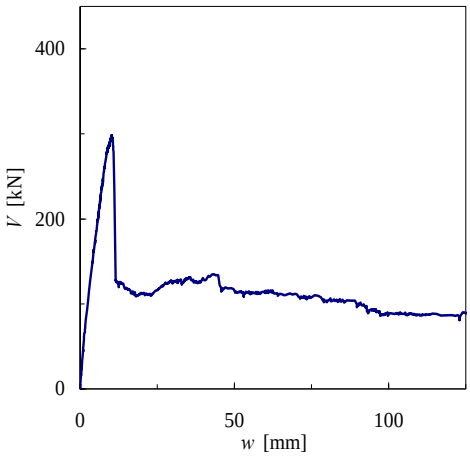

(a) *Load - central deflection*

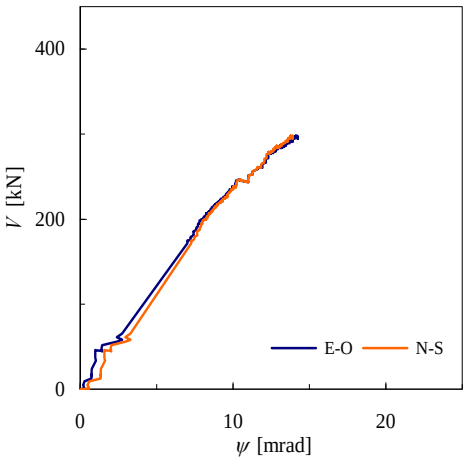

(b) *Load - rotation up to punching*

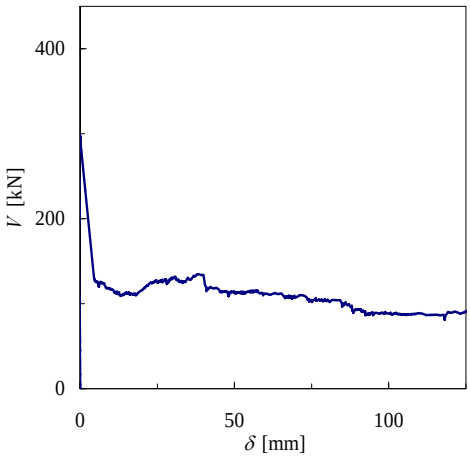

(c) *Load - penetration displacement*

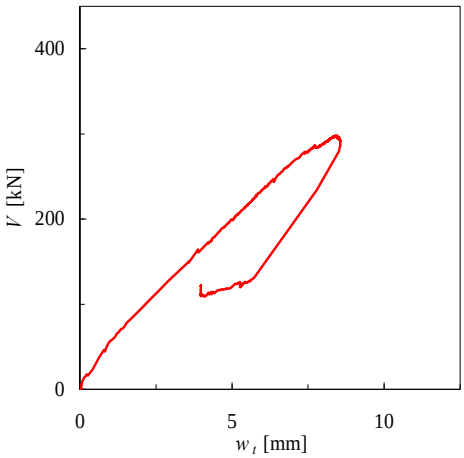

(d) *Load - compression side deflection*

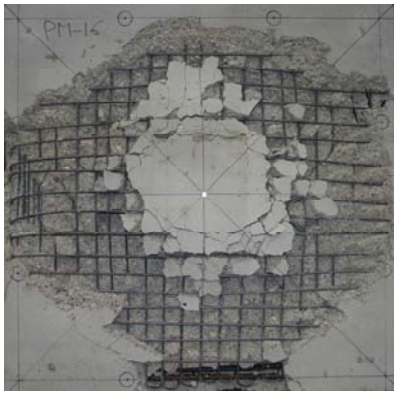

(e) *Slab plan view after testing*

Figure A-4.12: Slab PM-16: bent-up-bars Ø14, insufficient anchorage

$\rho = 0.82\%$ $f_c = 39.7$ MPa

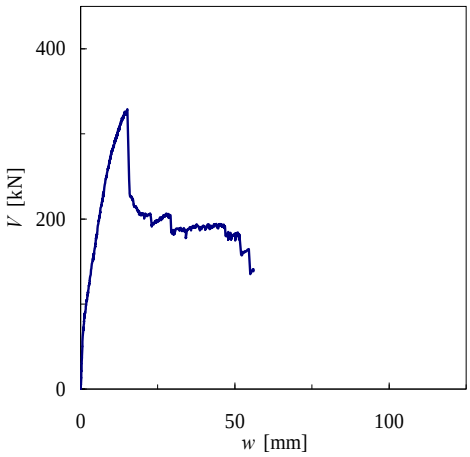

(a) *Load - central deflection*

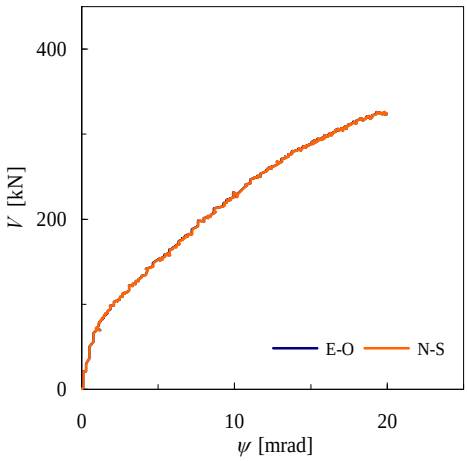

(b) *Load - rotation up to punching*

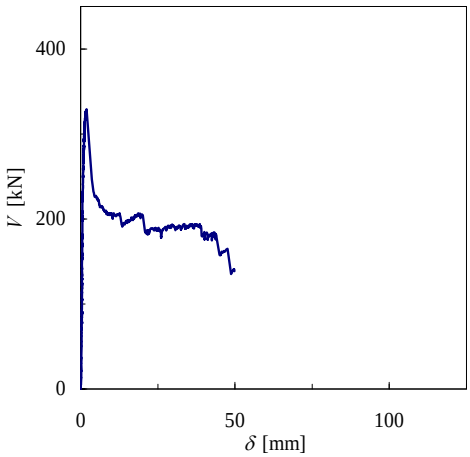

(c) *Load - penetration displacement*

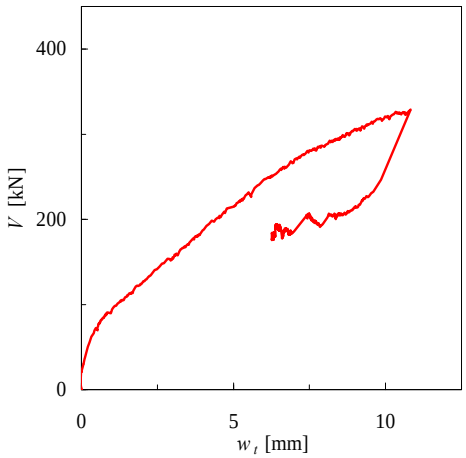

(d) *Load - compression side deflection*

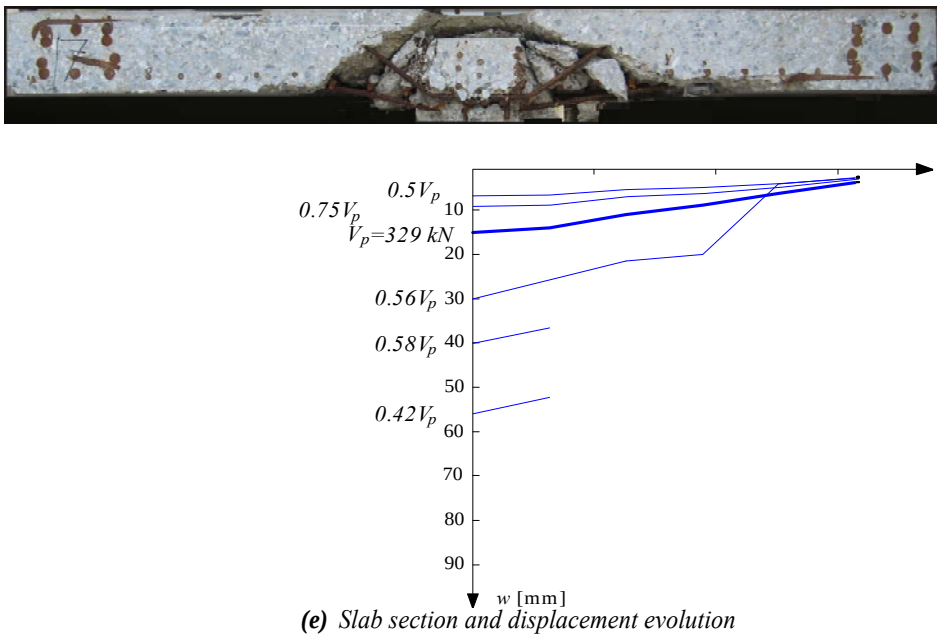

(e) *Slab section and displacement evolution*

Figure A-4.13: Slab PM-17: fully anchored bent-up-bars Ø8

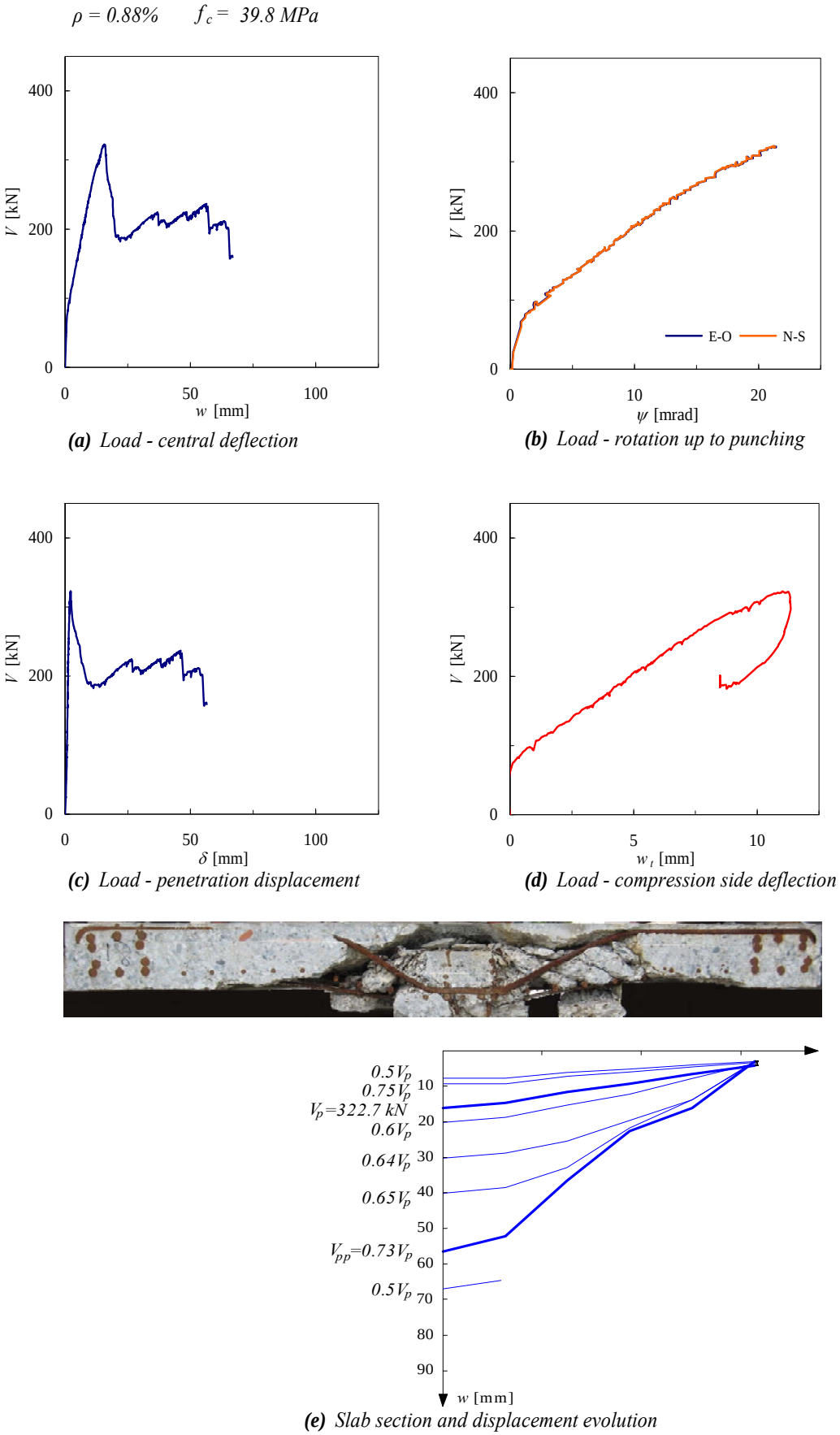

(a) *Load - central deflection*

(b) *Load - rotation up to punching*

(c) *Load - penetration displacement*

(d) *Load - compression side deflection*

(e) *Slab section and displacement evolution*

Figure A-4.14: Slab PM-18: fully anchored bent-up-bars Ø10

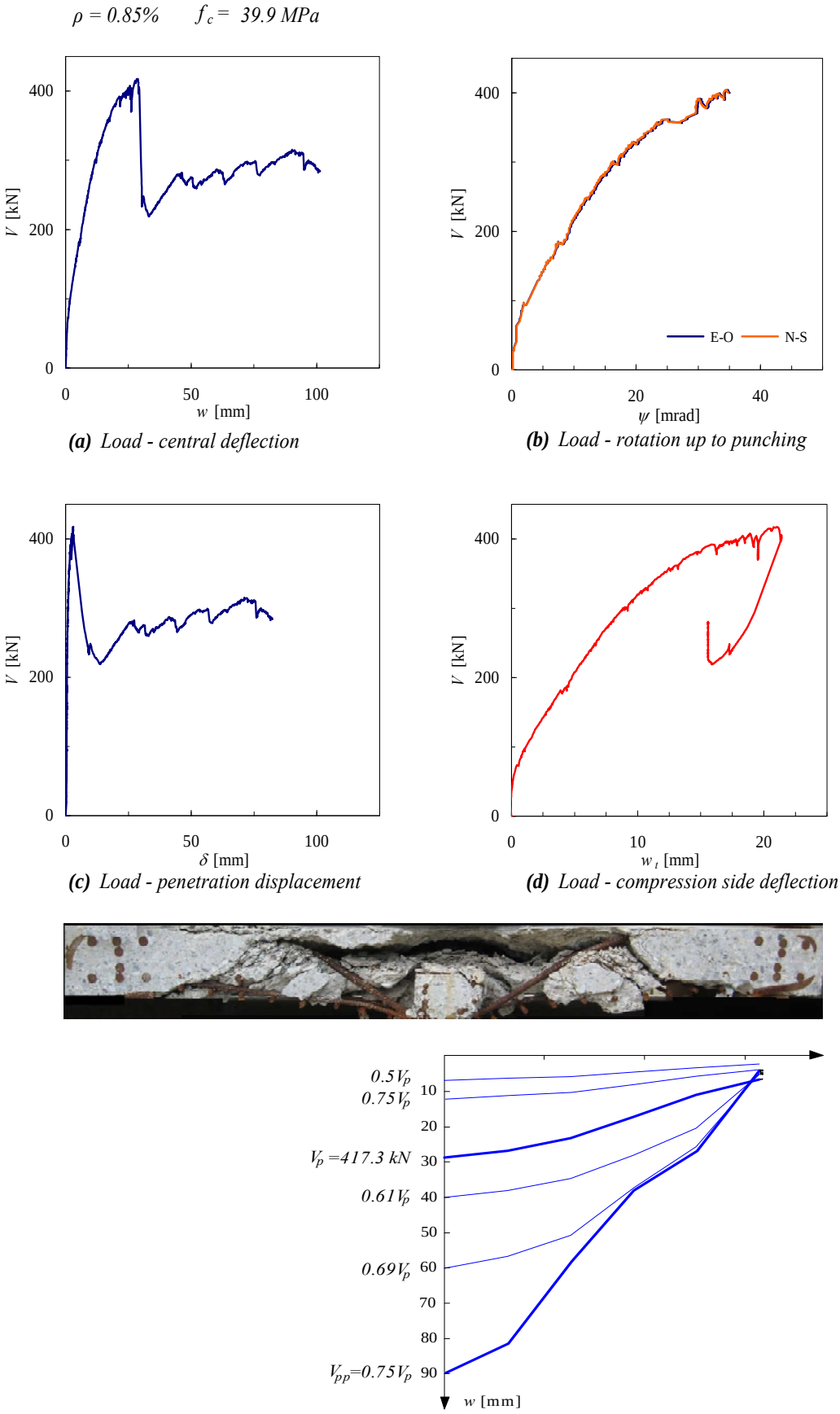

(a) *Load - central deflection*

(b) *Load - rotation up to punching*

(c) *Load - penetration displacement*

(d) *Load - compression side deflection*

(e) *Slab section and displacement evolution*

Figure A-4.15: Slab PM-19: fully anchored bent-up-bars Ø12

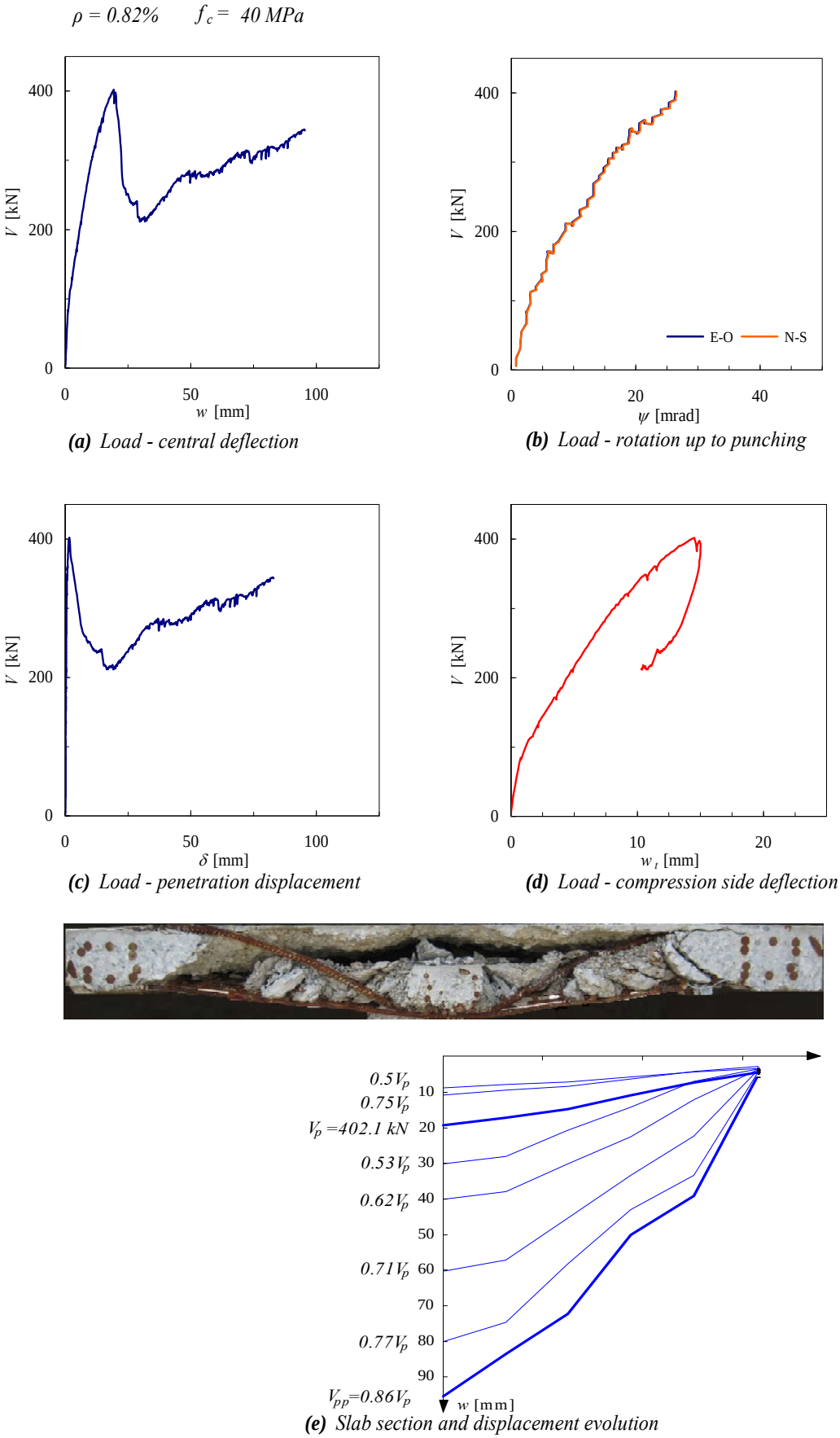

(a) *Load - central deflection*

(b) *Load - rotation up to punching*

(c) *Load - penetration displacement*

(d) *Load - compression side deflection*

(e) *Slab section and displacement evolution*

Figure A-4.16: Slab PM-20: fully anchored bent-up-bars Ø14

$\rho = 0.81\%$ $f_c = 40.2$ MPa

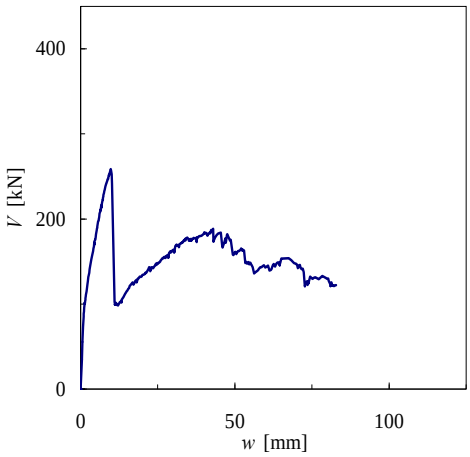

(a) *Load - central deflection*

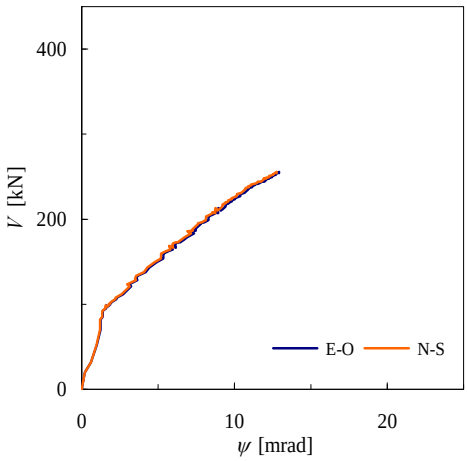

(b) *Load - rotation up to punching*

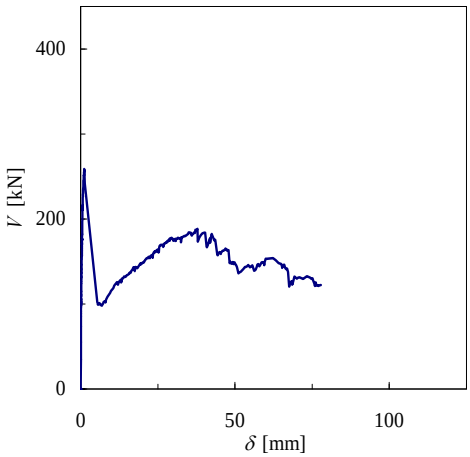

(c) *Load - penetration displacement*

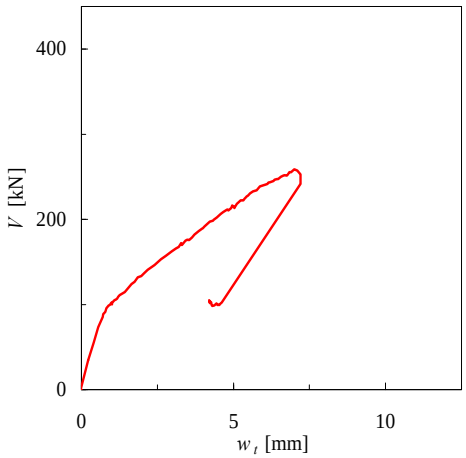

(d) *Load - compression side deflection*

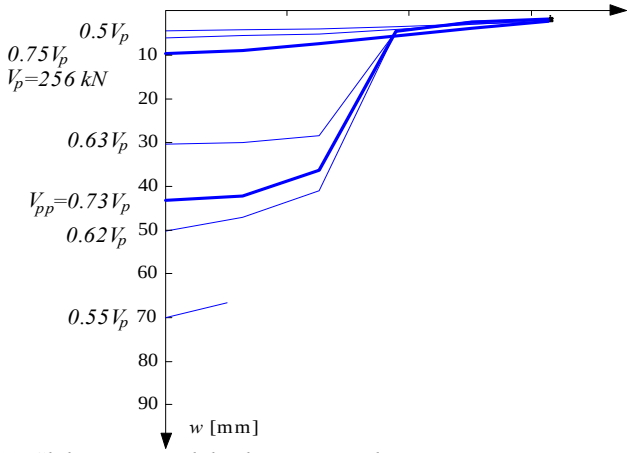

(e) *Slab section and displacement evolution*

Figure A-4.17: Slab PM-21: straight integrity reinforcement Ø8

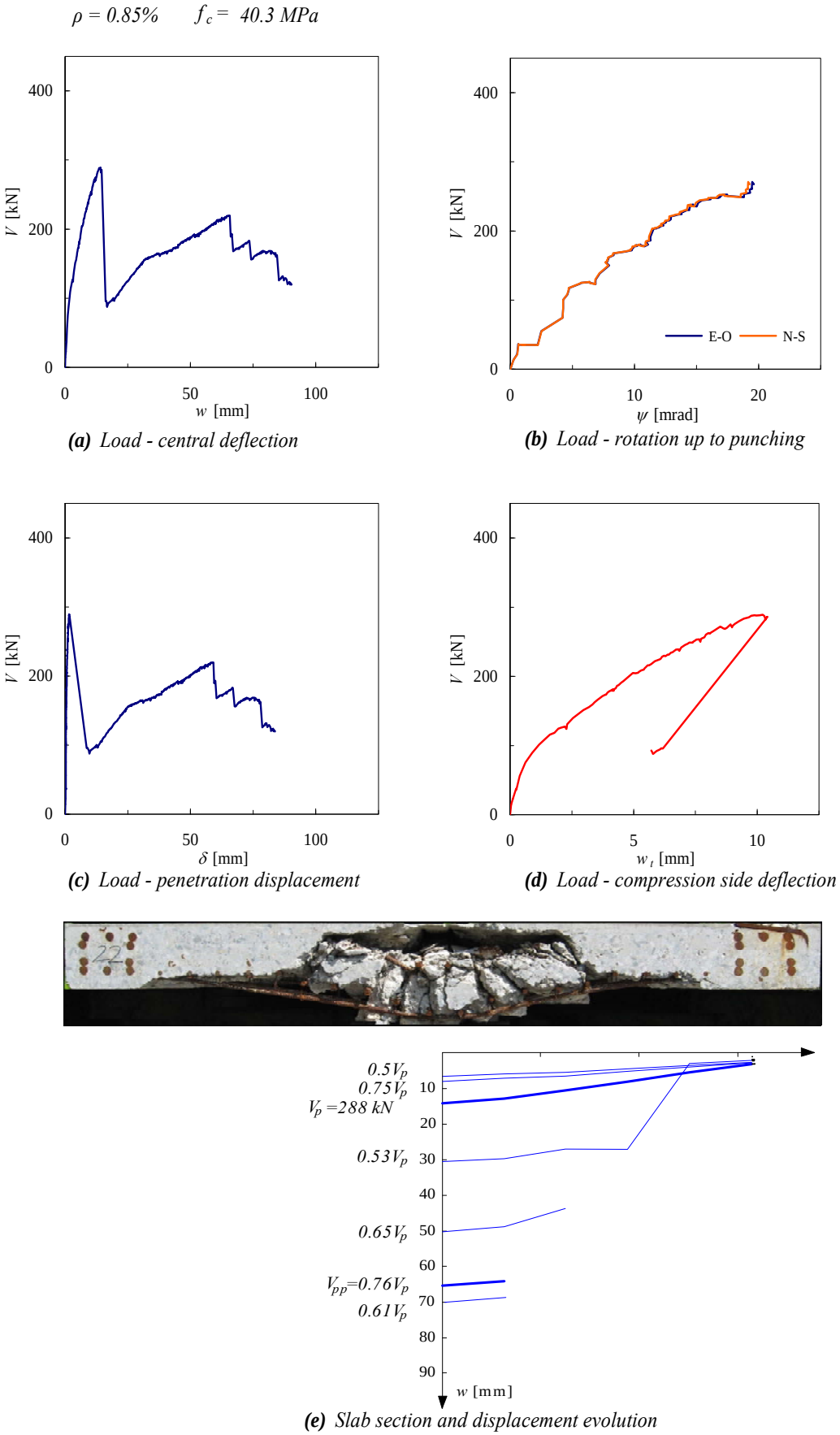

(a) *Load - central deflection*

(b) *Load - rotation up to punching*

(c) *Load - penetration displacement*

(d) *Load - compression side deflection*

(e) *Slab section and displacement evolution*

Figure A-4.18: Slab PM-22: straight integrity reinforcement Ø10, hot-rolled steel

$\rho = 0.88\%$ $f_c = 40.4$ MPa

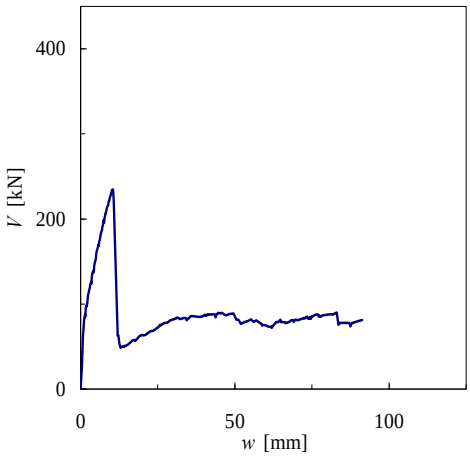

(a) *Load - central deflection*

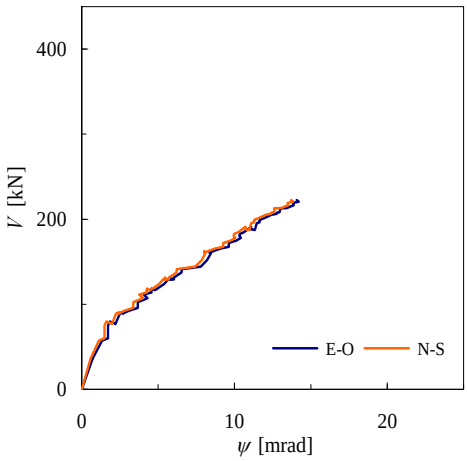

(b) *Load - rotation up to punching*

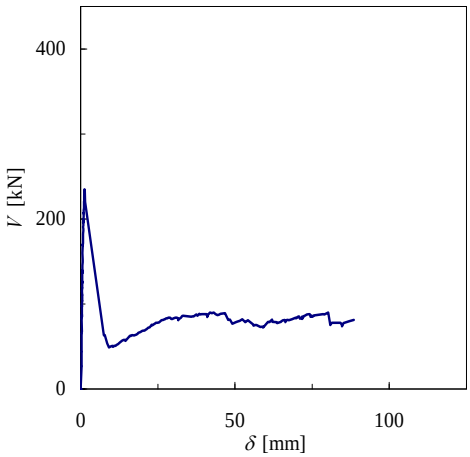

(c) *Load - penetration displacement*

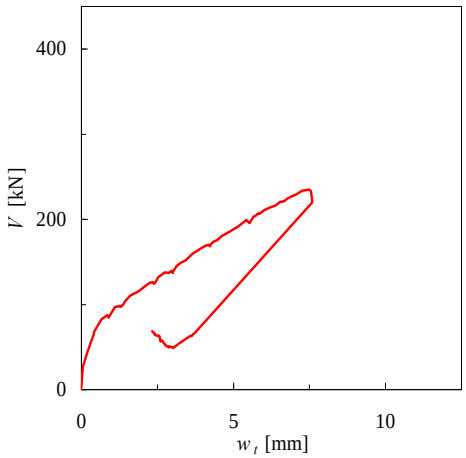

(d) *Load - compression side deflection*

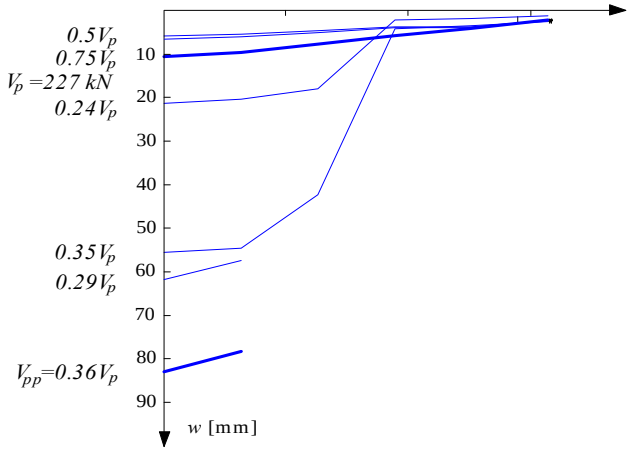

(e) *Slab section and displacement evolution*

Figure A-4.19: Slab PM-23, ρ = 0.88 %

$\rho = 0.86\%$ $f_c = 40.4$ MPa

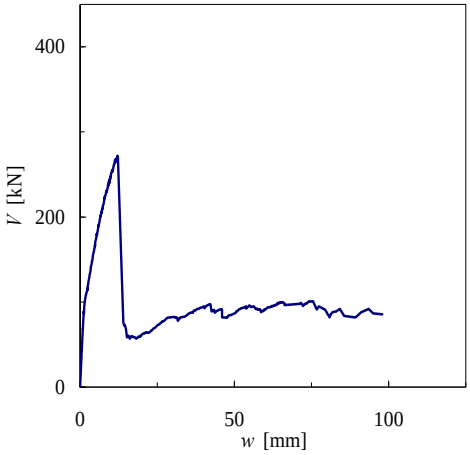

(a) *Load - central deflection*

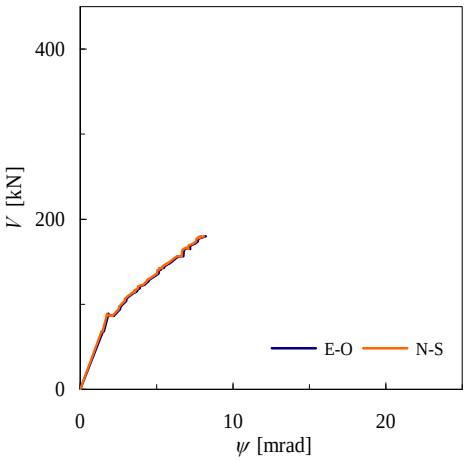

(b) *Load - rotation up to punching*

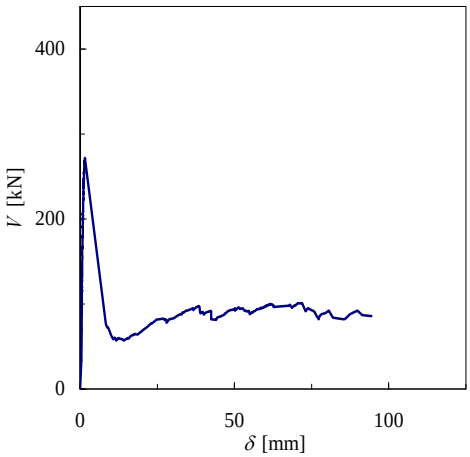

(c) *Load - penetration displacement*

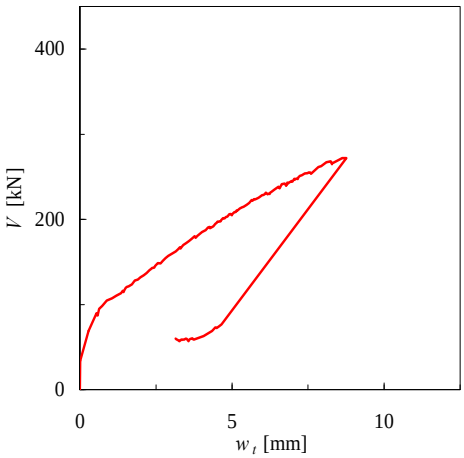

(d) *Load - compression side deflection*

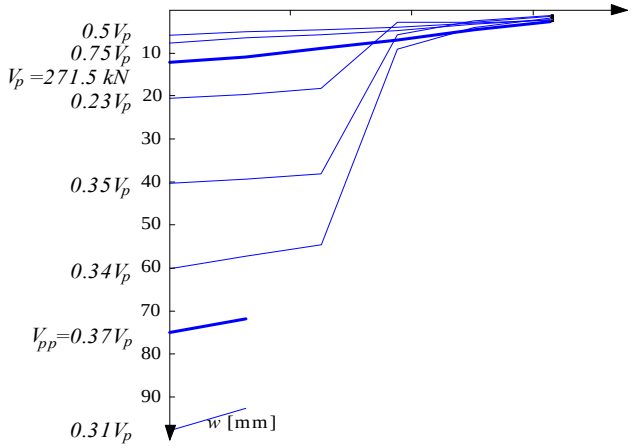

(e) *Slab section and displacement evolution*

Figure A-4.20: Slab PM-24, ρ = 0.85 %, confinement reinforcement

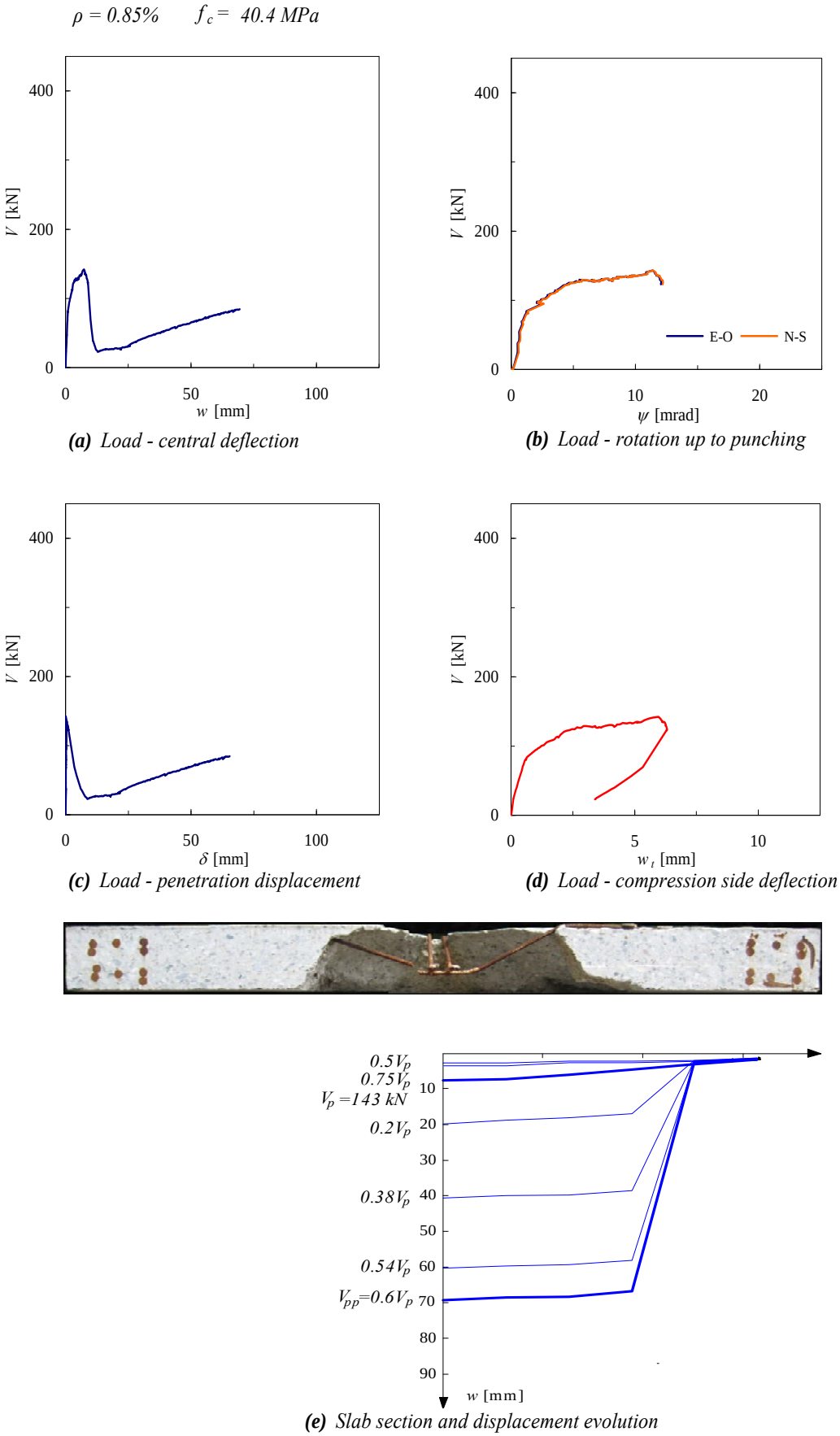

(a) *Load - central deflection*

(b) *Load - rotation up to punching*

(c) *Load - penetration displacement*

(d) *Load - compression side deflection*

(e) *Slab section and displacement evolution*

Figure A-4.21: Slab PM-25: cut-off tensile reinforcement + integrity reinforcement Ø8

$\rho = 0.83\%$ $f_c = 40.3$ MPa

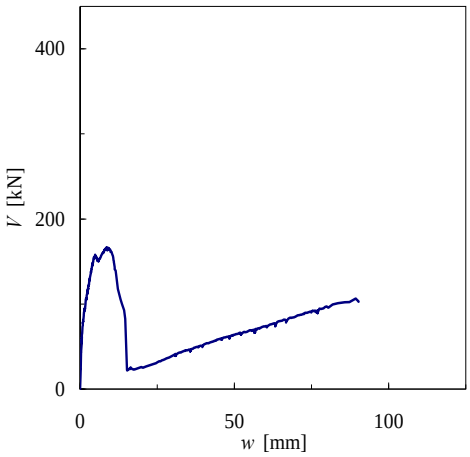

(a) *Load - central deflection*

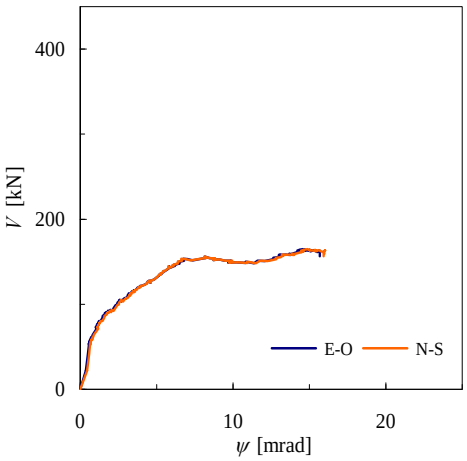

(b) *Load - rotation up to punching*

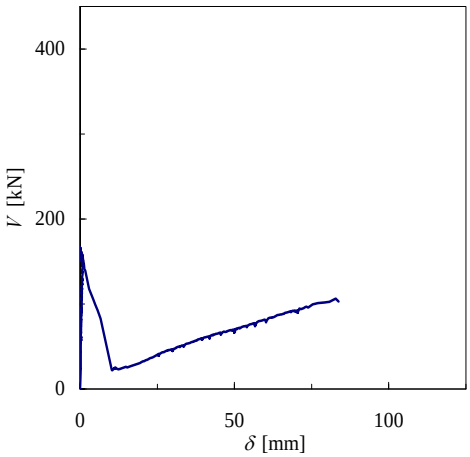

(c) *Load - penetration displacement*

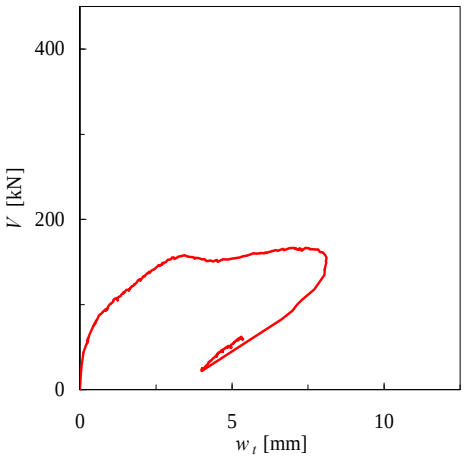

(d) *Load - compression side deflection*

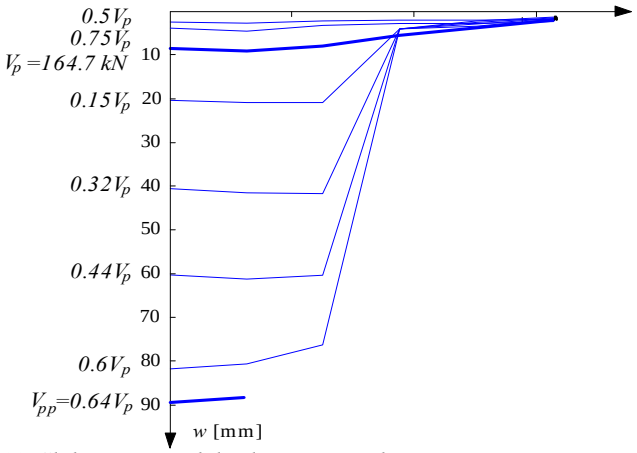

(e) *Slab section and displacement evolution*

Figure A-4.22: Slab PM-26: cut-off tensile reinforcement + integrity reinforcement Ø10

$\rho = 0.81\%$ $f_c = 40.3$ MPa

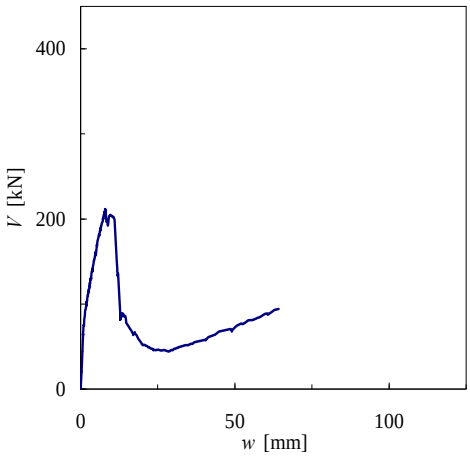

(a) *Load - central deflection*

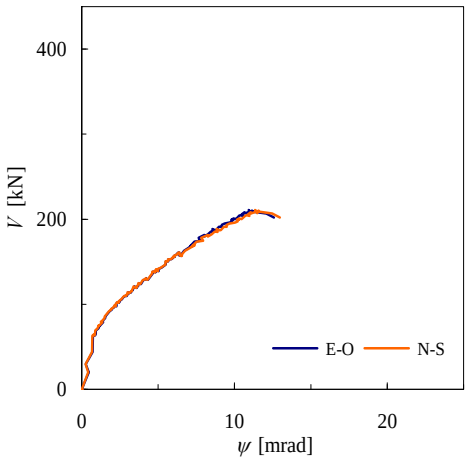

(b) *Load - rotation up to punching*

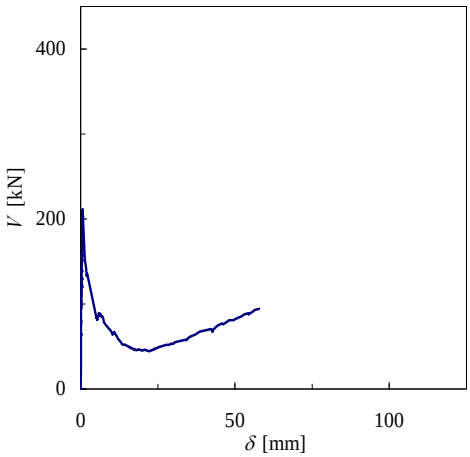

(c) *Load - penetration displacement*

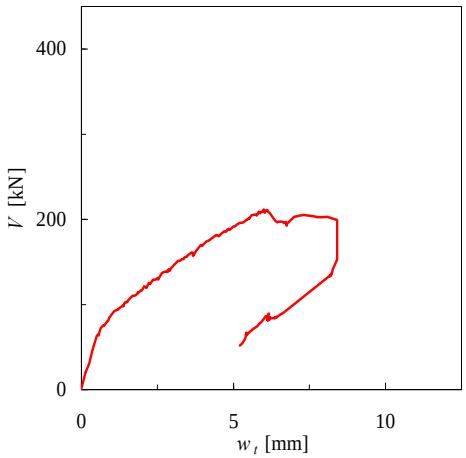

(d) *Load - compression side deflection*

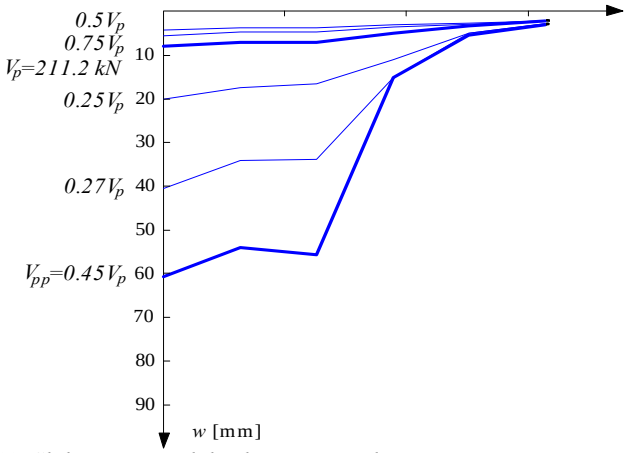

(e) *Slab section and displacement evolution*

Figure A-4.23: Slab PM-27: cut-off tensile reinforcement + integrity reinforcement Ø12

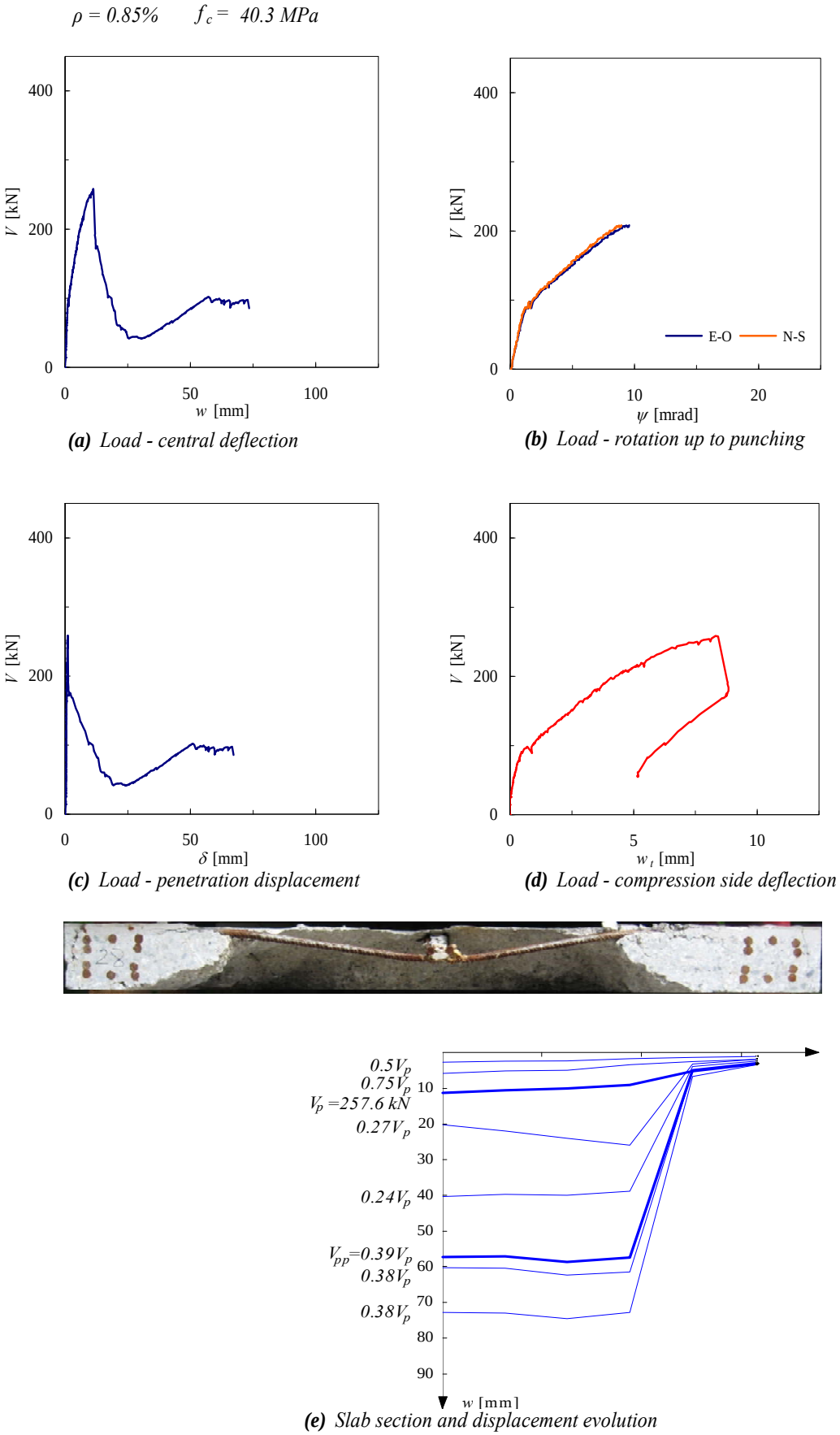

(a) *Load - central deflection*

(b) *Load - rotation up to punching*

(c) *Load - penetration displacement*

(d) *Load - compression side deflection*

(e) *Slab section and displacement evolution*

Figure A-4.24: Slab PM-28: cut-off tensile reinforcement + integrity reinforcement Ø14

A-5 Summary of experimental results

The test results are compared to gain a better understanding of the influence of various parameters on the post-punching behavior of flat slabs supported by columns. It was generally observed that after the punching shear strength has been reached, the load decreases rapidly. Then it starts increasing with further deflection in the post-punching phase. In all specimens, tensile reinforcement tends to tear out of concrete by a combination of bond failure and vertical tearing, especially in the vicinity of the column. At this stage, because of the large strains at the slab tension surface, cracks propagate through the slab and yielding of reinforcement spreads throughout the slab.

PM-1 to PM-4: Tensile reinforcement

Fig. A-5.1 shows the load-deflection responses of slabs PM-1 to PM-4, with the same geometry but different reinforcement ratios. As expected, the punching shear capacity increases as the reinforcement ratio increases. All specimens experienced punching shear failure and their post-punching behavior was observed. As Fig. A-5.1 shows, the punching strength of PM-3 is slightly higher than that of PM-4. This difference in their response can be explained by the fact that the concrete compressive strength at the time of testing was 39.5 MPa and 36.8 MPa for PM-3 and PM-4, respectively. It should also be mentioned that the punching shear strength of flat slabs is significantly influenced by the concrete compressive strength. However, in this case, slab PM-4 had a larger reinforcement ratio. In this series of test, the only connection between truncated punching cone and the rest of the slab after punching failure was the tensile reinforcement. This connection made it possible for slabs to carry load after punching failure. The ratio of the maximum post-punching strength to the maximum punching strength was 0.21, 0.30, 0.36 and 0.37 for slabs PM-1, PM-2, PM-3 and PM-4, respectively. The relative small post-punching strength of these specimens was due to the fact that the tensile reinforcement almost completely spalled of concrete. Fig. A-5.1 also shows the main results of these specimens.

It should be noted that all experiments, PM-1 to PM-28, were terminated when the main measurement equipments were no longer able to record meaningful values due to the destruction of the punching cone.

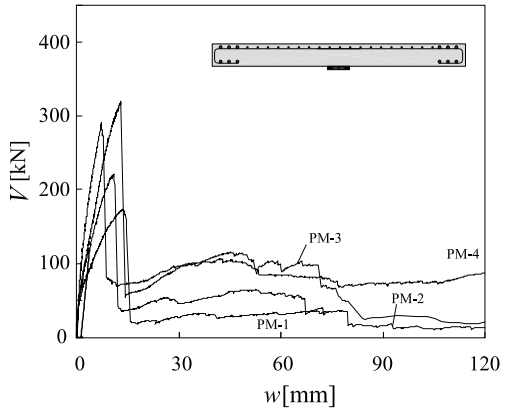

Test	f_c [MPa]	ρ [%]	A_{sb}	V_p [kN]	w_p [mm]	V_{pp} [kN]
PM-1	36.6	0.82	-	175.8	13.6	37.2
PM-2	36.5	0.82	-	223.7	11.0	66.0
PM-3	37.8	0.82	-	324.3	13.1	117.4
PM-4	36.8	0.82	-	295.2	7.4	107.8

Figure A-5.1: Load–deflection curve and main results for slabs PM-1 to PM-4

PM-9 to PM-12: Integrity reinforcement

Fig. A-5.2 shows the load versus the central deflection for slabs PM-9 to PM-12. Ø8, Ø10, Ø12 and Ø14 straight bar were used in the compression zone of these slabs. In this test series, the post-punching behavior was influenced not only by the tensile reinforcement but also by the integrity reinforcement. As load increases, cracks open, and interlocking of aggregate reduces quickly. Therefore, in the absence of shear reinforcement, longitudinal reinforcing bars play a significant role in transferring shear when other contributions to the shear transfer are negligible as in the case of post-punching behavior of flat slabs. It can be observed that in these tests where the integrity reinforcing bars pass through the column, the post-punching load were clearly larger than that observed in the specimens without integrity reinforcement. The ratio of the maximum post-punching strength to the maximum punching strength was 0.55, 0.70, 0.98 and 0.98 for slabs PM-9, PM-10, PM-11 and PM-12, respectively. Although the punching strength was approximately the same for all specimens in this test series, there was a considerable difference in the post critical behavior of the first two specimens (PM-9 and PM-10), and the last two (PM-11 and PM-12). This can be attributed to the type of steel reinforcement. Cold-worked steel was used for the former slabs, whereas hot rolled steel was used for the latter slabs. The sudden drops in the graphs are caused by the fracture of the steel bars.

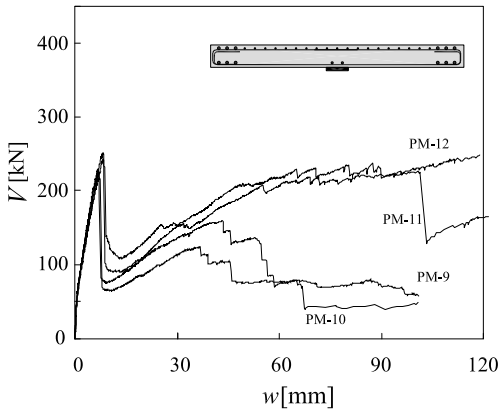

Test	f_c [MPa]	ρ [%]	A_{sb}	V_p [kN]	w_p [mm]	V_{pp} [kN]
PM-9	31.0	0.82	4Ø8*	224	7.1	123
PM-10	31.1	0.82	4Ø10*	227	6.7	159
PM-11	32.3	0.82	4Ø12**	241	8.2	236
PM-12	32.4	0.82	4Ø14**	249	8.2	245

* cold–worked steel
** hot–rolled steel

Figure A-5.2: Load–deflection curve and main results for slabs PM-9 to PM-12

PM-13 to PM-16: Bent-up-bars, insufficient anchorage

Fig. A-5.4 shows the load-deflection responses of slabs PM-13 to PM-16, each having the same geometry and tensile reinforcement but a different bent-up-bar diameter. All specimens experienced punching shear failure. As can be seen in Fig. A-5.4, these test specimens have the same initial stiffness but their punching strengths are slightly different. As it pointed out earlier, the punching shear strength of flat slabs is significantly influenced by the concrete compressive strength. According to Table 2.5 the concrete compressive strength of slabs PM-13, PM-14, PM-15 and PM-16 ranged from 30 to 34.5 MPa. This may partially explain the different punching strengths of these specimens. The ratio of the maximum post-punching strength to the maximum punching strength was 0.46, 0.53, 0.64 and 0.45 for slabs PM-13, PM-14, PM-15 and PM-16, respectively. The relative small post-punching strength of these specimens was due to the fact that the bent-up bars were not properly anchored as can occur in existing structures. According to the Swiss code SIA 262 the minimal anchorage length in the tension zone equals to forty times the bar diameter for the concrete type of C30/37 which is about 480 and 560 mm for Ø12 and Ø14, respectively. Fig. A-5.3 shows the anchorage condition for the various integrity reinforcement as well as the possible cracking before punching failure. There is no concern for integrity reinforcement crossing the column as well as for full-anchored bent-up bars (Fig. A-5.3 a and c). However, with the increase of the load and opening the punching cracks in the absence of the hook (Fig. A-5.3 b), the bent-up bars experienced the bond failure thus losing their effectiveness. This can be attributed to the short anchorage length of 455 mm in combination with premature punching cracks along the bar.

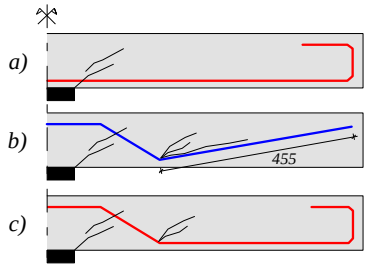

Figure A-5.3: Anchorage condition for the various integrity reinforcement

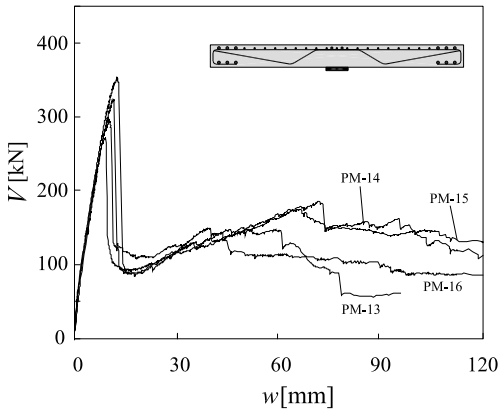

Test	f_c [MPa]	ρ [%]	A_{sb}	V_p [kN]	w_p [mm]	V_{pp} [kN]
PM-13	32.6	0.82	4Ø8	327	11.4	151
PM-14	32.7	0.82	4Ø10	356	12.6	187
PM-15	32.7	0.84	4Ø12	274	9.1	177
PM-16	32.8	0.83	4Ø14	298	10.1	135

Figure A-5.4: Load–deflection curve and main results for slabs PM-13 to PM-16

PM-17 to PM-20: Well-anchored bent-up-bars

Fig. A-5.5 shows the load-deflection responses for slabs PM-17 to PM-20. The bent-up bars which function as shear reinforcement were fully anchored. These specimens exhibited an improved punching behavior and larger post-punching strength. Detachment of the top reinforcement was observed. Compared to the other specimens, PM-19 and PM-20 exhibited a different behavior prior to the punching failure. The punching strength showed an increase of 28% and 23% to the respective experimental punching load for PM-19 and PM-20, respectively. They also experienced a very large deflection at punching failure showing a much more ductile behavior than the other specimens. The slab deflection at punching shear failure was 28.7 mm and 19.3 mm for PM-19 and PM-20, respectively.

The maximum loads obtained in the post-punching phase were clearly larger than those obtained in the slabs with integrity reinforcement passing through the column. The ratio of the maximum post-punching strength to the maximum punching strength was 0.75, 0.73, 0.75 and 0.86 for slabs PM-17, PM-18, PM-19 and PM-20, respectively. Although the ratio of the maximum post-punching strength to the punching shear strength for these two specimens were lower than those in slabs PM-11 and PM-12, the maximum post-punching load of PM-19 and PM-20 were 33% and 41% higher than those of slabs PM-11 and PM-12, respectively. These specimens showed that using bent-up bars passing through the column is probably more effective than integrity reinforcing bars in preventing the progressive collapse.

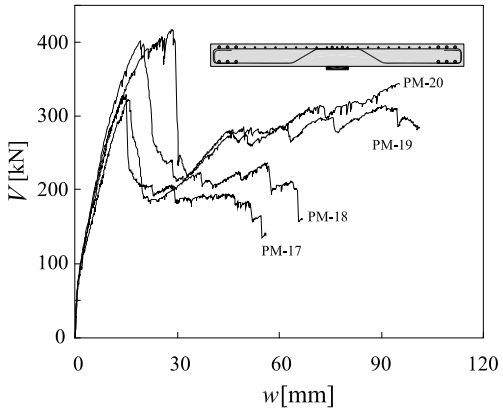

Test	f_c [MPa]	ρ [%]	A_{sb}	V_p [kN]	w_p [mm]	V_{pp} [kN]
PM-17	39.7	0.82	4Ø8	329	15.1	247
PM-18	39.8	0.88	4Ø10	323	15.7	237
PM-19	39.9	0.85	4Ø12	417	28.7	315*
PM-20	40.0	0.82	4Ø14	402	19.3	345*

* Test terminated because the main measurement equipments were no longer able to record meaningful values

Figure A-5.5: Load–deflection curve and main results for slabs PM-17 to PM-20

PM-21 and PM-22: Ductility

Fig. A-5.6 shows the load-deflection responses of slabs PM-21, PM-22. These test specimens were similar to PM-9 and PM-10 respectively, however PM-22 had a different steel type. Cold-worked steel had been used for PM-10 and hot-rolled steel was used for the slab specimen PM-22. The aim was to investigate the effect of the type and ductility of steel on the post-punching behavior. Using hot-rolled steel bars provided a better post-punching behavior and increased not only the punching strength but also the maximum post-punching strength and its corresponding displacement. The ratio of the maximum post-punching load to the maximum punching strength was 0.73 and 0.76 for slabs PM-21 and PM-22, respectively. The concrete compressive strength

for PM-9 and PM-10 was about 31 MPa and for PM-21 and PM-22 was about 40 MPa and thus the punching strength as well as the post-punching strength were influenced by the effect of the concrete compressive strength (up to 15%).

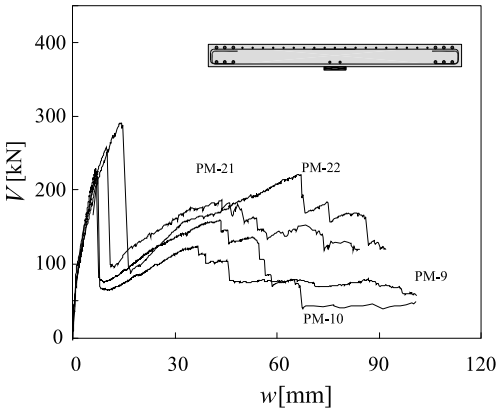

Test	f_c [MPa]	f_{sv} [MPa]	ρ [%]	A_{sb}	V_p [kN]	w_p [mm]	V_{pp} [kN]
PM-9	31.0	616*	0.82	4Ø8	224	7.1	123
PM-10	31.1	560*	0.82	4Ø10	227	6.7	159
PM-21	40.2	625*	0.81	4Ø8	256	9.7	185
PM-22	40.3	605**	0.85	4Ø10	288	14.1	219

* cold–worked steel
** hot–rolled steel

Figure A-5.6: Load–deflection curve and main results for slabs PM-21, PM-22, PM-9, and PM-10

PM-23 and PM-24: Confinement

Fig. A-5.7 shows the load versus the central deflection for slabs PM-23 and PM-24. These specimens were geometrically similar and hence the punching and the post-punching behavior of them were nearly the same. No additional reinforcement was used and thus tensile reinforcement was the only factor influencing the post-punching response. The ratio of the maximum post-punching strength to the maximum punching strength was 0.36 and 0.37 for slabs PM-23 and PM-24, respectively. Slab PM-23 was the reference slab and thus only tensile reinforcement was used, whereas for slab PM-24 some stirrups were also placed above the column to investigate the effect of confinement reinforcement on the punching and post-punching behavior. As Fig. A-5.7 shows, using confinement reinforcement above the column slightly increased the punching strength as well as the post-punching strength.

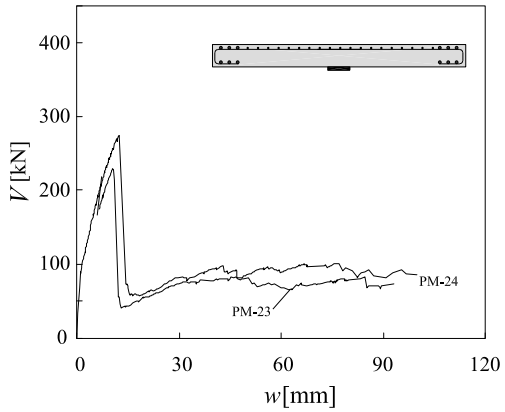

Test	f_c [MPa]	ρ [%]	A_{sb}	V_p [kN]	w_p [mm]	V_{pp} [kN]
PM-23	40.4	0.81	-	227	10.4	82
PM-24	40.4	0.85	-	272	12.1	101

Figure A-5.7: Load–deflection curve and main results for slabs PM-23 and PM-24

PM-25 to PM-28: Cut-off tensile reinforcement

Fig. A-5.8 shows the load-deflection responses for slabs PM-25 to PM-28. In this test series, tensile reinforcing bars were cut off at the specified points, to specifically investigate the effect of the integrity reinforcement on the post-punching behavior. Cutting-off the tensile reinforcing bars localized the punching cracks at the end of the bars and as a result, the tensile reinforcing bars were not activated after punching failure. Therefore, the only factor affecting the post-punching response was the integrity reinforcement. The ratio of the maximum post-punching strength to the maximum punching strength was 0.60, 0.64, 0.45 and 0.39 for slabs PM-25, PM-26, PM-27 and PM-28, respectively. It was observed that using improper anchored tensile reinforcement (cut-off of tensile reinforcement) significantly reduced the punching strength, the post-punching strength and also the ductility of the slab-column connection. These specimens provided the opportunity of studying the effect of integrity reinforcement passing through the column. However, due to the fact that the only connection between the punching cone and the rest of slab was a small portion of the integrity reinforcing bars over the column, the risk of falling down the punching cone and other technical problems the tests were stopped before the specimens reached to their maximum post-punching strength. In addition, the punching cone was completely separated of the slab at the end of these experiments.

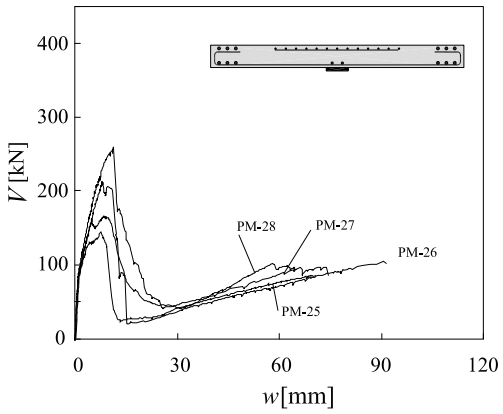

Test	f_c [MPa]	f_{sy} [MPa]	ρ [%]	A_{sb}	V_p [kN]	w_p [mm]	V_{pp} [kN]
PM-25	40.4	625	0.85	4Ø8	143	7.7	85
PM-26	40.3	605	0.83	4Ø10	165	8.5	105
PM-27	40.3	559	0.81	4Ø12	211	8	94
PM-28	40.3	578	0.85	4Ø14	258	11.2	101

Figure A-5.8: Load–deflection curve and main results for slabs PM-25 to PM-28

A-6 Post-punching provision in SIA 262

The design of reinforced concrete flat slabs is governed by punching shear strength at ultimate limit state and by deflection at serviceability limit state. Numerous experiments have been performed in the past to gain a better understanding of the punching behavior of flat slabs. However, the current codes of practice deal with this context differently and therefore the calculation of the punching or post-punching strength and the relevant detailing of reinforcement depend considerably on the code applied. Therefore, the reinforcement layout might be very different in different countries.

Experience has shown that the overall integrity of a structure can be significantly enhanced by minor changes in reinforcement detailing. The tendency of the codes of practice is to increase the redundancy and ductility in structures so that in the event of damage to a major supporting element or an abnormal loading event, the resulting damage may be confined to a relatively small area. Therefore the structure will have a better chance to maintain overall stability. Redistribution of loads following a local damage to a structure depends on strength, continuity, redundancy, and deformation and energy dissipation capacities of the structure; however, in the case of punching failure, the drop in resistance can be large and can thus trigger failure at adjacent columns and lead to the progressive collapse of a large part of the structure. Alternate load path and integrity provisions are means of providing redundancy or continuity to mitigate possible progressive collapse. When punching failure occurs, top reinforcement that is continuous over the support, but not confined by stirrups in the case of flat slabs without shear reinforcement, will tend to tear out of concrete and will not provide the catenary action needed to connect the damaged parts of structure. By making a portion of compressive reinforcement continuous, the overall stability could be obtained and the likelihood of that a local punching failure could lead to progressive collapse is reduced.

To prevent the slab from totally collapsing after a possible punching, the Swiss Code SIA 262-03 [1] requires that some reinforcement shall be provided on the flexural compression side. The reinforcement shall be extended over the supported area and dimensioned as follows:

$$V_d = A_{sb} \cdot f_{sd} \cdot \sin\psi \tag{A-6.1}$$

Assuming $\psi = 42°$ leads to:

$$A_{sb} > 1.5 \frac{V_d}{f_{sd}} \tag{A-6.2}$$

Where A_{sb} is the total cross-sectional area of the reinforcing bars crossing the column core, f_{sd} is the design yield strength of the reinforcing steel, V_d is the dimensioning value of the shear transferred to the column at accidental situation, and ψ is the angle of inclination of reinforcing bars in the vicinity of the punching crack at failure.

A-7 References

1. SIA, *SIA 262:2003, Construction en béton*, Société Suisse des Ingénieurs et des Architectes, Norme suisse SN 505 262, Switzerland, French, 2003.

2 . MUTTONI A., FERNÁNDEZ RUIZ M., *Shear strength of members without transverse reinforcement as function of critical shear crack width*, ACI Structural Journal, V. 105, No 2, pp. 163-172, Farmington Hills, USA, 2008.

3 . MUTTONI A., *Punching shear strength of reinforced concrete slabs without transverse reinforcement*, ACI Structural Journal, V. 105, N° 4, pp. 440-450, USA, 2008.

4 . MUTTONI A., GUANDALINI S., FERNÁNDEZ RUIZ M., *Comportement mécanique des dalles et planchers-dalles en béton armé*, Documentation SIA, D 0226 : Sécurité structurale des parkings couverts, pp. 13-28, Zürich, Switzerland, French, 2008.

5 . MUTTONI A., FERNÁNDEZ RUIZ M., *Shear strength in one- and two-way slabs according to the critical shear crack theory,* fib Symposium, Amsterdam 2008, Amsterdam, Netherlands, 2008.

6. BROMS C. E., *Elimination of Flat Plate Punching Failure Mode*, ACI Structural Journal, V. 97, No. 1, p. 94 - 101, 2000.

7. CSA STANDARD A23.3-04, *Canadian Standard Association*, 232 p, 2004.

8. ACI, Building Code Requirements for Structural Concrete, ACI American Concrete Institute, ACI 318-05, 430 p., USA, 2005.

9. ACI 352.1R-89, Recommendations for Design of Slab-Column Connections in Monolithic Reinforced Concrete (Reapproved 1997), ACI American Concrete Institute, 22 p., USA, 1997.

10. DIN, *DIN 1045-1 Tragwerke aus Beton und Stahlbeton*, DIN 1045-1, Deutsches Institut für Normung, 2nd Edition, 148 p., Berlin, Germany, German, 2005.

11. EUROCODE , *Eurocode 2: Design of concrete structures - Part 1-1: General rules and rules for buildings*, European Committee for Standardization (CEN), Brussels, 2004.

12. BS 8110-97, Structural use of concrete: Part 1: Code of practice for design and construction, British Standard Institute, London, p.117.

13. VAZ RODRIGUES R., *Shear Strength of Reinforced Concrete Bridge Deck Slabs*, EPFL, PhD thesis, n° 3739, 289 p., Lausanne, Switzerland, 2007.

14. CEB, CEB-FIP Model Code 1990, *Bulletin d'information No. 213/214*, may, 1993.

Appendix B

Estimation of the projected area A_{ch}

When the thickness of the concrete over the integrity bars are not sufficient for the failure mode associate with the fracture of the bars, the post-punching strength of the slab is limited by the maximum concrete breakout strength:

$$V_{con,max} = A_{ch} f_{ct,eff} \tag{B.1}$$

where A_{ch} is the horizontal projection of the conical failure surface . It was shown in Chapter 4 that for two integrity bars passing through the column, the total projected area can be expressed as

$$\begin{aligned} A_{ch} &= 8\left(\frac{\pi}{2} d_1^2 - A_1\right) \\ A_1 &= \frac{\theta_j}{2} d_1^2 - \frac{s}{4} d_1 \sin\theta_j \\ \theta_j &= \cos^{-1}(s / 2d_1) \end{aligned} \tag{B.2}$$

where the parameters involved are shown in Fig. B.1.

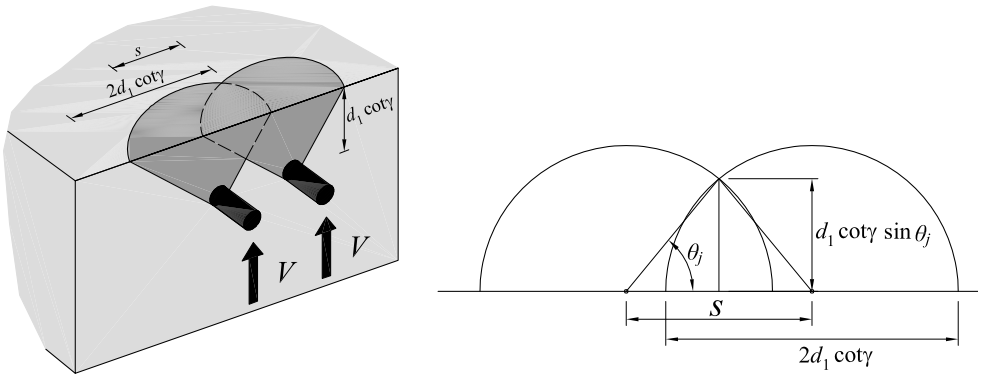

Figure B.1: Horizontal projection of the conical failure surface for two reinforcing bars

If more than two integrity reinforcing g bars pass through the column, the projected area for each bar can be calculated by the geometrical conditions. Fig. B.2 shows the horizontal projected area in the case of three or four reinforcing bars passing through the column. When three integrity bars pass through the column in each direction, the total horizontal area associated to the maximum concrete breakout can be calculated by

$$A_{ch} = \frac{3}{2}\pi d_1^2 - 2d_1^2\theta_j + sd_1 \sin\theta_j \tag{B.3}$$

As the number of bars passing through the columns increases, the total horizontal projected area increases systematically. The projected area for each reinforcing bar can be estimated as

$$\begin{cases} \frac{1}{2}d_1^2(\pi-\theta_j)+\frac{1}{4}sd_1\sin\theta_j & \text{external bars} \\ \frac{1}{2}d_1^2(\pi-2\theta_j)+\frac{1}{2}sd_1\sin\theta_j & \text{internal bars} \end{cases} \tag{B.4}$$

Therefore, the total projected area when n integrity bars pass through the column in each direction is

$$A_{ch}=4\{[\theta_j+\frac{n}{2}(\pi-2\theta_j)]d_1^2+\frac{n-1}{2}sd_1\sin\theta_j\} \tag{B.5}$$

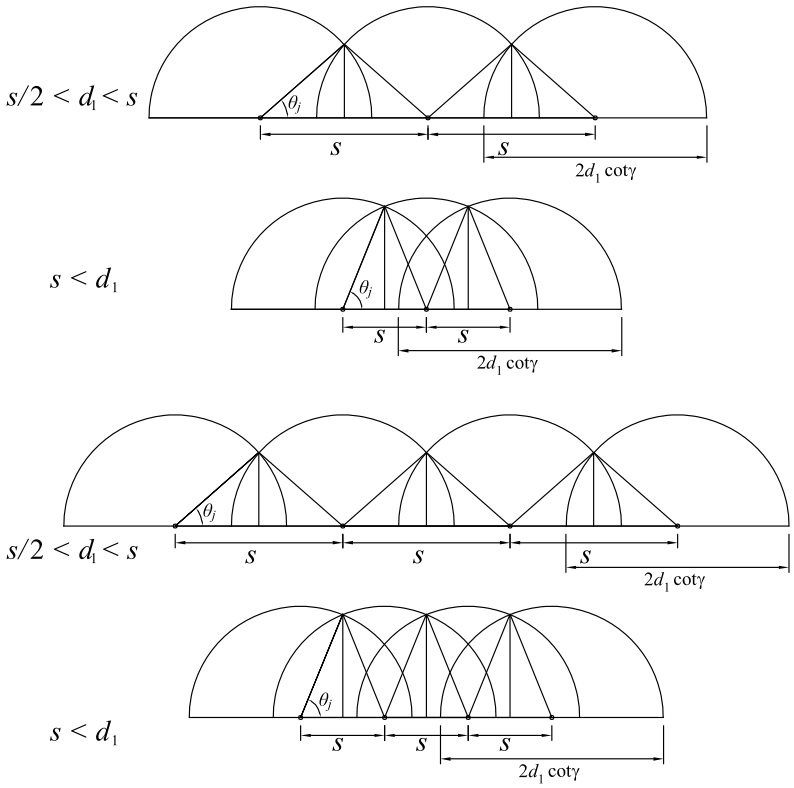

Figure B.2: Horizontal projection of the conical failure surface for three and four reinforcing bars passing through the column

Appendix C

Summary of experimental results

	Test	age	f_c	f_{ct}	E_c	d	ρ	Tensile reinf. f_{sy}	Tensile reinf. f_{su}	Tensile reinf. ε_{su}	Tensile reinf. E_s	A_{sb}	Integrity reinf. f_{sy}	Integrity reinf. f_{su}	Integrity reinf. ε_{su}	Integrity reinf. E_s	V_p	w_p	V_{pp}	w_{pp}	$\frac{V_{pp}}{V_p}$	Reinforcement layout	A_s	A_{sb}	Test
		[day]	[MPa]	[MPa]	[GPa]	[mm]	[%]	[MPa]	[MPa]	[%]	[GPa]		[MPa]	[MPa]	[%]	[GPa]	[kN]	[mm]	[kN]	[mm]					
Series 1	PM-1	33	36.6	2.9	36.9	102	0.25	601	664	7.4	201	-	-	-	-	-	176	13.6	37	70.5	0.21	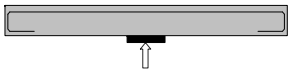	Ø8@200	-	PM-1
	PM-2	30	36.5	2.8	36.7	102	0.49	601	664	7.4	201	-	-	-	-	-	224	11.0	66	52.7	0.30		Ø8@100	-	PM-2
	PM-3	71	37.8	3.4	37.9	102	0.82	601	664	7.4	201	-	-	-	-	-	324	13.1	117	45.3	0.36		Ø8@60	-	PM-3
	PM-4	38	36.8	3.0	37.1	102	1.41	601	664	7.4	201	-	-	-	-	-	295	7.4	108	42.6	0.37		Ø8@35	-	PM-4
Series 2	PM-9	35	31.0	2.3	33.3	102	0.82	601	664	7.4	201	4Ø8	616	680	7.4	202	224	7.1	123	36.2	0.55	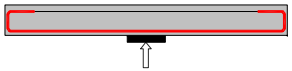	Ø8@60	4Ø8	PM-9
	PM-10	37	31.1	2.3	33.3	102	0.82	601	664	7.4	201	4Ø10	560	599	7.9	195	228	6.7	159	42.9	0.70		Ø8@60	4Ø10	PM-10
	PM-11	56	32.3	2.5	33.7	102	0.82	601	664	7.4	201	4Ø12	548	625	10.5	201	241	8.2	237	86.3	0.98		Ø8@60	4Ø12	PM-11
	PM-12	58	32.4	2.6	33.7	102	0.82	601	664	7.4	201	4Ø14	527	629	13.5	199	249	8.2	245	116.9	0.98		Ø8@60	4Ø14	PM-12
	PM-13*	62	32.6	2.6	33.8	102	0.82	601	664	7.4	201	4Ø8	616	680	7.4	202	327	11.4	151	39.9	0.46	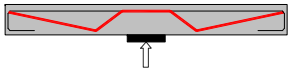	Ø8@60	4Ø8	PM-13
	PM-14*	64	32.7	2.6	33.8	102	0.82	601	664	7.4	201	4Ø10	560	599	7.9	195	356	12.6	188	71.7	0.53		Ø8@60	4Ø10	PM-14
	PM-15*	65	32.7	2.6	33.8	100	0.84	601	664	7.4	201	4Ø12	548	625	10.5	201	274	9.1	177	66.5	0.64		Ø8@60	4Ø12	PM-15
	PM-16*	68	32.8	2.6	33.9	101	0.83	601	664	7.4	201	4Ø14	527	629	13.5	199	298	10.1	135	43.4	0.45		Ø8@60	4Ø14	PM-16
Series 3	PM-17	35	39.7	2.8	28.7	102	0.82	625	641	6.1	200	4Ø8	625	641	6.1	200	329	15.1	204	50.0	0.75	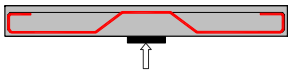	Ø8@60	4Ø8	PM-17
	PM-18	36	39.8	2.8	28.8	95	0.88	625	641	6.1	200	4Ø10	605	658	7.8	194	323	15.7	237	56.5	0.73		Ø8@60	4Ø10	PM-18
	PM-19	37	39.9	2.8	28.8	99	0.85	625	641	6.1	200	4Ø12	559	618	7.9	197	417	28.7	315	90.1	0.75		Ø8@60	4Ø12	PM-19
	PM-20	39	40.0	2.9	29.0	102	0.82	625	641	6.1	200	4Ø14	578	695	12.0	203	402	19.3	345	95.2	0.86		Ø8@60	4Ø14	PM-20
	PM-21	43	40.2	2.9	29.3	103	0.81	625	641	6.1	200	4Ø8	625	641	8.9	200	256	9.7	185	42.9	0.73	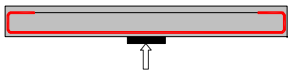	Ø8@60	4Ø8	PM-21
	PM-22	46	40.3	2.9	29.5	99	0.85	625	641	6.1	200	4Ø10	605	658	10.3	194	288	14.1	219	65.2	0.76		Ø8@60	4Ø10	PM-22
	PM-23	50	40.4	2.9	29.7	95	0.88	625	641	6.1	200	-	-	-	-	-	227	10.4	82	83.0	0.36		Ø8@60	-	PM-23
	PM-24	53	40.4	3.0	29.9	97	0.86	625	641	6.1	200	-	-	-	-	-	272	12.1	101	74.2	0.37		Ø8@60	-	PM-24
	PM-25$^+$	56	40.4	3.0	30.1	98	0.85	625	641	6.1	200	4Ø8	625	641	6.1	200	143	7.7	85	69.8	0.60	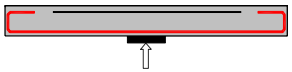	Ø8@60	4Ø8	PM-25
	PM-26$^+$	57	40.3	3.0	30.1	101	0.83	625	641	6.1	200	4Ø10	605	658	7.8	194	165	8.5	105	89.3	0.64		Ø8@60	4Ø10	PM-26
	PM-27$^+$	58	40.3	3.0	30.2	104	0.81	625	641	6.1	200	4Ø12	559	618	7.9	197	211	8.0	94	64.1	0.45		Ø8@60	4Ø12	PM-27
	PM-28$^+$	60	40.3	3.0	30.3	99	0.85	625	641	6.1	200	4Ø14	578	695	12.0	203	258	11.2	101	57.2	0.39		Ø8@60	4Ø14	PM-28

+ : Test deliberately terminated due to the risk of falling down the punching cone
* : Anchorage failure

Yaser Mirzaei

Address: Av. d'Echallens 63, 1004 Lausanne, Switzerland
Tel: +41 78 841 8823
Email: yaser.mirzaei@epfl.ch

Education

10/2005-03/2010 **Ecole Polytechnique Fédérale de Lausanne (EPFL), Lausanne, Switzerland**
- Ph.D. candidate in Structural Concrete Laboratory (IBETON)
- Thesis title: "Post-punching behavior of concrete flat slabs"

10/2002-03/2005 **Sharif University of Technology, Tehran, Iran**
- Master of Science in Earthquake Engineering, GPA: 17.22 / 20.00
- Ranked 32nd among 10,000 participants in the M.Sc. entrance exam

10/1998-10/2002 **Sharif University of Technology, Tehran, Iran**
- Bachelor of Science in Civil Engineering, GPA: 16.57 / 20.00
- Ranked 1st in ACI-Iranian chapter's educational program
- Ranked 110th among 300,000 participants in the university entrance exam

10/1994-07/1998 **Sadegh High School, Tehran, Iran**
- Diploma in Mathematics and Physics, GPA: 19.13 / 20.00

Professional Experience

04/2004-09/2005 **Structural Engineer, Namvaran Consulting Engineers, Tehran, Iran**
- Designed foundations for petrochemical equipments (e.g. pumps, reservoirs, and pipe lines)
- Member of design team for large-scale petrochemical infra-structures
- Managed and designed projects of low-rise residential buildings
- Prepared design tables for various steel bolted connections

Academic Experience

10/2005-03/2010 **Teaching and research assistant, EPFL, Lausanne, Switzerland**
- Held tutorial sessions for Concrete Structures I & II, Statics I & II, and Prestressed Concrete Bridges
- Assisted in preparation of assignments
- Taught courses based on the Swiss code series (SIA 2003)

10/2002-07/2004 **Teaching and research assistant, Sharif University of Technology, Tehran, Iran**
- Held tutorial sessions for Theory of Structures I & II, Solid Mechanics, and Theory of Plates and Shells
- Assisted in preparation of assignments

Publications

- Mirzaei, Y., and Muttoni, A., *Post-failure shear transfer through flexural reinforcement in slab-column connections* (to be published)
- Mirzaei, Y., and Muttoni, A., *Experimental investigation into the post-punching behavior of reinforced concrete flat slabs* (to be published)
- Mirzaei, Y., *Post-punching behavior of reinforced concrete slab-column connections*, 7th International fib Symposium, Stuttgart, 2008.
- Mirzaei, Y., and Muttoni, A., *Tests of the post-punching behavior of the reinforced concrete flat slabs*, IBETON, Switzerland, 2008.
- Mirzaei, Y., *Seismic behavior of steel structures using nonlinear pushover analysis*, Master of Science dissertation, Tehran, March 2005.
- Mirzaei, Y., and Mofid, M., *Application of nonlinear pushover analysis for seismic demand estimation*, 3rd national civil engineering congress, Tehran, May 2004.